GEOCHEMICAL PROCESSES IN THE EARTH'S MANTLE

AND THE NATURE OF CRUST-MANTLE INTERACTIONS:

EVIDENCE FROM STUDIES OF Nd AND Sr ISOTOPE RATIOS

IN MANTLE-DERIVED IGNEOUS ROCKS AND LHERZOLITE NODULES

by

ALAN ZINDLER
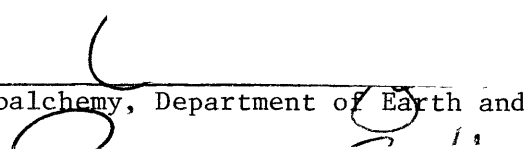
B.S., Florida State University
(1976)

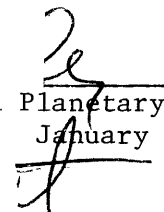SUBMITTED IN PARTIAL FULFILLMENT
OF THE REQUIREMENTS FOR THE
DEGREE OF

DOCTOR OF PHILOSOPHY

at the

MASSACHUSETTS INSTITUTE OF TECHNOLOGY

JANUARY, 1980

Signature of Author_____
    Center for Geoalchemy, Department of Earth and Planetary Science
                                                January 21, 1980

Certified by_____
                                                Stanley R. Hart
                                                Thesis Supervisor

Accepted by_____
                                                Frederick A. Frey
                                                Chairman, Department Committee

GEOCHEMICAL PROCESSES IN THE EARTH'S MANTLE

AND THE NATURE OF CRUST-MANTLE INTERACTIONS:

EVIDENCE FROM STUDIES OF ND AND SR ISOTOPE RATIOS

IN MANTLE-DERIVED IGNEOUS ROCKS AND LHERZOLITE NODULES

by

ALAN   ZINDLER

Submitted to the

Department of Earth and Planetary Science on

January 28, 1980 in partial fulfillment of the

requirements for the degree of Ph.D.

ABSTRACT

Investigations have been undertaken to provide constraints on the
nature of geochemically active processes in the mantle and their effects
on mantle evolution and magma generation. Three types of approaches have
been implemented: (1) To study isotopic systematics and trace element abun-
dances in young, mantle-derived volcanic rocks, which, because of their tecto-
nic setting, had little or no chance for interaction with crustal material
prior to their eruption. (2) To compare and contrast the Precambrian mantle
with the present-day  mantle via geochronological studies of ultramafic and
mafic igneous rocks from Archean and Proterozoic greenstone belts. (3) To
examine isotopic systematics and trace element distributions in mantle-de-
rived lherzolite nodules, in an effort to reconcile first order observations
of mantle materials with models of magma production in the mantle.
     Picritic basalts to quartz-normative tholeiites from the western Rey-
kjanes Peninsula have been analyzed  for Nd and Sr isotopic ratios and rare
earth element (REE) abundances. The results of this study show that the mantle
beneath the Reykjanes Peninsula is both vertically and laterally zoned with
respect to LIL elements, and that mixing of liquids produced in different
mantle segments must be called upon to explain the chemical variation in the
basalts. Alkalic volcanics from Central Europe have also been investigated
and are found to lie  within the range defined by young oceanic volcanic
rocks. The mantle source region for these lavas has changed in character from
the Miocene to the Quaternary, as reflected by changes in the Nd and Sr iso-
topic compositions of these rocks to lower and higher values respectively.
     Sm-Nd systematics for the Abitibi belt and the Cape Smith belt yield ages

2622 and 1871 m.y. respectively. However,Rb-Sr systematics in both areas have been affected by alteration processes subsequent to crystallization and no longer carry information about the primary crystallization ages. Relative to a model for the bulk earth which predicts chondritic relative abundances for REE's, the Abitibi magmas appear to be derived from an unfractionated, "chondritic", reservoir, while the Cape Smith magmas are derived from a reservoir with a history of LREE depletion. Sr isotopic systematics in inclusion-free clinopyroxenes provide evidence for both old oceanic crust and island arc material in the Cape Smith belt.

Nd and Sr isotopic data show that the magma which crystallized as gabbro of the Shobogamo Intrusive Suite was contaminated by crustal component prior to crystallization. The nature of the process whereby a mantle-derived magma is contaminated, is constrained by Nd and Sr isotope ratios and concentrations. The process described is considered applicable to modern volcanic provinces which have been interpreted as being derived from "enriched" mantle source regions.

The constituent phases of some ultramafic nodules from San Carlos, Arizona, ranging from dunite to "fertile" spinel lherzolite have been analyzed for Nd and Sr isotopes and trace element concentrations. Adjacent phases with different parent-daughter ratios were found to be in isotopic equilibrium suggesting recent equilibration events in the mantle, a result which is contrary to that expected on the basis of previous work. Alkali element budgets of the nodules are not accounted for by the alkalies in silicate phases, and liquid inclusions and sulfides are thought to play an important role. Sr, Nd, and Sm are shown to reside in clean silicate phases in both the LREE-depleted, "fertile" nodules, and the LREE-enriched harzburgitic nodules. The processes which have affected these nodules are complex and multi-facetted, and involve the migration,within the mantle,of liquids or fluids enriched in alkali and LIL elements. It is proposed that these metasomatic components can play an important role in determining the chemistry of magmas generated in the mantle.

Thesis supervisor:   Stanley R. Hart, Professor of Geology and Geochemistry

## Acknowledgements

TABLE OF CONTENTS

Introduction

This thesis represents a compilation of data and conclusions from

six independent investigations completed during the author's tenure at

M.I.T.  Although these studies involve various rock types of different

ages from apparently unrelated localities, there is an underlying theme

which has provided the impetus for the undertaking of each of the

projects: to understand geochemically active processes in the mantle

and their effects on mantle evolution and magma generation.  Within

the context of this theme, it was considered that three types of

approaches were relevant: (1) To study isotopic systematics and trace

element abundances in young, mantle-derived volcanic rocks, which,

because of their tectonic setting, had little or no chance for inter-

action with crustal material prior to their eruption.  It was expected

that this would enable development of constraints both on the nature

of magma generation and on the character of chemical heterogeneity in

the mantle. (2)   To compare and contrast the Precambrian mantle with

the present-day mantle via geochronological studies of ultramafic and

mafic igneous rocks from Archean and Proterozoic greenstone belts.

Through this type of investigation, evolutionary parameters may be

derived for the mantle and, in addition, Precambrian and present-day

magma generation processes may be compared.   (3) To examine isotopic

systematics and trace element distributions in mantle-derived

lherzolite nodules, in an effort to reconcile first-order observations

of mantle materials with models of magma production in the mantle.  It

was hoped that this approach would also provide insight into the

geochemically active processes which have caused the mantle to evolve to it's present state.

The first type of approach has been applied in two different modern tectonic settings: the Reykjanes Peninsula, Iceland (Chapter 1), and volcanic provinces of Central Germany (Chapter 2). A sequence of basalts from the Reykjanes Peninsula, the northeastward extension of the Reykjanes Ridge onto Iceland, were analyzed for Nd and Sr isotope ratios and rare earth element (REE) abundances. These basalts, which range from olivine-rich "picrite" basalts to quartz-normative tholeiites, are erupted in a region which is transitional between mid-ocean-ridge (MOR) and ocean-island tectonic settings, providing an ideal format for investigation of possible mantle heterogeneity and variations in the petrogenetic processes responsible for the observed differences in chemistry between successive flows. The results of this study show that the mantle beneath the Reykjanes Peninsula is both vertically and laterally zoned with respect to LIL elements, and that mixing of liquids produced in different mantle segments must be called upon to explain the chemical variations in the basalts.

Nd and Sr isotope ratios have been measured in alkalic volcanic rocks from central Europe. These volcanics range in composition from feldspathoid-bearing basanites to phonolites, and are erupted through a once-stable shield area which was reactivated during the Miocene. As this may represent the early stages of, or an aborted attempt at rifting of a stable craton, it is an attractive region for observing changes in mantle chemistry which may accompany the development of a new tectonic regime. Preliminary results suggest that the mantle source for these lavas

has changed in character from the Miocene to the Quaternary, as reflected by changes in the Nd and Sr isotopic compositions of the rocks.

The second approach has been employed in two areas of the Canadian shield: the Abitibi belt of the Superior Province and the Cape Smith-Wakeham Bay of the Churchill Province (Chapter 3). In both studies, komatiitic and tholeiitic volcanic rocks and hypabyssal intrusives have been analyzed for Nd and Sr isotope ratios and Sm, Nd, Rb and Sr concentrations. Sm-Nd systematics define ages of 2622±120 m.y. for the Abitibi belt and 1871±75 m.y. for the Cape Smith belt, which are consistent with age estimates for these rocks based on other techniques. However, Rb-Sr systematics in both areas have been affected by alteration processes subsequent to crystallization and no longer carry information about the primary crystallization ages. Because the mafic to ultramafic chemistry of these rocks precludes a significant role for older crustal material in their genesis, initial $^{143}Nd/^{144}Nd$ ratios are interpreted as mantle values at the respective emplacement times. Relative to a model for the bulk earth which predicts chondritic relative abundances for REE's, the Abitibi magmas appear to be derived from an unfractionated, "chondritic", reservoir, while the Cape Smith magmas are derived from a reservoir with a history of LREE depletion. The results from Abitibi suggest that the peridotitic komatiite liquids must be generated by melting of a residue from a previous melting event. No such conclusion is made for the Cape Smith rocks, where komatiites and tholeiites appear to be a continuum in a single magma series. It is proposed that the Cape

Smith belt represents an intercratonic tectonic setting which is transitional between Archean greenstone belts and modern island arcs.

A Nd and Sr isotopic study of the Shabogamo Intrusive Suite was undertaken in the spirit of the second approach (Chapter 4). However, during the course of the investigation, it was determined that the magma which crystallized as gabbros of the Shabogamo Intrusive Suite was contaminated by a crustal component prior to crystallization. The nature of the process whereby a mantle-derived magma is contaminated, is constrained by Nd and Sr isotope ratios and concentrations. The process described is considered applicable to modern volcanic provinces which have been interpreted as being derived from "enriched" mantle source regions.

The third approach has been implemented in a detailed geochemical study of constituent phases of ultramafic nodules from San Carlos, Arizona (Chapter 5). The nodules studied show a large variation in mineralogy from dunite to "fertile" spinel lherzolite. This project was undertaken to quantitatively characterize the chemical differences which accompany the mineralogical variations in the nodules. In this way, it was thought to understand the processes responsible for the chemical and mineralogical differences between rocks, which must have a bearing on the nature of basalt genesis in the mantle. Many signficant conclusions are drawn from this study, while many significant problems remain to be solved by future investigations. Adjacent phases with different parent-daughter ratios were found to be in isotopic equilibrium suggesting recent equilibration events in the mantle, a result which is contrary to that expected on the basis of

previous work.  Alkali element budgets of the nodules are not accounted for by the alkalis in silicate phases, and liquid inclusions and sulfides are thought to play an important role.  Sr, Nd and Sm are shown to reside in clean silicate phases in both the LREE-depleted, "fertile" nodules, and in the LREE enriched harzburgitic nodules.  The processes which have affected these nodules are complex and multi-faceted, and involve the migration within the mantle of liquids or fluids enriched in alkali and LIL elements.  It is proposed that these metasomatic components can play an important role in determining the chemistry of magmas generated in the mantle.

The conclusions drawn on the basis of results from investigations presented in this thesis represent a significant contribution to the understanding of chemical processes in the mantle and their bearing on magma generation and time-integrated mantle evolution.  However, time may show that a more important contribution has been to show where current theory is inadequate to explain observations, thus providing an impetus for further work.

CHAPTER 1

Nd AND Sr ISOTOPE RATIOS

AND RARE EARTH ELEMENT ABUNDANCES

IN REYKJANES PENINSULA BASALTS:

EVIDENCE FOR MANTLE HETEROGENEITY

BENEATH ICELAND

## 1.1 Introduction

The Reykjanes Peninsula, in southwestern Iceland, is the subaerial, northeastward extension of the active Reykjanes Ridge spreading center. However, it is established (Schilling, 1973; Hart et al., 1973; Sun et al., 1975; White et al., 1976; O'Nions and Gronvold, 1973; O'Nions and Pankhurst, 1974; Sigvaldason, 1974; O'Nions et al., 1976) that trace element and isotopic characteristics of Icelandic tholeiitic basalts are distinct from axial tholeiitic basalts of the Reykjanes Ridge south of $61^{\circ}N$. These geochemical differences have commonly been attributed to mantle heterogeneity; thus, the Reykjanes Peninsula is an excellent area for studying mantle heterogeneity and the petrogenetic processes creating island tholeiites (e.g., Iceland) which are markedly enriched in incompatible trace elements relative to "normal" (O'Nions and Pankhurst, 1974) mid-ocean ridge basalts (MORB).

Our collaborative research on Holocene tholeiites from the western Reykjanes Peninsula combines isotopic and trace element abundance data with the field, petrologic and major element data of Jakobsson et al. (1978). Based on these data we conclude that: (1) the mantle source region for Reykjanes Peninsula basalts is heterogeneous, with respect to rare earth element (REE) contents and $^{143}Nd/^{144}$; (2) on a time averaged basis these mantle sources are all relatively depleted in light REE compared to chondrites; and (3) a model of vertical heterogeneity with mixing of magmas produced in different mantle portions is most consistent with the data.

1.2  Background

Jakobsson et al. (1978) discussed the general geology of the

Reykjanes Peninsula, and the petrographic, major element composition and

field relations of the samples studied.  Briefly, the post-glacial basalts

studied group into distinct swarms along the Reykjanes Peninsula,

with fissures arranged en enchelon to the trend of the Reykjanes Ridge.

This trend strikes about N70E and is interpreted as a plate boundary

with the direction of spreading approximately perpendicular to the

fissures (Tryggvason, 1973; Klein et al., 1973; Klein et al., 1977; Frey

et al., 1974; and Fig. 1).  We report data for the westernmost swarms

on the peninsula, the Reykjanes, the Grindavik, and the Krisuvik swarms

(Fig. 1).  Within each swarm, eruption fissures dominate the central or

axial portions and lava shield craters lie on the periphery.

Based on major element composition and petrography three types of

basaltic lavas are identified.  Picrite basalts, averaging 25% normative

olivine, are erupted from lava shield craters and are the oldest Holocene

basalts in each swarm.  Olivine tholeiites, also erupted from lava shield

craters, follow the picrite basalts and contain from 7 to 25% normative

olivine.  The youngest phase of volcanism is characterized by fissure

eruption of tholeiitic basalts, which range from slightly (<7%) olivine

to slightly (<2%) quartz normative.  Estimated lava volumes extruded

during the three eruptive phases are, respectively, 0.2, 9.7 and 3.2 km$^3$.

Jakobsson et al. (1978) recognize two petrochemical groups, the picrite

basalt-olivine tholeiite series, which define coherent geochemical trends,

and the fissure tholeiites which are geochemically distinct from the first

Figure 1.

Map of the active volcanic zone of the Reykjanes Peninsula, S.W.-
Iceland. Volcanic fissure swarms are indicated by dashed lines. Also
shown are the distribution of various types of Holocene eruption sites.
Figure taken from Jakobsson et al. (1978).
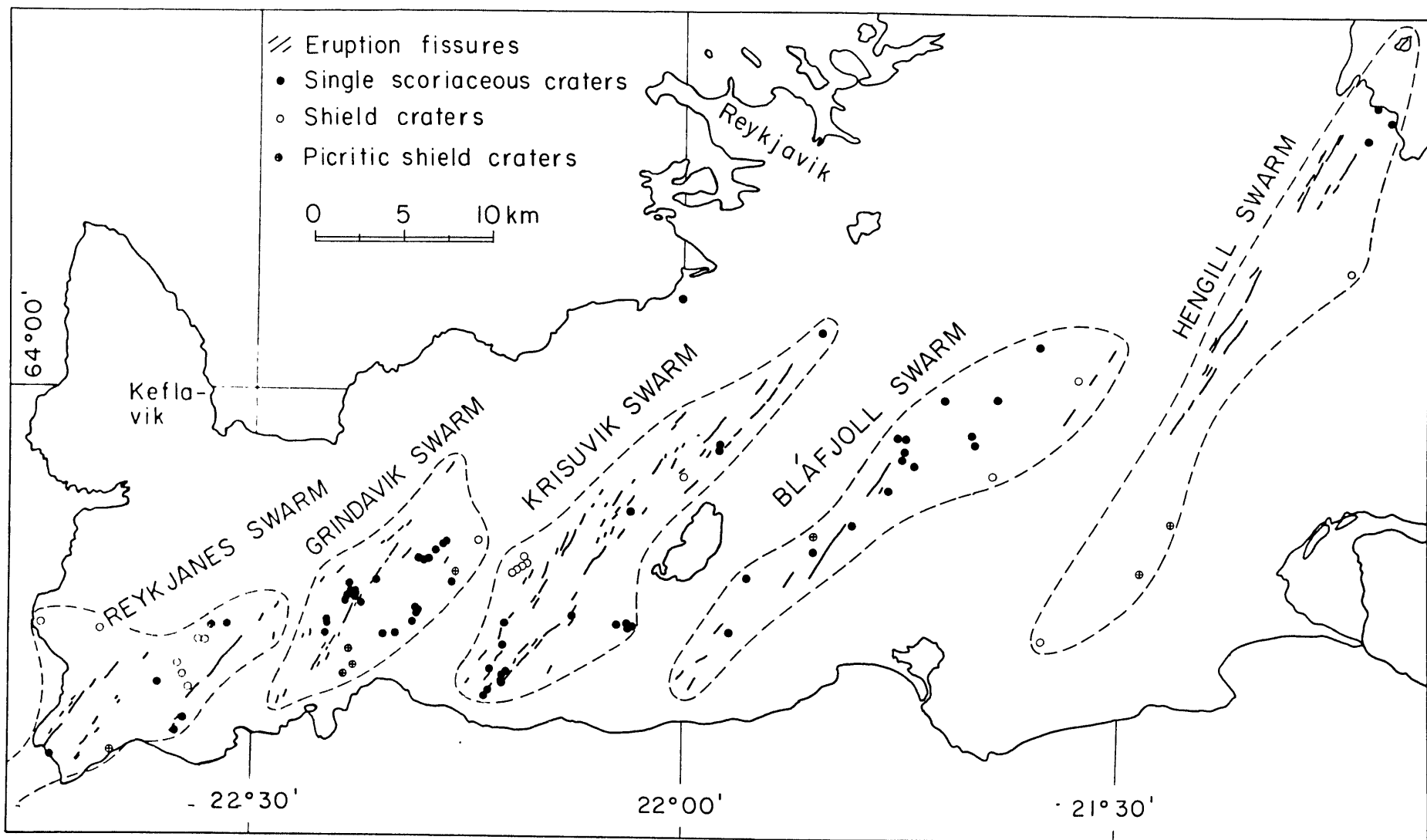
Figure 1

group. Although they recognized an important role for fractional crystallization Jakobsson et al. (1978) concluded that "the volume/chemistry (especially $K_2O$, $TiO_2$ and $P_2O_5$ contents) relations strongly indicate that other processes must be sought to explain the main compositional variation".

1.3 <u>Results</u>

Rare earth elements.

Eighteen samples showing the complete range in major element composition (Jakobsson, 1978) have been analyzed for REE abundances (Table 1 and Fig. 2). As seen in Fig. 3, the grouping of lavas based on major element composition is supported by their separation into groups on the basis of relative REE abundances and light REE (LREE) fractionation. Although the fields for the tholeiites and olivine tholeiites overlap considerably, this is largely due to samples RE 81 and RE 25, the most mafic tholeiites (Jakobsson, 1978). There is extreme variation in La abundance from the most LREE depleted picrite basalt to the most enriched fissure tholeiite. In fact, the range in $(La/Sm)_N$ from 0.33 to 1.25 (Table 1) encompasses almost the entire range of $(La/Sm)_N$, 0.25 to 1.37, found in a transect from $57^{o}N$ on the Reykjanes Ridge to $64^{o}$ on the Reykjanes Peninsula (Schilling, 1973; Schilling et al., 1978). $(La/Sm)_N$ values previously reported by Schilling (Schilling, 1973; Schilling et al., 1978) for the Reykjanes Peninsula range from 1.26 to 1.37.

Table 1-1

Rare earth element concentrations * in Reykjanes Peninsula basalts

Reykjanes swarm

| | picrite basalts | | | olivine tholeiites | | fissure tholeiites | | |
|------|-------|-------|---------|-------|-------------------|-------|-------|-------|
| | RE 47 | RE 46 | RE 36-I | RE 61 | RE 34 (average) | RE 25 | RE 29 | Re 21 |
| La | 0.26 | 0.63 | 0.53 | 3.54 | 4.00 ± 0.23 | 3.34 | 5.69 | 8.25 |
| Ce | 1.50 | 3.6 | 3.6 | 9.8 | 10.75 ± 0.86 | 8.6 | 16.0 | 23.0 |
| Nd | 1.20 | 2.6 | 2.9 | 6.6 | 6.95 ± 0.83 | 5.9 | 11.0 | 14.0 |
| Sm | 0.45 | 1.14 | 1.02 | 2.12 | 2.23 ± 0.10 | 2.03 | 2.60 | 3.73 |
| Eu | 0.21 | 0.50 | 0.44 | 0.78 | 0.93 ± 0.02 | 0.88 | 1.12 | 1.41 |
| Tb | 0.20 | 0.33 | 0.32 | 0.40 | 0.49 ± 0.02 | 0.49 | 0.68 | 0.86 |
| Ho | 0.20 | 0.60 | 0.60 | — | 0.55 ± 0.05 | 0.70 | 0.80 | 1.0 |
| Yb | 0.70 | 1.70 | 0.65 | 1.79 | 2.05 ± 0.14 | 2.19 | 2.61 | 3.16 |
| Lu · | 0.12 | 0.29 | 0.25 | 0.29 | 0.29 ± 0 | 0.36 | 0.43 | 0.50 |

Grindavik swarm

| | picrite basalts | | | olivine tholeiites | fissure tholeiites | | |
|------|-------|--------|--------|-------|-------|-------|-------|
| | RE 78 | RE 149 | RE 100 | RE 56 | RE 81 | RE 15 | RE 16 |
| La | 0.38 | 0.50 | 1.80 | 5.92 | 4.12 | 8.22 | 8.27 |
| Ce | 2.4 | 1.30 | 6.3 | 16.0 | 13.0 | 20.0 | 23.0 |
| Nd | 1.0 | 1.20 | 4,0 | 11.0 | 6.8 | 14.0 | 15.0 |
| Sm | 0.76 | 0.51 | 1.57 | — | 2.05 | 3.75 | 3.81 |
| Eu | 0.36 | 0.25 | 0.59 | 1.15 | 0.83 | 1.37 | 1.49 |
| Tb | 0.24 | 0.17 | 0.34 | 0.62 | 0.46 | 0.70 | 0.80 |
| Ho | 0.34 | — | 0.60 | — | — | 1.00 | 1.10 |
| Yb | 1.25 | 0.89 | 1.82 | 2.17 | 1.97 | 3.08 | 3.51 |
| Lu | 0.20 | 0.16 | 0.29 | 0.36 | 0.32 | 0.50 | 0.56 |

Krisuvik swarm

| | olivine tholeiites | fissure tholeiites | |
|------|-------|------|------|
| | 119 | 39-1 | 103 |
| La | 4.90 | 6.0 | 5.8 |
| Ce | 11.0 | 14.0 | 16.0 |
| Nd | 7.2 | 9.3 | 9.7 |
| Sm | 2.38 | 2.85 | 3.27 |
| Eu | 0.94 | 1.07 | 1.24 |
| Tb | 0.52 | 0.67 | 0.66 |
| Ho | 0.60 | 0.90 | 1.00 |
| Yb | 2.09 | 2.44 | 3.11 |
| Lu | 0.31 | 0.37 | 0.51 |

* All REE's in ppm, determined by INAA.

Figure 2.

Rare earth element abundances of Reykjanes Peninsula basalts
(data are normalized to an average of chondrites from Nakamura (1974),
Tb and Ho from Frey et al. (1968). Sm and Nd data from Table 2. a-
tholeiites; b - olivine tholeiites; c - picrite basalts.
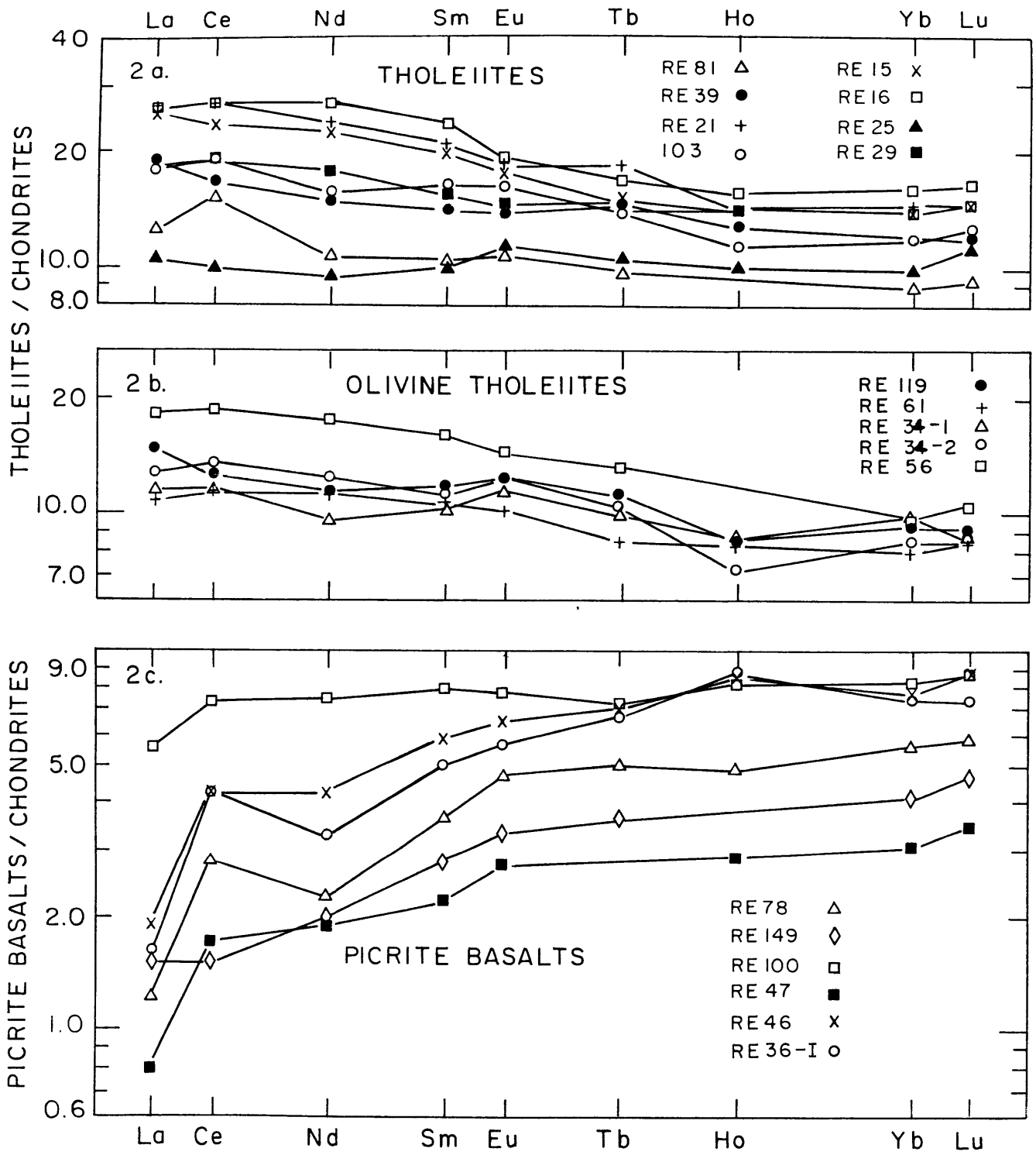
Figure 2

Figure 3.

    Fields for different basalts types, Reykjanes Peninsula (from Fig. 2).

Figure 3

REYKJANES PENINSULA BASALTS

THOLEIITE

OLIVINE THOLEIITES

PICRITE BASALTS

BASALTS / CHONDRITES

50

20

10.0

5.0

2.0

1.0

La  Ce  Nd  Sm  Eu  Tb  Ho  Yb  Lu

23
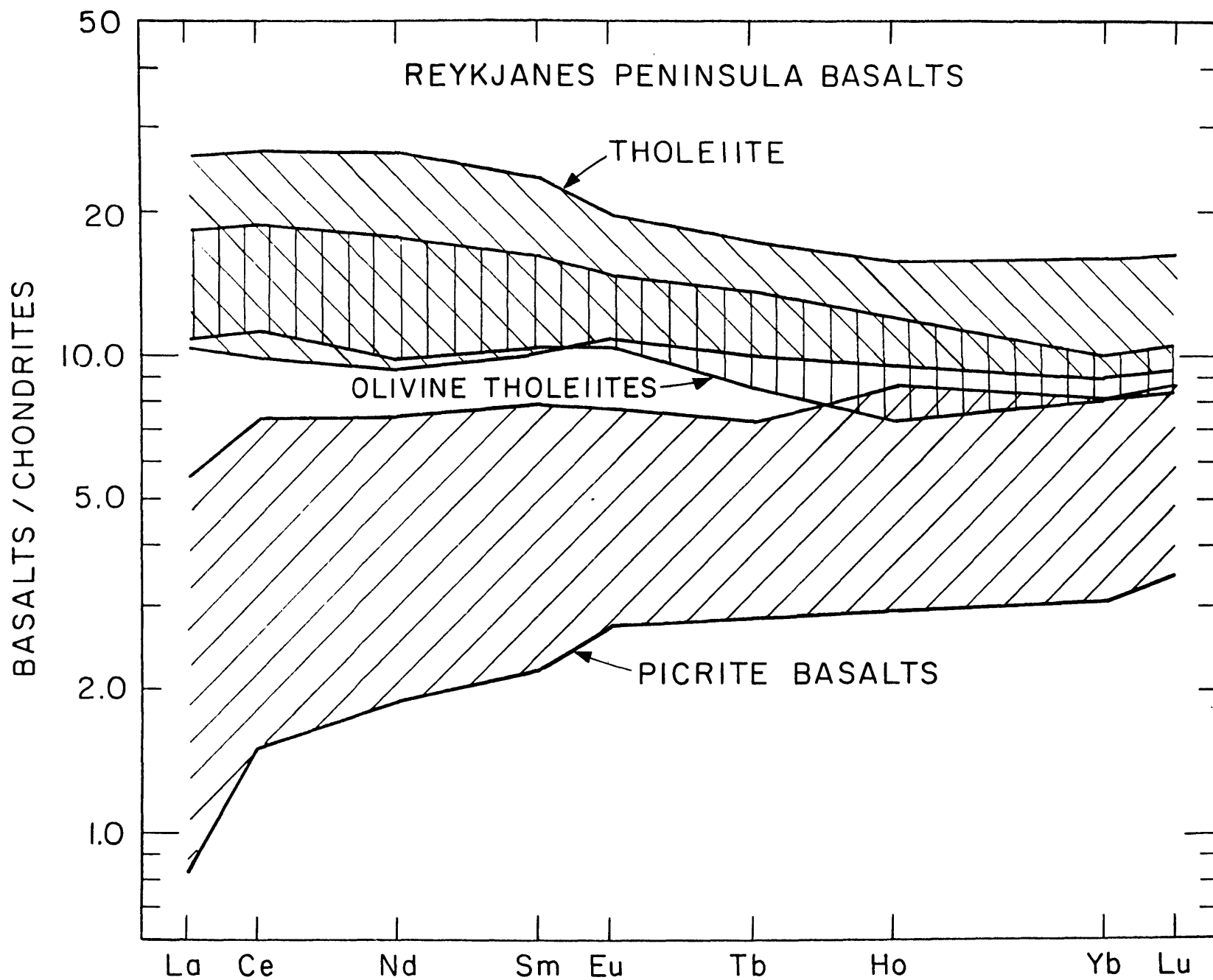
Nd and Sr isotopes.

Nine samples, representative of the observed range in $(La/Sm)_N$ values, were chosen for $^{143}Nd/^{144}Nd$ and $^{87}Sr/^{86}Sr$ measurements (Table 2). $^{87}Sr/^{86}Sr$ ratios fall in a very restricted range from 0.7031 to 0.7032, increasing slightly from the picrite basalts to the tholeiites. This range is consistent with previously reported $^{87}Sr/^{86}Sr$ values from the Reykjanes Peninsula (Hart et al., 1973; O'Nions and Gronvold, 1973; O'Nions et al., 1976) and is completely distinct from the range of reported values for the Reykjanes Ridge (from 0.7026 to 0.7029, from Hart et al., 1973; White et al., 1976; O'Nions and Pankhurst, 1974; O'Nions et al., 1976). The small $^{87}Sr/^{86}Sr$ variation is surprising in light of the variation in $^{143}Nd/^{144}Nd$, from 0.51299 in the tholeiite fissure basalts, to 0.51317 in the picrite basalts. This range is very large when compared to $^{143}Nd/^{144}Nd$ ratios reported by O'Nions et al. (1977) for several post-glacial tholeiites from Iceland (0.51300-0.51304). In fact, it is somewhat larger than the total range observed by O'Nions et al. (1977) for tholeiite basalts from the Reykjanes Ridge and Iceland (0.51313 at 52°N to 0.51300 on Iceland), and represents more than one third of the total measured range in most oceanic islands and MORB (DePaolo and Wasserburg, 1976; O'Nions et al., 1977; DePaolo and Wasserburg, 1976b). In contrast, the range of $^{87}Sr/^{86}Sr$, 0.7031-0.7032, in the Reykjanes Peninsula basalts is very small when compared to the range for islands and MORB (0.7023-0.7065) (Hoffman and Hart, 1978).

Though there may be a negative correlation between $^{143}Nd/^{144}Nd$ and $^{87}Sr/^{86}Sr$ (Fig. 4), errors associated with the relatively small variations in $^{87}Sr/^{86}Sr$ are critical in evaluating this correlation.

Table 1-2

Nd and Sr isotopic compositions and Rb, Sr, Sm and Nd concentrations [*] for Reykjanes peninsula basalts

| Sample No. | Rock type | Rb | Sr | Sm | Nd | $^{87}Sr/^{86}Sr$[**] | $^{143}Nd/^{144}Nd$[**] | $t_{ND}$ |
|---|---|---|---|---|---|---|---|---|
| RE 15 | tholeiite | 3.647 | 165.8 | 4.058 | 14.23 | $\begin{cases} 0.70316 \pm 4 \\ 0.70317 \pm 5 \end{cases}$ | $0.512990 \pm 14$ | 7.3 |
| RE 16 | tholeiite | 4.032 | 152.9 | 4.803 | 16.67 | $0.70319 \pm 5$ | $0.513037 \pm 16$ | 8.2 |
| RE 21 | tholeiite | 4.005 | 159.7 | 4.227 | 14.38 | $\begin{cases} 0.70323 \pm 5 \\ 0.70318 \pm 4 \end{cases}$ | $0.512995 \pm 15$ | 7.4 |
| RE 29 | tholeiite | – | – | 3.203 | 10.62 | – | $0.513015 \pm 28$ | 7.8 |
| RE 46 | picrite basalt | 0.1795 | 61.7 | 1.191 | 2.658 | $0.70320 \pm 11$ | $0.513168 \pm 18$ | 10.8 |
| RE 56 | olivine tholeiite | 1.897 | 189.4 | 3.240 | 10.89 | $\begin{cases} 0.70317 \pm 5 \\ 0.70315 \pm 5 \end{cases}$ | $0.513032 \pm 18$ | 8.1 |
| RE 61 | olivine | 1.509 | 149.4 | $\begin{cases} 2.176 \\ 2.177 \end{cases}$ | $\begin{cases} 6.995 \\ 6.993 \end{cases}$ | $0.70310 \pm 4$ | $0.513053 \pm 14$ | 8.5 |
| RE 78 | picrite basalt | 0.132 | 58.8 | 0.750 | 1.434 | $0.70313 \pm 7$ | $0.513119 \pm 44$ | 9.8 |
| RE 100 | picrite basalt | 1.022 | 75.2 | 1.598 | 4.680 | $\begin{cases} 0.70311 \pm 7 \\ 0.70314 \pm 5 \end{cases}$ | $\begin{cases} 0.513083 \pm 25 \\ 0.513078 \pm 19 \end{cases}$ | $\begin{cases} 9.1 \\ 9.0 \end{cases}$ |
| RE 149 | picrite basalt | 0.086 | 42.8 | 0.565 | 1.208 | $0.70313 \pm 6$ | $0.513115 \pm 25$ | 9.7 |
| RE 361 | picrite basalt | – | – | 1.026 | 2.042 | – | $0.513158 \pm 25$ | 10.6 |
| BCR-1 | U.S.G.S. standard | – | – | – | – | – | $\begin{cases} 0.51265 \pm 3 \\ 0.51263 \pm 3 \\ 0.51265 \pm 2 \\ 0.51264 \pm 2 \end{cases}$ | – |

[*] All concentrations are in ppm, by isotope dilution.

[**] Errors are in last significant digits, and represent $2\sigma$ confidence level. $^{87}Sr/^{86}Sr$ values are relative to 0.70800 for the E and A standard. $^{143}Nd/^{144}Nd$ normalized to $^{146}Nd/^{144}Nd = 0.72190$ [38].

Figure 4.

Nd-Sr correlation diagram showing $^{143}Nd/^{144}Nd$ vs. $^{87}Sr/^{86}Sr$ for Reykjanes Peninsula basalts. Note the large range in $^{143}Nd/^{144}Nd$ compared to a range in $^{87}Sr/^{86}Sr$ which is only slightly beyond analytical error.

Figure 4
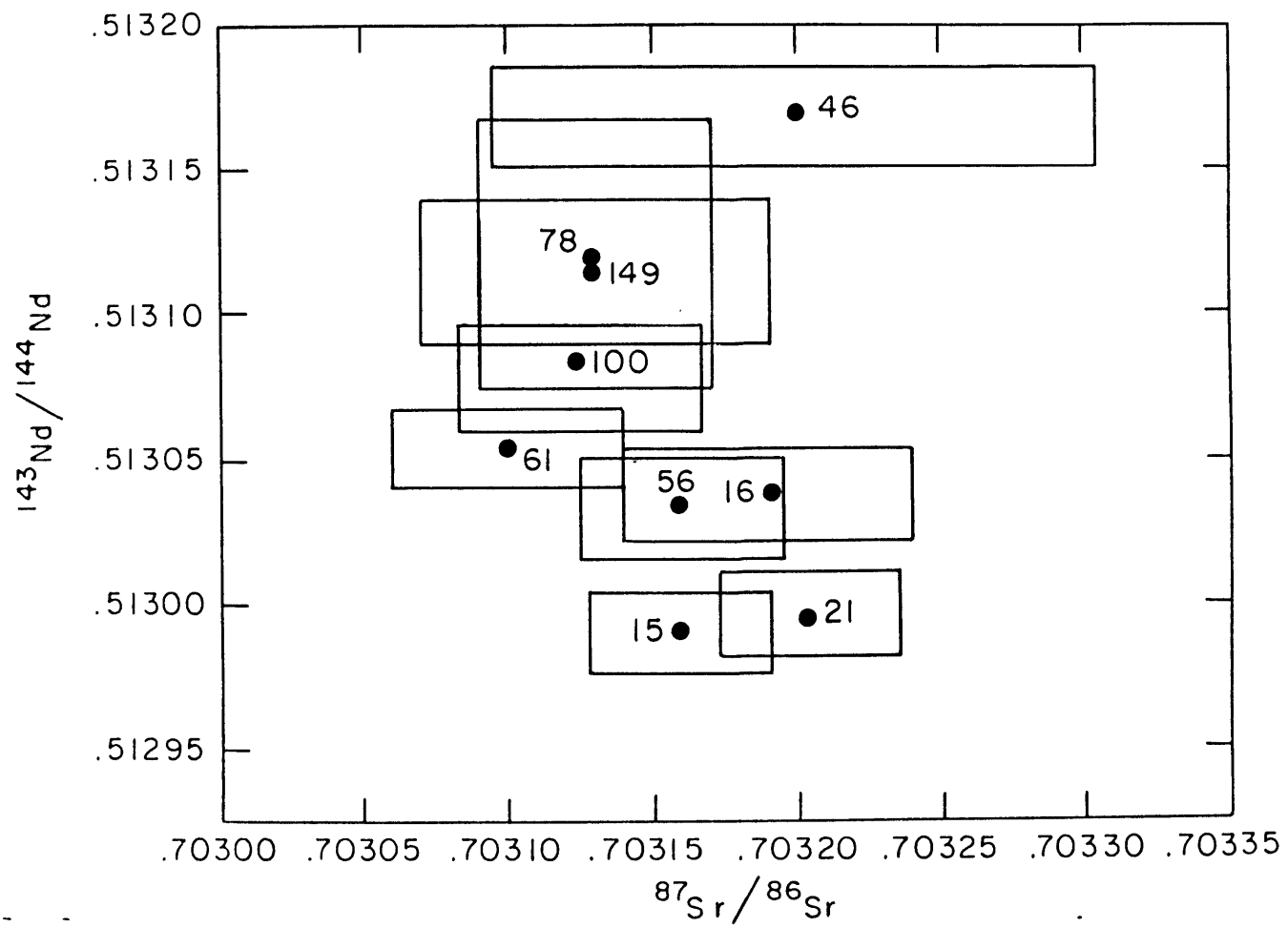
Further, when these data are plotted on a Nd-Sr correlation diagram

with existing data for ocean islands and MOR basalts (Fig. 5), it can

be seen that although they lie within the "oceanic trend" defined by

the existing data, the slope of the Reykjanes Peninsula data diverges

signficantly from that of the "oceanic trend". At present, we are not

able to evaluate the significance of Hiis divergence of trends, with

coincidence of fields, on a Nd-Sr correlation diagram, but we propose

that this is an important observation which should be considered in any

quantitative attempt to explain the Nd-Sr correlation in oceanic rocks.


## 1.4   The case for a heterogeneous mantle

The large variation in $^{143}$Nd/$^{144}$Nd in these basalts strongly indicates

a heterogeneous mantle source of the Reykjanes Peninsula basalts.  Because

of the relatively small variations in $^{87}$Sr/$^{86}$Sr (Fig. 4), the processes

creating such heterogeneity in the source mantle must have caused more

relative fractionation of Sm/Nd than Rb/Sr.  Clinopyroxene and garnet

are mantle phases that can markedly change the ratio of Sm/Nd while

causing little change in Rb/Sr.  For example, in Fig. 6, Nd/Sm and Rb/Sr

are plotted as a function of percent melting in a garnet peridotite.

For different sets of partition coefficients and various mineral

proportions, there is always a range of melting where Nd/Sm changes

significantly while Rb/Sr remains essentially constant.  Therefore, the

observed mantle heterogeneity could be a result of melt migration within

the mantle.

Alternatively, disequilibrium melting processes have been invoked

(O'Nions and Pankhurst, 1974; Flower et al., 1975; Beswick and Carmichael,

Figure 5.

Nd-Sr correlation diagram showing Reykjanes Peninsula data from this study compared to data for other young volcanic rocks. Data sources: MORB, Hawaii, Bouvet, Tristan da Cunha, Ascension and Iceland from O'Nions et al. (1977); flood basalts, MORB, and Hawaii from DePaolo and Wasserburg (1976b); MORB, Iceland, and Azores from Richard et al. (1976); East Eifel from Staudigel and Zindler (1978). $\varepsilon_{Nd}$ is defined as:

$$\varepsilon_{Nd} = \left[ \frac{(^{143}Nd/^{144}Nd)}{(0.512616)_{JUV}} - 1 \right] \times 10^{4}$$

where 0.512616 is the present-day $^{143}Nd/^{144}Nd$ in the basaltic achondrite Juvinas (DePaolo and Wasserburg, 1976). All $^{143}Nd/^{144}Nd$ are normalized to $^{146}Nd/^{144}Nd = 0.72190$.

Nd-Sr CORRELATION DIAGRAM

REYKJANES
PENINSULA
TREND

- ● MORB
- × ICELAND (THIS STUDY)
- ▲ ICELAND (PREVIOUS STUDIES)
- ⌀ AZORES
- ○ ASCENSION
- + TRISTAN Da CUNHA
- □ BOUVET
- ■ HAWAII
- △ FLOOD BASALTS
- ◇ EIFEL, GERMANY

"OCEANIC TREND"

DATA FROM:

RICHARD et.al. 1976
DEPAOLO & WASSERBURG 1976b
O'NIONS et.al. 1977
STAUDIGEL & ZINDLER 1978

$^{143}Nd/^{144}Nd$

$\epsilon_{Nd}$

$^{87}Sr/^{86}Sr$   Figure 5

30
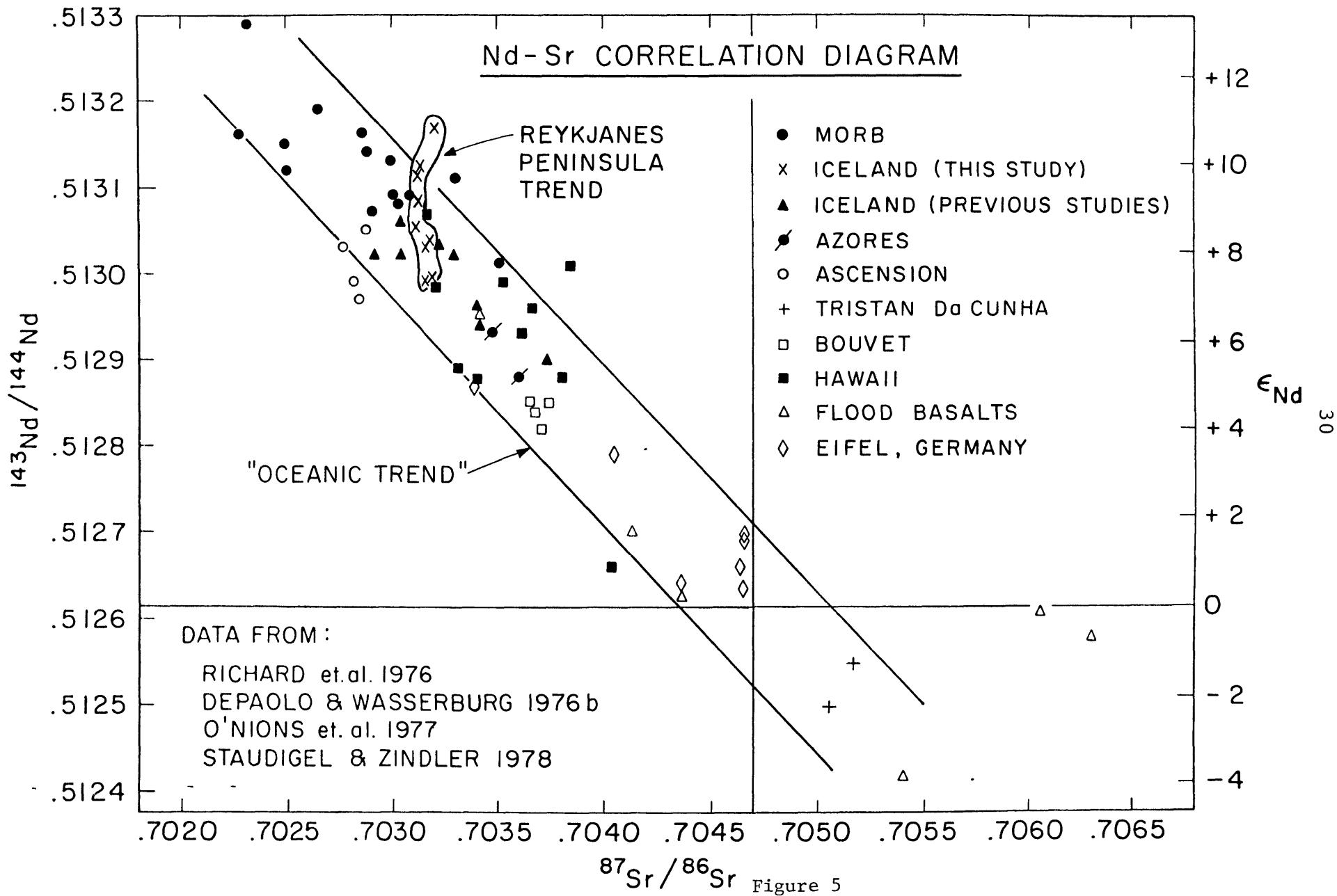
Figure 6.

Theoretical curves showing changes in Nd/Sm and Rb/Sr as a function

of melting in a garnet lherzolite.  Nd/Sm and Rb/Sr in the original solid

are taken as unity.  Fractional melting equations of Shaw (1970) are

used in the calculations.  Solid curves are for a mantle where

ol:opx:cpx:gnt = 55:25:10:10 and dashed curves are for ol:opx:cpx:gnt: =

55:25:5:15.  Curves A and B are calculated using partition coefficient

sets #2 and #3, respectively, from Frey et al. (1978).  Curves C and D

represent a "reasonable" range in partition coefficients for Rb and Sr,

in the four mantle phases, taken from the literature.  $K_{D\ Rb}^{cpx/l} = 0.00141$

to 0.027 and $K_{D\ Sr}^{cpx/l} = 0.072$ to 0.095, from Hart and Brooks (1974),

Philpotts and Schnetzler (1970), and Shimizu (1974).  $K_{D\ Rb}^{ol/l} = 0.00018$

to 0.011 and $K_{D\ Sr}^{ol/l} = 0.00019$ to 0.019; high values from Arth (1976),

low values from Hart and Brooks (1974).  $K_{D\ Rb}^{opx/l} = 0.015$ to 0.29  and

$K_{D\ Sr}^{opx/l} = 0.010$ to 0.024, from Arth (1976).  $K_{D\ Rb}^{gnt/l} = 0.002$ to 0.037

and $K_{D\ Sr}^{gnt/l} = 0.007$ to 0.01, calculated from cpx/l $K_D$'s using gnt/cpx

values from Philpotts et al. (1972).

Rb/Sr AND Nd/Sm IN MELTS OF
GARNET PERIDOTITE AS A FUNCTION
OF PERCENT MELTING
SOLID CURVES – GNT : CPX = 1:1
DASHED CURVES – GNT : CPX = 3:1

PERCENT MELTING
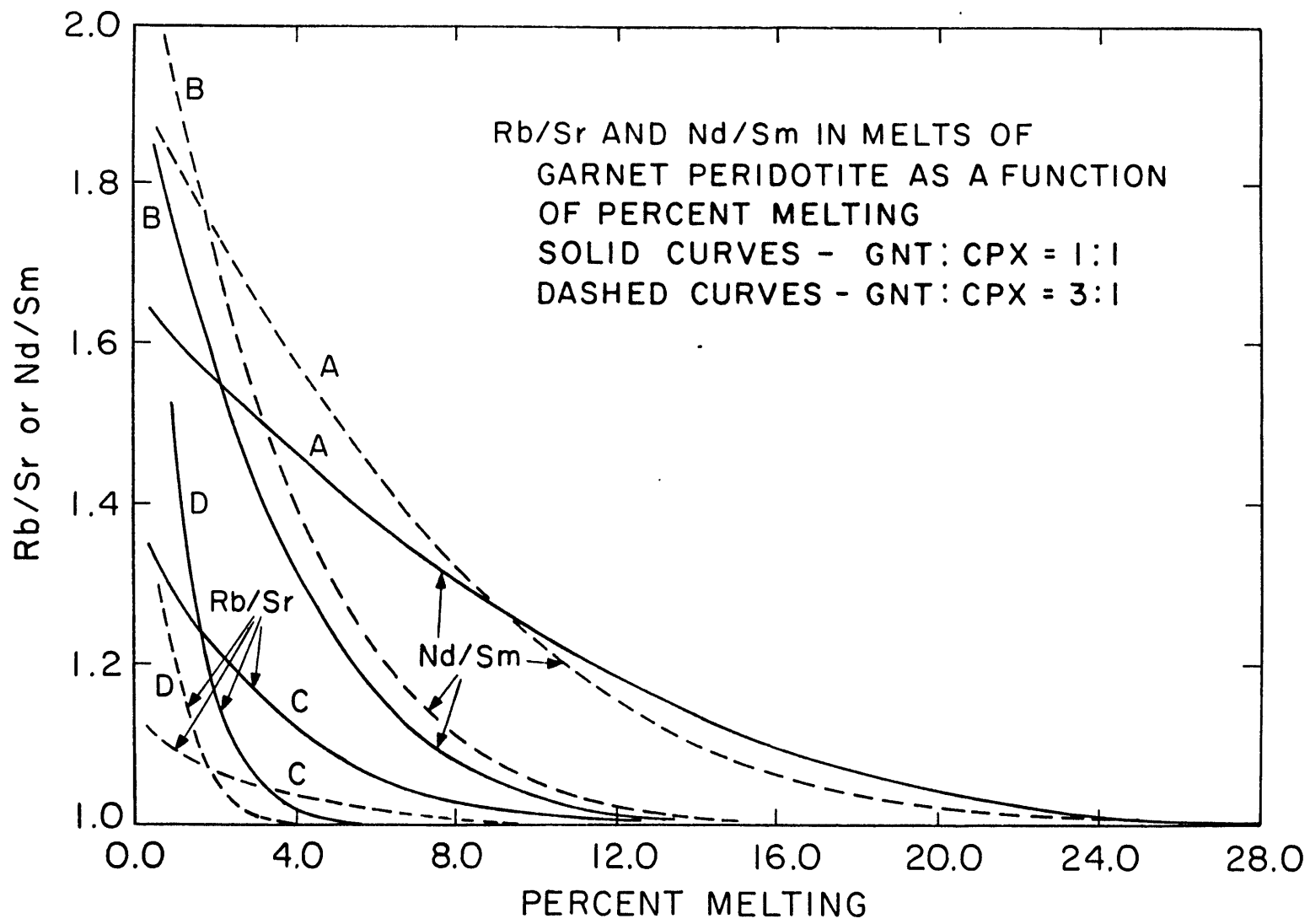
Figure 6

1977; Sigvaldason et al., 1974) to account for large isotopic variations in volcanic suites. Recently, Beswick (1978) has maintained that the arguments of Hofmann and Hart (1978), based on kinetic data, have no bearing on "isotopic diffusion" in systems where $\mu_{Sr}^{\alpha} = \mu_{Sr}^{\beta}$ but $\mu_{87Sr}^{\alpha} \neq \mu_{87Sr}^{\beta}$. In the limit of low concentrations, simple "random walk" diffusion theory predicts that isotopic exchange will occur at a rate close to that predicted from tracer diffusion experiments, even in the absence of "chemical" concentration gradients. Beswick's arguments thus involve a misconception of the diffusion process and do not affect the conclusions of Hofmann and Hart (1978).

Large variations in REE concentrations are also very difficult to reconcile with a homogeneous mantle model. The factor of 12 difference in La concentration from the most LREE-depleted to the most LREE-enriched basalt (Fig. 2) requires more than an order of magnitude difference in percent melting to produce these liquids from a homogeneous source. For example, if the picrite basalts were produced by, arbitrarily, 30% melting, the fissure tholeiites must result from less than 3% melting. Such low degrees of melting are believed to yield alkaline basalts rather than tholeiites (Green, 1971; Bysen and Kushiro, 1977; Frey et al., 1978). Similarly, an unrealistically large range in melting degree is required to account for the variation in $(La/Sm)_N$ from 0.3 in the picrite basalts to 1.25 in the fissure tholeiites. If the relative REE pattern in the picrite basalts is that of the mantle source, the degree of melting for the fissure tholeiites must be 1% (Schilling et al., 1978; and Fig. 8). We emphasize that the age relationships (from oldest to youngest: picrite basalts-olivine tholeiites-tholeiites) determined by Jakobsson et al.

(1978) are important in interpreting the wide range in REE abundances.
For example, if the picrite basalts were the youngest basalts, a
fractional melting or two-stage melting model would be applicable (e.g.,
Smewing and Potts, 1976), but such models are inconsistent with the time
sequence of these Reykjanes Peninsula basalts.

Another alternative to the heterogeneous mantle model is that
assimilation of altered crustal material might account for the isotopic
and abundance variations (O'Hara, 1977). As relatively little is known
about quantitative chemical changes in altered Icelandic crust, this
is a difficult process to evaluate. However, several lines of evidence
suggest that the crustal assimilation has not been a major influence.
First, the positive correlation of $(La/Sm)_N$, $^{143}Nd/^{144}Nd$ (Fig. 7) and
major element composition would be a most fortuitious result of a random
assimilation process. Second, there is no source of "anomalous"
Nd except seawater, and it has been shown (Hawkesworth et al., 1977;
DePaolo and Wasserburg, 1977; O'Nions et al., 1978) that Sr isotope
ratios will be much more severely affected by basalt-seawater inter-
actions than Nd. Third, Muehlenbachs et al. (1974; and personal
communication, 1978) have determined that the $\delta^{18}O$ values range from
5.1 to 5.6 for the Reykjanes Peninsula basalts studied. Though there
is a mild correlation of $\delta^{18}O$ with $^{143}Nd/^{144}Nd$ and La/Sm the normal
range of $\delta^{18}O$ in these basalts precludes a significant role for
assimilation of altered basaltic crust.

Therefore, we conclude that the source mantle for the Reykjanes
Peninsula is heterogeneous, at least with respect to $^{143}Nd/^{144}Nd$ and
relative REE abundances.

Figure 7.

Plot of $^{143}Nd/^{144}Nd$ vs. $(La/Sm)_N$ for Reykjanes Peninsula basalts.

Sample numbers given next to data boxes. Boxes represent estimated

2 σ errrors for analyses (see analytical section for discussion).
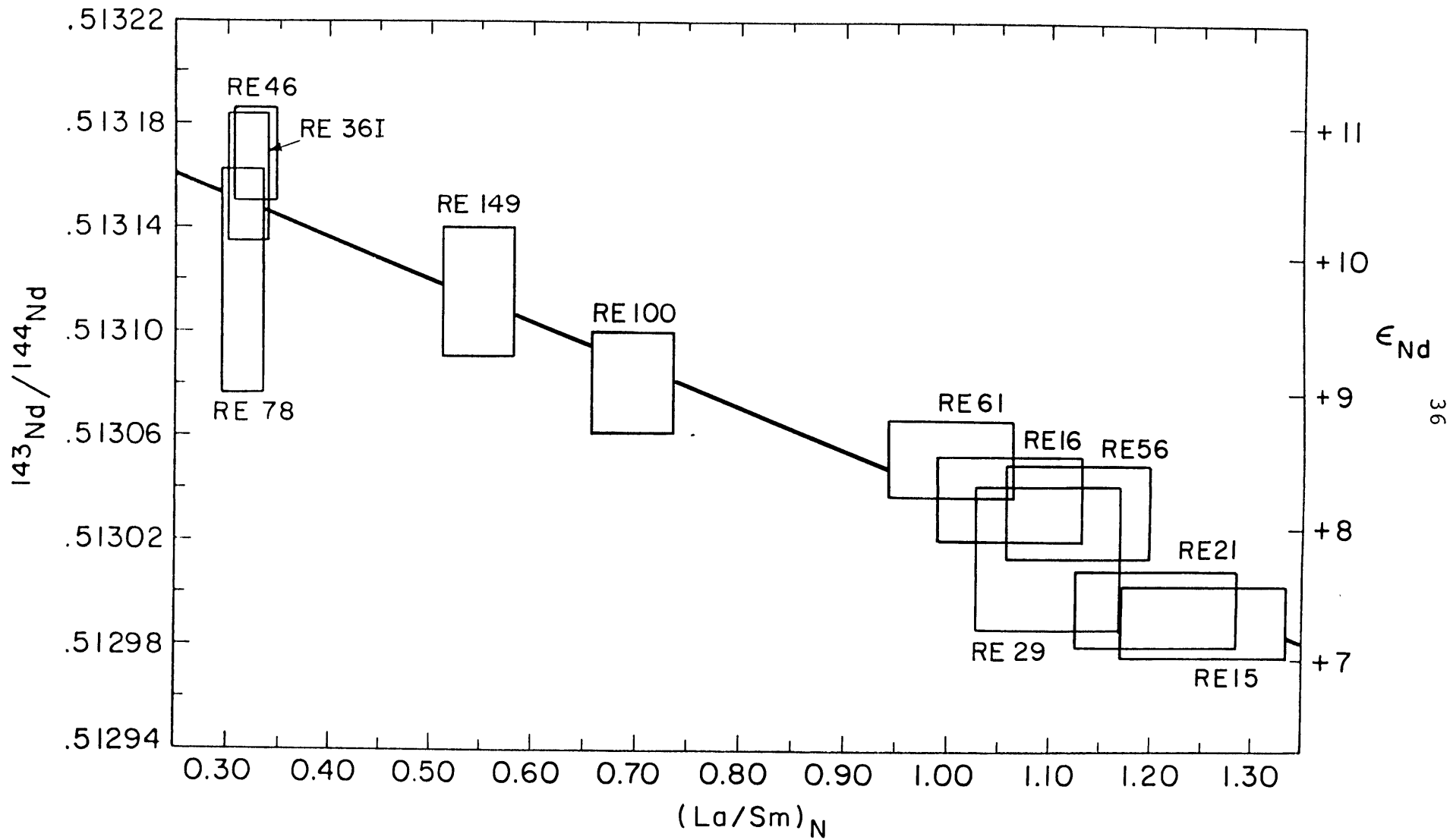
Figure 7

Having established the heterogeneity of the mantle beneath the Reykjanes Peninsula we must consider the hypothesis that the basalts result from the mixing of different components in the mantle as opposed to being derived from discrete mantle segments. Mixing processes may be evaluated by looking at the covariation of various chemical parameters, such as are shown in Figs. 7-10, where, in the simplest case of two-component mixing, linear arrays (mixing lines) would be expected for most of the cases shown (for a detailed discussion of the interpretation of mixing diagrams, see Langmuir et al. (1978).

Previous detailed studies of basalts from Iceland and the Reykjanes Ridge (O'Nions and Gronvold, 1973; O'Nions and Pankhurst, 1974; Schilling et al., 1978) have demonstrated that there exists a strong positive correlation between $^{87}Sr/^{86}Sr$ and $(La/Sm)_N$. Further, O'Nions et al. (1977) have demonstrated a negative correlation between $^{143}Nd/^{144}Nd$ and $^{87}Sr/^{86}Sr$ for Icelandic basalts. From this, one would expect to see a negative correlation of $^{143}Nd/^{144}Nd$ and $(La/Sm)_N$, which is shown to be the case on the Reykjanes Peninsula (Fig. 7). Because a mixing line is not linear on this diagram and there are few constraints on the low $^{143}Nd/^{144}Nd$, high $(La/Sm)_N$ end-member, we are unable to quantitatively test the mixing hypothesis on this diagram. With reference to this trend, one should note that the relative ages of the rocks increase from the tholeiites (e.g. RE 15) to picrites (e.g. RE 46). A plot which is very similar to the $(La/Sm)_N$ versus $^{143}Nd/^{144}Nd$, but which may have very different implications, is the Sm-Nd isochron diagram (Fig. 8). It can be seen in Fig. 8 that although the data do not fall on a line, they do form a "linear trend" which may be interpreted either as a mixing

Figure 8.

Sm—Nd isochron diagram. Sample numbers given next to data boxes, which represent 2 $\sigma$ confidence levels. $^{143}$Nd/$^{144}$Nd ratios are normalized to $^{146}$Nd/$^{144}$Nd = 0.72190.
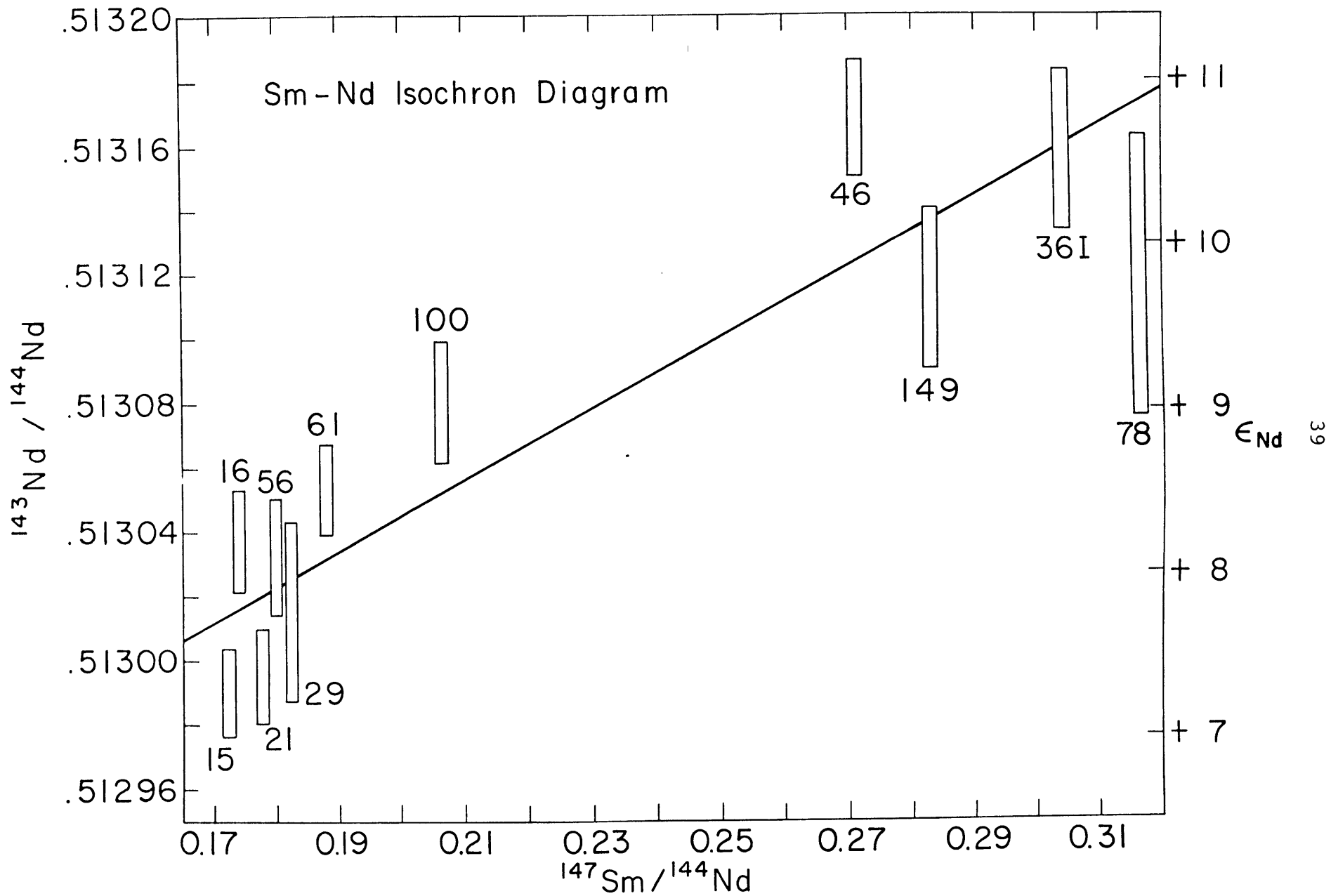
Figure 8

trend or an isochron.  The interpretation of the data on this diagram

will be dealt with in a subsequent section.

To test the feasibility of mixing for both the LREE's and HREE's,

$(La/Sm)_N$ is plotted versus $(Lu/Sm)_N$ in Fig. 9.  It can be seen that again

the data lie along a linear trend consistent with two-component mixing.

A convenient method of constraining the isotopic character of one

end member in a two-component mixture is to plot the isotopic ratio of

a given element versus the inverse concentration of that element.  In

Fig. 10, $^{143}Nd/^{144}Nd$ is plotted against 1/Nd.  The data do not define a

line, but they form a trend which can be extrapolated to 1/Nd = 0

("infinite enrichment" of Nd) thus constraining the $^{143}Nd/^{144}Nd$ ratio,

in the low $^{143}Nd/^{144}Nd$ end-member to greater than 0.5129 (note that,

in this diagram, the 1/Nd values may be changed considerably due to

accumulation or loss of olivine.  RE 46, for example, is the olivine-

free upper portion of a picritic flow (Jakobsson et al., 1978), thus

will have a lower 1/Nd value than the original liquid.  Re 15 is

essentially phenocryst-free, but even assuming a loss of 50% olivine,

would originally have had a 1/Nd less than 0.14.  RE 78, 149, and 361

contain on the order of 25% phenocryst olivine and may be displaced

to greater values of 1/Nd than the original liquids.)  Although this

value is not tightly constrained it is an important result because it

requires the mantle source for this end-member to have a long-term

history of relative LREE depletion compared to chondrites.  In other

words, we see no evidence of a "primitive" or "chondritic" mantle in

this environment.

Figure 9.

Plot of $(Lu/Sm)_N$ vs. $(La/Sm)_N$ for Reykjanes Peninsula basalts. Sample numbers and boxes as in previous figures.
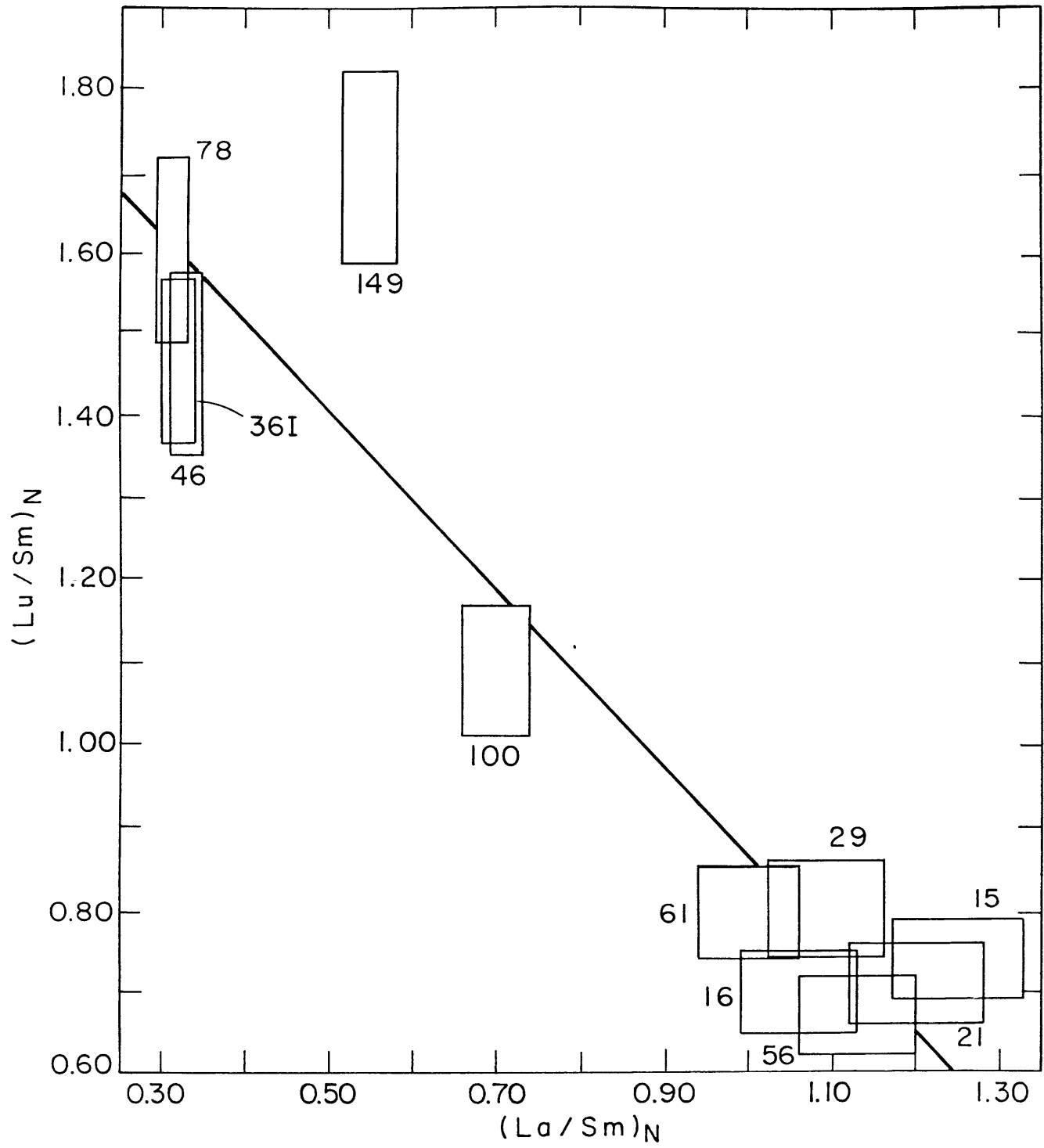
Figure 9

Figure 10.

Plot of $^{143}Nd/^{144}Nd$ vs. 1/Nd for Reykjanes Peninsula basalts. A line is fit to the data trend to show intercept of 0.51300 at 1/Nd = 0. As is discussed in the text, the Nd concentrations of many of the basalts may have been changed by fractionation or accumulation of olivine. Making liberal allowances for these processes, we may still constrain the $^{143}Nd/^{144}Nd$ value at 1/Nd = 0 to 0.5129. Taking the present-day $^{143}Nd/^{144}Nd$ value for Juvinas (Lugmair et al., 1975) as a "primordial" or "chondritic" value, this extrapolated value of $^{143}Nd/^{144}Nd$ at 1/Nd = 0 precludes the involvement of a "primordial" or "chondritic" mantle in the production of the Reykjanes Peninsula basalts.
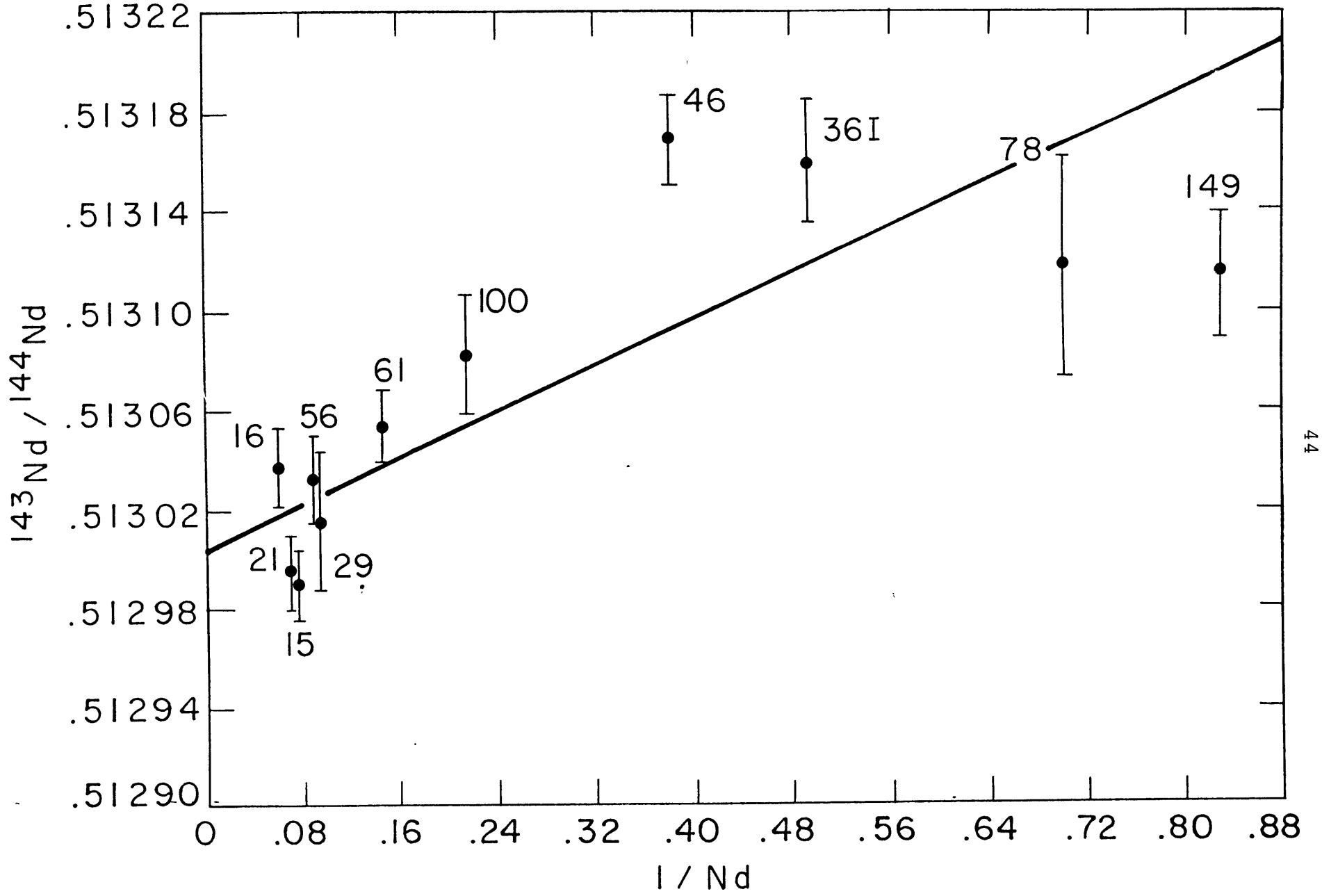
Figure 10

1.5  Conceptual models for a heterogeneous mantle beneath the Reykjanes

Peninsula

Before considering different mantle models, we summarize the

characteristics required by our data.  The model must explain: (1) major

and trace element abundance variations consistent with the time-

stratigraphic relationships of the Reykjanes Peninsula basalts; (2) the

variations in $^{143}Nd/^{144}Nd$ which are all greater than the chondritic

ratio; and (3) the variations in La/Sm which must be generated from time-

averaged mantle sources that are relatively depleted in LREE compared

to chondrites.  We also emphasize that the proposed models are applicable

only to the mantle beneath Iceland, because $^{87}Sr/^{86}Sr$ of Icelandic basalts

are distinct from $^{87}Sr/^{86}Sr$ ratios of Reykjanes Ridge basalts (Hart et

al., 1973; O'Nions and Gronvold, 1973; O'Nions and Pankhurst, 1974).

To facilitate evaluation of different mantle models, we propose the

scheme outlined in Fig. 11.  The arbitrary divisions of scale and age

in Fig. 11 are simplistic, but are probably as sophisticated as is

warranted by our understanding of the mantle.  Intuitively, the three

parameters in Fig. 11 are not independently variable and we propose two

"end-member" models, LOM and SYS (for explanation, see caption for Figs.

12 and 13), which we will evaluate in terms of the Reykjanes Peninsula

data.  Other permutations of the three parameters are possible, but we

consider that, within the framework of the SYS and LOM models, we can

demonstrate the ways in which different types of data can constrain the

different parameters.

In the SYS model, we envision a homogeneous mantle some few hundred

million years ago, with a chondrite-normalized REE pattern similar to

Figure 11.

Mantle model schematic depicts a simple three-fold scheme for
the classification of models of mantle heterogeneity. Two "end-member"
values are identified for each column: arrows indicate the range of
possibilities between end-members. (For the scale of heterogeneity,
30 km may be read as "larger than the scale of melting", and 10 m may
be read as "smaller than the scale of melting".) Circled letters,
one from each column, are used to refer to specific models (i.e., LOM,
SYS, etc.).

# MANTLE   MODEL SCHEMATIC

| SCALE OF HETEROGENEITY | AGE OF HETEROGENEITY | STATE OF MIXING |
|---|---|---|
| L — LARGE SCALE > 30 km ↕ S — SMALL SCALE ≤ 10 m | O — OLD ≫ 170 m.y. ↕ Y — YOUNG < 170 m.y. | M — MIXING OF MELTS ↕ S — SOLID STATE (MIXING OF MANTLES) |
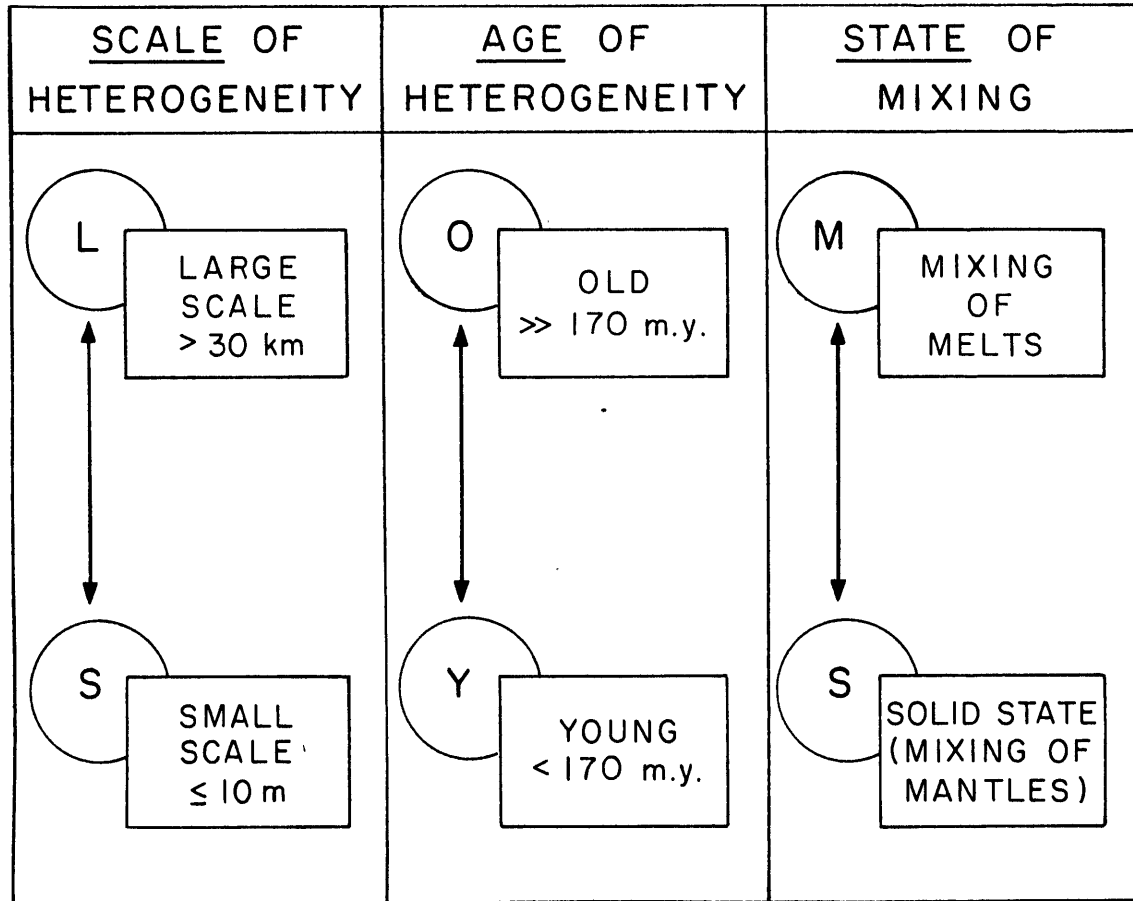
Figure 11

picrite RE 46, but with lower absolute REE abundances (Fig. 12a, a cartoon depicting the SYS model). About 170 m.y. ago ( the approximate time given by the correlation on the $^{147}Sm/^{144}Nd$ versus $^{143}Nd/^{144}Nd$ isochron diagram, Fig. 8), a liquid with highly fractionated REE abundances is produced by a small degree of melting of garnet peridotite. This liquid is distributed as veins or blobs throughout the "proto-Reykjanes Peninsula source mantle" (Fig. 12b). This proto-source mantle evolves as a subsolidus system until about 12, 000 years ago. Because of their different Sm/Nd ratios during this time period, the surrounding mantle develops much higher $^{143}Nd/^{144}Nd$ than the vein or blob material. Subsequently, melting of mantle segments with different "mantle : vein" or "mantle : blob" ratios is capable of producing the Reykjanes Peninsula basalts with their wide variations in LREE content and $^{143}ND/^{144}Nd$ ratios (Fig. 12c). Within the context of the SYS model we interpret the correlation on the Sm-Nd isochron diagram (Fig.8) as a "mantle isochron" ( or "errorchron"), documenting the "age" of the heterogeneity, rather than a mixing line. Although, in the SYS model, abundance variations in strongly incompatible elements must reflect mixing, major element abundances may not show mixing relationships because major element concentrations are controlled by residual mantle phases (Langmuir,1978).

In the LOM model, we envision two mantle portions ( Mantle A and B of Fig. 13a, a cartoon depicting the LOM model) which have existed as separate mantle systems for a long period of time ( >> 170 m.y.). Mantle A has a relative REE abundances and $^{143}Nd/^{144}Nd$ similar to picrite RE 46 and Mantle B has lower $^{143}Nd/^{144}Nd$ ( ~0.5129) and higher $(La/Sm)_N$ $(0.3 < (La/Sm)_N <1)$, typical of an "ocean-island" type mantle. About 12,000 years ago, a picrite basalt melt is produced in Mantle A, by a relatively

Figure 12.

SYS mantle model cartoon (see text for discussion). (a) Depicts a homogeneous mantle which has existed for an indefinite amount of time prior to 170 m.y. ago. (b) Depicts the formation of heterogeneities in the "proto-Reykjanes Peninsula source mantle" by invasion of a LREE-enriched phase produced in equilibrium with garnet. The LREE-enriched phase is pictured as either "blobs" or "veins" within the source mantle. The system then undergoes sub-solidus, closed-system evolution until, (c), about 12,000 years ago, when melting ensues. Different mantle segments, A, B, and C, with variable "mantle/vein" or "mantle/blob" ratios, melt to produce the Reykjanes Peninsula basalts.

SYS MANTLE MODEL

a.

HOMOGENEOUS
MANTLE

t > 170 m.y.

b.

PROTO-R.P. SOURCE MANTLE

LREE ENRICHED PHASE

t ≈ 170 m.y.

c.

C

B

A

CRUST
AND
LITHOSPHERE

SPINEL
LHERZOLITE

GARNET
LHERZOLITE

FROM 12,000 yrs. ago
to PRESENT

Figure 12

50
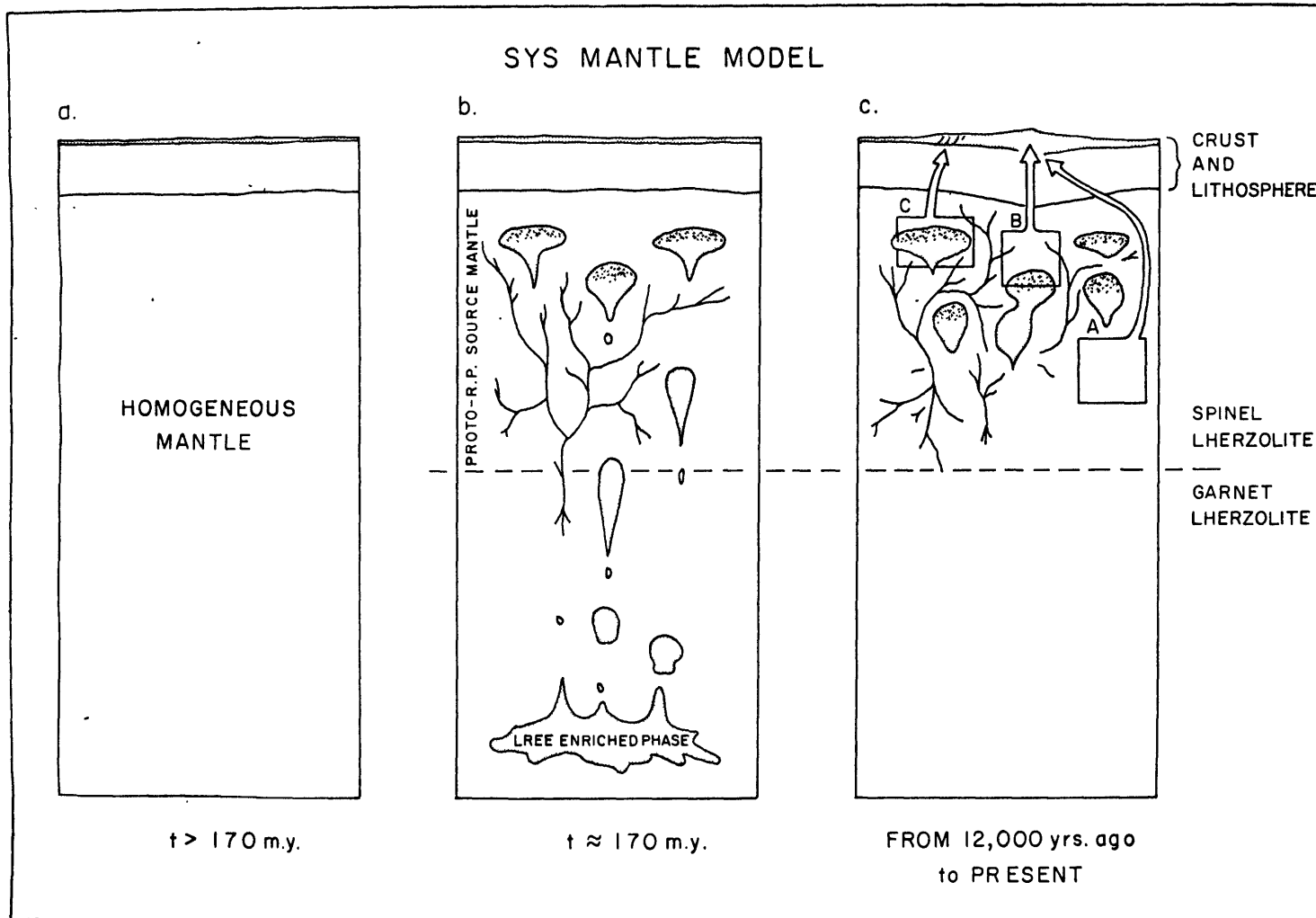
large degree of melting, while a LREE-enriched fluid, resulting from a small degree of melting in equilibrium with garnet peridotite, is produced in Mantle B (Fig. 13b). The LREE-enriched fluid from Mantle B is then "leaked" into the picrite basalt melt at a relatively constant rate, so that successive melts erupted at the surface show effects of increasing "contamination" of the primary picrite basalt melt with the LREE-enriched fluid (Fig. 13b). REE modeling calculations show that it is possible to mix a liquid, produced by 1-2% melting of garnet peridotite, with picrite RE 46, to obtain the relative REE abundances in the olivine and fissure tholeiites. However, detailed quantitative modeling of REE is not justified until further evaluation of the role of fractional crystallization is completed. Within the context of the LOM model, abundance variations of all elements must show mixing relationships.

In the preceding discussion we qualitatively demonstrated that SYS and LOM models are capable of producing the isotopic ratio and REE abundance variations of the Reykjanes Peninsula basalts. However, one major point makes the SYS model seem unlikely. Within the SYS scheme, it would be extremely fortuitious to find, as in the case on the Reykjanes Peninsula, that successively younger lavas have successively lower $^{143}Nd/^{144}Nd$ and higher La/Sm. In fact, we would expect random correlations of geochemical parameters with time, or, possibly, increasing $^{143}Nd/^{144}Nd$ and decreasing La/Sm with time because the LREE-enriched mantle portions form the low-melting component. This objection, based on time-stratigraphic relationships of the Reykjanes Peninsula basalts, applies equally to any mantle model involving mixing in the solid state (e.g., LOS, SOS, etc.). Furthermore, models with small scale heterogeneity, that is,

Figure 13.

    LOM mantle model cartoon (see text for discussion). (a) Depicts

a long-term mantle heterogeneity, with characteristics of Mantle A and

B outlined in the diagram. $\varepsilon_{Nd}$ values are deviations, in parts $10^4$,

from the "chondrite evolution line" defined by primordial Nd in Juvinas

(Lugmair, et. al., 1975). The two-box model is intended to be a

simplification of what must certainly be a more complex situation.

(b) About 12,000 years ago, a LREE-enriched phase is produced in Mantle

B, in equilibrium with garnet and is "leaked" into the "primary" picrite

basalt melt in Mantle A, at a more-or-less constant rate. Successive

eruptions from Mantle A will show increasing effects of contamination

by the LREE-enriched phase.

# LOM MODEL

a. FROM >> 170 my to 12,000 yrs. ago

b. FROM 12,000 yrs. ago to PRESENT
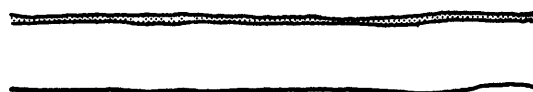
MANTLE A
$(La/Sm)_N \sim 0.3$
$\epsilon_{Nd} \sim +12$

CLOSED SYSTEM
EVOLUTION

MANTLE B
$0.3 < (La/Sm)_N < 1.0$
$\epsilon_{Nd} \sim +7$

CRUST AND
LITHOSPHERE

MANTLE
A

PICRITE BASALT MELT

SPINEL
LHERZOLITE

GARNET
LHERZOLITE

MANTLE
B

LREE ENRICHED PHASE

Figure 13

smaller than the scale of melting, necessarily imply mixing in the solid state, and therefore, are subject to the same objection. Thus, we consider that the LOM model is the most reasonable model which is consistent with the Reykjanes Peninsula data.

In Fig. 13, the heterogeneity in the LOM model is depicted as being vertical within the mantle. This is in contrast to the LOM (or LOS) model of lateral heterogeneity proposed by Schilling (1973, 1978) where only one source, the Primordial Hot Mantle Plume, is available beneath Iceland. We depict the heterogeneity <u>within</u> the mantle beneath Iceland (i.e., within the Primordial Hot Mantle Plume) as being vertical, because of the need to produce a LREE-enriched liquid, and the convenience of doing this in the garnet stability field. However, the Sr isotope data which show steep gradients from the Reykjanes Peninsula to Reykjanes Ridge (Hart et al., 1973; White et al., 1976; O'Nions and Gronvold, 1973; O'Nions and Pankhurst, 1974; O'Nions et al., 1976) suggest that there are also lateral chemical gradients in the mantle beneath Iceland and the Reykjanes Ridge. Therefore, the main features of our model, which contrasts with Schilling's Mantle Plume, are: (1) we see no evidence for a "primordial" or "chondritic" mantle beneath the Reykjanes Peninsula (Schilling et al., 1978); (2) we find the mantle beneath Iceland, within the region of Schilling's plume, to be markedly heterogeneous; and (3) we have evidence that at least some mantle segments beneath Iceland have $(La/Sm)_N$ and $^{143}Nd/^{144}Nd$ ratios similar to the mantle beneath "normal" mid-ocean ridges; however, $^{87}Sr/^{86}Sr$ ratios are considerably higher in the mantle source of the Reykjanes Peninsula basalts.

## 1.6 Conclusions

Reykjanes Peninsula basalts are derived from a source mantle which is heterogeneous with respect to relative REE concentrations and $^{143}Nd/^{144}Nd$. Furthermore, all portions of the source mantle have been depleted in light REE relative to chondrites for a long period of time. The range of Reykjanes Peninsula lavas from picrites to tholeiites results from mixing of magmas produced by different degrees of melting in different parts of the heterogeneous source mantle.

In the Reykjanes Peninsula basalts, $^{87}Sr/^{86}Sr$ ratios, which are usually considered as reliable indicators of source heterogeneity, are much less variable than $^{143}Nd/^{144}Nd$. If decoupling of Sm-Nd and Rb-Sr systems within the mantle commonly occurs, many conclusions about mantle heterogeneity based on Sr isotope data will have to be reassessed.

Although we present a model of vertical heterogeneity in the mantle beneath the Reykjanes Peninsula, the high $^{87}Sr/^{86}Sr$ ratios ($\geq 0.7031$) in Reykjanes Peninsula basalts precludes involvement of a "normal" mid-ocean ridge mantle source. Thus, there are vertical and lateral chemical gradients in the mantle beneath Iceland and the Reykjanes Ridge.

CHAPTER 2

Nd AND Sr ISOTOPIC VARIATIONS

IN CENTRAL EUROPEAN VOLCANICS

## 2.1 Introduction

Nd and Sr isotopic compositions have been measured in alkalic volcanics associated with Tertiary-Quaternary rifting in central Europe. Samples were chosen so as to minimize the possibility of crustal contamination in their genesis, and enable the investigation of changes in mantle chemistry which might be associated with the evolution of rifting in a continental setting. Volcanic centers from within zones of rifting are also compared to off-rift centers, to observe possible tectonic influence on source composition.

The results presented here represent preliminary findings of a continuing investigation of central European volcanics by the author and Hubert Staudigel. Major conclusions are not possible on the basis of these data, and their inclusion here is so that all work pursued by the author at M. I. T. is available to interested parties.

## 2.2 Geologic Setting

Samples analysed in this study come predominantly from the East Eifel volcanic field (see Figure 2-1). One sample comes from the West Eifel and four represent Tertiary nodule bearing localities from central Europe, which became active during the early stages of rifting in the Rhine Graben.

The Eifel province is within the western portion of the Rheinisches Schiefergebirge (RS) which comprises a 4-10 km thick sequence of limestones, graywackes, slates and quartzites of Devonian to lower Carboniferous age. The RS represents a portion of the European Variscan mountain range, which is correlated with the Appalachian mountains in the eastern United States, and was folded and metamorphosed during the Hercynian orogeny (for summary, see Illies et al. 1979). The region has been subjected to several phases of uplift, erosion and subsidence since the Permian, with the most recent phase starting in the Pliocene.

The tectonic setting of the RS, which extends NE-SW across the region between the Rhine Graben and the Lower Rhine Embayment, has been discussed by Illies et al. (1970). The Rhine Graben developed in two tectonic stages (Illies, 1978): (1) an extensional event between 48-18 m. y. ago resulting in the main development of the Rhine Graben, and accompanied by extensive nodule-bearing, alkalic volcanics throughout central Europe and, (2) a reactivation of rifting about 4 m. y. ago, with a rotated stress field, resulting in uplift of the Rhenish Shield and formation of the Lower Rhine Embayment. Volcanism associated with this second stage of rifting is restricted to the Eifel province.

As seen in Figure 2-1, the East Eifel volcanic field is located in the central portion of the Rhenish Shield along the trend of the Lower

Figure 2-1 Tectonic map of the Alpine foreland of Western Europe. Rifting has occurred along the Rhine Graben, south of Frankfurt and the Lower Rhine Embayment, north of Bonn. The East Eifel volcanic field (EE) is located ∿70 km southwest of Bonn. The connection between the Lower Rhine Embayment and the Rhine Graben is evidenced by the path of earthquake epicenters which extends across the Rhenish shield, through the East Eifel province. (Figure is taken from Illies et al. (1979).
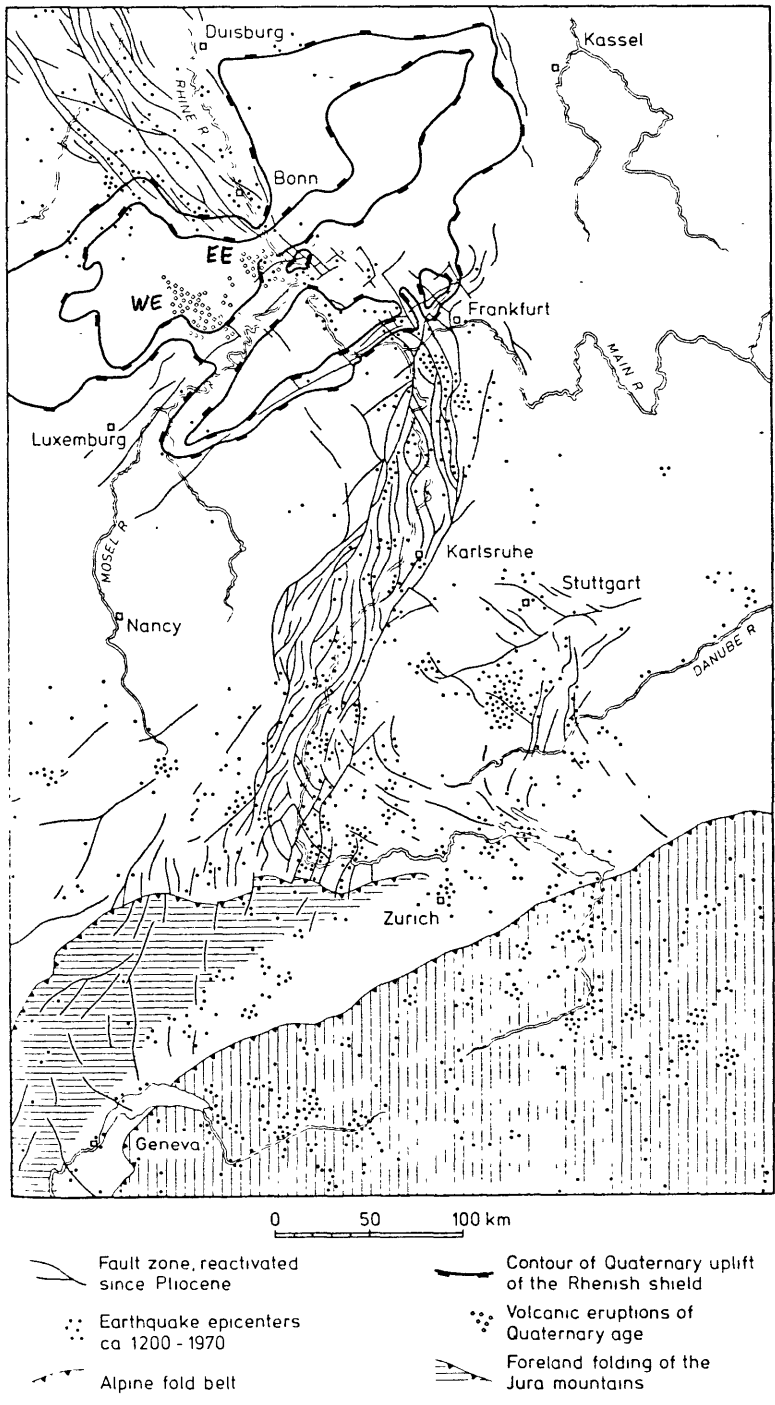
Figure 2-1

Rhine Embayment toward the Rhine Graben. Because the Rhenish Shield has acted as a competent block during rifting, no faulting has occurred in the vicinity of the East Eifel. However the sub-surface presence of the Lower Rhine Embayment is evidenced by the line of earthquake epicenters which crosses the East Eifel volcanic field (see Figure 2-1; Illies and Greiner, 1979; Illies et al, 1979). The West Eifel volcanic field is located significantly to the west of the major axis of rifting and is situated in a seismically quiet zone.

Recent volcanic activity in the Eifel began about 600,000 yrs. ago and continued until ∿8000 yrs. ago (Frechen and Lippolt, 1965; Windheuser, 1977; Lorenz and Büchel, 1978; Mertes and Schmincke 1980). Major chemical differences are observed between volcanics of the East and West Eifel (Schmincke et al. 1979). While the East Eifel is predominantly characterized by basanites, the West Eifel has only minor basanites and is mainly characterized by nephelinites, melilite nephelinites, and leucitites. Lavas from both volcanic fields are slightly potassic, with $K_2O/Na_2O \sim 1$ in the west and $K_2O/Na_2O > 1$ in the east. Ultramafic nodules occur throughout the Eifel but are more common in the west.

2.3  Results

Nd and Sr isotopic compositions have been measured in five Quaternary and two Tertiary samples from the Eifel province (Table 2-1). All Quaternary samples represent undersaturated, "primitive" compositions and as such, are considered to have experienced little interaction with continental crust. The two Tertiary samples are alkali basalts and have been collected from eroded volcanic "necks" in the East Eifel volcanic field. Eifel sample localities are shown in Figure 2-2 and are described in Table 2-1. Four ultramafic nodule-bearing, Tertiary volcanic rocks from central Europe have also been analyzed, and the data and sample localities are listed in Table 2-1.

Figure 2-3 is a plot of $^{143}Nd/^{144}Nd$ versus $^{87}Sr/^{86}Sr$ for all samples analyzed. A negative correlation between the two parameters is evident, and comparison to Figure 1-5 shows that all samples lie within the field defined by young oceanic volcanic rocks. This may be taken as evidence for the primary, "uncontaminated" nature of these volcanic rocks, but, as will be shown in Chapter 4, this is not necessarily the case. Only one of the samples analysed to date is from the West Eifel field, and this falls within the range defined by the four Quaternary East Eifel samples. However, preliminary Sr data (Staudigel, unpublished data) for additional West Eifel samples suggest that a lower range of $^{87}Sr/^{86}Sr$ may be typical.

$^{143}Nd/^{144}Nd$ and $^{87}Sr/^{86}Sr$, respectively, are plotted versus eruption ages (Schmincke, pers. comm.) in Figures 2-4a and 2-4b. Clear differences in both parameters are seen to exist between the Tertiary and Quaternary volcanics independent of locality. Tertiary samples have $^{87}Sr/^{86}Sr$

ratios in the range of 0.7033-0.7044 and $^{143}Nd/^{144}Nd$ ratios from

0.5128-0.5129, while Quaternary samples display ranges of 0.7044-0.7047

and 0.5126-0.5127 for $^{87}Sr/^{86}Sr$ and $^{143}Nd/^{144}Nd$ respectively. Nd and

Sr isotopic compositions of the Quaternary samples are within the pre-

dicted range of unfractionated, bulk-earth values (see Figures 3-6 and

3-7) while the Tertiary compositions are within a range more typical of

young oceanic volcanic rocks (see Figure 2-4b).

Table 2-1    Nd and Sr isotopic compositions[1] and Rb and Sr concentrations[2] from Central German volcanic provinces

| Sample # | Locality | Rock Type | Age (millions of years) | Rb | Sr | $^{87}Sr/^{86}Sr$ | $^{143}Nd/^{144}Nd$ |
|---|---|---|---|---|---|---|---|
| NM 41 | Rothenberg (E) | basanite | 0.3 | 81.4 | 896 | 0.70464±6 | 0.51266±2 |
| E 292 | Hochstein (E) | nephelinite | 0.3 | 102.4 | 1578 | 0.70466±4 | 0.51270±2 |
| E 306 | Perler Kopf (E) | leucitite | 0.43 | 164 | 1816 | 0.70466±6 | 0.51263±3 |
| E 308 | Herchenberg (E) | mel. nephelinite | 0.48 | 79.1 | 1154 | 0.70436±5 | 0.51264±2 |
| E 382 | Larchenhof (E) | alkali basalt | 35.1 | 27.3 | 927 | 0.70342±3 | 0.51287±2 |
| E 392 | Hohe Buche (E) | basanite | 0.37 | 81.2 | 768 | 0.70467±4 | 0.51269±2 |
| E 393 | Steinbergs Kopf (E) | alkali basalt | 24 | 39.1 | 782 | 0.70409±5 | 0.51279±3 |
| E 358 | Hohenfels(W) | mel.nephelinite | ∿ 0.8 | 67.6 | 635 | 0.70443±3 | 0.51265±2 |
| Rhö 11a | Suhl/Rhon | basanite | Tert. | 67.4 | 790 | 0.70332±7 | 0.512899±2 |
| HBG 2a | Zeilberg Heldburg dike/swarm | basanite | Tert. | 66.6 | 1345 | 0.70437±4 | 0.512801±3 |
| XKU 190 | Hochbron/URACN | ol-melilitite | Tert. | 47.0 | 1250 | 0.70402±4 | 0.512831±3 |
| NHS 9 | Westberg Lower Hessia depression | ol-melilitite | Tert. | 32.6 | 2008 | 0.70360±6 | 0.512824±4 |

1.  Errors are in last significant figures and represent $2\sigma_m$ confidence level. $^{143}Nd/^{144}Nd$ normalized to $^{146}Nd/^{144}Nd$ = 0.72190. $^{87}Sr/^{86}Sr$ relative to 0.70800 for E & A SrCO$_3$, and normalized to $^{86}Sr/^{88}Sr$ = 0.11940.

2.  Rb and Sr concentrations in ppm.

3.  (E) indicates East Eifel volcanic province.  (W) indicates West Eifel volcanic province.

Figure 2-2  Sample locations for Tertiary and Qua-

ternary volcanics in the Eifel Mts., Rhenish Shield,

W. Germany.
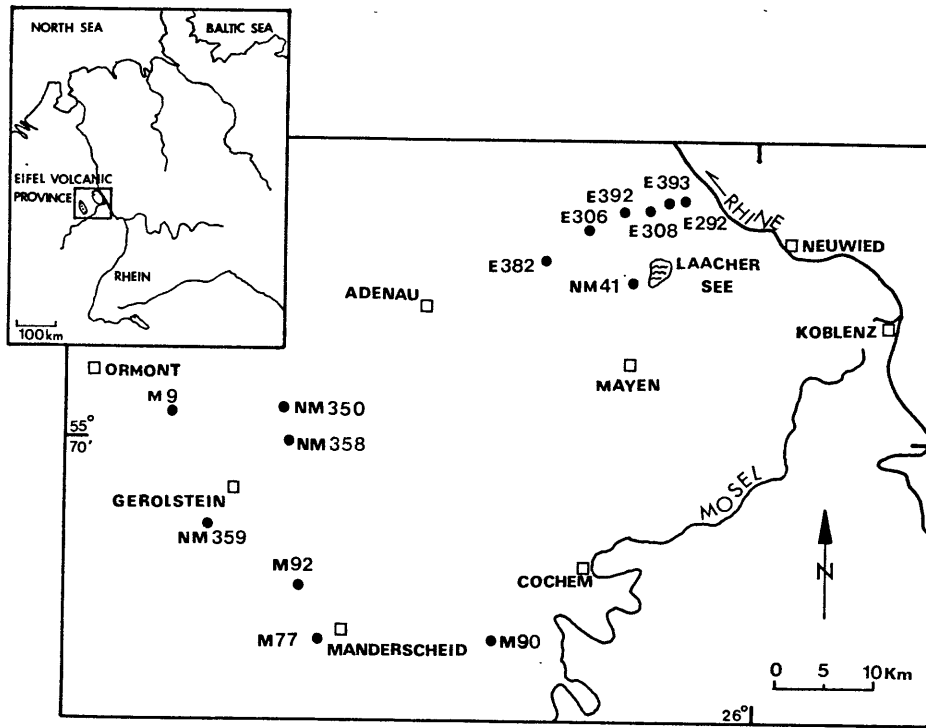
Figure 2-2

Figure 2-3  $^{143}$Nd /$^{144}$Nd versus $^{87}$Sr/$^{86}$Sr for alkalic

volcanic rocks from central Europe.  Tertiary and

Quaternary rocks are indicated with brackets.
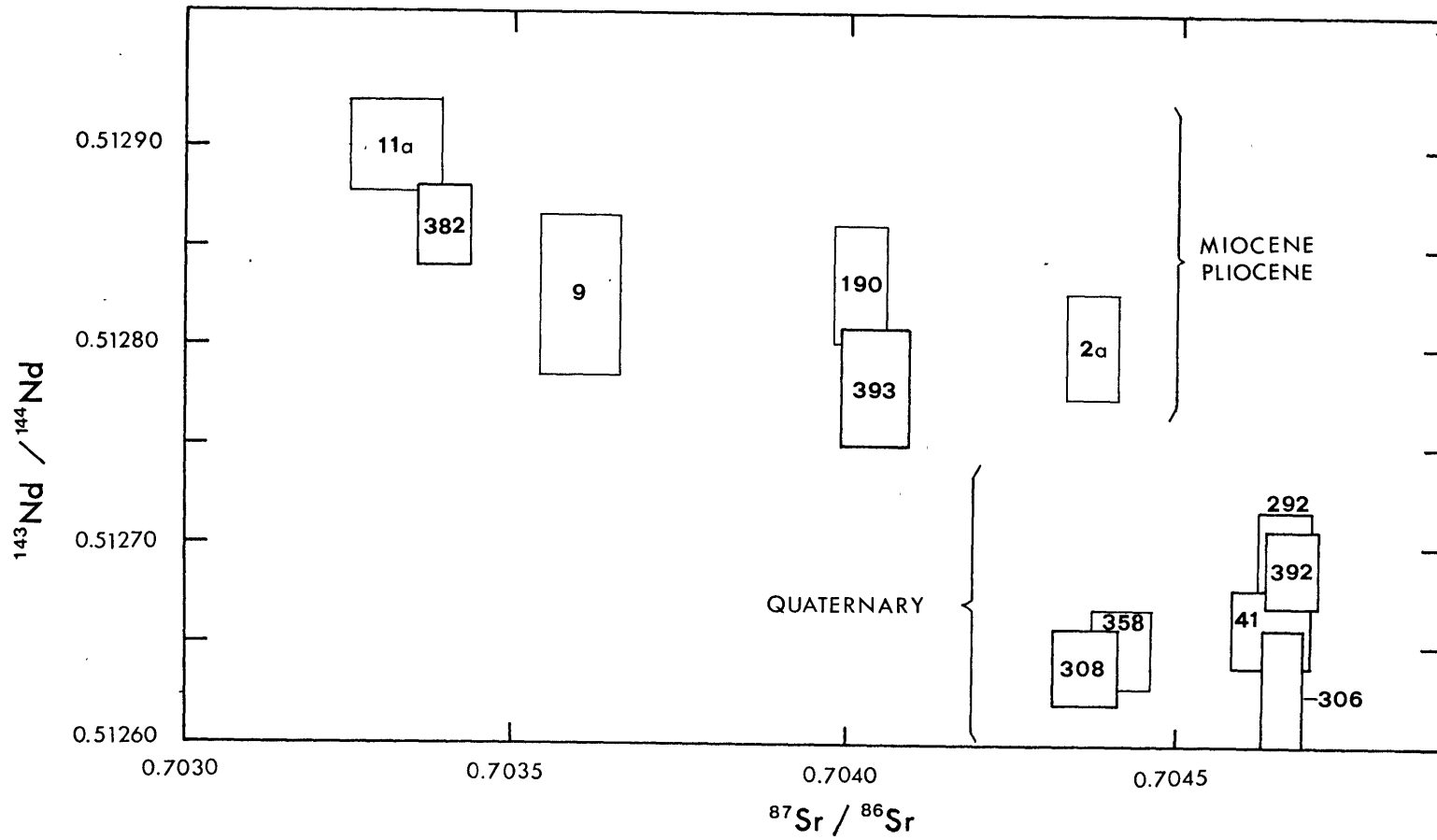
Figure 2-3

Figure 2-4a $^{143}$Nd/$^{144}$Nd versus eruption age for vol-

canics from the East Eifel and West Eifel volcanic
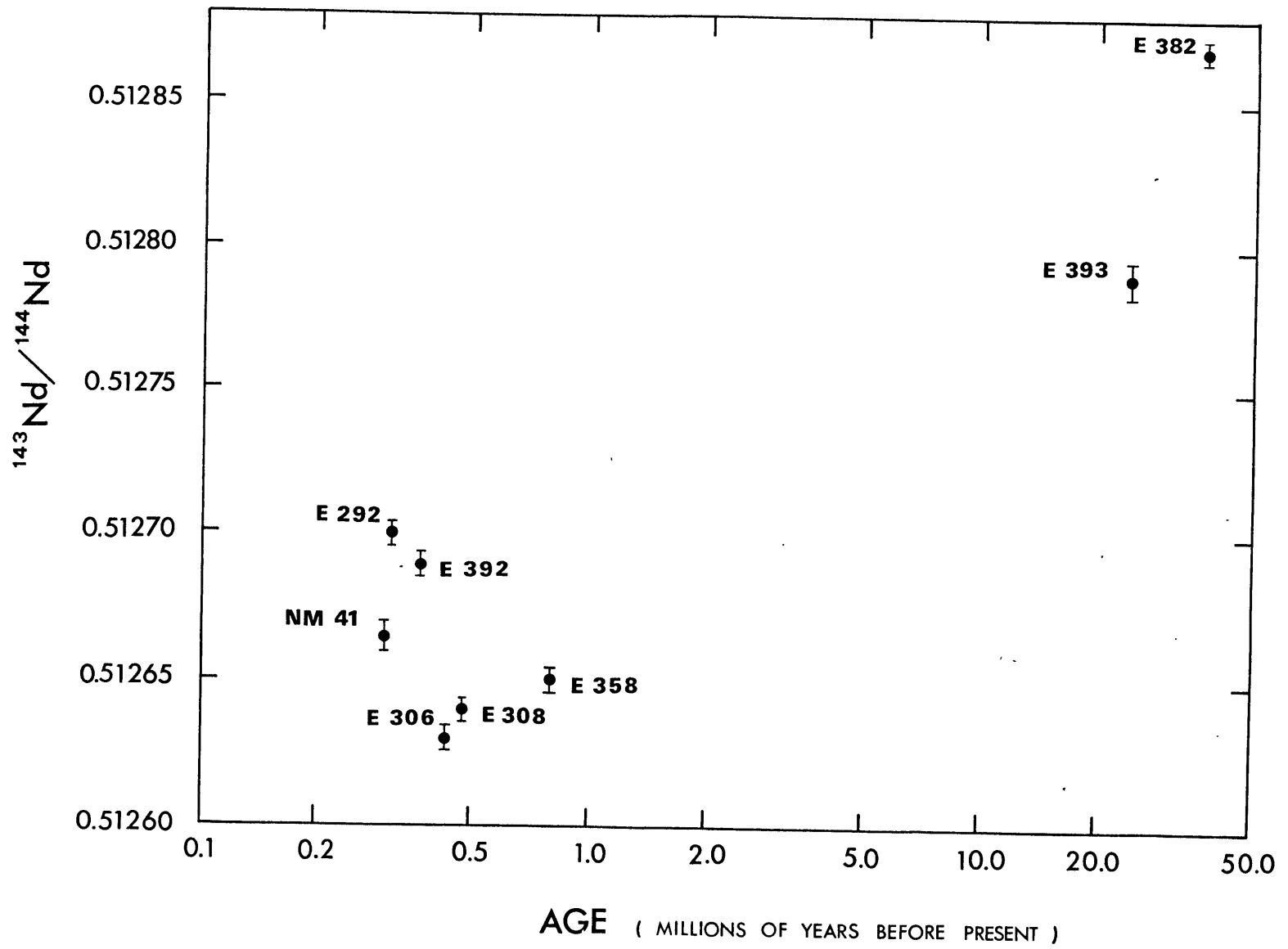
fields.

Figure 2-4a

Figure 2-4b $^{87}Sr/^{86}Sr$ versus eruption age for vol-
canics from the East Eifel and West Eifel volcanic
fields.
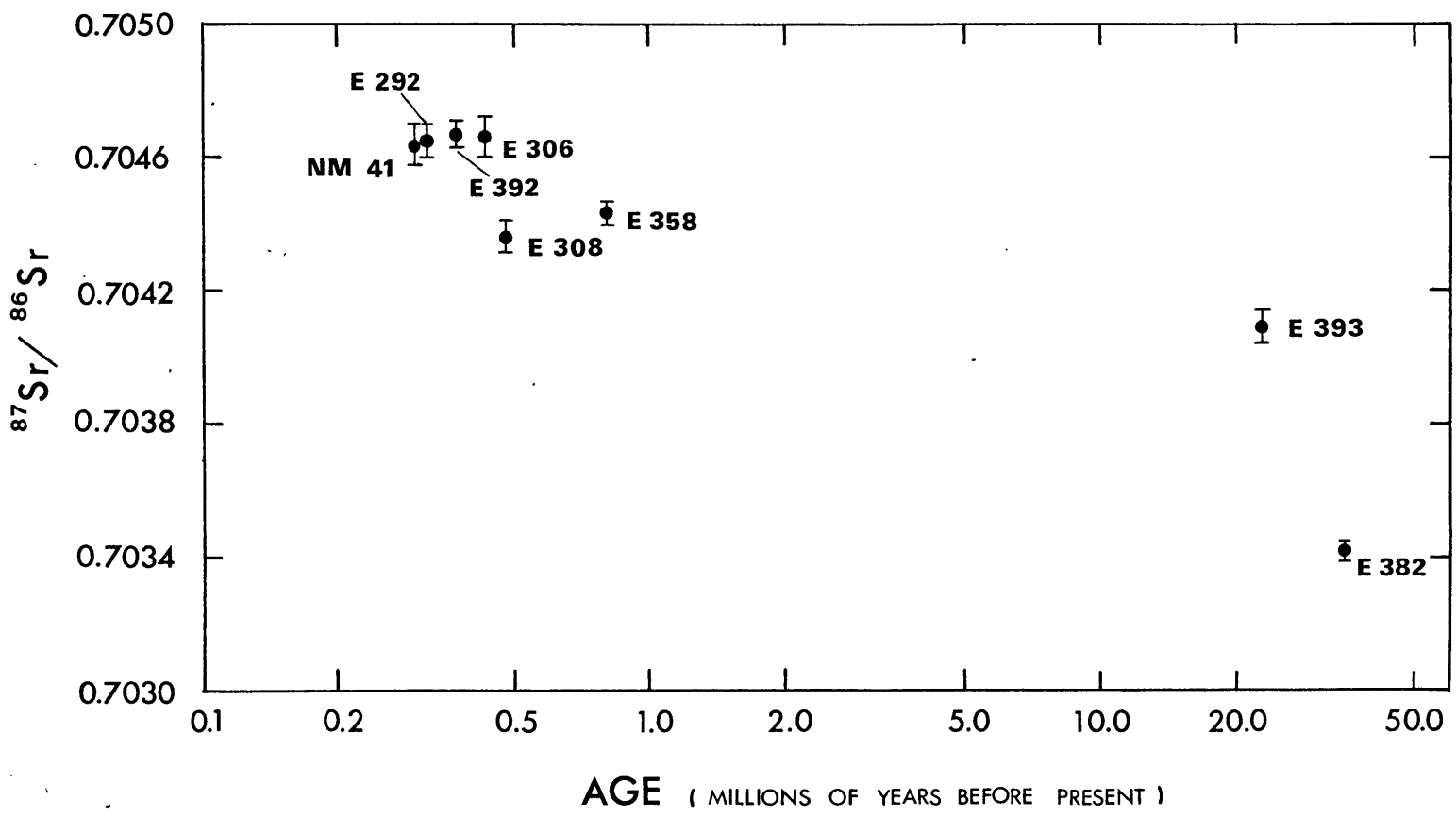
Figure 2-4b

## 2.4 Discussion

One might predict, intuitively, that with the progressive evolution of an intracontinental rift system, the sub-rift mantle would evolve toward a more "oceanic" character. In the context of this study, oceanic character would indicate a mantle generally more depleted in LIL elements with consequently higher $^{143}Nd/^{144}Nd$ and lower $^{87}Sr/^{86}Sr$ ratios. That the opposite is observed in central Europe is somewhat of an enigma, and forces one to consider the possibility that the younger lavas are contaminated by a crustal component. Although magma compositions similar to the samples which were analyzed are not typically assumed to reside in crustal magma chambers, this possibility cannot be eliminated. In Chapter 4, it is demonstrated that mantle- and crustal-derived melts may mix, and result in the displacement of the mantle melt composition toward bulk-earth values for $^{143}Nd/^{144}Nd$ and $^{87}Sr/^{86}Sr$. This type of mixing is capable of explaining the isotopic composition of the Quaternary volcanics relative to those erupted during the Tertiary without resorting to temporal or spatial heterogeneities in the mantle. It is considered, however, that the small range in $^{143}Nd/^{144}Nd$ and $^{87}Sr/^{86}Sr$ observed for the Quaternary, East Eifel volcanics, which are erupted from different volcanic centers, makes a random assimilation process seem unlikely. The author and H. Staudigel are currently involved in extending this project to include known ultramatic nodule-bearing flows from the West Eifel, in an effort to further evaluate the possibility for crustal contamination of the lavas. As mentioned previously, preliminary results do indicate that lower $^{87}Sr/^{86}Sr$ may be typical of the West Eifel.

If one assumes that the volcanics do represent uncontaminated mantle compositions, two possible scenarios would explain the observed

isotopic variations: (1) the mantle beneath central Europe has changed in composition since the Tertiary, possibly by the upwelling of deeper, less "depleted", mantle in a process related to the extensional tectonics observed in the crust, or; (2) the mantle beneath central Europe is vertically heterogenous with respect to $^{143}Nd/^{144}Nd$ and $^{87}Sr/^{86}Sr$, and magma generation during the Tertiary and Quaternary tapped different segments of this mantle. Resolution of these problems is not possible at this stage and must await the outcome of the further investigations.

A range of REE abundances measured in Quaternary and Tertiary volcanics from the East Eifel (Duda and Schmincke, unpublished data) is shown in Figure 2-5. These rocks are very enriched in LREE's but are constrained by $^{143}Nd/^{144}Nd$ ratios to be derived from mantle with time-integrated Sm/Nd ratios equal to or greater than average chondrite values. In the most favorable case, it is shown that $\sim$1% fractional melting of garnet lherzolite with chondritic Sm/Nd will produce the observed LREE enrichments. For the undersaturated, alkaline compositions of the East Eifel volcanics, 1% melting may be a reasonable figure. However, the situation is similar to that observed for the Reykjanes Peninsula tholeiites, and it may be that these rocks are derived by a magma generation process similar to that described in Chapter 1.

Figure 2-5  REE abundances in East Eifel volcanics

(Data from Duda and Schmincke, unpublished data).

A 1% melt of a garnet lherzolite source is shown to

approximate LREE enrichment in Eifel samples (frac-

tional melting equations of Shaw, 1970).
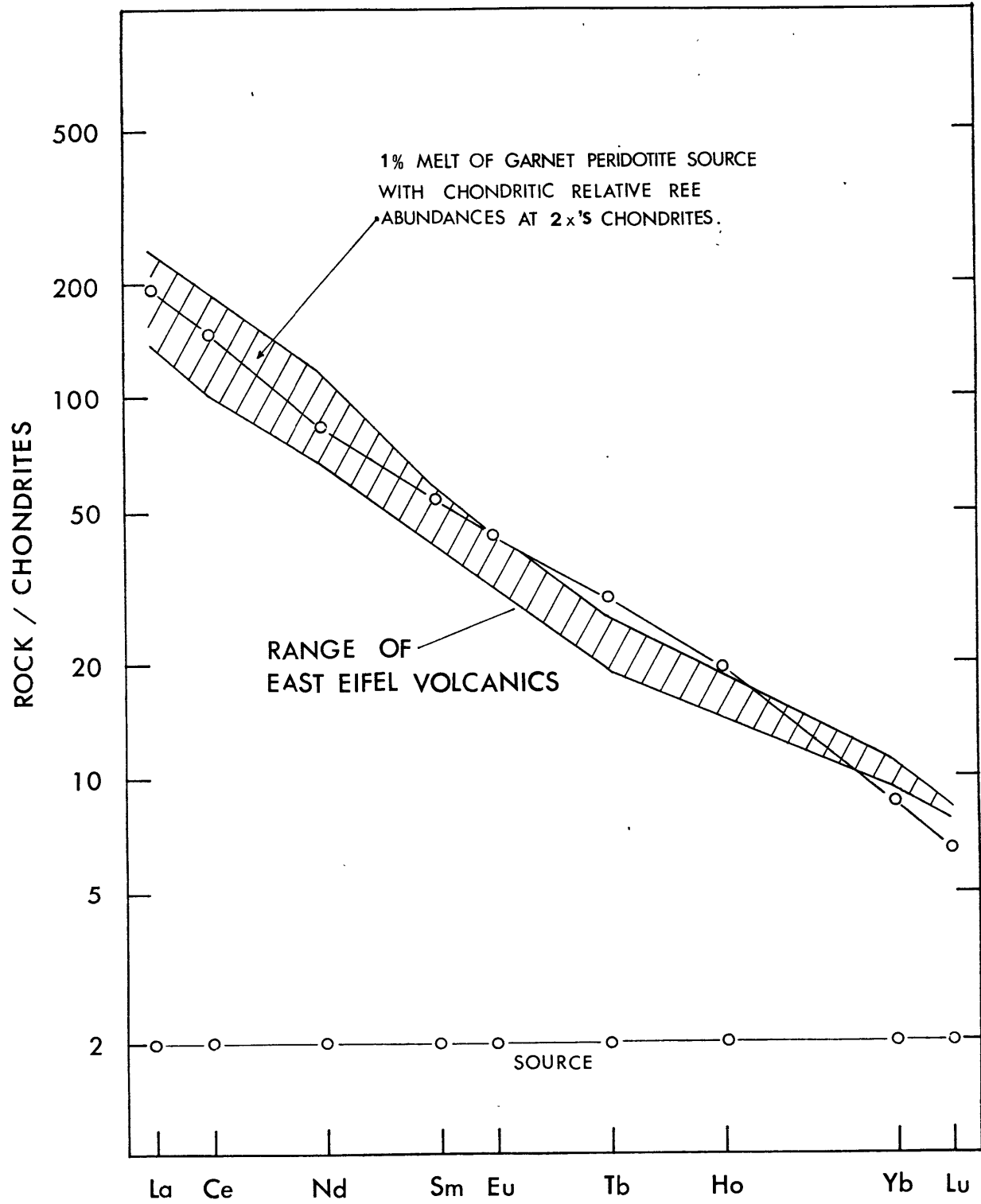
Figure 2-5

## 2.5   Conclusions and summary of chapter 2

Nd and Sr isotope ratios for central European volcanics fall within the range observed for young oceanic basalts. The Quaternary volcanics of the East Eifel are apparently derived from source regions with bulk-earth $^{143}Nd/^{144}Nd$ and $^{87}Sr/^{86}Sr$ ratios, while the Tertiary centers have compositions more typical of young ocean islands (higher $^{143}Nd/^{144}Nd$ and lower $^{87}Sr/^{86}Sr$). Preliminary Sr data suggest a possible shift toward lower $^{87}Sr/^{86}Sr$ ratios for off-rift volcanic activity (i.e., W. Eifel).

The data from this study do not rule out the possibility that interaction with continental crust has produced the low $^{143}Nd/^{144}Nd$ and high $^{87}Sr/^{86}Sr$ ratios in the Quaternary volcanics, which would allow all of the central European volcanics to be derived from a single homogenous mantle source. Resolution of this problem requires further investigation, which is currently underway.

REE concentrations in the Eifel volcanics are consistent with their derivation by $\sim$1% melting of a garnet peridotite source, with chondritic relative REE abundances. This does not preclude the possibility of their generation via a melting model similar to that proposed for the W. Reykjanes Peninsula in Chapter 1.

CHAPTER 3

Nd AND Sr ISOTOPE RATIOS IN KOMATIITES

AND ASSOCIATED ROCKS:   IMPLICATIONS FOR

THE NATURE OF MANTLE EVOLUTION

3.1 <u>Introduction</u>

Komatiites and associated rocks have received considerable attention
from geochemists in recent years, as numerous descriptions of their
occurence have appeared in the literature.  These rocks typically
represent the mafic to ultramafic end members of Precambrian greenstone
associations which are situated within or between ancient sialic cratons.
As such, they offer a unique opportunity both to investigate geochemical
aspects of magma generation during the Precambrian and to define constraints
on the chemical composition of the Precambrian mantle.  In this respect,
the distinct advantage of studying komatiitic and tholeiitic rocks as
opposed to their more differentiated, acidic associates, is that their
mafic nature precludes significant involvement of sialic crust in the
generation of magmas from which they have crystallized.  In short, we are
provided with a "window" through which to view the Precambrian mantle
which is of similar quality to that available via the study of young
oceanic basalts.

Sm-Nd and Rb-Sr isotopic studies of komatiites and tholeiites
provide three types of information not attainable through conventional
trace element studies.  The most obvious of these is manifest in the
ability to date the time of crystallization of individual rock units.
Recently, there has been appreciable success with this type of endeavor
due to advances in technology which have allowed high-precision
measurements of $^{143}Nd/^{144}Nd$ and, thus, the application of the Sm-Nd
system to dating of mafic rocks (Hamilton et al., 1977, 1978, 1979;
DePaolo, 1979; Jacobsen, 1980).  Previously, applications of the Rb-Sr

system (e.g. Allsopp et al., 1973) met with serious difficulties due to the now-documented mobility of Rb and/or Sr during deuteric and low grade metamorphic processes in mafic rocks (Hamilton et al., 1979; Smith and Erlank, 1978). However, it has been shown by Hart and Brooks (1977) that Rb-Sr systematics in fresh clinopyroxene provide reliable estimates of initial $^{87}Sr/^{86}Sr$.

The second type of information is attained by virtue of the chemical similarity of isotopes of a single element, i.e., that isotopes of a heavy element are not significantly fractionated during magma generation processes. This fact, combined with arguments based on experimentally determined diffusion coefficients (Hoffman and Hart, 1978), predicts that a liquid produced by melting of a segment of mantle will have Nd and Sr isotopic compositions identical to the bulk mantle which was melted. As a result, where one is able to estimate the initial isotopic composition of an igneous rock unit and exclude the possible involvement of a crustal component in its genesis, this isotopic composition may be assigned to the mantle at the time of crystallization of the rock.

The third type of information has a direct bearing on the petrogenesis of komatiites and associated tholeiites and is available because of the well-understood behavior of Sm and Nd during magmatic processes. Unlike Rb and Sr or U and Pb, Nd and Sm are geochemically similar, refractory elements whose absolute and relative behavior have been the subject of many intensive studies (see Frey, 1979). Initial $^{143}Nd/^{144}Nd$ ratios, together with hypotheses which predict chondritic relative Sm/Nd ratios in the bulk earth, enable one to estimate Sm/Nd ratios in the source mantle for the rocks of interest. Comparison of

mantle Sm/Nd ratios with those measured in komatiites and tholeiites, furnishes constraints on the nature of petrogenetic processes which have been active.

A problem which is particularly relevant to Sm/Nd dating of mafic rocks deserves a short discussion here. Strictly speaking, the theory whereby ages are estimated on the basis of isochrons is applicable only where all samples analysed come from a single rock unit. Where it is necessary to work with whole rock samples, because of a paucity of primary phases, it is very difficult to obtain a large enough range of Sm/Nd ratios from a single unit to provide an accurate age estimate. This is due both to the chemical similarity of parent and daughter and to the long half-life of $^{147}$Sm ($\lambda^{147}$Sm$=6.54$x$10^{-12}$y$^{-1}$). To circumvent this problem, investigators, to the occasional dismay of classical geochronologists, have analysed samples from spatially related rock units which afford the necessary range in Sm/Nd ratios. Implicitly, this approach assumes that adjacent rock units have crystallized simultaneously from magmas with identical $^{143}$Nd/$^{144}$Nd. Although the time constraint becomes less important in older rocks, arguments made to justify this approach are invariably circular. What can be said, is that the apparently consistent results of studies to date support the validity of the assumptions, and further that the results of these studies have provided information about the petrogenesis of komatiite-tholeiite associations and Precambrian mantle evolution, which could not otherwise have been obtained.

This report consists of a summary of Rb-Sr and Sm-Nd isotopic studies of komatiites and related rocks. Previously unpublished data on komatiites

from the Abitibi belt and the Cape Smith-Wakeham Bay belt are presented

in detail. Data and age constraints from other regions are summarized

and important conclusions are discussed on the basis of all of the data.

## 3.2 Cape Smith-Wakeham Bay belt, New Quebec

The E-W trending Cape Smith-Wakeham Bay belt extends for approximately 400 km. across the northern tip of the Ungava Peninsula in New Quebec, and forms the central sector of the Circum-Ungava geosyncline.

Tectonically, it is flanked to the southeast by the Labrador trough and to the southwest by the Belcher Islands fold belt, both of which trend approximately N-S (See Fig. 3-1). The variably metamorphosed volcanic and sedimentary rocks of the Cape Smith belt have been divided into two major groups, the lower Povungnituk Group and the upper Chukotat Group, which are in contact across an angular unconformity, which has been interpreted as a thrust fault by Hynes and Francis (1980). The general geology of the belt has been described by Dimroth (1970), and more recently, Francis and Hynes have begun a detailed petrological and chemical field investigation of rocks of the Cape Smith belt (Francis and Hynes, 1979; Hynes and Francis, 1980). The Cape Smith belt shares similarities with both Archean greenstone belts and Paleozoic and younger island arcs and ophiolites, and hence, offers an ideal opportunity to characterize the evolution of continental margin tectonics from the poorly defined tectonic settings of the Archean to modern regimes which are easily understood within the context of plate tectonic theory.

Early attempts at dating rocks of the Cape Smith belt have been restricted to K-Ar investigations of greenschist facies metasediments, and ages range from 1430 to 1650 m.y. for the Povungnituk Group and from 1430 to 1490 m.y. for the Chukotat Group (Beall et. al., 1963). However, the belt has been presumed to be late Aphebian in age based on

Figure 3-1

    Regional geologic outline of the Cape Smith-

Wakeham Bay belt (after Taylor, 1974)

Agg  -  high grade, granitic to dioritic

        Hudsonian gneiss complex

Arg  -  Archean gneiss complex

 Av  -  basalt, andesite, volcanic breccia

Aab  -  amphibolite and hornblende gneiss

Adr  -  granodiorite, diorite and granite

 As  -  slate, siltstone, mudstone, sandstone,

        greywacke, phyllite and mica schist

 ●  -  gabbro, peridotite, pyroxenite, serpentinite.
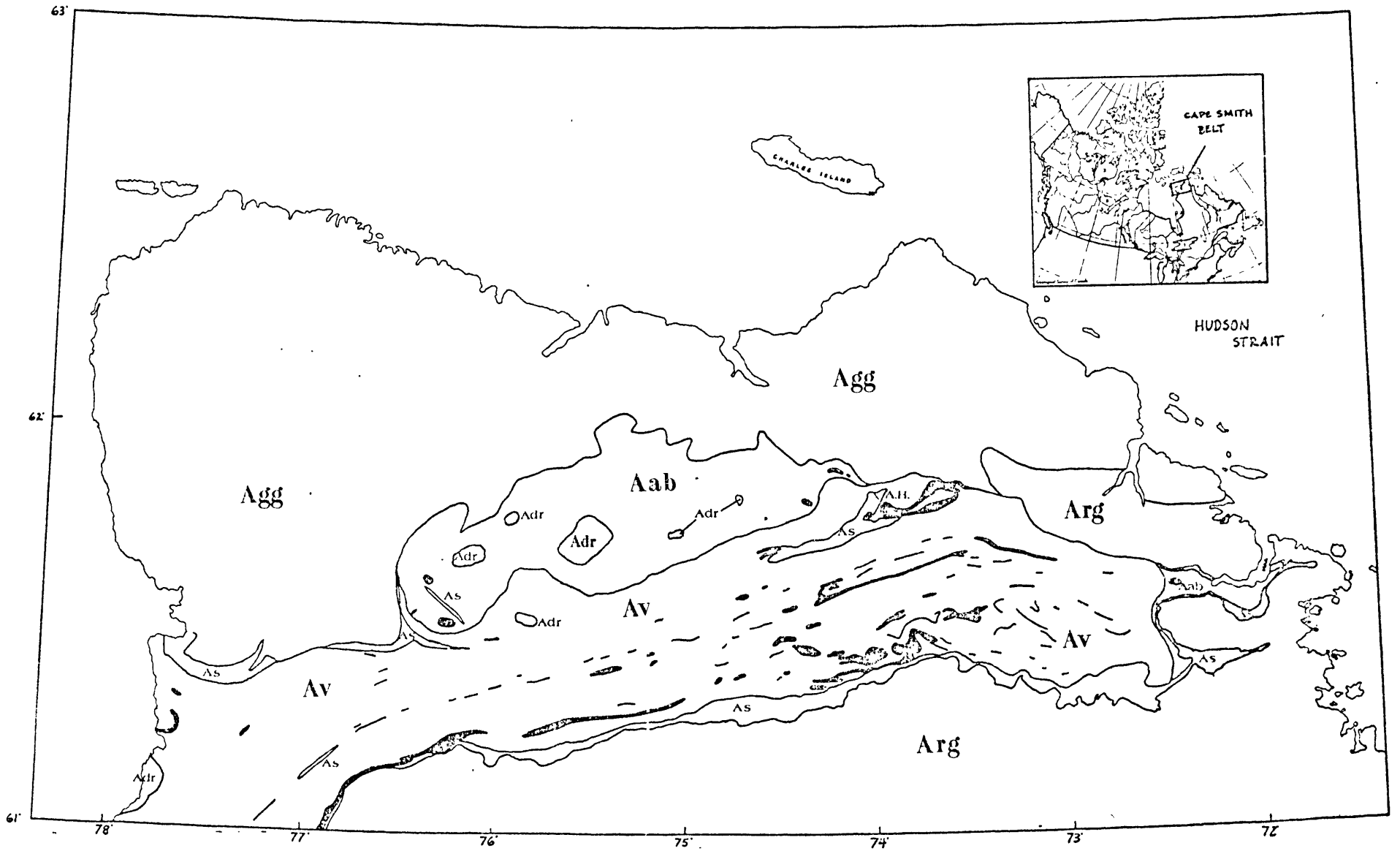
Figure 3-1

correlations with volcanic rocks of the Belcher Island fold belt and slates from the central Labrador trough, which yield Rb-Sr isochron ages of 1700±151 m.y. and 1816±148 m.y. respectively (errors represent $2\sigma$m and are recalculated from Freyer, 1972, using the revised decay constant for $^{87}$Rb: $\lambda^{87}$Rb$=1.42$x$10^{-11}$y$^{-1}$).

The data presented here represent preliminary results from an ongoing Sm-Nd and Rb-Sr isotopic investigation of ultramafic sills from the upper Po$^V$ungnituk Group and high-Mg, differentiated flows from the Chukotat Group, all of which have crystallized from liquids having komatiitic affinities (Francis and Hynes, 1979). Samples come from: (1) the Vaillant Sill, an ultramafic sill approximately 450 m in thickness, which is differentiated from leucogabbro to peridotite (Beall, 1962; Francis and Hynes, 1979); and (2) two differentiated, high-Mg flows from the upper part of a thrust sheet which consists of a several km thick section of mafic pillow volcanics and flows with minor gabbroic intrusives (Hynes and Francis, 1980). The Vaillant Sill is intruded into a sequence of pelitic metasediments and volcanics, characteristic of a near-shore environment, in the upper part of the Povungnituk Group. On the other hand, the allochthonous volcanic associations of the Chukotat thrust sheets show little or no influence of a nearby continent, and must have originated in a wholly oceanic environment.

Sm-Nd and Rb-Sr data for Cape Smith samples are given in Table 3-1. Analytical techniques for Sm-Nd are described in Appendix I; Rb-Sr analytical techniques have been described by Hart and Brooks (1977). Three whole rocks and two clinopyroxene separates from the Vaillant Sill, and three whole rocks from Nick's flow, a differentiated flow from the lowermost Chukotat thrust sheet, have been analysed for Sm-Nd.

Table 3-1 Sm-Nd and Rb-Sr data for Cape Smith samples

| Sample No. | Rb(ppm) | Sr(ppm) | Sm(ppm) | Nd(ppm) | $^{87}Rb/^{86}Sr$ [1] | $^{147}Sm/^{144}Nd$ [2] | $^{87}Sr/^{86}Sr$ [3] | $^{143}Nd/^{144}Nd$ [4] |
|---|---|---|---|---|---|---|---|---|
| VA 3 WR | 0.0864 | 16.96 | 0.6531 | 1.776 | 0.01473 | 0.2223 | 0.70635±4 | 0.513147±19 |
| VA 3 CPX | 0.0880 | 21.14 | 0.6911 | 1.525 | 0.01204 | 0.2741 | 0.70603±4 | 0.513727±15 |
| VA 13 WR | 1.115 | 6.200 | 3.668 | 1.131 | 0.5205 | 0.1960 | 0.71779±4 | 0.512792±14 |
| VA 13 CPX | 0.0406 | 9.846 | 0.8770 | 1.903 | 0.01192 | 0.2786 | 0.70339±7 | 0.513826±24 |
| VA 19 WR | 0.999 | 84.98 | 2.440 | 7.784 | 0.03400 | 0.1895 | 0.70704±3 | 0.512678±17<br>0.512700±20 |
| A 19 AMPH | ·0.264 | 10.19 | | | 0.07493 | | 0.70803±4 | |
| 78-148 CPX | 0.1530 | 7.810 | | | 0.05664 | | 0.70322±10 | |
| 78-152 CPX | 0.0429 | 7.838 | | | 0.01582 | | 0.70257±7 | |
| SS 120 WR | | | 1.436 | 4.176 | | 0.2080 | | 0.512918±26 |
| SS 123 WR | | | 2.036 | 6.073 | | 0.2027 | | 0.512907±30 |
| SS 124 WR | | | 6.119 | 18.16 | | 0.2037 | | 0.512894±22 |

1 - error estimated from replicate analyses to be better than ±0.7% ($2\sigma m$).
2 - error estimated from replicate analyses to be better than ±0.3% ($2\sigma_m$).
3 - errors represent $2\sigma_m$. $^{87}Sr/^{86}Sr$ relative to $^{86}Sr/^{88}Sr$ = 0.1194. Values corrected to $^{87}Sr/^{86}Sr$ of 0.70800 in E & A SrCO$_3$.
4 - errors represent $2\sigma_m$. $^{143}Nd/^{144}Nd$ relative to $^{146}Nd/^{144}Nd$ = 0.72190.

VA 13 is a <sup>cumulate</sup> peridotite from the lower part of the Vaillant

Sill; VA 3 is a pyroxenitic pod from within the cumulate zone; and VA 19

is a gabbro from the upper part of the sill.  All samples have been

metamorphosed and, while some fresh olivine remains in the peridotite,

clinopyroxene in VA 19 has been completely converted to amphibole and

plagioclase in the gabbros is albitized.  SS 120 and SS 124 come from

the bottom and top of Nick's flow, respectively, and contain some fresh

clinopyroxene, in addition to epidote and carbonate.  SS 123 is a gabbroic

textured lava from the center of the flow and consists entirely of a

secondary mineral assemblage.

With the exception of VA 3 CPX, all points lie within a best-fit

isochron (Figure 3-2) and define an age of 1871±75 m.y. and an initial

$^{143}Nd/^{144}Nd$ of 0.51038±9 (all errors quoted at $2\sigma$m confidence level).

Clinopyroxene in VA 3, unlike VA 13, is extremely cloudy, a condition

which may explain its anomalous position on the isochron diagram.  In

short, the Sm-Nd data are consistent with the Vaillant Sill and Nick's

flow having crystallized from magmas with similar Nd isotopic composi-

tion at about 1871 m.y.

Figure 3-3 is a Rb-Sr isochron diagram for whole rocks and minerals

from Cape Smith.  Samples previously described from the Vaillant Sill

appear in this diagram along with an analysis of amphibole from VA 19.

While samples from Nick's flow were not analyzed for Rb-Sr, two

clinopyroxene separates from an underlying flow (Summit flow, Hynes,

pers. comm.) have been measured.  78-148 is a gabbroic textured lava

from the middle of the 100 m thick flow and 78-152 is just above the

chilled margin at the bottom of the flow.  Clinopyroxenes from 78-148

and 78-152 are clear and inclusion-free, similar to VA 13 cpx.

Figure 3-2    Sm-Nd isochron diagram for Cape Smith
samples. SS-samples from Nick's Flow; VA-samples from
the Vaillant sill. Regression analysis, after York
(1966), yields an age of $1871 \pm 75$ m.y. $(2\sigma m)$ and an
initial $^{143}Nd/^{144}Nd$ ratio of $0.51038 \pm 9$ $(2\sigma m)$.
$(\lambda^{147}Sm = 6.54 \times 10^{-12} y^{-1})$.
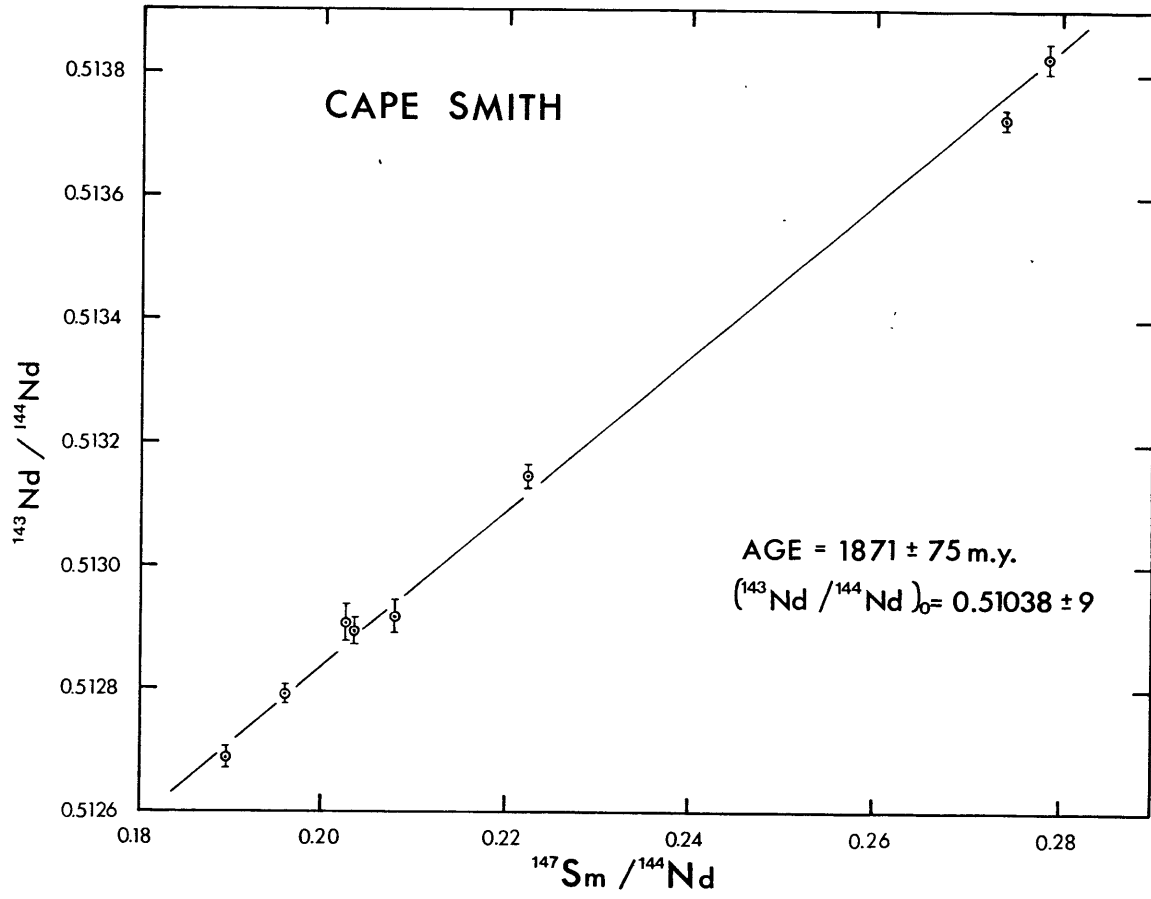
Figure 3-2

In Figure 3-3 it can be seen that the three clean clinopyroxene samples lie significantly below a regression line through the remaining data points, which defines an age of 1586±150 m.y. and an initial $^{87}Sr/^{86}Sr$ of 0.70608±28. Because of similarity with K-Ar ages, this may be interpreted as a metamorphic age, however the age might also be meaningless and simply be an indication of the degree of alteration of the rocks.

The most significant results from the Rb-Sr data are the low $^{87}Sr/^{86}Sr$ ratios measured in the clean clinopyroxenes. Hart and Brooks (1977) have demonstrated the utility of this approach for determining initial $^{87}Sr/^{86}Sr$ ratios in metamorphosed mafic rocks. When the measured $^{87}Sr/^{86}Sr$ ratios in the clinopyroxenes are corrected to initial ratios at 1871 m.y., 78-148 and 78-152 yield, respectively, 0.70170±10 and 0.70214±7 while VA 13 yields 0.70307±7. It is considered that the large amount of Rb measured in 78-148 is not in the clinopyroxene but concentrated, by relatively recent processes, along cracks or sub-grain boundaries, resulting in too large a correction for $^{87}Sr/^{86}Sr$. Regardless, the results suggest that the Summit flow has crystallized from a magma with significantly lower $^{87}Sr/^{86}Sr$ than that which crystallized as the Vaillant Sill. Further implications of these data will be discussed in a later section.

Figure 3-3   Rb-Sr isochron diagram for Cape Smith

samples. VA samples from Vaillant sill; 78-samples from

the Summit Flow.  Regression analysis yields an age of

1586±150 m.y. (2σm), for samples excluding clean cpx,

and an initial ratio of 0.70608±28 (2σm).  Initial

ratios at 1871 m.y. for clean cpx are 0.70307±7, 0.70170±10,

and 0.70214±7 for VA13, 78-148, and 78-152, respectively.

($\lambda^{87}$Rb = 1.42 X $10^{-11}y^{-1}$).
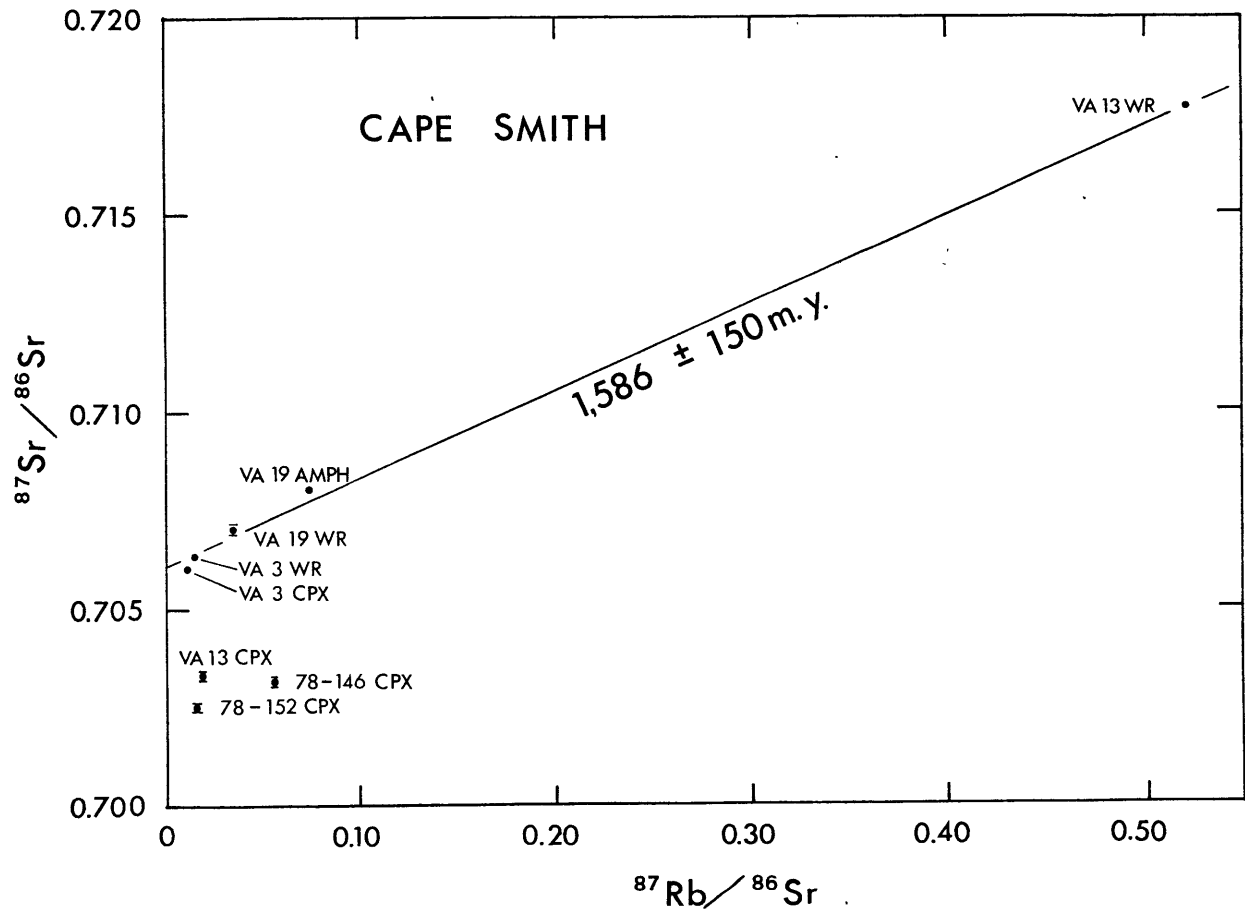
Figure 3-3

## 3.3  Abitibi belt, Superior Province

(The following geologic outline is summarized from Hart and Brooks, 1977). The Superior Province in southern Quebec and Ontario (inset, Fig. 3-4) consists of E-W trending belts of metavolcanic rocks, alternating with belts of metasedimentary rocks. The metavolcanic belts are typically arcuate and complexly deformed, with lenticular granitic bodies intruded along antiforms. The Abitibi volcanic belt, described by Goodwin and Ridler (1970) (Fig. 3-4), is one of the most extensive of these Archean belts, and from size consideration alone, is unique even when compared to South African and Australian examples. The belt is folded about generally E-W trending axes with major ultramafic, mafic, and volcano-sedimentary horizons being oriented primarily E-W.

The belt contains large-scale isoclinal folds and subvertical minor folds which generally display two superposed schistosities (Dimroth et. al, 1973). Intensity of deformation within the belt varies considerably, and strongly deformed zones have been used to define structural provinces. Even so, the state of penetrative deformation is usually low, as evidenced by the preservation of delicate quench textures in komatiitic and more differentiated volcanic rocks (Gelinas and Brooks, 1974). The overall metamorphic grade of the belt is prehnite-pumpellyite to lower greenschist facies, and while secondary mineral assemblages predominate, primary igneous clinopyroxene is preserved in some of the thicker flows and sills (Hart and Brooks, 1977).

Reliable age estimates from the Abitibi belt have come primarily from U-Pb investigations of zircon populations taken from acidic volcanic rocks. Rhyolitic to dacitic volcanic rocks have yielded zircon ages in

Figure 3-4 Regional geologic outline of the Abitibi
metavolcanic belt (after Goodwin and Ridler, 1970).
The inset shows the position of the belt within The
Superior Province. The no. 1 indicates the location
of Munro Township.

Figure 3-4

LEGEND

| | |
|---|---|
| + + | Granitic rocks |
| ‖‖‖ | Mafic intrusions |
| ░░░ | Ultramafic rocks |
| ▒▒▒ | Archean sediments |
| ≡≡≡ | Proterozoic sediments |
| ☐ | Volcanics |

SCALE

0    50    100 KM

Ontario
Quebec
U.S.A.

KAPUSKASING GNEISS BELT

ONTARIO
QUEBEC

GRENVILLE PROVINCE

Matagami
Chibougamau
Rouyn-Noranda
Val-d'or
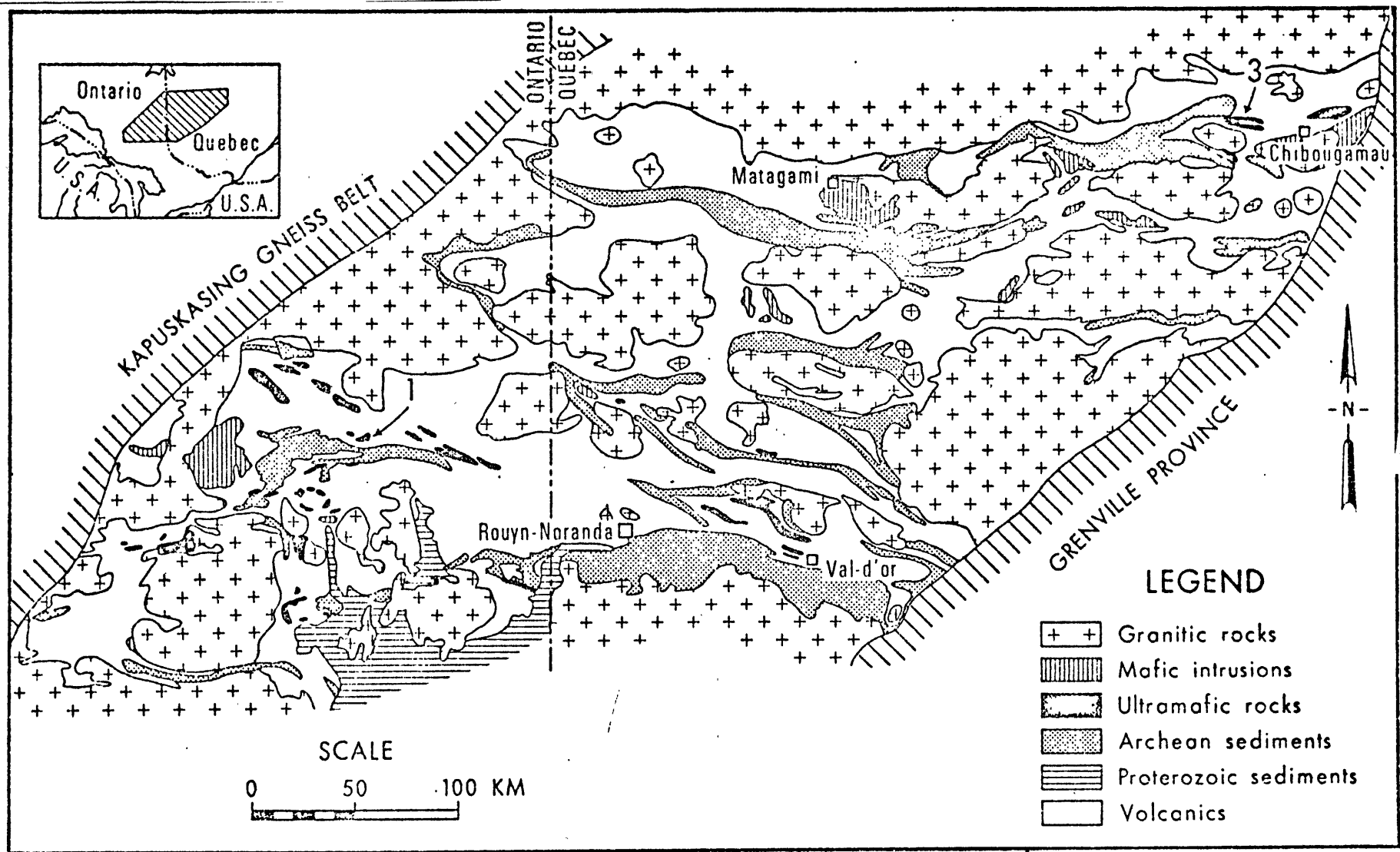
-N-

the range of 2700-2725 m.y. (Nunes and Pyke, 1980; Nunes and Jensen, 1980).
Krogh and Davis (1971) have determined zircon ages for granitic rocks
within the volcanic pile at Noranda which, when corrected for the new
decay constants are consistent with the range found by Nunes.

Nd and Sr isotopic compositions have been measured in komatiitic
and tholeiitic rocks which occur as flows and hypabyssal sills in the
Munro Township (see location, Figure 3-4). Whole rock samples analyzed
in this study are metamorphosed to lower greenschist facies and, while
some fresh clinopyroxene remains, olivine is completely serpentinized
and plagioclase in the gabbroic rocks is highly sausseritized.

The nine samples analyzed for Sm-Nd come from : (1) the Munro-
Warden Sill, a tholeiitic layered sill differentiated from dunitic
peridotite to leuco-gabbro (MacRae, 1969); and (2) Fred's Flow, a
komatiitic layered flow, differentiated from dunite to gabbro and
containing spinifex-textured pyroxene and olivine (Arndt et. al, 1977;
Arndt, 1977). The results are listed in Table 3-2 and plotted on a
Sm-Nd isochron diagram, Figure 3-5. All samples fall within error of
a best fit isochron defining an age of $2622 \pm 120$ m.y. ($2\sigma m$) and an
initial $^{143}Nd/^{144}Nd$ ratio of $0.50933 \pm 16$. The relatively large error
associated with this age is due in part to the restricted range of
Sm/Nd ratios in these rocks but may also be attributed to some geologic
error resulting from the metamorphic grade of the rocks. Nevertheless,
the age is in agreement with the more precise age measurements of the
acidic volcanics and is considered to document the crystallization age
of tholeiites and komatiites from Munro Township. In addition, the data
are consistent with the tholeiitic and komatiitic rocks having crystallized
from magmas with similar $^{143}Nd/^{144}Nd$.

Table 3-2   Sm-Nd data for Munro Township samples

| Sample No. | Rock Type | Locality | Nd(ppm) | Sm(ppm) | $^{147}Sm/^{144}Nd$ [1] | $^{143}Nd/^{144}Nd$ [2] | Method [3] |
|---|---|---|---|---|---|---|---|
| MT-MW-1 | Gabbro | Munro-Warden Sill | 8.977 | 2.527 | 0.1702 | 0.512272±23 | 2 |
| MT-MW-2 | Gabbro | Munro-Warden Sill | 4.881 | 1.432 | 0.1773 | 0.512367±21 | 2 |
| MT-MW-3 | Gabbro | Munro-Warden Sill | 9.071 | 2.695 | 0.1796 | 0.512466±23 | 2 |
| MT-MW-4 | Pyroxenite | Munro-Warden Sill | 4.83 | 1.599 | 0.2003 | 0.512822±14 | 1 |
| MT-MW-6 | Pyroxenite | Munro-Warden Sill | 2.185 | 0.7496 | 0.2074 | 0.512916±24 | 1 |
| P9-105 | Gabbro Textured Lava | Fred's Flow | 5.21 | 1.918 | 0.2220 | 0.513168±37 | 1 |
| P9-106 | Gabbro Textured Lava | Fred's Flow | 4.50 | 1.706 | 0.2289 | 0.513262±36 | 1 |
| P9-107 | Pyroxene Spinifex Textured Lava | Fred's Flow | 3.072 | 1.190 | 0.2353 | 0.513445±20 | 1 |
| P9-167 | Olivine Spinifex Textured Lava | Fred's Flow | 3.26 | 1.285 | 0.2348 | 0.513363±30 | 1 |

1 – Estimated error in Sm/Nd ± 0. 3% ($2\sigma_m$).

2 – Errors quoted at $2\sigma_m$ confidence level.   $^{143}Nd/^{144}Nd$ relative to $^{146}Nd/^{144}Nd$ = 0.72190.

3 – Method 1 – concentrations measured in powder aliquots;   Method 2 – concentrations measured in liquid aliquots.

Figure 3-5    Sm-Nd isochron diagram for samples from
Munro Township.    P9-samples from Fred's Flow; MTMW-
samples from the Munro Warden Sill.    Regression analysis
yields an age of 2622±120 m.y. (2σm) and an initial
ratio of 0.50933±16 (2σm).
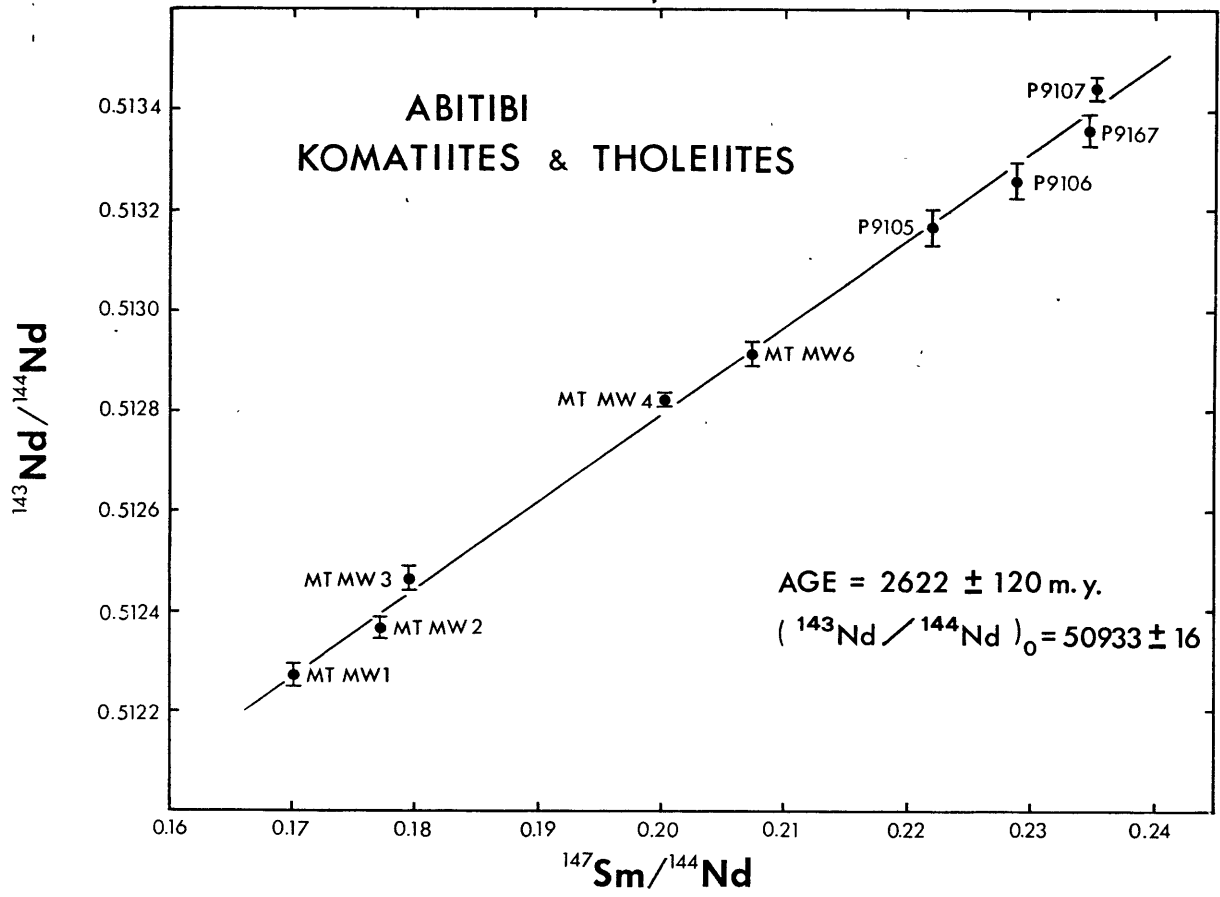
Figure 3-5

3.4  Results from other studies

In this section, results from recent Sm-Nd investigations of

komatiities and associated rocks from Rhodesia and South Africa are

reviewed.  A Sm-Nd study of basic volcanic rocks from the Garben

Schiefer unit, West Greenland, is also discussed.  These studies

represent the work of P.J. Hamilton, R.K. O'Nions, and N.M. Evensen,

and the discussion here is summarized from their publications (Hamilton

et al. 1977; Hamilton et. al, 1978; Hamilton et. al, 1979).

Rhodesia

Major greenstone belts from the Rhodesian craton comprise successions

of ultramafic to mafic and more differentiated volcanic rocks, typically

overlain by volcano-sedimentary sequences (Harrison, 1970; Stowe, 1971;

Wilson, 1973; Bickle et al. 1975).  Attempts at Rb-Sr chronology of

greenstone belts near Belingwe and Fort Victoria did not provide useful

age information (Hawkesworth et. al, 1975), however the age of these

belts is constrained to be younger than the 2.97±0.16 b.y. Mashabe

tonalite (Hawkesworth and Bickle, 1977) and older than the emplacement of

the Great Dyke, which has been dated by the Rb-Sr method at 2.51±0.02 b.y.

(Hamilton, 1977).

$^{143}Nd/^{144}Nd$ and Sm/Nd ratios were measured by Hamilton et. al.

(1977) in ten samples which range in composition from ultramafic komatiites

to basaltic andesites.  Samples come from Fort Victoria, Belwinge and

Que Que, and display low-grade metamorphic mineral assemblages.  The

Sm-Nd data define an age of 2.64±0.14 b.y. and an initial $^{143}Nd/^{144}Nd$

of 0.50919±18, and are consistent with the formation of the different

greenstone belts within a restricted time interval from magmas with

similar $^{143}Nd/^{144}Nd$.

## Onverwacht Group, South Africa

The Onverwacht Group, in Swaziland and the Transvaal of South Africa, forms the basal portion of the Barberton greenstone belt and consists of two distinct volcanic units (Viljoen and Viljoen, 1969). The lower ultramafic unit is separated from the upper mafic-to-felsic unit by a persistent sedimentary layer, the Middle Marker Horizon. Greenschist facies metamorphisim in the Onverwacht Group (Viljoen and Viljoen, 1969) has disturbed Rb-Sr systematics so that the age of volcanism has remained in question. Rb-Sr data from whole-rock samples of the felsic volcanics have defined an age of 2570±40 m.y. (Allsopp, et. al, 1968) in contrast to U-Pb results from zircon and sulfide separates which yield an age of approximately 3310 m.y. (Van Niekerk, 1969). Sediments of the Middle Marker Horizon and the Fig Tree Group, which overlies the mafic to felsic unit, have been dated by the Rb-Sr whole rock method at 3280±70 m.y. and 2920±20 m.y., respectively (Hurley et. al, 1972; Allsopp, et. al, 1968). Jahn and Shih (1974) obtained no useful age information from a Rb-Sr whole rock study of mafic volcanic rocks but were able to generate an age of 3430±200 m.y. from density separates of a completely altered basaltic komatiite.

Hamilton et. al. (1979) measured $^{143}Nd/^{144}Nd$ and Sm/Nd ratios in ten samples from the lower ultramafic unit which range in composition from ultramafic komatiites to a sodic porphyry. Together, these data define an age of 3540±30 m.y. and an initial $^{143}Nd/^{144}Nd$ ratio of 0.50809±4, again demonstrating the utility of the Sm-Nd decay system where Rb-Sr systematics have been affected by metamorphism.

## Isua Supracrustals, West Greenland

The supracrustals of the Isua series consist of metasediments, metavolcanics and associated hypabyssal intrusives, and have been described by Bridgewater and McGregor (1974), Bridgewater et. al. (1974) and Allaart (1976). The basic volcanics and ultramafic intrusives have been metamorphased at greenschist to lower amphibolite facies and, although no komatiites "per se" have been described, the author interprets this as a matter of discretion. Pb-Pb and Rb-Sr whole rock investigations of iron formation, an acid conglomerate unit, and leucocratic schists, show good agreement and define a well-constrained age of about 3720 m.y. (Moorbath et. al, 1973 and 1975; and Moorbath et. al, 1977).

Sm-Nd data for a basic intrusive unit, the Garben Schiefer, and the acid conglomerate unit which it intrudes define an age of 3770±42 m.y. and an initial $^{143}Nd/^{144}Nd$ of 0.50783±46. Data for the Garben Schiefer alone yield an age of 3772±134 m.y. and an initial ratio of 0.50783±17, which agrees extremely well with the combined age and initial ratio for the two units. Therefore, although no simple genetic relationship exists between the two units, they are derived during a restricted time period from sources with indistinguishable $^{143}Nd/^{144}Nd$ (Hamilton et. al, 1978).

3.5  Comparison of Sm-Nd and Rb-Sr

The utility of the Sm-Nd decay system for dating metamorphosed,

mafic to ultramafic igneous rocks is amply demonstrated by the studies

discussed in this chapter.  In four of the five investigations, it was

shown that the Rb-Sr system had been open subsequent to crystallization,

and was not able to provide an accurate age estimate for the rocks of

interest.  Although U-Pb zircon ages from acidic volcanics, which may

be associated with the mafic or ultramafic rocks, provide more precise

age determinations than are generally possible with Sm-Nd, structural

interpretation of Archean greenstone belts is not always such that

relationships between acid and mafic units are well understood.  As

was discussed in the introduction, a major drawback of the Sm-Nd system

is the difficulty in obtaining a sufficient range in Sm/Nd ratios, from

a single igneous rock unit, to allow determination of a precise age.

The author considers that the approach of combining data from spatially

associated rock units, as was the case in each of the studies presented,

is justified by the apparent consistency of the results, especially

where Rb-Sr systematics failed to provide any useful information.

That Sm-Nd has proven much more useful than Rb-Sr in dating meta-

basic rocks is hardly suprising in view of the volatile chemistry of Rb.

Rb is known to be mobile during low-grade metamorphic processes, which

are often manifest by the formation of sheet silicates that significantly

concentrate Rb.  Even in "pristine" igneous gabbros, deuteric processes

can render Rb-Sr systematics unreliable (Chapter 4).  Hamilton et. al.

(1979) and Smith and Erlank (1978) have conclusively demonstrated the

refractory behavior of Sm and Nd, when compared to Rb and Sr, in altered

pillow lavas of the Onverwacht Group.  Pillow margin-interior pairs, which showed insignificant variation in Sm and Nd concentrations and Sm/Nd ratios, were subject to 20-400% variation in Rb/Sr ratios.

In short, precise measurements of $^{143}$Nd/$^{144}$Nd provide reliable age estimates for metamorphosed mafic to ultramafic rocks, which are not amenable to dating by Rb-Sr or U-Pb methods.

## 3.6  Bulk earth evolution of $^{143}Nd/^{144}Nd$ and $^{87}Sr/^{86}Sr$

Before considering the implications of initial isotopic compositions

from komatiitic rocks with regard to mantle evolution, currently popular

theories for bulk-earth evolution of $^{143}Nd/^{144}Nd$ and $^{87}Sr/^{86}Sr$ will

be described.  Evolutionary parameters and their sources are outlined

in Table 3-3.  Choice of these parameters is necessarily somewhat

arbitrary, but the values chosen, and their respective uncertainties,

are considered to accurately describe the bulk earth to the limit of

currently available data.

This model is built entirely upon the long-standing hypothesis that

the bulk earth contains chondritic relative abundances of rare-earth

elements.  Accretionary theory and numerous investigations of REE

concentrations in terrestrial rocks (see Frey, 1979) have substantiated

this hypothesis.  Accepting it, we are able to estimate the Sm/Nd ratio

in the bulk earth by averaging Sm/Nd values from a large number of

meteorites.  Many such compilations are available but the best of these

are considered to be from Nakamura (1974) and Evensen (1978), with Sm/Nd

ratios of 0.3091 and 0.3118 respectively (given as atomic ratios).

Another value which must be considered, by virtue of its frequent usage

(e.g. DePaolo and Wasserburg, 1976a, 1976b, 1979; DePaolo, 1979;

McCulloch and Wasserburg, 1978; Jacobsen and Wasserburg, 1978, 1980a,

1980b), is that measured in the basaltic achondrite Juvinas (Sm/Nd = 0.3072;

Lugmair et. al, 1975).  Faced with this significant range in Sm/Nd

ratios, this author has made the arbitrary choice of averaging the

Juvinas value with Evensen's value, resulting in Sm/Nd = 0.3095±23

(Table 3-3), which is similar to Nakamura's value, and within error,

includes the other two values. The importance of this value and its

uncertainty will become clear in the discussion which follows.

Theories of accretion predict that planetary material formed with

similar isotopic compositions of the heavy elements, approximately 4.55

to 4.60 billion years ago (see O'Nions et. al, 1979). Consequently, it

can be assumed that initial $^{143}Nd/^{144}Nd$ and $^{87}Sr/^{86}Sr$ ratios measured

in meteorites approximate these ratios in the earth at the time of its

formation. The value chosen for $^{143}Nd/^{144}Nd$, initially in the bulk earth,

is 0.50679 (Table 3-3), which represents an average of initial ratios

determined for the basaltic achondrites Juvinas and Angra dos Reis

(Lugmair et. al, 1975; Lugmair and Marti, 1977). This value agrees with

other initial ratios determined for achondrites, within stated errors

(Lugmair and Scheinin, 1976; Unruh et. al, 1977; Nakamura et. al, 1977),

and together with the bulk earth Sm/Nd ratio defines present day $^{143}Nd/^{144}Nd$

as 0.51268±7. The bulk earth initial ratio for $^{87}Sr/^{86}Sr$ is taken to

be Allende, 0.69877 (Gray et. al, 1973); use of BABI, 0.69898 (Papanastassiou

and Wasserburg, 1969) or Angra dos Reis, 0.69884 (Papanastassiou, 1970),

will not significantly affect the model. The age of the earth is

estimated at 4.55 billion years, which agrees with results from Sm-Nd,

U-Pb, and Rb-Sr systematics in meteorites (e.g., Lugmair and Marti, 1977;

Wasserburg et. al, 1977; Minster et. al, 1979).

Because of the volatile chemistry of Rb, it is not possible to

estimate bulk earth Rb/Sr in a manner analogous to Sm/Nd. However, the

observed correlation of $^{143}Nd/^{144}Nd$ and $^{87}Sr/^{86}Sr$ in young basalts

(Richard et. al, 1976; O'Nions et. al, 1977; DePaolo and Wasserburg, 1977)

facilitates an estimate of $^{87}Sr/^{86}Sr$ in the present-day bulk earth, by

comparison to present-day $^{143}Nd/^{144}Nd$ (see Table 3-3). The error in

Table 3-3

Bulk earth Sm-Nd and Rb-Sr evolutionary parameters

| Parameter | Value | Source |
|---|---|---|
| $(^{143}Nd/^{144}Nd)$ present day | $0.51268 \pm 7$** | from single-stage evolution of $(^{143}Nd/^{144}Nd)_o$ at 4.55 b.y. to present |
| (Sm/Nd) atomic | $0.3095 \pm 23$** | average of Sm/Nd in Juvinas[1] and CI chondrites[2]; similar to average of chondrites reported by 3. |
| $(^{87}Sr/^{86}Sr)$ present day | $0.7045 \pm 3$*** | obtained from comparing present-day value for $(^{143}Nd/^{144}Nd)$ with observed correlation of $^{143}Nd/^{144}Nd$ and $(^{87}Sr/^{86}Sr)_o$ in young basalts. |
| (Rb/Sr) atomic | $0.0304 \pm 16$*** | from single stage evolution of $(^{87}Sr/^{86}Sr)_o$ at 4.55 b.y. to present-day $(^{87}Sr/^{86}Sr)$. |
| $(^{143}Nd/^{144}Nd)_o$ | 0.50679* | average of initial values for Juvinas[1] and Angra dos Reis[4] at 4.55 b.y. |
| $(^{87}Sr/^{86}Sr)_o$ | 0.69877* | initial value for Allende[5] at 4.55 b.y. |

* initial $^{143}Nd/^{144}Nd$ and $^{87}Sr/^{86}Sr$ values are assumed to be without error for the sake of the model; if errors in these values were included, errors in other parameters would increase by 50%, depending on the handling of correlations between $(^{143}Nd/^{144}Nd)_o$, age and Sm/Nd.

** errors result from range in Sm/Nd from Juvinas to CI chondrites.

*** errors result from arbitrary bracketing of correlation of $^{87}Sr/^{86}Sr$ and $^{147}Nd/^{144}Nd$ in young basalts.

1-Lugmair et. al., 1975;  2 - Evensen et. al., 1978;  3 - Nakamura, 1974;  4 - Lugmair and Marti, 1977.
5-Minster et al., 1979.

this value reflects the scatter in the Nd-Sr correlation. Present-day $^{87}Sr/^{86}Sr$, taken together with the 4.55 billion year value from Allende, defines a Rb-Sr ratio in the bulk earth of $0.0304\pm16$.

The parameters discussed in the preceeding section are sufficient to define bulk earth evolution models for Nd and Sr, which are depicted in Figures 3-6 (Nd) and 3-7 (Sr). For comparison, present-day estimates for MORB are shown in these figures, along with first-order rate models describing evolution from the bulk earth at 4.55 billion years to present-day MORB (see captions, Figures 3-6 and 3-7).

3.7  Evolutionary implications of initial $^{143}Nd/^{144}Nd$ and $^{87}Sr/^{86}Sr$

from komatiites and associated rocks

Ages and initial $^{143}Nd/^{144}Nd$ ratios from studies discussed in this chapter are plotted in Figure 3-6 (the error ellipse representation is after Minster et. al, 1979) and tabulated in Table 3-4. The data from Archean belts plot within error of the single-stage bulk earth evolution path for $^{143}Nd/^{144}Nd$. This is evidenced by time-integrated Sm/Nd ratios, $(Sm/Nd)_{ti}$, calculated for each of the rock sites (Table 3-5). Within error, these ratios are identical with each other and the bulk earth Sm/Nd ratio from Table 3-3. However, because of the long half-life of $^{147}Sm$, changes in the Sm/Nd ratio of the mantle are slow to produce changes in $^{143}Nd/^{144}Nd$, so that the data support either a first-order rate model or the single-stage model for the evolution of $^{143}Nd/^{144}Nd$ in the Archean mantle (see Figure 3-6). The first-order rate model describes the situation where Sm/Nd in the mantle changes as a first-order function of time (see caption of Figure 3-6 for a mathematical definition). Consequently, the major implications of the Sm-Nd results from Archean rocks are: (1) to provide support for the bulk earth evolutionary parameters in Table 3-3; and (2) to preclude the formation of a major portion of the earth's crust prior to 3.5 billion years ago.

Reliable estimates of Archean mantle $^{87}Sr/^{86}Sr$ are scarce, for reasons discussed previously. The only such estimate currently available is for pure clinopyroxene from the Abitibi belt (Hart and Brooks,1977; Machado et. al, 1980). This value is plotted in Figure 3-7 using the age estimate derived from Sm-Nd systematics. As was the case for

Table 3-4

---

Sm-Nd and Rb-Sr evolutionary parameters** for Precambrian komatiite associations

| Rock Suite | Age (m.y.) | $(^{143}Nd/^{144}Nd)_o$ | $(Sm/Nd)^*_{ti}$ | $(^{87}Sr/^{86}Sr)_o$ | $(Rb/Sr)^*_{ti}$ |
|---|---|---|---|---|---|
| Cape Smith | $1871^{+}_{-}75$ | $0.51038^{+}_{-}9$ | $0.322^{+}_{-}0.006$ | $\begin{bmatrix}0.70192^{+}_{-}7\\0.70307^{+}_{-}7\end{bmatrix}$ | $\begin{bmatrix}0.0288^{+}_{-}0.0006\\0.0393^{+}_{-}0.0007\end{bmatrix}$ |
| Abitibi[1] | $2622^{+}_{-}120$ | $0.50933^{+}_{-}16$ | $0.318^{+}_{-}0.014$ | $0.70120^{+}_{-}5$ | $0.0310^{+}_{-}0.0015$ |
| Onverwacht[2] | $3540^{+}_{-}30$ | $0.50809^{+}_{-}4$ | $0.311^{+}_{-}0.007$ | $(0.70045^{+}_{-}5)$ | $(0.0420^{+}_{-}0.0012)$ |
| Rhodesia[3] | $2640^{+}_{-}140$ | $0.50919^{+}_{-}18$ | $0.303^{+}_{-}0.016$ | | |
| Isua[4] | $3770^{+}_{-}40$ | $0.50783^{+}_{-}5$ | $0.323^{+}_{-}0.011$ | | |

---

* ti - time-integrated ratios for single-stage evolution relative to bulk-earth parameters for calculations:
$\lambda^{147}Sm = 6.54 \times 10^{-12} y.^{-1}$; $\lambda^{87}Rb = 1.42 \times 10^{-11} y.^{-1}$.

** all errors quoted at $2\sigma_m$ confidence level.

1 - $(^{87}Sr/^{86}Sr)_o$ from Jahn and Shih, 1974; 2 - Hamilton et al., 1979; 3 - Hamilton et al., 1977;

4 - Hamilton et al., 1978.

Figure 3-6  $^{143}Nd/^{144}Nd$ evolution diagram. Bulk earth

evolutionary parameters are given in Table 3-3.  Present-

day MORB is modeled using highest $^{143}Nd/^{144}Nd$ measured

in MORB (0.51329 for Mid-Atlantic Ridge sample AD-3

from O'Nions et.al., 1977). Straight line from present-

day MORB to bulk-earth evolution path derives from the

Sm/Nd ratio of 0.433 measured in DSDP 3-14, a tholeiite

from the Mid-Atlantic Ridge (Carlson et.al., 1978).

Archean crustal evolution defined by measurements of New

Quebec and North Quebec composites of Archean crustal

material by McCulloch and Wasserburg (1978).  First-

order rate model evolution from the bulk earth at 4.55

billion years to present-day MORB is described by the

equation:

$$(^{143}Nd/^{144}Nd)t = (^{143}Nd/^{144}Nd)o + [(^{147}Sm/^{144}Nd)o+kt] (e^{\lambda t}-1),$$

where $k=4.4290 \times 10^{-12}y^{-1}$, $\lambda=6.54 \times 10^{-12}y^{-1}$, and initial

values come from Table 3-3.  Error ellipses for Pre-

cambrian greenstone  belts are discussed in the text.

$^{143}Nd/^{144}Nd$ ratios are relative to $^{146}Nd/^{144}Nd=0.72190$.

$^{143}Nd/^{144}Nd$ EVOLUTION DIAGRAM

BAY OF ISLANDS

MORB-TYPE MANTLE EVOLUTION

BULK EARTH EVOLUTION

1$^{st}$ ORDER RATE MODEL

QUEBEC COMPOSITE

SHABOGAMO I.S.

ARCHEAN CRUSTAL EVOLUTION

CAPE SMITH KOMATIITES

ABITIBI KOMATIITES & THOLEIITES

RHODESIAN GREENSTONES

ONVERWACHT VOLCANICS

ISUA SUPRACPUSTALS

ANGRA DOS REIS
JUVINAS

$^{143}Nd/^{144}Nd$

TIME ( BILLIONS OF YEARS BEFORE PRESENT )
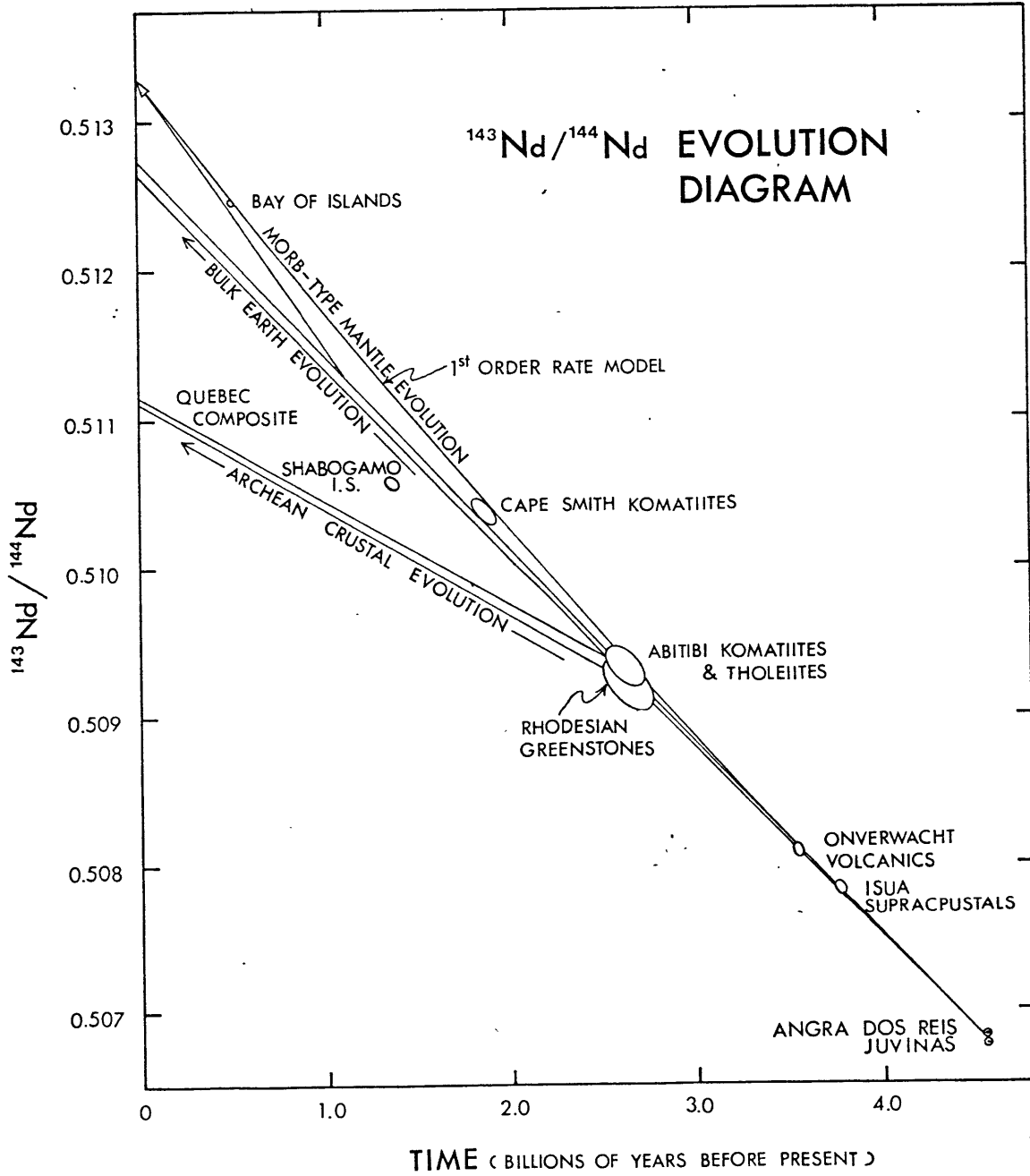
Figure 3-6

$(Sm/Nd)_{ti}$ from Abitibi, the calculated $(Rb/Sr)_{ti}$ (Table 3-4) is

indistinguishable from the bulk earth Rb/Sr ratio (Table 3-3). However,

because the half-life of $^{87}Rb$ is considerably shorter than $^{147}Sm$, the

first-order rate model for $^{87}Sr/^{86}Sr$ passes significantly below the

Abitibi data at 2.6 billion years. If present-day "MORB-type" mantle

is derived from undifferentiated mantle by a first-order rate process,

the rock samples in Abitibi do not represent the ancient equivalents

of modern oceanic crust. On the other hand, if the rocks from Abitibi

represent Archean island arc material, then one would expect the $^{143}Nd/^{144}Nd$

to lie along the MORB evolution line, and the $^{87}Sr/^{86}Sr$ to be higher

than MORB, based on isotopic studies of young island arc material

(DePaolo and Wasserburg, 1977; Hawkesworth et. al, 1977).

Jahn and Shih (1974) determined an initial $^{87}Sr/^{86}Sr$ ratio of

0.70048±5, for a basaltic komatiite from the Onverwacht Group, by

analysing density separates. The rock was composed entirely of secondary

minerals and this author does not consider the data to be reliable.

Whereas the age obtained, 3430±200 m.y., is within error of the Sm-Nd

age of 3540±30 m.y., it almost certainly documents the amphibolite grade

metamorphism which the rock has suffered. Numerous studies have shown

that mafic whole rocks are not closed systems for Rb-Sr during amphibolite

and lower grades of metamorphism (Abitibi and Cape Smith studies in this

Chapter; Hamilton et. al, 1979; Smith and Erlank, 1978).

$^{143}Nd/^{144}Nd$ and $^{87}Sr/^{86}Sr$ initial ratios from Cape Smith are plotted

on Figures 3-6 and 3-7 respectively, and, due to the Proterozoic age of

the belt, prove to be particularly interesting. The $(Sm/Nd)_{ti}$ value for

Cape Smith is significantly higher than that defined for the bulk earth

and provides a positive indication that the mantle has begun to evolve toward modern oceanic mantle by 1871 m.y. The age-corrected $^{87}Sr/^{86}Sr$ ratios for the three clinopyroxene separates, discussed in section 3.2, define a large range in $^{87}Sr/^{86}Sr$ on Figure 3-7. The lowest value is near to the first order growth curve for $^{87}Sr/^{86}Sr$ while the highest value is significantly higher than the bulk earth at 1871 m.y. This range, an apparent enigma, may be understood in terms of the different tectonic settings from which the clinopyroxenes were taken. The Vaillant Sill, which yields the highest $^{87}Sr/^{86}Sr$ value, is intruded into a volcano-sedimentary sequence typical of a "slope and rise" environment, while the Summit Flow is part of an allochthonous sequence of mafic to ultramafic volcanics (Hynes and Francis, 1980). One may speculate that the Cape Smith belt represents the preserved remains of a marginal basin which closed during the Proterozoic, with southward subduction of an oceanic plate. In this context, the Vaillant Sill would represent a subduction-related intrusive, while the volcanic sequence in the thrust sheet would be a slice of obducted oceanic crust. The $^{87}Sr/^{86}Sr$ ratio from the Vaillant Sill then results from subduction-related magmatism and the low values from the Summit Flow represent mantle values at 1871 m.y. As mentioned above, high $^{87}Sr/^{86}Sr$ ratios typically occur in igneous rocks which are associated with convergent plate margins.

Of course, this sort of speculation is hardly justified on the basis of three clinopyroxene analyses, and the author and colleagues will continue to pursue this problem as will Francis and Hynes with their field-based approach. Finally, it should be noted that the initial $^{87}Sr/^{86}Sr$ ratios from Cape Smith do not differentiate between first-order rate processes and multi-stage evolution models for MORB-type mantle, but are broadly compatible with either.

Figure 3-7   $^{87}$Sr/$^{86}$Sr evolution diagram.  Bulk earth
evolutionary parameters are given in Table 3-3.  Present-
day $^{87}$Sr/$^{86}$Sr in MORB is taken as 0.70265 (ave. of
28 samples from Atlantic and Pacific oceans by Brooks
et.al., 1976).  Straight line from present-day MORB
to bulk-earth evolution path uses an average Rb/Sr of
0.00844 from Hart (1976).  Archean crustal evolution
defined by measurements of New Quebec and North Quebec
composites of Archean crustal material by McCulloch and
Wasserburg (1978).  First-order rate model evolution
from the bulk earth at 4.55 billion years to present-
day MORB is described by the equation:

$$(^{87}Sr/^{86}Sr)t = (^{87}Sr/^{86}Sr)o + [(^{87}Rb/^{86}Sr)o+kt](e^{\lambda t}-1),$$

where k=-6.09154 x $10^{-12}y^{-1}$, $\lambda$=1.42 x $10^{-11}y^{-1}$, and
initial values come from Table 3-3. Abitibi and Cape
Smith points are discussed in the text.  $^{87}$Sr/$^{86}$Sr
ratios are relative to $^{86}$Sr/$^{88}$Sr=0.11940.

$^{87}Sr/^{86}Sr$ EVOLUTION DIAGRAM
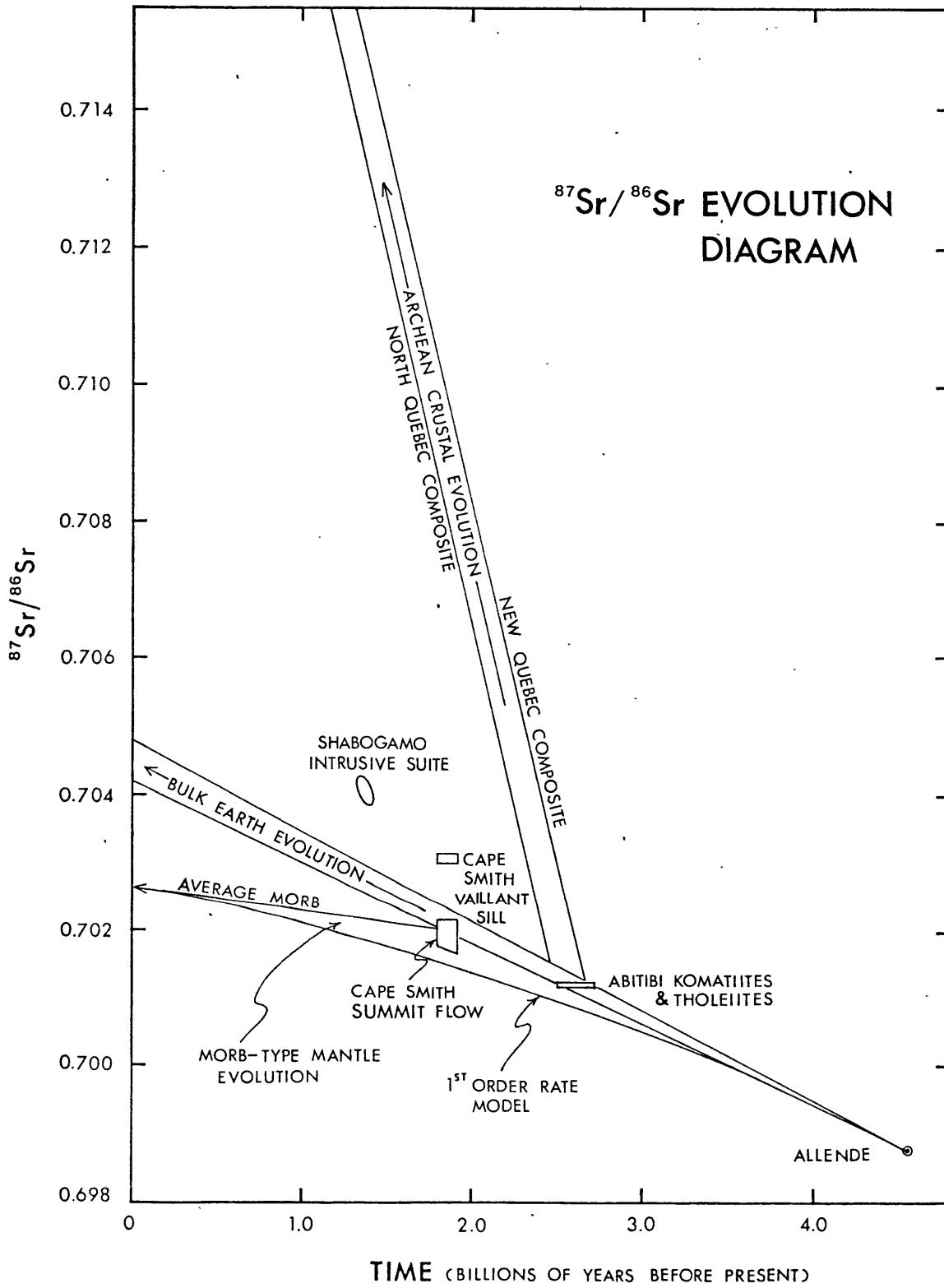
Figure 3-7

## 3.8  Constraints on Petrogenetic Processes

Time-integrated Sm/Nd ratios for the Archean rocks discussed in
this Chapter are consistent with the derivation of these rocks from source
regions in the mantle with bulk earth Sm/Nd ratios.  However, the fairly
large errors associated with these time-integrated ratios permit signi-
ficant latitude in this constraint.  Perhaps the more important petro-
genetic constraint resulting from the Sm-Nd investigations is that mafic
to ultramafic rocks, which exhibit a significant range of Sm/Nd ratios,
are derived from a mantle reservoir with a single time-integrated Sm/Nd
ratio and a single $^{143}Nd/^{144}Nd$ ratio.

Because of their mafic to ultramafic chemistry, komatiites and
associated tholeiites are presumed to "mimic" the REE patterns in their
mantle source regions.  Hence, the observed range in measured Sm/Nd ratios
for adjacent units (e.g., from 0.276 to 0.435 in Munro Township; Arth
et. al, 1977; Whitford and Arndt, 1977) has been interpreted as evidence
for chemical heterogeneity in the Archean mantle (e.g., Sun and Nesbitt,
1978).  If this interpretation is correct, Sm/Nd systematics in a given
suite of rocks constrain the heterogeneity to have been created in a
short time interval prior to magma generation.  This so-called "creation
of heterogeneities" may in fact be an aspect of the magma generation process,
in a fashion similar to that proposed for the Reykjanes  Peninsula
basalts in Chapter 1.

Alternatively, the magma generation process which produces the
komatiitic and tholeiitic liquids may act on a homogeneous mantle segment
to produce the observed range in Sm/Nd ratios.  Such a process would imply
the comagmatic character of LREE-depleted ultramafic komatiites and LREE-

enriched tholeiites, where they occur together. From a mass-balance standpoint, it is conceivable to derive LREE-enriched and LREE-depleted liquids from a mantle with a bulk earth Sm/Nd ratio. Such a process may be modeled by "continuous melting" of a garnet peridotite mantle, in a manner similar to that described in Langmuir (1977). This necessarily results in the eruption of tholeiites prior to the ultramafic komatiites, which is the sequence described by Arndt et. al (1977) for Munro Township, but is not commonly observed in other belts.

## 3.9  Summary and Conclusions from Chapter 3

Sm-Nd systematics provide reliable age estimates for suites of variably metamorphosed komatiites and associated rocks from Precambrian greenstone belts.  This is a particularly important result because in each of the areas discussed, Rb-Sr systematics have failed to provide unambiguous geochronologic information, due to the documented open-system behavior of Rb and Sr during low-grade metamorphism of mafic rocks.

Time-integrated Sm/Nd ratios for Rhodesia, Abitibi, Isua, and the Onverwacht are consistent with derivation of these rocks from mantle source regions with bulk-earth Sm/Nd ratios.  However, due to the uncertainties associated with the time-integrated values, the data are also consistent with derivation from mantle which is evolving toward present-day oceanic mantle via first-order rate processes.  The time-integrated Rb/Sr ratio for clinopyroxenes from Abitibi is identical, within error, to predicted bulk-earth Rb/Sr ratios.  Because of the relatively short-half-life of $^{87}$Rb, the first order rate evolution curve for $^{87}Sr/^{86}Sr$ has diverged significantly from the bulk earth path at $\sim$2.6 billion years, so that the initial $^{87}Sr/^{86}Sr$ ratio from Abitibi is significantly higher than the value predicted by the first-order rate model.  These data, however, do not preclude the first-order rate model, because the rocks from Abitibi may be generated during a subduction-related process, which would predict high $^{87}Sr/^{86}Sr$ ratios and normal $^{143}Nd/^{144}Nd$ ratios.

The time-integrated Sm/Nd ratio from Cape Smith provides the first indication that the mantle had begun its evolution toward modern-day

oceanic mantle by ∿1.9 billion years. This age agrees quite well with times predicted for the divergence of previously undifferentiated mantle toward modern oceanic mantle, on the basis of Rb/Sr (Brooks et. al, 1976) and U-Pb (Tatsumoto, 1978) systematics in young oceanic basalts. Regardless, it must be stressed that the Sm-Nd systematics are equally consistent with a first-order rate process and a two-stage evolution process of the type suggested by Rb-Sr and U-Pb systematics.

Initial $^{87}Sr/^{86}Sr$ from Cape Smith clinopyroxenes suggest a subduction-related genesis for the Proterozoic belt. High $^{87}Sr/^{86}Sr$ ratios from an ultramafic sill, which intrudes a volcano-sedimentary, "slope and rise" sequence, may result from the involvement of altered oceanic crust in the magma generation process. Significantly lower $^{87}Sr/^{86}Sr$ from an allochthonous mafic volcanic association suggest that this may represent a slab of obducted oceanic crust. Again, this data does not distinguish between a first-order rate process and a two-stage evolution process for the oceanic mantle.

Constraints defined by Sm-Nd systematics in komatiites and associated rocks can be satisfied by two types of magma generation in the mantle: (1) heterogeneities created immediately prior to or during magma generation result in the production of liquids with variable Sm/Nd ratios; or (2) ultramafic komatiites result from the continued melting of mantle which is residual after tholeiite generation ("continuous melting"). Resolution of these processes awaits further experimental and geochemical constraints.

CHAPTER 4


THE SHABOGAMO INTRUSIVE SUITE, LABRADOR:

Sr AND Nd ISOTOPIC EVIDENCE FOR

CONTAMINATED MAFIC MAGMAS IN THE PROTEROZOIC

## 4.1  Introduction

The Shabogamo Intrusive Suite is a unit composed largely of gabbro
which intrudes Archean, Aphebian and Helikian sequences at the junction of
the Superior, Churchill and Grenville structural provinces in western
Labrador (Figure 4-1). The suite intrudes, post-tectonically, rocks of the
Churchill Province deformed during the Hudsonian Orogeny ($\sim$1800 m.y.;
Stockwell, 1972), and within the Grenville Province has been variably
affected by Grenvillian deformation and metamorphism ($\sim$1000 m.y.; Stock-
well, 1972).  On this basis the age of the suite has been broadly defined
as Helikian, but evidence for a more precise age assessment has been
lacking.  However, a general similarity between leucogabbroic phases of
the suite and early gabbroic phases of the Elsonian anorthosites (intruded
about 1400 m.y.; Stockwell, 1972) has led some workers (e.g., Fahrig, 1967)
to imply a correlation.

Direct attempts at dating the gabbro using radiometric techniques have
not clarified the situation.  Minerals from the mildly metamorphosed
Gabbro Lake intrusion yield K-Ar ages of $2570^{+}_{-}180$ m.y. and $3520^{+}_{-}72$ m.y.
(Wanless et. al., 1966; Wanless et. al., 1974) grossly in excess of the
age of the Aphebian rocks which the gabbros intrude.  Zodrow (1971) has
determined a Rb-Sr age of $1600^{+}_{-}130$ m.y. for amphibolite facies gabbros
within the Grenville Province.  This age has remained in question both
because of the high metamorphic grade of the rocks and because mineral
ages from these rocks have yielded approximately 1000 m.y. ages (e.g.,
biotite:  $1050^{+}_{-}140$ m.y.; Zodrow, 1971).

A detailed Sm-Nd and Rb-Sr isotopic investigation was initiated on
four gabbroic intrusions of the Shabogamo Intrusive suite representing

Figure 4-1. Regional geologic outline of southwestern Labrador

showing distribution of gabbros of the Shabogamo Intrusive

Suite. 1-McLean Lake area (ML); 2-Gabbro Lake area (GL);

3-Wabush-Labrador City, Locality 1 (WLC-1); 4-Wabush-Labrador

City, Locality 2 (WLC-2). Inset shows location of study area

relative to Grenville, Superior, and Churcill structural

provinces.
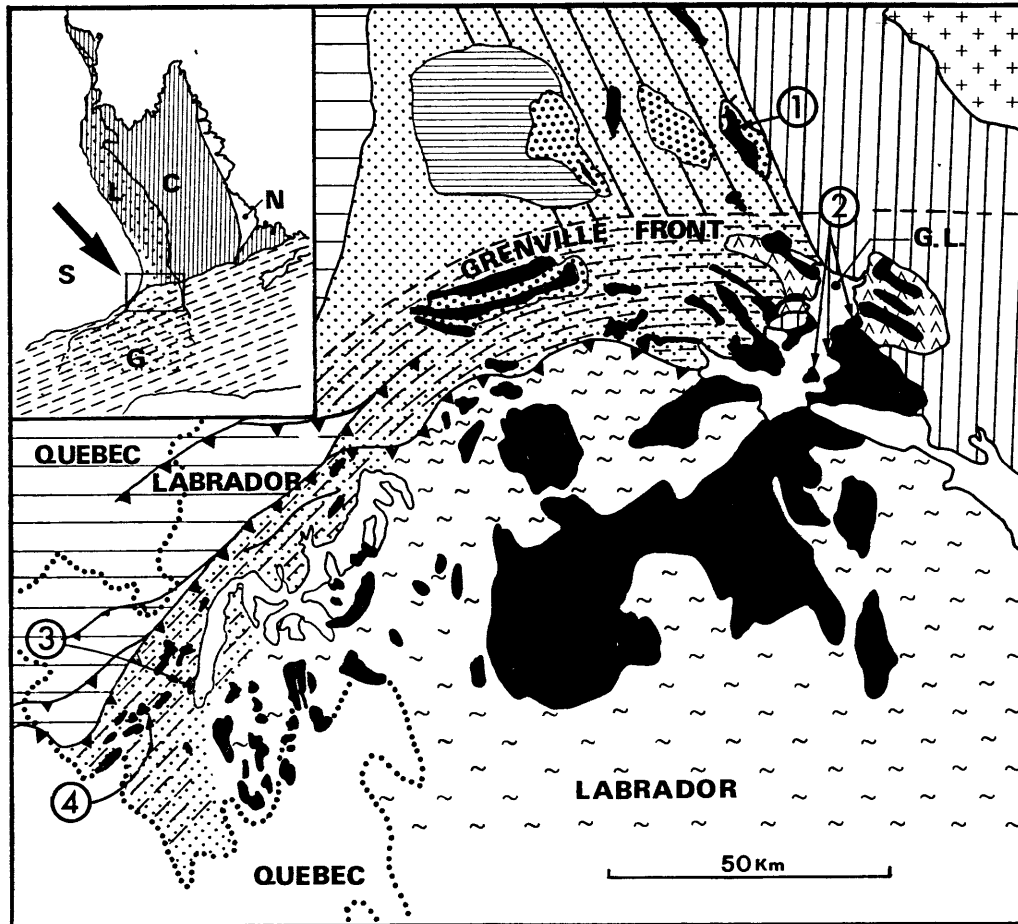
KANIAPISKAU SUPERGROUP

QUARTZOFELDSPATHIC SCHIST
AND GNEISS

ASHUANIPI METAMORHIC
COMPLEX

BLUEBERRY LAKE GROUP

HELIKIAN GRANITES

EASTERN BASEMENT METAMORPHIC
COMPLEX

SHABOGAMO INTRUSIVE SUITE

SIMS FORMATION

TAMARACK RIVER FORMATION

HUDSONIAN STRUCTURAL TRENDS

GRENVILLE STRUCTURAL TRENDS

Figure 4-1

(1) one body of unmetamorphosed gabbro from within the Churchill Province (MacLean Lake area; hereafter referred to as the ML body), (2) one body of mildly metamorphosed gabbro (greenschist facies) which lies on the eastern margin of the Labrador trough 30 km. south of the Grenville front (Gabbro Lake area; hereafter the GL body), and (3) two bodies of strongly metamorphosed gabbro (amphibolite facies) situated along the western margin of the Labrador trough, approximately 50 km. south of the Grenville front (Wabush-Labrador City area; hereafter referred to as WLC-1 and WLC-2). We considered that this investigation would enable us to contrast the behavior of the Sm-Nd and Rb-Sr systems under variable degrees of metamorphism. We also wished to precisely date the age of intrusion of the suite because its distribution across the Churchill-Grenville Province boundary makes the unit an ideal time-stratigraphic marker for establishing the absolute and relative chronology of events in the area.

This paper records the results of our investigation. It will be shown that while the Rb-Sr systematics are ambiguous, even in the unmetamorphosed gabbro, the Sm-Nd systematics are independent of metamorphic grade and provide a reliable age estimate for the time of intrusion at $1375 \pm 50$ m.y. Furthermore, it will be shown that coupled Sm-Nd and Rb-Sr systematics constrain the composition of the mantle-derived parental magma of the Shabogamo Intrusive suite. Mixing of this magma with a crustal component results in the liquid which crystallizes as the Shabogamo Gabbros.

4.2  Geological Outline


The area of investigation in Western Labrador lies at the junction of

the Superior, Churchill and Grenville structural provinces (Figure 1).

The following account of the stratigraphy and structural development of

this area is summarized from Brooks et. al.(in prep.).

The Superior Province, known locally as the Ashuanipi Metamorphic

Complex, consists of pyroxene bearing upper amphibolite to granulite

facies gneisses formed during the Kenoran Orogney.

The Churchill Province comprises a western zone (Labrador Trough) of

Aphebian sedimentary and volcanic rocks termed the Kanipiskau Super-group

and an eastern zone of granitic gneisses, locally termed the Eastern

Basement Complex by Wardle (1979).  The gneisses are probably of Archean

age (Dimroth et. al., 1970; Wardle, 1979), and represent a reworked

easterly extension of the Ashuanipi Metamorphic Complex.  Overlying the

Kaniapiskau Supergroup in the southwestern part of the Labrador Trough

(Figure 1) is a sequence of algal dolomite, arkose and argillite termed

the Tamarack River Formation, believed to be of late Aphebian age (Ware,

1979; Ware and Wardle, 1979).  This in turn is unconformably overlain

by the Helikian (?) clastic rocks (conglomerate, arkose, orthoquartzite)

of the Sims Formation (Ware and Wardle, 1979).  Within the Trough, the

Sims Formation and all older units are intruded by gabbros and associated

rocks of the Shabogamo Intrusive Suite.

The Grenville Province adjacent to the southwest projection of the

Labrador Trough is predominantly underlain by a continuation of the

Kaniapiskau Supergroup lithologies that occur within the Churchill

Province.  Subordinate amounts of migmatitic gneisses of the Ashuanipi

Metamorphic Complex occur near the contact with the Superior Province and many of the units have been intruded by gabbro and associated lithologies correlated with the Shabogamo Intrusive Suite.

Structural trends in the Churchill Province, in both the Labrador Trough and the Eastern Basement Complex, are typically northwest-southeast and were developed during the Hudsonian Orogeny. In the Grenville Province, the Kaniapiskau Supergroup has undergone polyphase deformation during the Grenvillian Orogeny (Rivers, 1978; Rivers and Massey, 1979). The northern limit of the province, known as the Grenville Front, is defined by a series of thrust faults (Rivers and Massey, 1979) and by the development of east-west and northeast-southwest trending cleavage superimposed on rocks of the adjacent structural provinces. Metamorphism within the Grenville Province increases southwards from greenschist facies in the Front zone to upper amphibolite facies 50 km south of the Front.

The gabbro intrusions (Figure 4-1) of this study have been chosen to reflect the varying metamorphic grade from (1) unmetamorphosed in the Labrador Trough (ML location) to (2) mildly metamorphosed (greenschist facies) in the Grenville Front zone where the Grenville effects are primarily manifest as narrow, widely spaced shear zones (GL location) to (3). strongly metamorphosed (amphibolite facies) in the Grenville Province, where the gabbros have been converted to garnet-hornblende-plagioclase-biotite assemblages (WLC locations). While the metamorphic effects in the Grenville Province are dominantly prograde, petrographic examination of the two WLC gabbros sampled reveals that one of the gabbros (WLC-2) has been retrograded, resulting in the partial conversion of the high grade metamorphic assemblage to diffuse aggregates of hydrous

phases accompanied by calcite.  A detailed account of the petrography of

the samples analyzed is given by Brooks et. al (1980).

## 4.3 Results

Isotopic data on rocks and minerals from the three areas are given in Table 4-1 (Rb-Sr) and Table 4-2 (Sm-Nd). Figure 4-2a is a Rb-Sr isochron diagram for whole rock samples from the unmetamorphosed area (ML) and the mildly metamorphosed area (GL). If we exclude CBL 23 (a pegmatitic differentiate), CBL 27 (a hornfels sediment), and CBL 35 (a highly altered gabbro), the remaining points define an isochron (errorchron) with an age of 1683±64 m.y. There is some scatter of data about this line over and above experimental error which must be ascribed to "geologic" effects. Figure 4-2b is a Rb-Sr isochron diagram of only the mafic rocks (Rb/Sr<.06), including minerals separated from samples CBL 25 and CBL 42. On this expanded plot, the deviation of points from a line (in excess of experimental error) is more clearly seen. The regression line to this data gives an age of 1366±171 m.y., significantly younger than the whole rock isochron discussed above. Biotites separated from CBL 25 and CBL 42 are not shown on this plot, but regression analyses of mineral-whole rock data (biotite-cpx-plag.-w.r.) for these two samples yields ages of 1425±22 m.y. and 1190±80 m.y., respectively. In other words, biotite CBL 42 (from the lightly metamorphosed area) is clearly younger than biotite CBL 25 (from the unmetamorphosed area). An isochron of approximately 1400 m.y. is thus a good representation of all the mafic whole rock (Rb/Sr<.06) and mineral data with the exception of the young biotite, CBL 42. As discussed above, the more felsic whole rocks define a distinctly older isochron (shown in Figure 4-2b as a dashed line).

Figure 4-3 is a Rb-Sr isochorn diagram for whole rock samples from the strongly metamorphosed areas, WLC-1 and WLC-2. Garnet amphibolites

Table 4-1

Sr Isotopic compositions and Rb and Sr concentrations for Shabogamo Intrusive Suite

| Sample No. | Locality | Rb (ppm) | Sr (ppm) | $^{87}Rb/^{86}Sr$** | $^{87}Sr/^{86}Sr$* |
|---|---|---|---|---|---|
| CBL 2 | WLC-1 | 14.31 | 373.0 | 0.1111 | 0.70626±5 |
| CBL 3 | WLC-1 | 16.15 | 381.1 | 0.1227 | 0.70644±9 |
| CBL 4 | WLC-1 | 15.61 | 368.7 | 0.1226 | 0.70659±5 |
| CBL 5 | WLC-1 | 11.71 | 423.6 | 0.0801 | 0.70608±4 |
| CBL 6 | WLC-1 | 21.79 | 312.9 | 0.2017 | 0.70766±5 |
| CLB 7 | WLC-1 | 15.67 | 433.6 | 0.1047 | 0.70667±8 |
| CBL 8 | WLC-1 | 18.43 | 392.6 | 0.1359 | 0.70687±5 |
| CBL 9 | WLC-1 | 21.09 | 452.5 | 0.1350 | 0.70662±6 |
| CBL 10 | WLC-1 | 9.93 | 923.3 | 0.03115 | 0.70528±4 |
| CBL 11 | WLC-1 | 34.52 | 215.7 | 0.4635 | 0.71383±5 |
| CBL 13 | WLC-2 | 20.48 | 319.7 | 0.1855 | 0.70809±4 |
| CBL 14 | WLC-2 | 21.13 | 384.8 | 0.1590 | 0.70790±6 |
| CBL 15 | WLC-2 | 20.88 | 309.3 | 0.1955 | 0.70801±4 |
| CBL 16 | WLC-2 | 39.65 | 244.2 | 0.470 | 0.71192±5 |
| CBL 18 | ML | 47.0 | 209.7 | 0.650 | 0.71933±8 |
| CBL 21 | ML | 13.02 | 289.2 | 0.1304 | 0.70687±8 |
| CBL 22 | ML | 11.95 | 256.9 | 0.1347 | 0.70668±7 |
| CBL 23 | ML | 28.65 | 206.4 | 0.402 | 0.71525±8 |
| CBL 25 | ML | 12.78 | 329.8 | 0.1122 | 0.70641±6 |
| CBL 25 CPX | ML | 0.532 | 21.83 | 0.0707 | 0.70582±5 |
| CBL 25 PL | ML | 5.18 | 565.8 | 0.0265 | 0.70473±4 |
| CBL 25 BT | ML | 427.0 | 25.41 | 53.8 | 1.80768±21 |
| CBL 26 | ML | 25.93 | 336.3 | 0.2233 | 0.70922±9 |
| CBL 27 | ML | 87.0 | 189.0 | 1.337 | 0.73857±12 |
| CBL 28 | ML | 11.78 | 315.7 | 0.1081 | 0.70616±7 |
| CBL 29 | GL | 7.86 | 344.6 | 0.0661 | 0.70551±7 |
| CBL 30 | GL | 12.49 | 326.1 | 0.1107 | 0.70588±8 |
| CBL 32 | GL | 8.80 | 375.0 | 0.0679 | 0.70523±7 |
| CBL 33 | GL | 8.94 | 352.7 | 0.0734 | 0.70540±8 |
| CBL 34 | GL | 11.92 | 302.6 | 0.1141 | 0.70625±5 |
| CBL 35 | GL | 30.93 | 155.1 | 0.576 | 0.71300±7 |
| CBL 41 | GL | 11.76 | 219.4 | 0.1551 | 0.70710±10 |
| CBL 42 | GL | 9.28 | 343.2 | 0.0783 | 0.70550±9 |
| CBL 42 CPX | GL | 0.663 | 22.18 | 0.0866 | 0.70579±5 |
| CBL 42 PL | GL | 3.075 | 634.8 | 0.0140 | 0.70418±4 |
| CBL 42 BT | GL | 340.8 | 31.63 | 32.85 | 1.26000±25 |
| CBL 43 | GL | 45.8 | 274.4 | 0.483 | 0.71527±5 |
| CBL 44 | GL | 15.17 | 340.1 | 0.1290 | 0.70653±6 |

* Errors are in last significant digits and represent $2\sigma_m$ confidence level.
  $^{87}Sr/^{86}Sr$ values are relative to 0.70800 for the E and A standard.

** Estimated errors, on the basis of replicate analyses, are better than ±0.7%.

Figure 4-2a. Rb-Sr isochron diagram for whole-rock samples from MacLean Lake and Gabbro Lake areas. A regression analysis for the data, excluding CBL 23, CBL 35 and CBL 27, yields an age of 1683±64 m.y. ($2\sigma_m$) and an initial $^{87}Sr/^{86}Sr$ ratio of 0.70357±16 ($2\sigma_m$). ($\lambda^{87}Rb = 1.42 \times 10^{-11} y^{-1}$).

Figure 4-2a

133
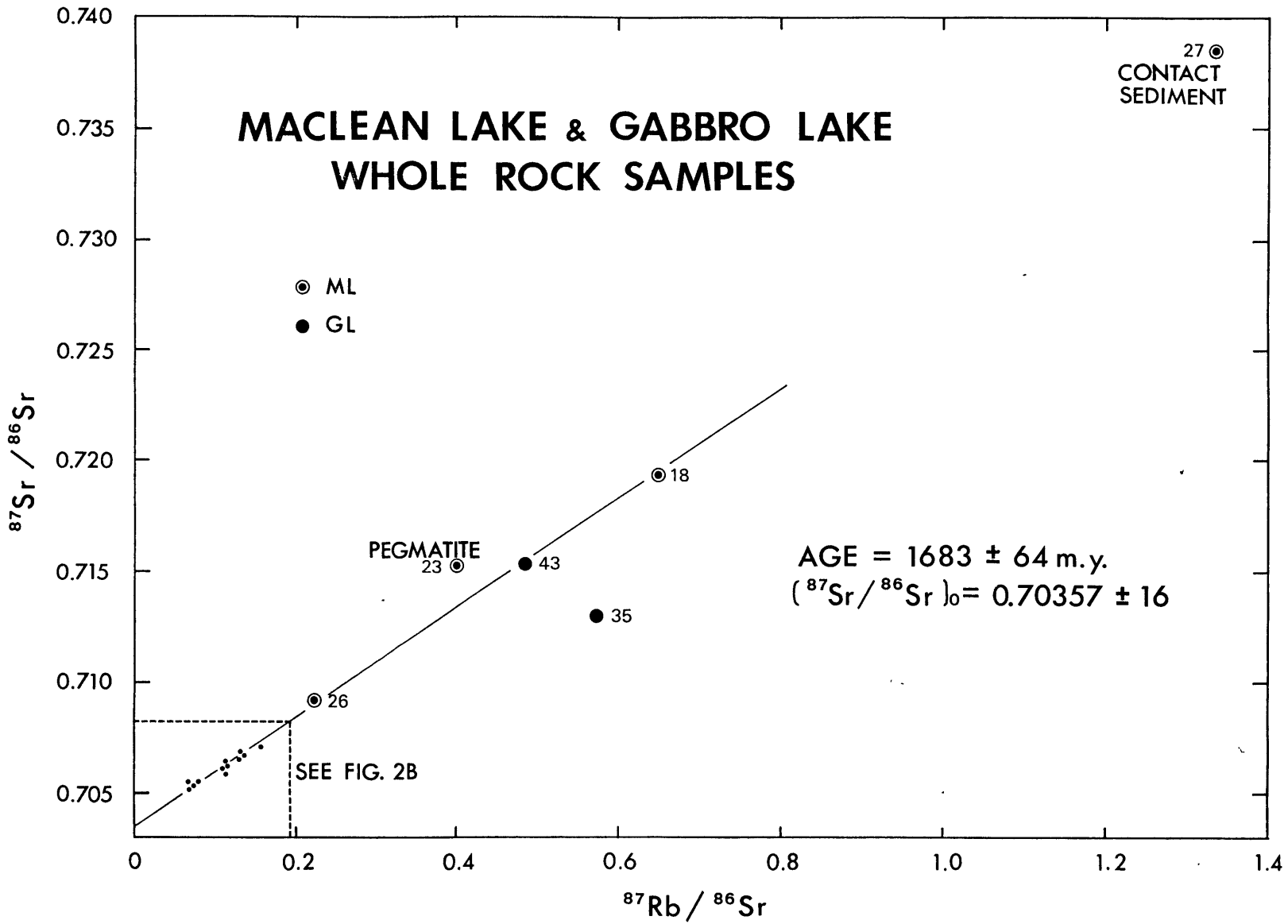
Figure 4-2b. Rb-Sr isochron diagram for whole-rocks and minerals, from MacLean Lake and Gabbro Lake areas, with $^{87}Rb/^{86}Sr<0.18$. The data define an age of $1366\pm171$ m.y. ($2\sigma_m$) and an initial $^{87}Sr/^{86}Sr$ ratio of $0.70407\pm24$ ($2\sigma_m$). Estimated errors in $^{87}Sr/^{86}Sr$ and $^{87}Rb/^{86}Sr$ are shown by error bars.

**MACLEAN LAKE & GABBRO LAKE**

$(^{87}Rb/^{86}Sr < 0.18)$

⊙ ML
● GL

25 CPX
42 CPX
25 PL
42 PL

29  32  33  42
28  30  34  25  44  22  21  41

AGE = 1366 ± 171 m.y.
$(^{87}Sr/^{86}Sr)_0 = 0.70407 ± 24$

$^{87}Rb/^{86}Sr$

$^{87}Sr/^{86}Sr$

Figure 4-2b

135
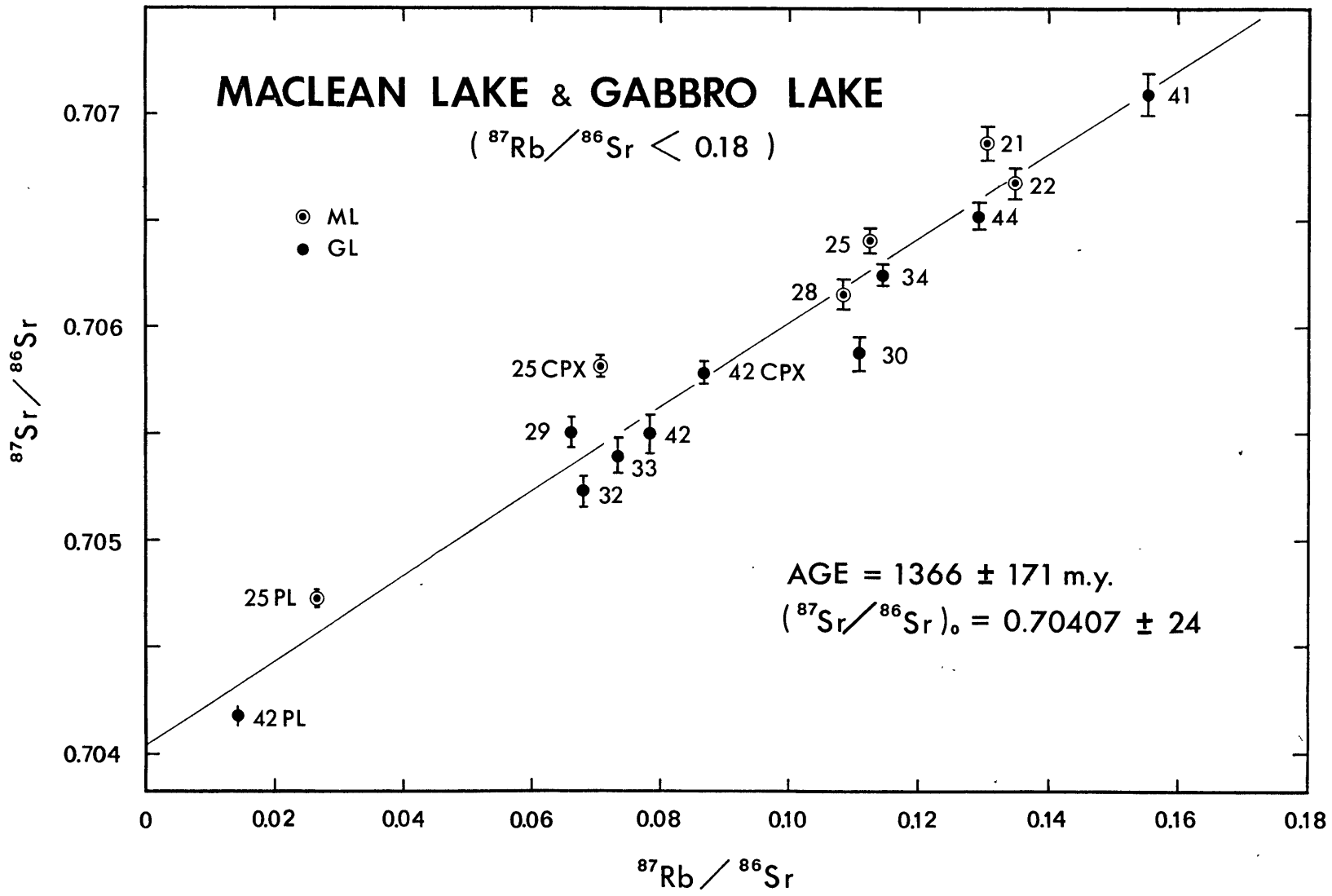
from the WLC-1 body (CBL-2-11) scatter about an errorchron which gives an

age of $1368^{+}_{-}170$ m.y. Samples from WLC-2 (CBL 13-16), which have mineral

assemblages indicative of retrogression from garnet amphibolite facies,

define a Rb-Sr isochron with an age of $934\pm128$m.y. The older age is

remarkably similar to the Rb-Sr 1375 m.y. age for the unmetamorphosed and

mildly metamorphosed mafic rocks.

Figure 4-4 is a Sm-Nd isochron diagram for rocks and minerals from all

four areas. With the exception of CBL 14 and CBL 16, all points lie within

experimental error of an isochron with an age of $1375^{+}_{-}50$ m.y. Separates

of calcic plagioclase and clinopyroxene from CBL 25 (from the unmetamor-

phosed ML body), together with the whole rock, define an isochron of

$1363^{+}_{-}47$ m.y. That CBL 14 and CBL 16 lie above the isochron outside of

experimental error may be explained in terms of the retrograde mineral

assemblage observed in these rocks. This is discussed in more detail in

a subsequent section.

Table 4-2

Nd isotopic compositions and Sm and Nd concentrations for Shabogamo Intrusive Suite

| Sample No. | locality | Sm (ppm) | Nd (ppm) | $^{147}Sm/^{144}Nd$ | $^{143}Nd/^{144}Nd*$ |
|---|---|---|---|---|---|
| CBL 6 | WLC-1 | 4.491 | 21.58 | 0.1258 | 0.511731±18 |
| CBL 10 | WLC-1 | 5.655 | 28.31 | 0.1208 | 0.511658±11 |
| CBL 11 | WLC-1 | 4.617 | 22.36 | 0.1249 | 0.511703±24 |
| CBL 14 | WLC-2 | 7.518 | 36.02 | 0.1262 | 0.511756±7 |
| CBL 16 | WLC-2 | 7.397 | 34.77 | 0.1286 | 0.511782±16 |
| CBL 25 | ML | 4.208 | 18.62 | 0.1366 | 0.511809±28 |
| CBL 25 CPX | ML | 5.445 | 17.09 | 0.1926 | 0.512319±22 |
| CBL 25 PL | ML | 0.6882 | 3.607 | 0.1153 | 0.511630±20 |
| CBL 42 | GL | 2.934 | 12.97 | 0.1367 | 0.511783±26 |
| CBL 42 CPX | GL | 3.791 | 11.32 | 0.2024 | 0.512403±20 |
| CBL 43 | GL | 6.610 | 31.04 | 0.1287 | 0.511724±14 |

* Errors are in last significant digit and represent $2\sigma_m$ confidence level. $^{143}Nd/^{144}Nd$ values are normalized to $^{146}Nd/^{144}Nd = 0.72190$.

** Estimated errors, on the basis of replicate analyses, are better than ±0.3% ($2\sigma_m$).

Figure 4-3. Rb-Sr isochron diagram for whole-rock samples from
Wabush-Labrador City areas (WLC-1 and WLC-2). Four analyses from
WLC-2 define an age of 934±128 m.y. and an initial ratio of
0.7056±5. Ten samples from WLC-1 define an age of 1368±170 m.y.
and an initial ratio of 0.7043±4. If CBL 11 is excluded, the
remaining data define an age of 946±182 m.y. and an initial ratio
of 0.7049±3 (all errors quoted at $2\sigma_m$ confidence level).

WABUSH-LABRADOR CITY AREA

☒ WLC-1
▲ WLC-2

1368 ± 170 m.y.

934 ± 128 m.y.

$^{87}Sr/^{86}Sr$

$^{87}Rb/^{86}Sr$

Figure 4-3

139
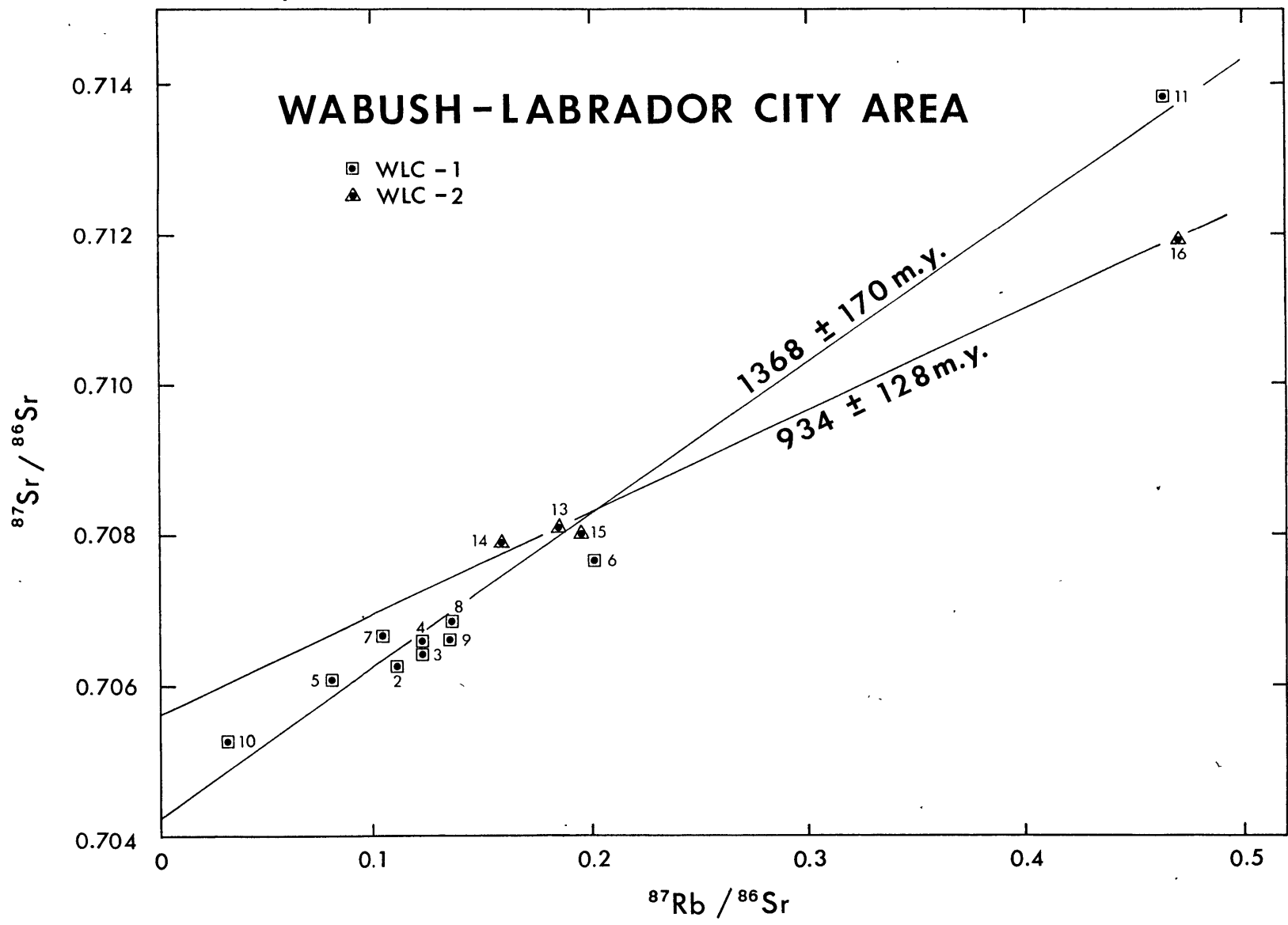
Figure 4-4. Sm-Nd isochron diagram for all samples from the

Shabogamo Intrusive Suite. Excluding CBL 14 and CBL 16 (see

discussion in text), the data yield an age of $1375\pm54$ $(2\sigma_m)$ and

an initial $^{143}$Nd/$^{144}$Nd ratio of $0.51057\pm6(2\sigma_m)$.

SHABOGAMO INTRUSIVE SITE

⊙ ML
● GL
⊡ WLC-1
▲ WLC-2

AGE = 1375 ± 54 m.y.

$\left(^{143}Nd/^{144}Nd\right)_0 = 0.51057 \pm 6$

Figure 4-4

141
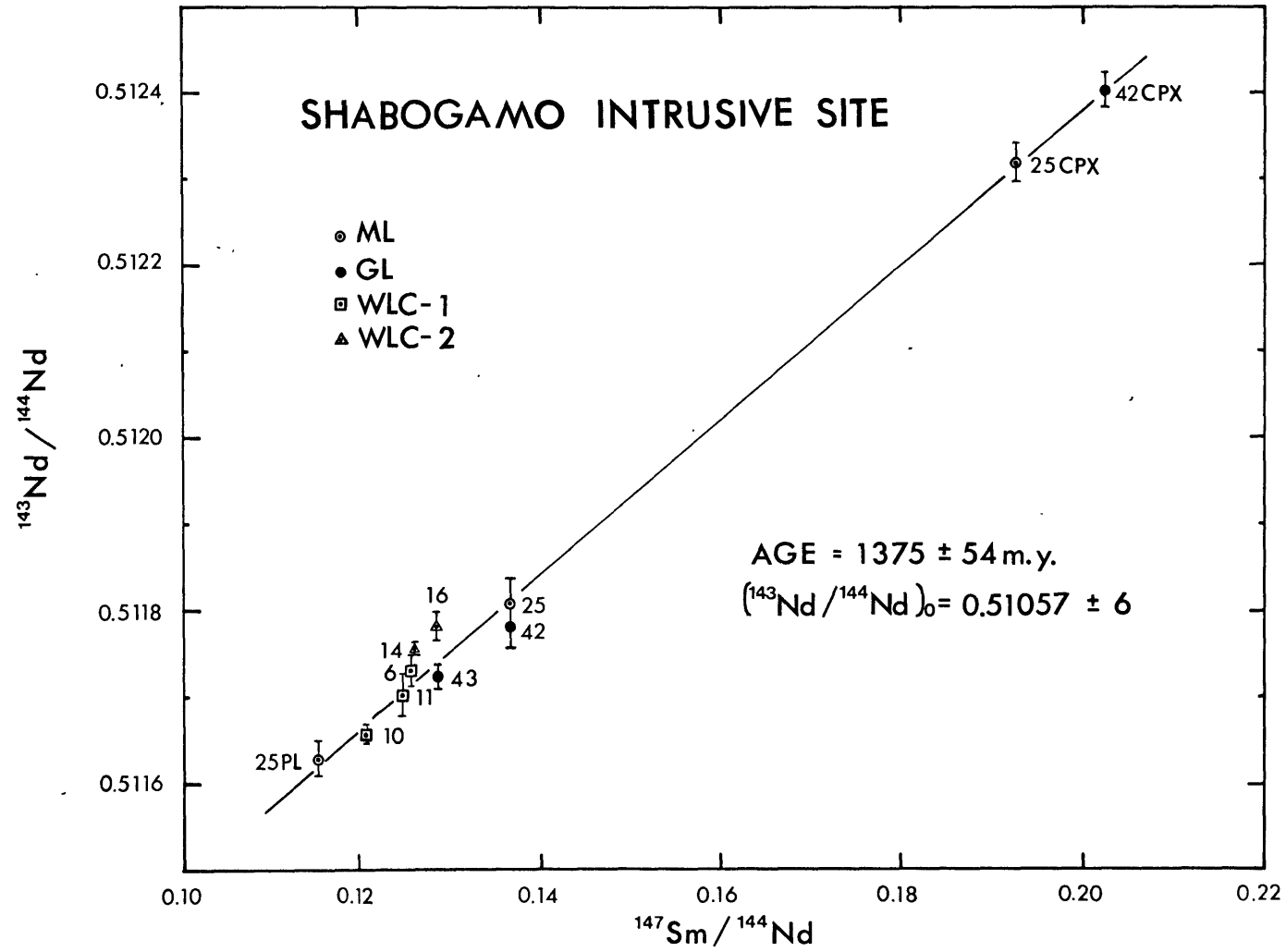
## 4.4 Timing of magmatism and metamorphism.

Determination of the time of emplacement of the unmetamorphosed and lightly metamorphosed gabbros of the ML and GL areas hinges on comparison of the 1690 m.y. Rb-Sr isochron and the 1375 m.y. Sm-Nd isochron. The clinopyroxenes and calcic plagioclase analysed for Sm-Nd represent primary phases in rocks where secondary phases are restricted to late-stage deuteric minerals (Brooks et al., 1980). We consider that these minerals, if crystallized at $\sim$1600 m.y., could not have been completely reset at $\sim$1375 m.y. without producing major changes in the primary mineralogy of the gabbros. In addition, there is no record of any regional metamorphism in the interval between 1750 m.y. (Hudsonian orogeny) and 1000 m.y. (Grenville orogeny). Consequently we consider that the 1375 m.y. Sm-Nd age, based on minerals and whole rocks from the ML and GL areas, documents the time of crystallization of the gabbro intrusives.

This interpretation is consistent with (1) the existence of a regional magmatic event in the Churchill Province at about 1400 m.y. and; (2) a 1540±40 m.y. Rb-Sr total rock isochron for felsic volcanics of the Blueberry Lake group (Brooks et. al., 1980) which are intruded by gabbros in the vicinity of GL. The Sm-Nd age is also consistent with the 1375±120 m.y. Rb-Sr isochron age for the more mafic gabbros from ML and GL, and with the 1427±67 m.y. Rb-Sr biotite age on CBL 25, from the unmetamorphosed ML body. The high Rb/Sr ratios in CBL 13, 23, 43, and 26 can be attributed to relatively large percentages of late-stage deuteric minerals (sericite, etc.). We consider two possible processes capable of explaining the displacement of these rocks to lower Rb/Sr and/or higher $^{87}Sr/^{86}Sr$, thereby defining the anomalously high 1660 m.y.

age: (1) fluids circulating during the final stages of crystallization became selectively enriched in radiogenic Sr through interaction with the country rock (support for the existence of fluids of this composition is seen in CBL 23, a pegmatite which represents the last liquid to crystallize in the ML body); (2) recent weathering at or near the surface may have selectively leached Rb from the sheet silicates, causing displacement of the rocks to lower Rb/Sr values by amounts proportional to the respective modal abundances of sheet silicates.

Sr and Nd isotopic data from the two strongly metamorphosed WLC bodies provides constraints on the timing of Grenville metamorphism in this region, as well as information about the effects of the metamorphism on the respective decay systems. Rb-Sr data for the WLC-2 body (CBL 13-16), which contains retrograde mineral assemblages, define as isochron with an age of $935^{+}_{-}60$ m.y. (Figure 4-3) and documents the waning stages of Grenville metamorphism in this region. Sm-Nd data for CBL 14 and 16 are displaced to the left of the isochron in Figure 4-4, and we consider that while the Sm-Nd system was not subject to large scale re-equilibration at circa 935 m.y., the partial breakdown of garnet during the retrograde process has caused the whole rocks to shift to lower Sm/Nd values.

Rb-Sr data for the WLC-1 body (CBL 2-11) scatter about an errorchron which gives an age of $1368^{+}_{-}170$ m.y. The Rb-Sr system has not been homogenized by the metamorphism in this body, as it was in WLC-2, though certainly it was severely distrubed. The disparity between the effects of the metamorphism on Rb-Sr systematics in the two WLC areas can be explained by the differences in mineralogy in the two bodies. Whereas it has already been mentioned that WLC-2 rocks show a retrograde mineral

assemblage, rocks of WLC-1 retain a mineral assemblage consistent with the garnet amphibolite metamorphic grade (Brooks et. al., in prep.). On this basis, we propose that more fluids were available in the WLC-2 area during the late stages of metamorphism.

Sm-Nd data on the WLC-body (CBL 6, 10, 11) is consistent with this hypothesis in that these rocks plot within error on the Sm-Nd isochron in Figure 4-3 along with rocks from the mildly metamorphosed GL body and the unmetamorphosed ML body.

## 4.5 Genesis of the magma series.

Nd and Sr isotopic data for the four intrusions studied are consistent with an origin by the crystallization of magmas of similar isotopic composition, approximately 1375 m.y. ago. Furthermore, the mafic nature of these intrusions precludes their derivation by melting of lower crustal material exclusively, and must involve some mantle-derived component. To develop constraints on the genesis of Shabogamo Intrusive Suite magmas, we have examined mixing relationships between proposed mantle-derived magmas and possible crustal sources for contamination of these magmas.

Before going on to describe specific models, we will summarize relevant current theories for bulk earth trace element content; we will then use this as the basis for estimating the isotopic composition of mantle-derived materials, at a particular time in the earth's history. Measurements of primordial Nd in the basaltic achondrites Juvinas and Angra dos Reis (Lugmair et. al., 1975; Lugmair and Scheinin, 1976) provide estimates of $^{143}Nd/^{144}Nd$ at the time of formation of planetary material, approximately 4.56 b.y. ago. These estimates, together with an average Sm/Nd value measured in chondritic material (Nakamura, 1974; Evensen et. al., 1978), enable one to model the evolution of $^{143}Nd/^{144}Nd$ in planetary material through time. Based on the long-standing hypothesis that the bulk earth contains chondritic-relative abundances of rare-earth elements, we may consider this as a bulk-earth evolution line for $^{143}Nd/^{144}Nd$ (Fig. 4-5a). The observed correlation of $^{143}Nd/^{144}Nd$ and $^{87}Sr/^{86}Sr$ in young mantle-derived volcanic rocks (Richard et. al., 1976; O'Nions et. al., 1977; DePaolo and Wasserburg, 1977) provides an estimate

Figure 4-5a.   $^{143}$Nd/$^{144}$Nd evolution diagram.   See text for

discussion of Shabogamo and Stillwater data.   Evolutionary

parameters are given in Table 3-3 and in caption for Figure 3-6.

$^{143}Nd/^{144}Nd$ EVOLUTION DIAGRAM

BAY OF ISLANDS

MORB-TYPE MANTLE EVOLUTION

BULK EARTH EVOLUTION

1st ORDER RATE MODEL

QUEBEC COMPOSITE

SHABOGAMO I.S.

ARCHEAN CRUSTAL EVOLUTION

CAPE SMITH KOMATIITES

ABITIBI KOMATIITES & THOLEIITES

RHODESIAN GREENSTONES

STILLWATER COMPLEX

ONVERWACHT VOLCANICS

ISUA SUPRACPUSTALS

ANGRA DOS REIS JUVINAS

TIME ( BILLIONS OF YEARS BEFORE PRESENT )

Figure 4-5a

Figure 4-5b. $^{87}Sr/^{86}Sr$ evolution diagram. See text for

discussion of Shabogamo and Stillwater data. Evolutionary

parameters are given in Table 3-3 and in caption for Figure 3-7.

⁸⁷Sr/⁸⁶Sr EVOLUTION DIAGRAM
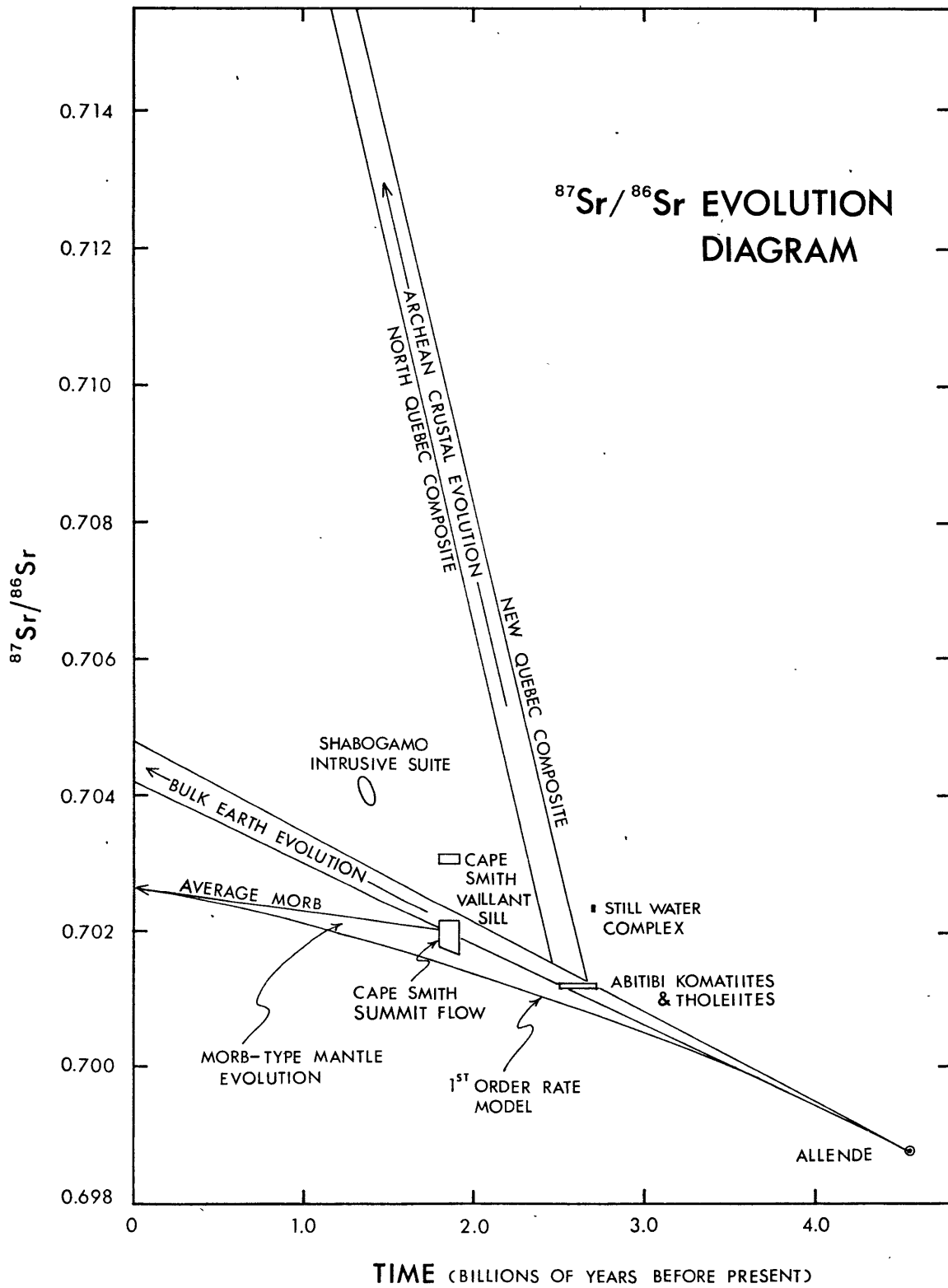
Figure 4-5b

for present-day $^{87}Sr/^{86}Sr$ in the bulk earth, and using arguments similar
to those set forth for Nd, we arrive at a bulk-earth evolution line for
$^{87}Sr/^{86}Sr$ (Fig. 4-5b). Initial ratios and crystallization ages for mantle-
derived rocks, shown as error ellipses in Fig. 4-5, have provided support
for the choice of these bulk-earth evolution lines (Hamilton et. al.,
1977; Hamilton et. al., 1978; Hamilton et. al., 1979; DePaolo and
Wasserburg, 1979; Jacobsen and Wasserburg, 1980; and Chapter 3).

Also plotted in Figure 4-5 are evolution lines for composites of
surface crustal material of Archean age analyzed for major and trace
elements by Shaw et. al. (1967) and for Nd and Sr isotopic compositions
by McCulloch and Wasserburg (1978). It can be seen that the initial
values of $^{143}Nd/^{144}Nd$ and $^{87}Sr/^{86}Sr$ for the Shabogamo Intrusive Suite
plot between the bulk-earth evolution lines and the evolution lines for
the Archean crustal material at 1375 m.y. Because there is no evidence
for "enriched" mantle (Rb/Sr> 0.03; Sm/Nd< 0.32) in Proterozoic time,
we conclude that the Shabogamo magma has resulted from mixing of a mantle-
derived magma with a crustal-derived component at the time of emplacement
into the crust. Furthermore, because young continental volcanic rocks
have been shown to have isotopic compositions broadly similar to present-
day bulk-earth values (DePaolo and Wasserburg, 1976; DePaolo and Wasserburg,
1979; and Chapter 2), we propose, for the sake of our model, that the
mantle-derived component of the Shabogamo magma had Nd and Sr isotopic
compositions similar to the bulk earth at 1375 m.y. Had we assumed a
mantle component derived from "MORB-type" mantle, the conclusions which
result from the modeling would not be qualitatively different.

Figure 4-6 is a plot of $^{143}Nd/^{144}Nd$ vs. $^{87}Sr/^{86}Sr$ at 1375 m.y., the
time of emplacement of the Shabogamo Intrusive Suite. Bulk-earth and

Figure 4-6. $^{143}$Nd/$^{144}$Nd vs. $^{87}$Sr/$^{86}$Sr at 1375 m.y. Bulk earth

and MORB values are calculated from data given in Table 3.3 and

in captions for Figures 3-6 and 3-7.

THE EARTH AT 1.375 B.Y.

MORB-TYPE MANTLE

BULK EARTH

SHABOGAMO INTRUSIVE SUITE

ARCHEAN CRUST AT 1.375 B.Y.

MIXING LINE BETWEEN BULK EARTH AND ARCHEAN CRUST

$^{143}Nd/^{144}Nd$

$^{87}Sr/^{86}Sr$
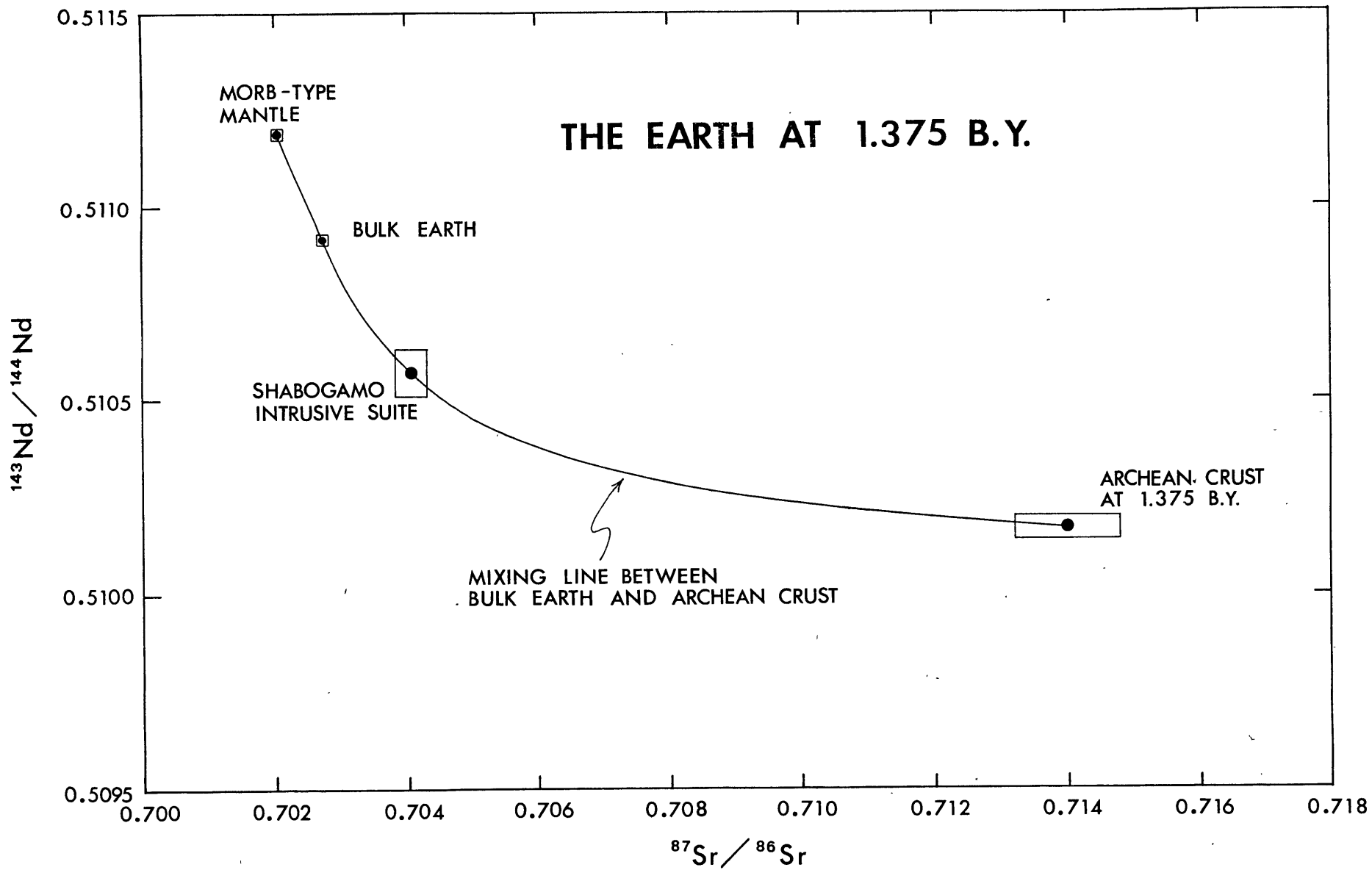
Figure 4-6

"MORB-type" mantle values are plotted on the diagram indicating the possible range of mantle compositions at that time. Also shown is a field for Archean rocks at 1375 m.y. taken from McCulloch and Wasserburg's analyses of New Quebec and North Quebec composites of Superior Province materials (McCullock and Wasserburg, 1978). These composites represent the best available estimates for cratonic materials which are in close spatial association with the area of this study. Consideration of the relationship of the Shabogamo Intrusive Suite to the bulk-earth and Archean field on this diagram constrains the fractions of Nd and Sr derived from each of the end members, to produce the Shabogamo magma. In addition, the shape of the mixing curve on this diagram also constrains the Sr/Nd ratios in both end members and we must examine these in terms of realistic Sr and Nd concentrations in magmas in order to assess the viability of the model. (For an in-depth discussion of the systematics of mixing relationships, the reader is referred to Langmuir et. al., 1978.)

Nd and Sr analyses for basalts, taken from the literature (Schnetzler and Philpotts, 1970; Philpotts and Schnetzler,1970; DePaolo and Wasserburg, 1976b; O'Nions et. al., 1977; DePaolo and Wasserburg, 1979; Shibata et al., 1979), are plotted in Fig. 4-7, a variation diagram of Sr vs. Nd. The Shabogamo Intrusive Suite values used in this diagram represent an average of gabbros with Rb/Sr <.06. For reference, we have drawn two curves which represent equilibrium batch melting of a mantle composed of 55% olivine, 25% orthopyroxene, 10% garnet and 10% clinopyroxene, and having, arbitrarily, three times Cl chondrite abundances of Sr (Jagoutz, pers. comm.) and Nd (Evensen, 1978). (See section 4.7 for discussion of partition coeffi-

Figure 4-7. Variation diagram of Nd vs. Sr mantle and crustal

melting parameters are discussed in section 4.7and listed in

Tables 4-3 and 4-4 . Numbers adjacent to melting curves indicate

the percentage of the total source which has melted. Olivine

and plagioclase fractionation curves are shown for reference (see

text), and dots on curves indicate 10% fractionation intervals.

Examples of mixing lines, between possible crustal and mantle melt

compositions, are shown. The lines labeled Sr/Nd = 23.4 and Sr/Nd =

3.65 are, respectively, possible mantle magma and possible contaminant

lines which result from the isotopic constraints. The shaded fields

around these lines represent $2\sigma$ error limits based on the uncertainties

in the initial $^{143}Nd/^{144}Nd$ and $^{87}Sr/^{86}Sr$. Data for oceanic basalts

are shown by open circles and data for continental basalts are shown

by open triangles. Localities and sources for the data are as

follows: 1- 10 basalts from Tortuga Islands, Batiza et al. (1979;

2- 4 mid-ocean ridge basalts, Philpotts et al. (1969); 3- 7 basalts

from the Bouvet ridge, Dickey et al. (1977); 4- 2 leg 34 basalts,

Hart (1976); 5- 4 basalts from the Scotia ridge, Sanders and Tarney

(1979); 6- 4 leg 15 basalts from the Caribbean,      et al. (1975);

7- 4 West Mariana Basin basalts, Dietrich et al. (1978); 8- 8 leg 49

basalts from 63°N-MAR, Wood et al. (1977); 9- 4 leg 49 basalts from

45°N-MAR, Wood et al. (1977); 10- 5 leg 49 basalts from 36°N-MAR,

Wood et al. (1977); 11- 6 mid-ocean ridge basalts, Sun et al. (1979);

12- 1 basalt from Greenland, Philpotts and Schnetzler (1970); 13-

2 basalts from 43°N-MAR, Shibata et al. (1979); 14-1 Karoo basalt,

DePaolo and Wasserburg (1976b); 15- 5 Hawaiian basalts, O'Nions et

al. (1977); 16- 9 basalts from the Reykjanes Peninsula (Chapter 1);

17 - 6 Siberian flood basalts, Depaolo and Wasserburg (1979);

18 - 3 Columbia River basalts, DePaolo and Wasserburg (1979).
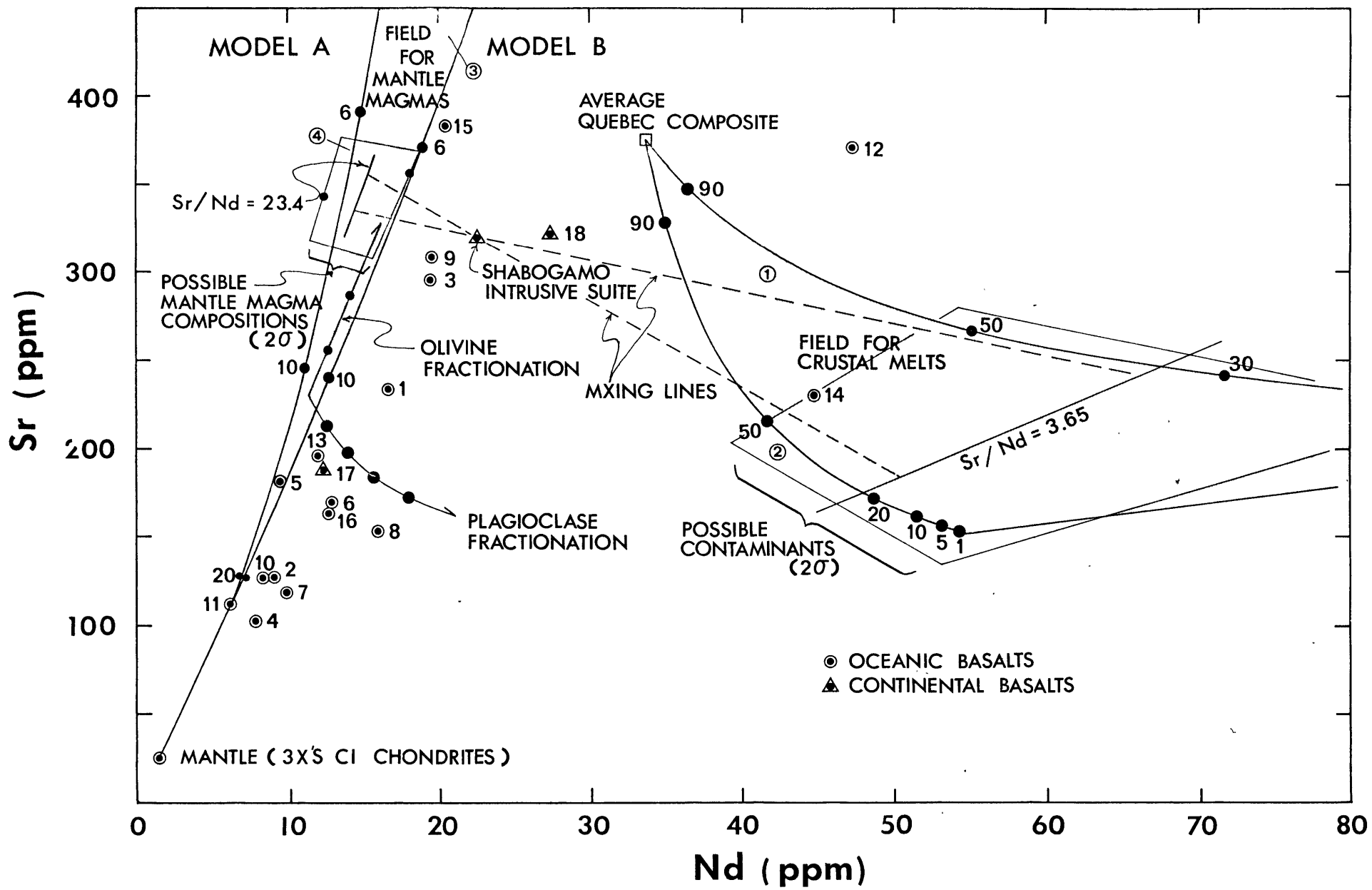
Figure 4-7

cients.) It can be seen in Fig. 4-7 that, although the basalts from oceanic regions form a coherent array which is sub-parallel to the mantle melting curve, they are always displaced to the right of this curve. We interpret the shift of these oceanic basalts to the right of predicted mantle melt compositions as being due to high level fractional crystallization of olivine and/or plagioclase (see examples in Fig. 4-7). Interpretation of this shift for the Shabogamo Intrusive Suite, as well as for basalts which have been erupted through old cratons, is not as straightforward because effects of contamination by continental material must be considered.

As was mentioned above, the Sr/Nd ratios in the mantle-derived melt and the proposed contaminant are fixed by consideration of Fig. 4-6, the $^{87}Sr/^{86}Sr$ vs. $^{143}Nd/^{144}Nd$ diagram. In order to satisfy the isotopic constraints, the mantle-derived melt must have Sr/Nd = 23.4, and the contaminant Sr/Nd = 3.65. Lines with these slopes are drawn in Fig. 4-7 and it can be seen that the necessary mantle-melt Sr/Nd ratio lies within the region predicted for mantle melt compositions by equilibrium batch melting models. Also, the Sr/Nd ratio in the average Quebec composite is very different from that required by the isotopic constraints for the contaminant and we conclude that mass assimilation, by a mantle-derived magma, of crustal material similar to that sampled in the Quebec composites, cannot produce the Shabogamo magma.

However, melting of crustal material, triggered by an elevated geotherm and intrusion of large quantities of basaltic magma into the crust, can produce liquids with Sr/Nd ratios in the range required by the isotopic constraints. In Fig 4-7, a field of liquid compositions is outlined which may be produced by melting of "granitic" material with the Sr and Nd

concentrations of the average Quebec composite. Two bulk partition

coefficients were chosen to represent a reasonable range for granitic

material (see Section 4.7).

In summary, a mantle-derived melt produced at 1375 m.y. with bulk-

earth Nd and Sr isotopic ratios can have mixed with a partial melt of

granitic material in the crust (approximately 5:1 by volume) to produce

the magma which crystallized as the Shabogamo Intrusive Suite. A similar

situation has been described by DePaolo and Wasserburg (1979) for the

Stillwater Complex (see Figure 4-5). DePaolo and Wasserburg acknowledge the

possibility of crustal contamination of the magma and we consider that

the model derived here would also be applicable for the Stillwater

Complex. However, this is a preferred model and does not constitute a

unique interpretation of the initial Nd and Sr isotopic compositions of the

Shabogamo gabbros. Faced with similar isotopic evidence for recent

volcanics, several authors have chosen to propose that the volcanics were

derived from "enriched" source regions in the mantle (Carter et. al., 1978;

Hawkesworth et. al., 1979). Rocks from Roccamonfina and Vesuvius, in

Italy, have been shown by Carter et. al. (1978) and Hawkesworth et. al.

(1979), respectively, to have $^{87}Sr/^{86}Sr$ which is higher than the present-

day bulk earth value and $^{143}Nd/^{144}Nd$ lower than the bulk earth value. In both

of these cases, magmas are erupted through older continental crust and we

believe that the isotopic compositions of these rocks may be explained by

contamination of mantle-derived magmas by crustal material, in a fashion

similar to that described in this paper.

## 4.6 Summary and conclusions from chapter 4.

Nd and Sr isotopic systematics in four intrusions of the Shabogamo Intrusive Suite are consistent with all four bodies having crystallized at $1375\pm54$ m.y. from magmas having identical $^{143}Nd/^{144}Nd$ and $^{87}Sr/^{86}Sr$. Nd-Sm systematics in unmetamorphosed and lightly metamorphosed rocks and minerals provide a reliable estimate of the timeof crystallization. In the unmetamorphosed and lightly metamorphosed gabbros, Rb-Sr systematics are less reliable in rocks with larger percentages of sheet silicates (higher Rb/Sr). During amphibolite grade metamorphism, Rb-Sr systematics may be severely affected or completely reset, while Sm-Nd systematics remain essentially unaffected on a whole rock scale. Where retrograde effects are observable in the amphibolites, whole rocks are displaced to lower Sm/Nd ratios, possibly due to the breakdown of garnet.

Initial Nd and Sr isotopic compositions for the Shabogamo Intrusive Suite are lower and higher, respectively, than bulk earth values at 1375 m.y. These values are consistent with a model of mixing of a mantle-derived magma with a partial melt of "granitic" crustal material (approximately 5:1 by volume) to produce the magma which crystallized as gabbro bodies of the Shabogamo Intrusive Suite. Processes involving the contamination of mantle-derived melts by crustal components may be called upon to explain occurrences of young volcanics with high $^{87}Sr/^{86}Sr$ and low $^{143}Nd/^{144}Nd$, which have previously been interpreted in terms of an "enriched" mantle source.

## 4.7 Note about model melting parameters.

The equilibrium batch melting equations of Shaw (1970) are used to calculate the mantle melting curves in Fig. 7. The modal composition of the mantle is taken to be: 55% olivine; 25% orthopyroxene; 10% clinopyroxene; 10% garnet. Mantle concentrations of Nd and Sr are taken to be three times CI chondrites: Nd = 1.422 ppm; Sr = 25.8 ppm. Partition coefficients are chosen for Models A and B so as to delimit a reasonable range of melt compositions based on the range of partition coefficients reported in the literature (Table 4-3). The ratios of garnet, clinopyroxene, orthopyroxene, and olivine initially entering the melt are: 5:5:1:1.

A mode for the average Quebec composite is estimated on the basis of the major element chemistry reported by Shaw et. al. (1967): 43% plagioclase; 15% potassium feldspar; 12% hornblende; 10% biotite; 15% quartz; + oxides and accessories. During melting, we assume that accessories which are present are consumed by the melt and do not affect the partitioning of Nd and Sr. The equilibrium batch melting equations of Shaw (1970) are used to calculate the melting curves, assuming modal melting. The field in Fig. 7 results from using a range of partition coefficients for Nd in hornblende and Sr in plagioclase, as these phases dominate the bulk $K_D$'s for Nd and Sr respectively. The partition coefficients used are reported in Table 4-4.

Olivine and plagioclase fractionation curves in Fig. 7 are calculated assuming total equilibrium with: $K_D^{ol/l}{}_{Sr} = 0.000055$ (see Chapter 5); $K_D^{ol/l}{}_{Nd} = 0.000604$ (see Chapter 5); $K_D^{Pl/l}{}_{Sr} = 1.83$ (Arth, 1976); $K_D^{Pl/l}{}_{Nd} = 0.081$ (Arth, 1976).

Table 4-3

Partition coefficients for mantle melting models

| | $K_D$ Sr | | | | $K_D$ Nd | | | |
|---|---|---|---|---|---|---|---|---|
| | 0l/$\ell$ | opx/$\ell$ | cpx/$\ell$ | gnt/$\ell$ | ol/$\ell$ | opx/$\ell$ | cpx/$\ell$ | gnt/$\ell$ |
| Model A | $0.000011^3$ | $0.000175^3$ | $0.072^1$ | $0.007^6$ | $0.00113^3$ | $0.00189^3$ | $0.382^5$ | $0.087^4$ |
| Model B | $0.000099^3$ | $0.000209^3$ | $0.111^1$ | $0.012^2$ | $0.000076^3$ | $0.00173^3$ | $0.182^7$ | $0.015^5$ |

1-Hart and Brooks, 1974;  2-Arth, 1976;   3-Chapter 5;  4-Shimizu and Kushiro, 1975;

5-Frey et al., 1979;  6-Philpotts et al., 1972;  7-Schnetzler and Philpotts, 1970.

Table 4-4

Partition coefficients used in crustal melting models

| | Plag/liq. | Kspar/liq. | Hbl/liq. | Bt/liq. |
|---|---|---|---|---|
| $K_{DSr}$ | $2.84^{2}-4.4^{1}$ | $3.87^{3}$ | $0.002^{1}$ | $0.12^{2}$ |
| $K_{DNd}$ | $0.19^{1,3}$ | $0.025^{3}$ | $1.03-4.26^{1}$ | $0.167^{1,3}$ |

1 - Nagasawa and Schnetzler (1971); 2 - Philpotts and Schnetzler (1970);

3 - Schnetzler and Philpotts (1970).

CHAPTER 5

GEOCHEMICALLY ACTIVE MANTLE PROCESSES:

EVIDENCE FROM TRACE ELEMENTS AND ISOTOPE

RATIOS IN PERIDOTITES FROM SAN CARLOS , ARIZONA

5.1 Introduction

Mantle-derived peridotites, which occur as xenoliths in alkalic volcanics from some ocean islands and continental regions, are an important source of primary information about the upper mantle. Through studies of these nodules, we can learn about the physico-chemical characteristics of upper-mantle material, while providing constraints on the geochemically active processes which have affected this material through time. The nature of the upper mantle, inferred from seismic investigations and the chemistry of mantle-derived volcanic rocks, is extremely model dependent. In fact, the primary goal of the proposed research is to reconcile current geophysical and petrogenetic models of the mantle with first-order observations of peridotite nodules.

Studies of petrographic relatioships and major element chemistry of nodules (e.g., Kuno and Aoki, 1970; Jackson and Wright, 1970; Chen, 1971; Nixon and Boyd, 1973; Frey and Green, 1974; Rhodes and Dawson, 1975; Boyd and Nixon, 1975; Francis, 1976; Frey and Prinz, 1978; Reid and Woods, 1979) have shown that observed variations in major elements are broadly consistent with the nodules having originated as residues from different degrees of partial melting (see Figure 5-1). Conversely, where major and trace element data are available for whole rocks and minerals from the same nodules (Philpotts et al., 1972; Nixon and Boyd, 1973; Frey and Green, 1974; Ridley and Dawson, 1975; Frey and Prinz, 1978; Ottonello, 1978; Kurat et al., 1979; Jagoutz, 1979), some investigators have noted that absolute and relative trace element concentrations are inconsistent with expectations based on major element chemistry (e.g., Frey and Green, 1974). These basic inconsistencies

Figure 5-1

Variation diagram of CaO vs. MgO for peridotite
nodules.  Open circles - spinel lherzolites; closed
amphibole lherzolites;  open squares - garnet lherzo-
lites; open triangles - harzburgites.  Note the
inverse correlation between CaO and MgO, indicative
of the depletion of clinopyroxene with the increasingly
residual nature of the peridotites.  Data from:
Philpotts et.al., 1972; Nixon and Boyd, 1973; Frey
and Green, 1974; Ridley and Dawson, 1975: Ottonello,
1978; Frey and Prinz, 1978;  Kurat et.al., 1980;
H. Stosch, unpublished data.
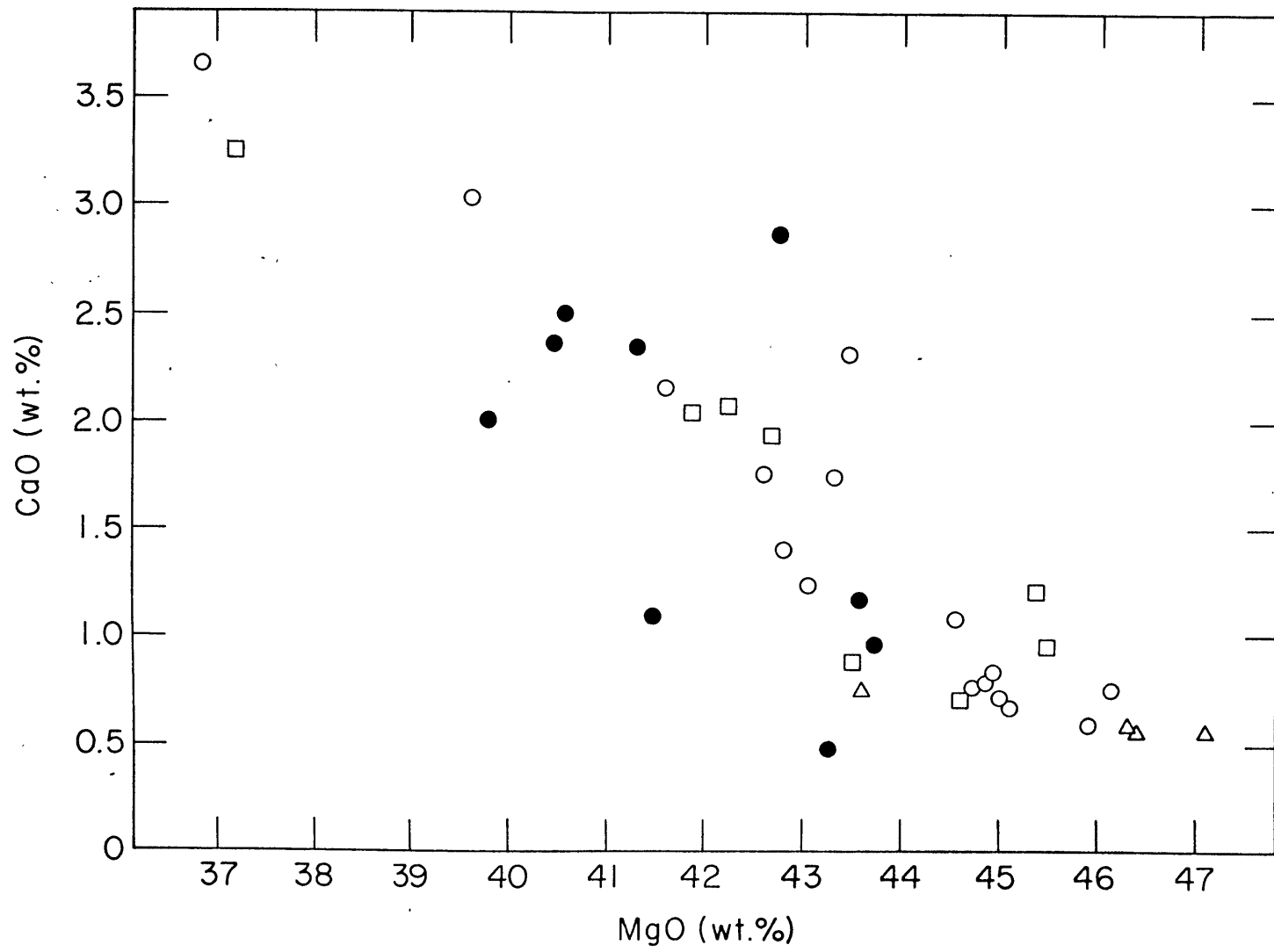
Figure 5-1

demonstrate the inadequacy of current theories for magma production in the mantle, and emphasize the need for a new approach in investigations of mantle material.

Results for trace elements in whole rocks and constituent minerals from San Carlos, Arizona, permit mass balance calculations for peridotites. Regardless of modal mineralogy, Ba and the alkali elements are found to reside almost exclusively in minor phases, while Sr, Nd and Sm in the whole rocks are consistent with the measured concentrations of these elements in clean silicates. These results indicate, as suggested previously (Griffin and Murthy, 1969; Basu and Murthy, 1977), that major lherzolite phases are too depleted in LIL elements to yield basaltic magma by partial melting.

## 5.2  Background

On the basis of measured trace element concentrations in basalts and associated rocks, detailed models have been applied in an effort to understand petrogenetic processes and to place constraints on the nature of "reasonable" source materials (e.g., Minster and Allegre, 1978; Sun and Hanson, 1975; Frey et al., 1978). These modelling exercises are typically carried out on suites of volcanic rocks which occur in tectonic settings that preclude significant crustal involvement in the magma generation process. As a result, trace element abundances in the source mantle are estimated in such a way as to explain variations in the volcanic rocks by simple melting processes, such as those described by Gast (1968). Trace element characteristics of the mantle seen through this "basalt window" are very different from observations of mantle-derived nodules, stressing the need to reconcile this seemingly anomalous nature of the nodules with theories of basalt petrogenesis.

Evidence which supports this latter observation is provided both by trace element systematics in nodules and by $^{143}Nd/^{144}Nd$ ratios measured in mantle-derived volcanic rocks. Despite the apparent difficulty in understanding trace element characteristics of nodules in terms of simple models, observed systematic relationships suggest that there are important chemically active mantle processes which have not been thoroughly considered. For example, a literature survey reveals that relative light rare earth element (LREE) enrichment (i.e., $[La/Sm]_N > 1$) is inversely correlated with bulk rock CaO, or modal clinopyroxene (Frey and Green, 1974; see Figure 5-2). It has

Figure 5-2

Variation diagrams for peridotite nodules.
Symbols and sources as in Figure 1.

a.    $(La/Sm)_N$ vs. CaO. Demonstrates
       inverse correlation between LREE
       enrichment and modal clinopyroxene.

b.    $(Yb)_N$ VS. CaO. Demonstrates
       positive correlation between HREE's
       and modal clinopyroxene.

c.    $(La/Sm)_N$ vs. (Yb) Demonstrates
       negative correlation between LREE
       enrichment and HREE concentration.
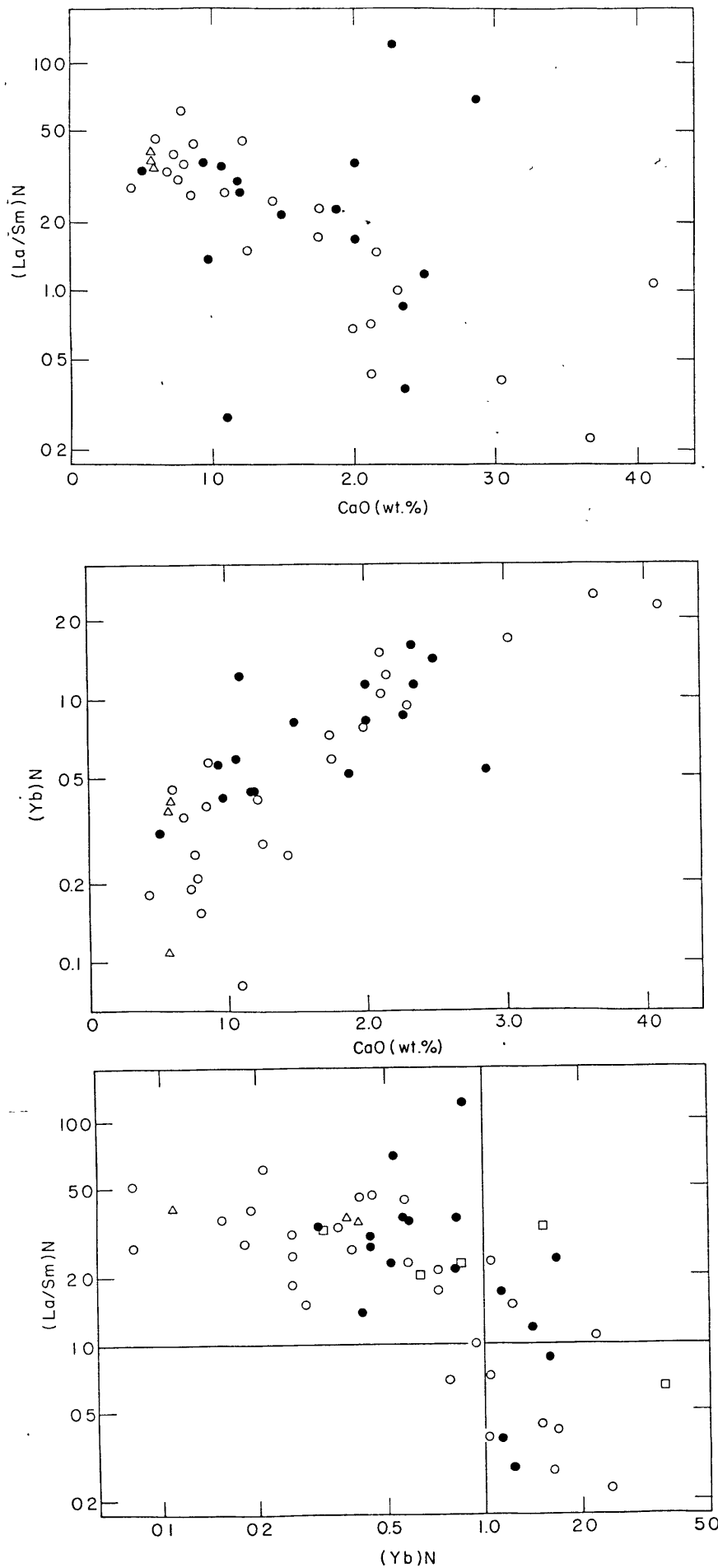
Figure 5-2

been shown that the eutectic in the mantle lherzolite system, at mantle pressures, lies much closer to clinopyroxene and the aluminous phase than to olivine or orthopyroxene (Davis and Schairer, 1965); Mysen and Kushiro, 1977). Thus, as lherzolite material is melted, clinopyroxene, and CaO, become increasingly depleted with greater degrees of partial melting. In addition, LREE's are known to be more incompatible than HREE's in major lherzolite phases (for review of partition coefficients, see Arth, 1976, or Frey et al., 1978), so that one would predict a positive correlation between $(La/Sm)_N$ ratios and bulk-rock CaO in nodules. That the opposite is observed is extremely interesting and suggests that magma generation in the mantle requires the subsequent metasomatism of material which is depleted during partial melting. Mantle metasomatism is certainly not a new idea as it has been suggested on the basis of several types of evidence by numerous authors (e.g., Wilshire and Trask, 1971; Best, 1974; Francis, 1976; Menzies and Murthy, 1980a and 1980b). However, its intimate connection to magma generation processes, which carries major implications for the chemical evolution of melts in the mantle, has not been suspected.

With the advent of high-precision measurements of $^{143}Nd/^{144}Nd$ ratios in volcanic rocks (Lugmair et al., 1975a and 1975b; DePaolo and Wasserburg, 1976a and 1976b; Richard et al., 1976; O'Nions et al., 1977), a powerful tool has become available which allows the unambiguous definition of time-integrated Sm/Nd ratios in mantle source regions. Whereas conventional trace element modeling has demonstrated the necessity for LREE enrichments in source regions for undersaturated alkaline

magmas (Minster and Allegre, 1978; Sun and Hanson, 1975; Frey et al.,

1978), Nd isotopic studies have very often shown such rocks to be

derived from mantle which has a long-term history of LREE abundances

which are unfractionated or depleted, relative to chondrites (e.g.,

O'Nions et al., 1977; Basu and Tatsumoto, 1979; Chapter 2). Usually

when such evidence is discussed (e.g., Menzies and Murthy, 1980b),

"recent enrichment events" in the souce mantle are arbitrarily pro-

posed. Again, it is considered that this information provides unescapa-

ble constraints which must be reconciled with modern petrogenetic

theory.

Until very recently, isotopic investigations of lherzolite

nodules have been primarily restricted to measurements of $^{87}Sr/^{86}Sr$

ratios in bulk rocks and constituent minerals (e.g., Hutchison and

Dawson, 1979; Paul, 1971; Laughlin et al., 1971; Stueber and Ikramuddin,

1977). A notable exception is the work of Kramers (1977), which pre-

sents both Pb and Sr isotopic data. A primary aim of much of the

earlier work was to investigate possible cognate relationships between

the nodules and their host basalts. Typically, while one or more

nodules of a given suite may have $^{87}Sr/^{86}Sr$ ratios similar to the en-

closing basalt, most do not. This provides support for non-cognate

relationships. Even more interesting have been the Rb-Sr systematics

displayed by nodules of a given suite or minerals from a single nodule.

In some cases, isochronous relationships are observed and have been

considered to document "relict mantle events" (Stueber and Ikramuddin,

1974; Basu and Murthy, 1977). However the more usual result has been

that suites of nodules and constituent mineralsfrom individual nodules

are not in isotopic equilibrium, and furthermore, do not display any

systematic relationship to one another. With regard to whole rocks,

this was considered to document mantle heterogeneity. For the minerals,

a complex history is indicated, in addition to prior residence in a

regime of sufficiently low temperature to prevent diffusive equili-

bration of $^{87}Sr/^{86}Sr$ between adjacent phases. (Hofmann and Hart,

1978).

Prior to completion of the work reported in this chapter, it

was considered that complex histories were preventing straightforward

interpretation of Rb-Sr systematics in the nodules. As a qualitatively

similar conclusion was justified on the basis of trace element data,

it was hoped that detailed separation of pure phases would yield mixing

relationships on isochron diagrams, eventually allowing definition of

time constraints for aspects of the nodules' evolution

Recent Sm-Nd investigations of lherzolite nodules and constituent

minerals have provided some additional insights (Basu and Tatsumoto,

1979; Jagoutz et al., 1980; Stosch et al., 1980; Menzies and Murthy,

1980a and 1980b). The work of Menzies and Murthy (1980a) has demon-

strated the apparent decoupling of Rb-Sr and Sm-Nd isotopic systems

during metasomatic processes in the mantle beneath S. Yemen. Aparently

fluids which crystallize as pargasite in the nodules are derived from

mantle with $^{87}Sr/^{86}Sr$ ratios similar to the primary lherzolite phases

(cpx), but with significantly different $^{143}Nd/^{144}Nd$ ratios. This result

is comparable to the decoupling of the two systems observed in basalts

from the Reykjanes Peninsula (Chapter 1).

Jagoutz et al., (1980), conducted a detailed Sm-Nd, Rb-Sr in-

vestigation of a clinopyroxene-rich spinel lherzolite from Kilbourne

Hole, New Mexico. They demonstrated the need to analyze clean mineral

separates, by showing that even where $^{143}Nd/^{144}Nd$ is in equilibrium between orthopyroxene and clinopyroxene, $^{87}Sr/^{86}Sr$ in the ortho-pyroxene showed effects of secondary contamination, possibly by caliche.

In total, isotopic data from peridotite nodules is not easily in-terpreted within the context of simple models. Complex histories in-volving metasomatic events in the mantle are indicated. As concluded on the basis of trace element evidence, it is necessary to implement new approaches in order to develop quantitative constraints on the processes which have affected the nodules, and which affect the chemical evolution of magmas in the mantle.

## 5.3  Sample descriptions

Nd and Sr isotope ratios and K, Rb, Cs, Ba, Sr, Nd, and Sm

concentrations have been measured in bulk rocks and separated phases

from three lherzolite nodules and one dunite from San Carlos,

Arizona (trace element concentrations determined by isotope dilution).

Three of the four samples studied have been previously described by

Frey and Prinz, (1978):  PA 15(A), a spinel lherzolite with ∿18%

clinopyroxene; PA 65(G), a spinel lherzolite with  ∿8% clinopyroxene;

and PA 10, a dunite, with only a trace of clinopyroxene.  SC 23, a

spinel lherzolite with  ∿3% clinopyroxene, was collected by Jagoutz.

Modal analyses for all samples are given in Table 5-1.  These samples

were chosen to enable investigation of chemical changes which might

accompany the increasing depletion of "basaltic constituents" in the

lherzolites.  Frey and Prinz (1978) have previously demonstrated sig-

nificant LREE enrichments in PA 10 and PA 65 and significant depletion

of LREE's in PA 15, displaying the invese correlation between modal

clinopyroxene and LREE enrichment discussed previously.  SC 23, despite

its residual mineralogy, was found to have a chondrite-normalized

REE pattern similar to PA 15, making it unique in terms of combined

trace and major element character.

TABLE    5-1

Modal analysis of San Carlos samples (in wt. percent)

| Sample | OL(neo) | OL(por) | OPX(neo) | OPX(por) | CPX(neo) | CPX(por) | SPN |
|---|---|---|---|---|---|---|---|
| SC 23 | 65.33 | 11.39 | 8.52 | 12.57 | 1.75 | 0.186 | 0.21 |
| PA 65 | 48.75 | 19.31 | 18.25 | 5.03 | 8.11 | -- | 0.52 |
| PA 15 | 23.54 | 16.55 | 15.44 | 23.65 | 11.74 | 6.48 | 2.55 |
| SC 23(corr.)[*] | 64.6 | 11.2 | 8.44 | 12.41 | 2.82 | 0.306 | 0.22 |
| PA 65(corr.)[*] | 50.14 | 19.86 | 18.74 | 5.16 | 5.45 | -- | 0.52 |

[*]Calculated to make Sm consistent from WR to clean bulk.

## 5.4  Results

The course of this investigation was guided by the hypothesis that if one were able to physically separate and analyze every constituent phase of a given nodule, an understanding of the chemical processes which had affected that nodule would emerge. Four basic strategies were employed to test this hypothesis: (1) 100% pure, inclusion-free separates were made for the major silicate phases; (2) separates of major phases with high concentrations of liquid and/or fluid inclusions were picked; (3) acid leaching was used to separate phases which were not physically separable; and (4) porphyroblastic and neoblastic habits of single phases were separated. In addition, likely sources for contamination of the nodules, i.e., basalt and caliche, were analyzed, so that their effects on mantle phases could be predicted. In retrospect, it is clear that this has helped to prevent erroneous conclusions on the basis of contaminated samples. As will become evident, it appears that this has been a significant source of ambiguity for data reported in the literature.

The results from this investigation are new and very exciting, but not completely definitive. As with every study in a little understood field, at least as many questions are raised as are answered. Part of the problem has been caused by the evolution of analytical techniques, during the course of the research, particularly with regard to mineral separation. As a result, samples made early in the study were of much lower quality than those which were produced later. Another problem results from the extremely low concentrations of LIL elements in clean silicates. Because these concentrations were much lower than expected, analyses were made of samples which were too small,

relative to blank levels (see Table 5-2) and which were typically

overspiked, sometimes to the point of introducing large uncertainties

in the measured concentration.

Trace element and isotopic data for nodule samples and basalt

and caliche from San Carlos are tabulated in Tables 5-3 to 5-7. For

trace element concentrations three qualities of data are reported:

(1) normal data, i.e., no significant problems with blanks or pre-

cision, level of precision is roughly estimated by the number of

significant figures which are reported; (2) questionable data

(values are underlined), which indicates that the total trace element

measured was within a factor of four of the blank (see Table 5-2);

and (3) maximum data, that is, the total amount of trace element

measured in the sample was less than or equal to the average blank

value for that element. In this last case, the measured weight of the

element is corrected by subtracting the minimum blank (Table 5-2) from

the total, resulting in a "maximum" concentration.

Nd and Sr isotope data were measured on samples with sufficient

amounts of these elements. $^{87}Sr/^{86}Sr$ has been measured on as little as 5.5 ng

of Sr (SC 23 POR) and $^{143}Nd/^{144}Nd$ on as little as 14 ng of Nd (PA 65 OPX),

but these were difficult measurements which could not be described as routine.

Salient aspects of these data, and consequent implications for

mantle processes are discussed in the sections which follow. Because

of sample size, blank problems, and the ever increasing purity of

samples, subtle facets of these data are difficult to interpret unam-

biguously. Therefore, due to the volume of data, many subtle aspects

are not discussed in the text. Before interpretation of fine-scale

TABLE 5-2

Procedural blanks for nodule analysis

| | K(ng) | Rb(ng) | Cs(pcg) | Ba(ng) | Sr(ng) | Nd(ng) | Sm(ng) |
|---------|-------|--------|---------|--------|--------|--------|--------|
| Average | 6.9 | 0.014 | 0.090 | 1.26 | 0.032 | 0.069 | 0.040 |
| Minimum | 3.2 | 0.008 | 0.051 | 0.63* | 0.016* | 0.035 | 0.020* |

*Where the range in blanks was small, the minimum value is taken

as one half of the average value.

phenomena in peridotites is possible, sample to sample reproducibility must be further investigated.

TABLE 5-3

Trace elements[1] and isotope ratios[2] in SC 23

| Sample | Weight[3] | K | Rb | Cs | Ba | Sr | Nd | Sm | $^{87}Sr/^{86}Sr$ | $^{143}Nd/^{144}Nd$ |
|---|---|---|---|---|---|---|---|---|---|---|
| WR UW | 0.28779 | 16.66 | 0.0543 | 4.00 | 0.347 | 5.110 | 0.1101 | 0.04686 | 0.70395±3 | 0.512655±74 |
| WR W | 0.11681 | 1.193 | 0.0023 | 0.073 | 0.0322 | 1.721 | 0.0898 | 0.0445 | 0.70321±3 | --- |
| CPX NEO | 0.08848 | 13.72 | 0.00260 | -- | 0.051 | 52.89 | 2.657 | 1.218 | 0.70316±3 | 0.512715±15 |
| CPX POR | 0.04975 | 12.64 | 0.00116 | 0.08 | 0.120 | 59.61 | 3.032 | 1.440 | 0.70318±2 | 0.512743±15 |
| OPX NEO LG | 0.06960 | 3,304 | 0.00454 | 0.061 | 0.009 | 0.1439 | 0.0161 | 0.0142 | --- | ---- |
| OPX NEO* | 0.02166 | <0.30 | <0.001 | -- | <0.019 | 0.1288 | 0.0163 | 0.016 | --- | ---- |
| OPX POR | 0.03061 | 0.29 | 0.0009 | 0.011 | 0.041 | 0.1852 | 0.0251 | 0.034 | 0.70338±18 | ---- |
| OL NEO | 0.08875 | <0.04 | <0.0007 | <0.016 | 0.012 | 0.0724 | <0.0003 | <0.0003 | --- | ---- |
| OL POR | 0.06555 | <0.07 | <0.0015 | <0.013 | 0.022 | 0.0248 | <0.0004 | <0.0002 | --- | ---- |
| HCL | 0.00395 | 865.6 | 1.84 | 161 | 14.5 | 118.4 | 1.938 | 0.399 | 0.70645±4 | ---- |
| HF | 0.03847 | 27.14 | 0.117 | 9.1 | 0.516 | 1.060 | 0.0508 | 0.0192 | 0.70457±8 | ----- |

* Indicates the cleaner of two mineral separates with the same designation.
1. Cs given as ppb. All other elements given as ppm. Underlining indicates data within a factor of four of average blank. Maximum concentrations are calculated using minimum blank values estimated errors indicated by a number of significant digits.
2. Errors, in last significant digits, represent 2σm confidence level. $^{143}Nd/^{144}Nd$ normalized to $^{146}ND/^{144}Nd$ = 0.721900. $^{87}Sr/^{86}Sr$ relative to 0.70800 for E & A $SrCO_3$ and normalized to $^{86}Sr/^{88}Sr$ = 0.11940.
3. Sample weights in grams.

TABLE 5-4

Trace elements[1] and isotope ratios[2] in PA 65

| Sample | Weight[3] | K | Rb | Cs | Ba | Sr | Nd | Sm | $^{87}Sr/^{86}Sr$ | $^{143}Nd/^{144}Nd$ |
|---|---|---|---|---|---|---|---|---|---|---|
| WR | 0.04193 | 68.8 | 0.0815 | 2.22 | 0.14 | 8.478 | 0.6769 | 0.1624 | 0.70314±4 | 0.513074±18 |
| CPX UW | 0.00628 | 87.3 | 0.1024 | 0.6 | 0.88 | --- | --- | --- | 0.70308±3 | 0.513084±13 |
| CPX W | 0.03829 | 11.25 | 0.0747 | 0.05 | 0.065 | 147.2 | 12.25 | 2.769 | 0.70306±3 | 0.513027±24 |
| CPX CL* | 0.00324 | 11.10 | 0.0045 | <0.4 | <0.3 | 148.7 | --- | --- | 0.70311±4 | --- |
| OPX | 0.13295 | 2.361 | 0.00354 | 0.058 | -- | 0.4265 | 0.1086 | 0.0481 | 0.70315±5 0.70309±4 | 0.512911±55 |
| OPX LIQ | 0.00190 | (228.9) | 0.026 | 0.49 | -- | 0.6950 | 0.113 | 0.03 | --- | --- |
| OPX CDY | 0.00940 | 35.74 | 0.0274 | 0.128 | <0.09 | 0.3745 | 0.0749 | 0.0322 | --- | --- |
| OL CLL | 0.88150 | 1.292 | 0.00348 | 0.077 | 1.61 | 0.744 | -- | --- | 0.70421±7 | --- |
| OL CLM* | 0.12790 | 3.3 | 0.0034 | 0.014 | <0.04 | 0.008 | 0.0035 | (0.064) | --- | --- |
| OL CLS** | 0.00428 | <0.3 | 0.0039 | <1.0 | <0.06 | 0.015 | 0.049 | (0.213) | --- | --- |
| OL LIQ L | 0.01271 | 3.39 | 0.0046 | <0.2 | <0.05 | 0.0361 | <0.002 | 0.0053 | --- | --- |
| OL LIQ S* | 0.00285 | 2.3 | 0.042 | <0.2 | <0.18 | 0.0751 | 0.035 | (0.047) | --- | --- |
| HCL[4] | -- | 1383 | 41.6 | 520 | 97.9 | 173.9 | 3.59 | 0.655 | 0.70786±8 | --- |
| SPN HCL[4] | -- | 99.2 | 0.51 | 11.9 | 22.2 | 40.98 | 1.52 | 0.279 | 0.70307±25 | --- |

\* Indicates the more pure of two mineral separates with the same designation.
\** Indicates the cleanest of the three clean olivine samples.
1. Cs given as ppb. All other elements given as ppm. Underlining indicates data which is within a factor of four of average blank. Maximum concentrations are calculated using minimum blank values. Estimated errors indicated by number of significant digits.
2. Errors, in last significant digits, represent $2\sigma m$ confidence level. $^{143}Nd/^{144}Nd$ normalized to $^{146}Nd/^{144}Nd$ = 0.721900. $^{87}Sr/^{86}Sr$ relative to 0.70800 for E&A $SrCO_3$ and normalized to $^{86}Sr/^{88}Sr$ = 0.11940.
3. Sample weights in grams.
4. Sample represents acid leach. Cs given as total pcg. All other elements given as total ng.

TABLE 5-5

Trace elements[1] and isotope ratios[2] in PA 15

| Sample | Weight[3] | K | Rb | Cs | Ba | Sr | Nd | Sm | $^{87}Sr/^{86}Sr$ | $^{143}Nd/^{144}Nd$ |
|---|---|---|---|---|---|---|---|---|---|---|
| WR | 0.04425 | 59.70 | 0.395 | 36.9 | 0.788 | 7.737 | 0.8115 | 0.3377 | 0.70555+3 | 0.512967+15 |
| WRC[5] | | 28.8 | 0.288 | 27.4 | 0.54 | 6.27 | 0.742 | 0.324 | | |
| CPX UW | 0.00605 | 37.30 | 0.109 | 0.79 | 0.56 | 55.38 | 3.859 | 1.712 | 0.70278+4 | 0.513052+27 |
| | | | | | | | | | 0.70274+4 | 0.513076+29 |
| CPX W | 0.01027 | 12.94 | 0.0077 | 0.3 | 0.27 | 34.07 | 3.817 | 1.724 | 0.70271+3 | 0.513063+19 |
| OPX CL | 0.0340 | 1.41 | 0.0028 | 0.045 | 0.082 | 0.0871 | 0.0235 | 0.0205 | --- | 0.51358+56 |
| OL WH | 0.26377 | 19.55 | 0.1345 | 7.5 | 0.647 | 0.6232 | 0.0602 | 0.0133 | --- | ---- |
| OL RED | 0.22406 | 18.76 | 0.0935 | 6.7 | 0.861 | 0.988 | 0.0954 | 0.0264 | --- | ---- |
| SPN HCL[4] | | 195.1 | 2.076 | 200 | 37.68 | 81.15 | 10.51 | 3.691 | 0.70377+14 | ---- |

1. Cs given as ppb. All other elements given as ppm. Underlining indicates data within a factor of four of average blank. Estimated errors indicated by number of significant digits.

2. Errors, in last significant digits, represent $2\sigma m$ confidence level. $^{143}Nd/^{144}Nd$ normalized to $^{146}Nd/^{144}Nd = 0.721900$. $^{87}Sr/^{86}Sr$ relative to 0.70800 for E & A $SrCO_3$ and normalized to $^{86}Sr/^{88}Sr = 0.11940$.

3. Sample weights in grams.

4. Sample represents an acid leach. Cs given as total pcg. All other elements given as total ng.

5. Whole rock analysis calculated by subtracting 0.00282g of caliche from WR.

TABLE 5-6

Trace elements[1] and isotopes ratios[2] in PA 10

| Sample | Weight[3] | K | Rb | Cs | Ba | Sr | Nd | Sm | $^{87}Sr/^{86}Sr$ | $^{143}Nd/^{144}Nd$ |
|--------|-----------|-----|------|--------|------|-------|--------|-------|-------------------|---------------------|
| CPX CL | 0.00422 | 24.97 | 0.0104 | <0.25 | 0.17 | 102.3 | 4.52 | 0.890 | 0.70276+4 | ---- |
| OL CL | 0.00781 | 0.74 | 0.0079 | <0.006 | 0.22 | 0.023 | <0.001 | 0.0014 | ---- | ---- |
| OL LIQ | 0.00609 | 17.18 | 0.0229 | 0.35 | 0.55 | 1.030 | 0.0419 | 0.859 | 0.70268+70 | ---- |
| DK Glass | 0.00324 | 47590 | 63.1 | 674 | 784 | 1428 | 34.07 | 6.907 | 0.70279+5 | 0.512896+51 |
| RED GLASS | 0.00437 | 21346 | 26.5 | 634 | 356 | 727.0 | 34.92 | 6.238 | 0.70285±4 | ---- |

1. Cs given as ppb. All other elements as ppm. Underlining indicate data within a factor of four of blank. Maximum concentrations calculated using minimum blank values. Estimated uncertainties indicated by number of significant digits.

2. Errors, in last significant digits, represent $2\sigma m$ confidence lived. $^{143}Nd/^{144}Nd$ normalized to $^{146}Nd/^{144}Nd = 0.721900$. $^{87}Sr/^{86}Sr$ relative to 0.70800 for E & A $SrCo_3$ and normalized to $^{86}Sr/^{88}Sr = 0.11940$.

3. Sample weights in grams.

TABLE  5-7

Trace elements[1] and isotope ratios[2] in basalt and caliche

| Sample | Weight | K | Rb | Cs | Ba | Sr | Nd | Sm | $^{87}Sr/^{86}Sr$ | $^{143}Nd/^{144}Nd$ |
|---|---|---|---|---|---|---|---|---|---|---|
| PA 53B | 0.15791 | 19965 | 26.6 | 111 | 357 | 2133 | 34.16 | 7.337 | 0.70298±4<br>0.70298±4 | 0.513050±14 |
| 23 CAL | 0.100 | 10954 | 37.8 | 3369 | ∿90 | 519.9 | 24.56 | 4.795 | 0.70571±3 | 0.512687±25 |

1.  Cs given as ppb.  All other elements as ppm.

2.  Errors, in last significant digits, represent 2σm confidence level.  $^{143}Nd/^{144}Nd$ normalized to $^{146}Nd/^{144}Nd = 0.721900.$  $^{87}Sr/^{86}Sr$ relative to 0.70800 from E & A $SrCO_3$ and normalized to $^{86}Sr/^{88}Sr = 0.11940.$

5.5 <u>Mass balance of trace elements</u>

A major advantage of the approach taken in this investigation
is the ability to calculate mass balances for trace elements in
the nodules, thereby determining the extent to which trace elements
reside in minor or unidentified phases. To facilitate this,
"clean bulk" samples were calculated using trace element concentra-
tions measured in pure mineral separates (Tables 5-3 to 5-5) and
the modal analyses of the samples (Table 5-1). The ensuing clean
bulk values(Table 5-8) were then corrected by adjusting clino-
pyroxene in the measured mode so that Sm in the whole rock samples
agreed with Sm in the calculated clean bulks (see Table 5-9). This
is justified from two viewpoints: (1) Sm always shows the best
agreement between clean bulk and whole rock values and (2) the
paucity of clinopyroxene, together with the coarse-grained nature
of the nodules,makes it very likely that discrepancies existed between
modal clinopyroxene in the two samples which were analyzed for modal
mineralogy and whole rock trace elements, respectively. The corrected
clean bulk values were used to normalize trace element concentrations
measured in individual mineral separates, and selected results are
plotted in Figures 5-3 to 5-5 versus ionic radius (ionic radii from
Whittaker and Muntus, 1970). Clean bulk values are not shown in the
diagrams but would be represented by horizontal lines at 1.0. Some
of the olivine data, particularly from SC 23, represent maximum con-
centrations. These maximum concentrations enhance the magnitude of
K "anomalies", as they were used for calculation of the clean bulk

TABLE  5-8

Clean bulk samples calculated from measured modes

| Sample | K | Rb | Cs | Ba | Sr | Nd | Sm |
|--------|------|---------|-------|-------|-------|-------|-------|
| SC 23  | 0.36 | 0.00087 | 0.016 | 0.018 | 1.12  | 0.057 | 0.030 |
| PA 65  | 1.7  | 0.0036  | 0.027 | 0.067 | 12.10 | 1.01  | 0.23  |
| PA 15  | 2.9  | 0.0031  | 0.077 | 0.09  | 6.27  | 0.705 | 0.32  |

TABLE 5-9

Corrected clean bulk samples

| Sample | K | Rb | Cs | Ba | Sr | Nd | Sm |
|--------|------|---------|-------|-------|------|-------|--------|
| SC23[1] | 0.52 | 0.00089 | 0.017 | 0.019 | 1.76 | 0.089 | 0.0445 |
| PA65[2] | 1.38 | 0.0035 | 0.026 | 0.053 | 8.16 | 0.688 | 0.162 |
| PA15[3] | 2.9 | 0.0031 | 0.077 | 0.09 | 6.27 | 0.705 | 0.32 |

1. calculated by increasing CPX in mode so that Sm is accounted for in SC 23 WRW.

2. calculated by increasing CPX in mode so that Sm is accounted for in PA 65 WR.

3. same as calculated clean bulk. Sr, Nd and Sm in clean bulk agree well with Pa 15 WR if 0.00282g of caliche is subtracted from whole rock.

Figure 5-3

Mineral separates and whole rocks from SC 23, normalized
to clean bulk values.  Abbreviations:  CPX - clinopyroxene;
OPX - orthopyroxene; OL - olivine;  CAL - caliche;
P - porphyroblast;  N - neoblast; UW - unwashed;
HF - HF leach; HCl - HCl leach.  PA 53B is the basalt
from San Carlos.

Figure 5-3

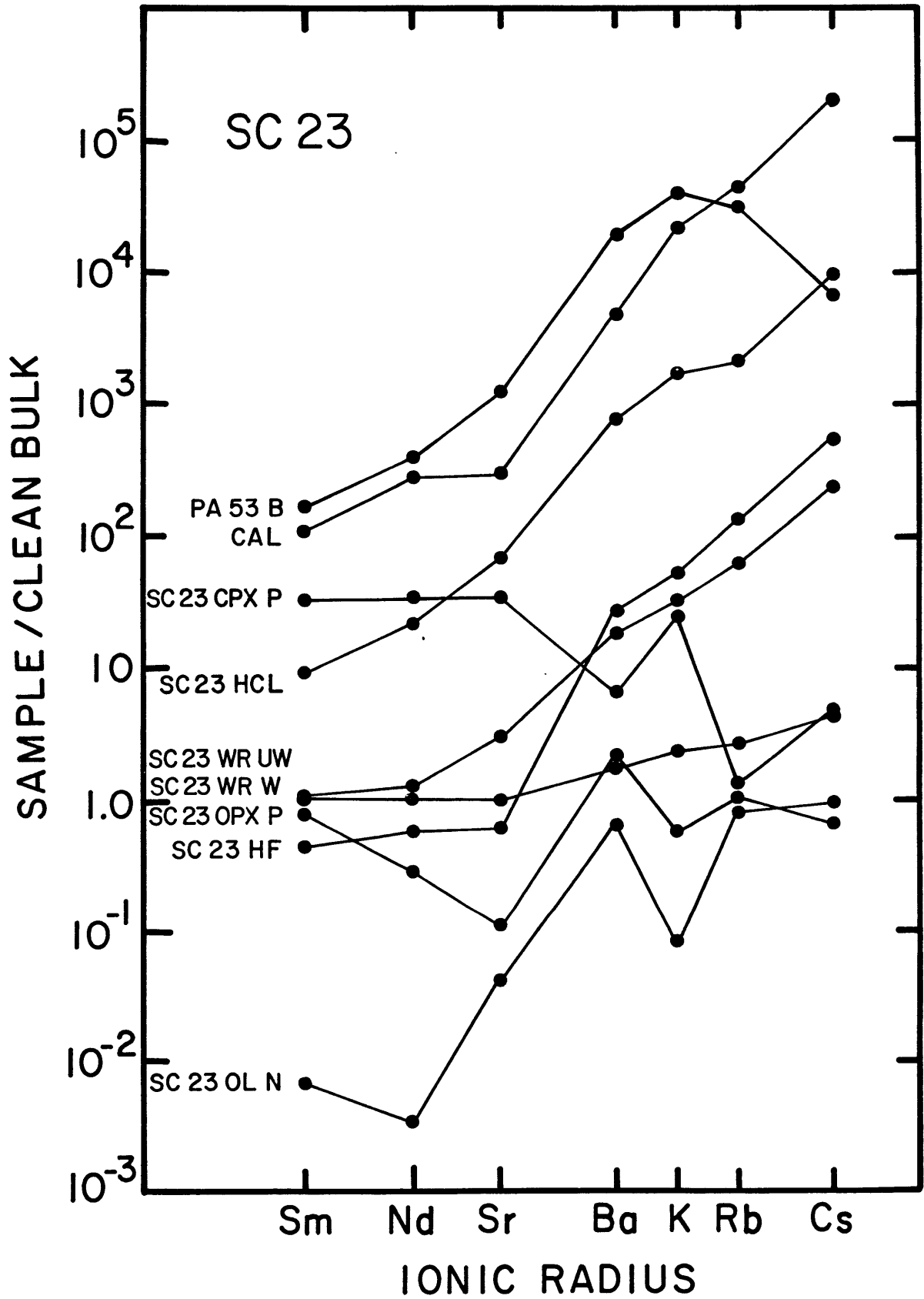Figure 5-4

Mineral separates and whole rock from PA 15, normalized
to clean bulk values.  Abbreviations are the same as
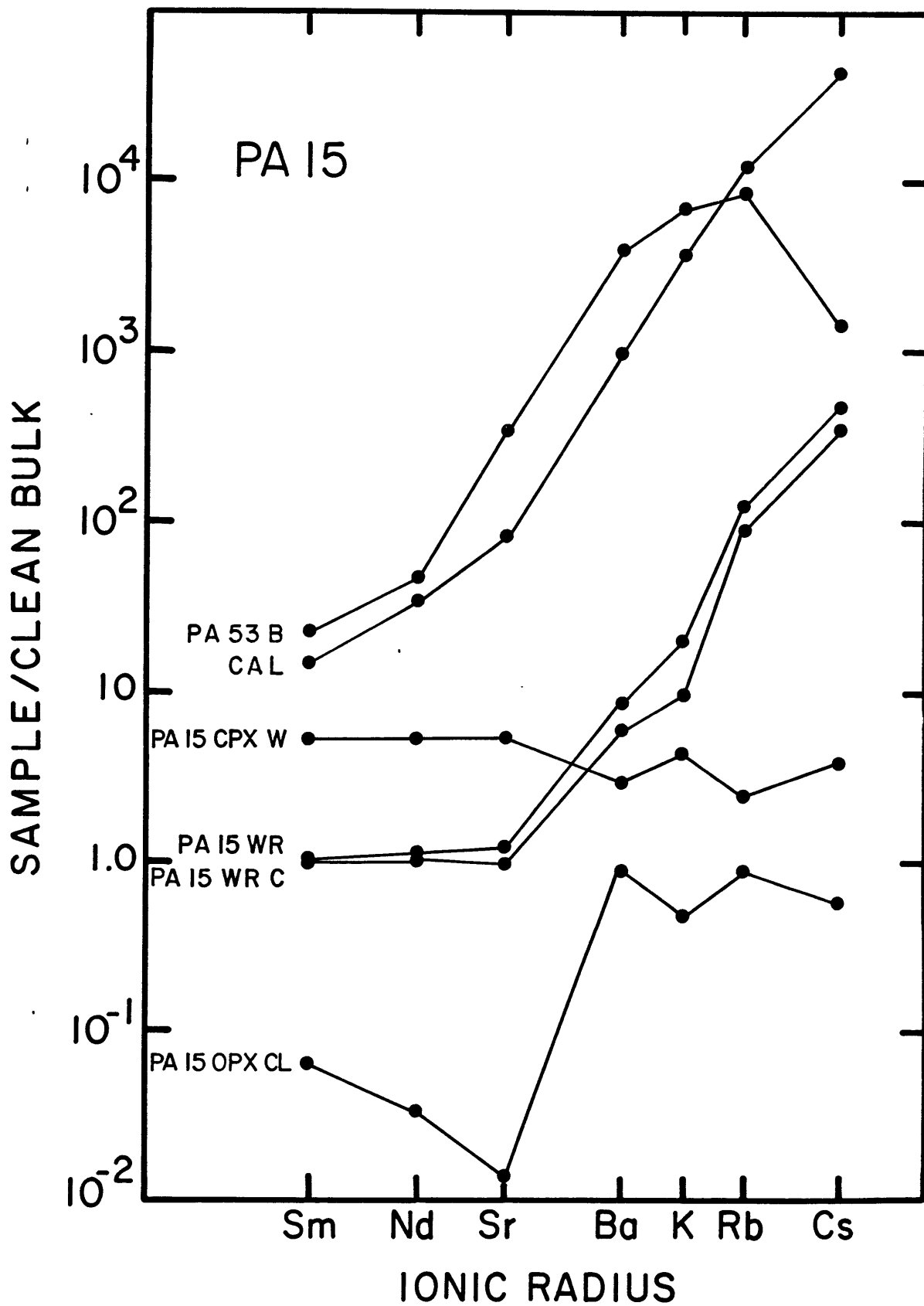for Figure 3 except that C and CL indicate "clean".

Figure 5-4

Figure 5-5

Mineral separates and whole rock from PA 65, normalized
to clean bulk values.  Abbreviations are the same as
in Figure 3, except:  CY - cloudy;  LQL - with liquid
inclusions;  CL - clean.
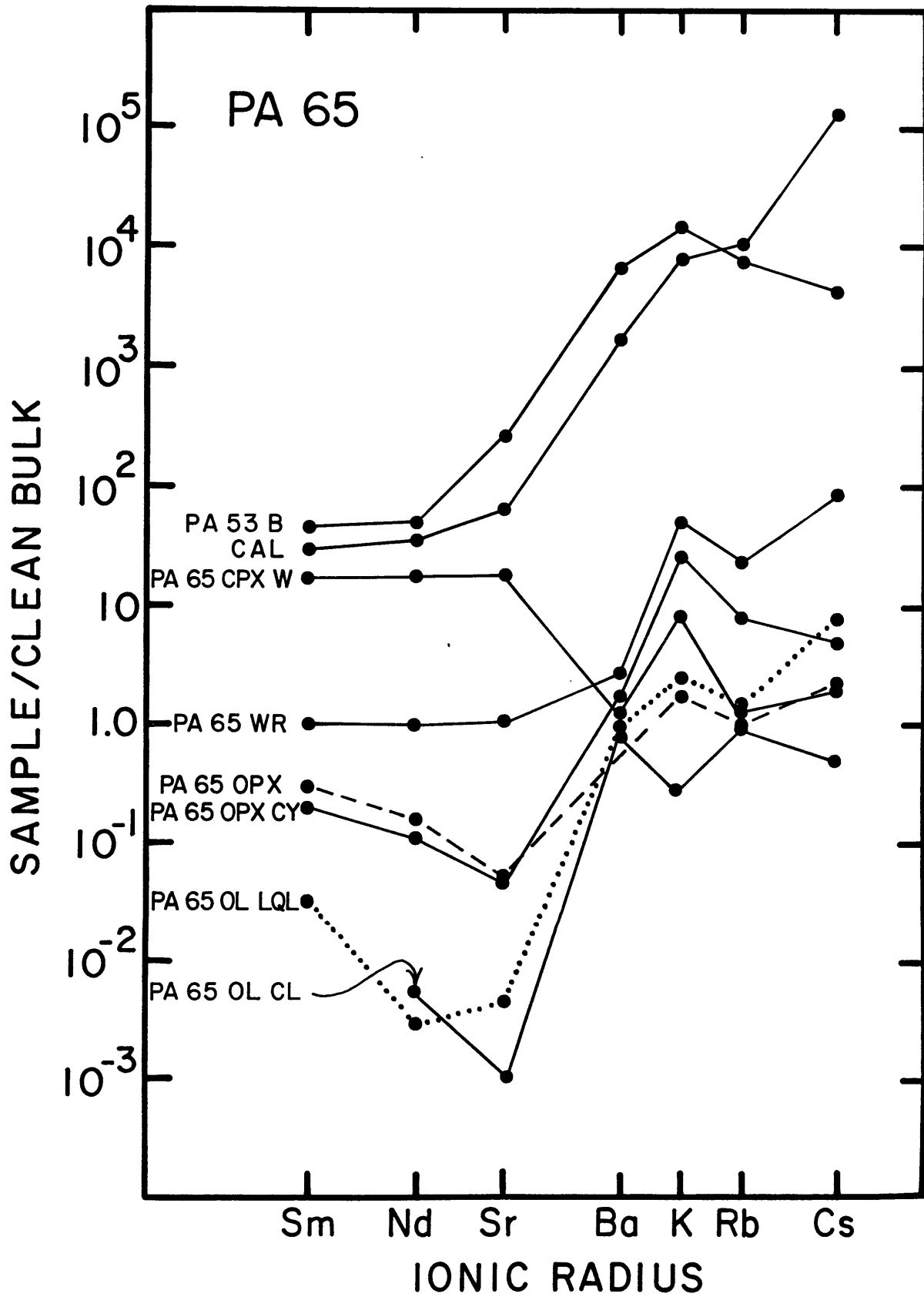
Figure 5-5

values. In each of the diagrams, caliche and alkali basalt (PA 53 B) from San Carlos are shown for reference.

Comparison of whole rock samples for the three lherzolites shows that in all cases, Ba and the alkali elements do not reside in the major silicate phases, and that the discrepancy increases with ionic radius. The alkali-enriched phases are seen to be most abundant in PA 15, which is also the only sample capable of producing a significant amount of basalt melt on the basis of major element chemistry. Furthermore, within reasonable limits, Sr, Nd and Sm are shown to be accounted for by the concentrations of these elements in the major silicate phases. Hence, there is a primary difference in the behavior of the smaller ions, Sr, Nd and Sm, compared to that of Ba and the alkalis. These data indicate that the mantle alkali budget, both for primary "fertile" lherzolite material (PA 15), and for depleted and subsequently metasomatized material (PA 65), is contained in minor phases. A major aim of future investigation will be to distinguish alkali metal-bearing phases in "fertile" lherzolites from those in residual peridotites.

It is important to note that, as suggested by Griffin and Murthy (1969) and Basu and Murthy (1977) for anhydrous lherzolite compositions, alkali element concentrations, in all three calculated clean bulk samples, are much too low to generate basalts by realistic degrees of partial melting. To produce a low-K tholeiite from PA 15, the clean bulk most enriched in K, requires significantly less than 1% melting. These observations require the existence of minor phases which have an important role in magma generation processes.

## 5.6 Importance of pure mineral separates

Previous investigators have recognized the need for pure mineral separates when analyzing trace element concentrations, as evidenced by their efforts to produce inclusion-free mineral separates and the development of various acid-washing techniques (e.g., Griffin and Murthy, 1969; Philpotts et al., 1972; Shimizu, 1974; Steuber and Ikramuddin, 1974; Basu and Murthy, 1977; Basu and Tatsumoto, 1979; Jagoutz et al., 1980; Stosch et al., 1980; Menzies and Murthy, 1980a and 1980b). During the course of this investigation, the ability to produce pure mineral separates increased substantially, as the early results showed this to be absolutely necessary. "Pure" refers not only to the complete absence of other major phases in a given separate, but also to the absence of included phases, liquid or gaseous inclusions, cracks, and all surface contamination.

Evaluation of the separation techniques is best accomplished by comparing our results for alkali elements in clean silicate phases from peridotites with data from the literature (Hutchison and Dawson, 1970; Paul, 1971; Philpotts et al., 1972; Steuber and Ikramuddin, 1974; Shimizu, 1975; Dasch and Green, 1975; Burwell, 1975; Basu and Murthy, 1977; Ottonello, 1978; Kurat et al., 1979). An attempt has been made to review all relevant literature, but undoubtedly, unintentional omissions have been made. Diopsides from the literature have ranges of 22-615 ppm and 0.05-2.1 ppm for K and Rb respectively, while our measurements range from 11.1-13.7 ppm K and from 0.0012-0.0077 ppm Rb. K and Rb concentrations in orthopyroxene reported in the literature range from 10-857 ppm and 0.047-3.07 ppm while our values range from

0.29-1.41 ppm and 0.0009-0.0028 ppm, respectively. A comparison of K and Rb in olivine is qualitatively similar. These results demonstrate the ease of alkali contamination in silicate phases. In fact, samples we considered to be pure at an early stage of our research were significantly higher in K and Rb than the same samples made with improved separation techniques.

Our measurements of Sr, Nd and Sm in olivine and orthopyroxene are also considerably lower than values reported in the literature. However, because these elements are concentrated in clinopyroxene, high values may result from a small amount of clinopyroxene included with an orthopyroxene or olivine separate, an explanation which is not possible for K and Rb. Sr in orthopyroxene and olivine reported in the literature show similar ranges of 0.3-15 ppm, while we have measured 0.087-0.19 ppm in orthopyroxene and 0.008-0.07 ppm in olivine. Nd concentrations in orthopyroxenes and olivines from the literature range from 0.05-0.27 ppm and 0.06-0.08 respectively. We have measured Nd concentrations from 0.016-0.025 ppm in orthopyroxene and 0.0003-0.050 in olivine. Again, these differences may largely result from a small amount of clinopyroxene in the olivine and orthopyroxene separates. Due to the relative compatibility of Sr, Nd and Sm in clinopyroxene, our determinations of these elements in clinopyroxene are very similar to literature values.

After consideration of the data reviewed above, one may be concerned that San Carlos is a particularly unusual nodule locality. However, Frey and Prinz (1978) have demonstrated similarities between San Carlos and other localities on the basis of major element and REE concentrations in whole rocks and clinopyroxene. Further, Steuber and

Ikramuddin (1974) determined Rb and Sr concentrations in one whole rock and constituent minerals from San Carlos, and their values were included in the above comparisons.

To obtain an accurate picture of trace element distributions in the mantle, one must consider data from clean silicate phases, as well as sources for contamination of these silicates.

## 5.7  Results from acid washing experiments

Washed and unwashed mineral separates have been analyzed because

of the marked effect acid washing was shown to have by previous in-

vestigators (e.g., Griffin and Murthy, 1969; Basu and Murthy, 1977;

Menzies and Murthy, 1980a).  Washing was accomplished by a procedure

similar to that outlined by Shimizu (1974), a considerably more potent

treatment than that utilized by Basu and Murthy.  For SC 23, a bulk

rock sample was prepared by crushing to individual grain size and

washed, first with warm 2.5N HCl, then with 5% HF.  The two washes

were analyzed separately.  In order to accurately estimate possible

contaminants, samples of caliche and basalt from San Carlos were also

analyzed.

The results are especially dramatic for the alkali elements.  In

clinopyroxene separates, washing was found to reduce alkali metal con-

centrations by approximately an order of magnitude, while having little

or no effect on Sr, Nd or Sm.  For the whole rock, all elements are

significantly affected by factors ranging from almost two orders of

magnitude for Cs to about 5% for Sm (See Figure 5-3).  Although washing

caused no significant change in the $^{87}Sr/^{86}Sr$ or $^{143}Nd/^{144}Nd$ ratios in

the clinopyroxene, there was a substantial change in the $^{87}Sr/^{86}Sr$ of

the whole rock, from 0.70395 ± 3 to 0.70321 ± 3.  (It should be noted

that SC 23 was chosen for its particularly well-preserved character,

with no cracks through the nodule and no apparent surface alteration

effects).  The shift in the $^{87}Sr/^{86}Sr$ is in the direction of caliche

(0.70571), and the normalized patterns for caliche and the unwashed

whole rock (Figure 5-3) are seen to be similar.  The $^{87}Sr/^{86}Sr$ ratio

in the HCl wash resembles that in caliche, supporting this interpretation.

It is interesting that the $^{87}Sr/^{86}Sr$ ratio in the basalt (0.70298) is

less than that in the clean nodule (0.70321); thus, if one were not cognizant of possible surface contamination, there would have been no reason to suspect the high $^{87}Sr/^{86}Sr$ ratio for the apparently pristine, unwashed whole rock. Further, the HF wash, which was made subsequent to the HCl wash on the same sample, has an $^{87}Sr/^{86}Sr$ ratio of 0.70457, significantly higher than the clean bulk rock, indicating that after ∿20 minutes in warm 2.5N HCl, some of the caliche still remained in the sample. Agreement between the $^{87}Sr/^{86}Sr$ in the washed whole rock and both the clean clinopyroxene (0.70318 ± 2) and the clean ortho-pyroxene (0.70338 ± 18) suggests that the HF wash did finally remove a major portion of the contaminant (the large error for $^{87}Sr/^{86}Sr$ in the OPX results from the small amount of Sr in the total sample, approximately 6 ng). (It should be noted that in PA 65, equilibrium of $^{87}Sr/^{86}Sr$ between clinopyroxene (0.70308 ± 2) and orthopyroxene (0.70312 ± 4) was also observed). Unwashed whole rock $^{87}Sr/^{86}Sr$ ratios from other samples were seen to go as high as 0.70555 in PA 15, where the clean mineral data was ∿0.70275. On the basis of these results, we conclude that mineral-mineral isotopic disequilibrium observed in some nodules, and anomalously high $^{87}Sr/^{86}Sr$ ratios measured in some whole rocks, may result from analysis of contaminated samples.

## 5.8 Possible mantle sources for contamination

The most likely mantle source for "contamination" of major

silicate phases, in lherzolites, is considered to be fluid or

liquid inclusions, which occur ubiquitously in all silicates and

spinel. To place constraints on the trace element characteritics

of inclusions, inclusion-rich mineral separates have been analyzed,

To date, these tests have been made primarily on olivine and ortho-

pyroxene, where interpretation of the data is straightforward, due

to the very low concentrations of all trace elements in these phases.

The liquid or fluid inclusions observed are similar to those des-

cribed in olivines by Roedder (1965). Because a technique for

estimating the mass of inclusions in a given mineral separate has not

yet been perfected, we are limited to comparing our clean mineral

data to analyses of separates with high concentrations of inclusions.

As was the case for the clean mineral separates, the inclusion-

bearing separates are cleaned by the acid-washing technique described

previously.

The results of these experiments have demonstrated conclusively

that the liquid and/or fluid inclusions have high concentrations of

trace elements, particularly the alkali metals. For example, K in

olivine with inclusions, from PA 10, is enriched by a factor of $\sim 25$

relative to inclusion-free olivine. In the same sample, Rb and Cs

are enriched by factors of $\sim 4$ and $\sim 50$, respectively. This yields a

K/Rb ratio in the inclusions of $\sim 750$, which is within the range of

alkali basalts and other alkali-rich, under-saturated volcanic rocks.

(The basalt from San Carlos which was analyzed, PA 53 B, has a K/Rb

ratio of 751; see Table 5-7). Similarly, inclusion-rich orthopyroxene

and olvine, from PA 65, suggest inclusion K/Rb ratios of 1300 and 740, respectively. Sr, Nd and Sm are all enriched in the inclusion-bearing concentrates, but, because clinopyroxene is very enriched in Sr, Nd and Sm, relative to orthopyroxene and olivine, the major effect of the inclusions is to increase the alkali element budget of the peridotites.

It has been concluded, on the basis of these results, that liquid and/or fluid inclusions represent a significant fraction of the mantle alkali metal budget, and consequently, have an important effect on the chemical evolution of melts during magma generation. The observation that inclusions occur primarily in porphyroblastic grains, dictates that inclusions are formed prior to the main phase of re-crystallization observed in many nodules. (Small, equidimensional, neoblastic grains are typically inclusion-free.) Other constraints on the time of formation of the inclusions may be derived from Sm-Nd and Rb-Sr isotopic systematics of inclusion-free and inclusion-rich samples of the same phase. Samples analyzed to date have been too small to permit isotopic analysis.

A second possible source of mantle "contamination" of clean silicates was considered to be a red, magnetic, surface coating, primarily observed on spinel and olivine grains. This was hypothesized to be a sulfide mineral on the basis of its magnetic properties and its solubility in HCl. To facilitate measurements of this phase, spinel concentrates, with relatively large amounts of the surface coating, were made from PA 65 and PA 15. The surface coatings were then dissolved in 2.5N HCl, leaving the spinel completely unaffected. Trace elements and $^{87}Sr/^{86}Sr$ ratios were measured in the HCl leaches. On the basis of the low K/Cs ratio and high $^{87}Sr/^{86}Sr$ ratio for the HCl from PA 15 (Table 5-5) this sample was believed to be contaminated by caliche. $^{87}Sr/^{86}Sr$ from the PA 65 HCl leach is identical to that in the clean silicates, excluding the possibility of caliche contamination. The K/Rb ratio of 200 in this sample is very different from that in the basalt,

eliminating this source for contamination. Gross estimates of the amount of sample analyzed yield concentrations as follows: K $\sim$ 5%; Sr $\sim$ 2%; Nd $\sim$ 750ppm; Rb $\sim$ 350ppm. Although the error in these estimates may be large, these rough calculations demonstrate the potential importance of this phase to mantle chemistry.

In summary, semiquantitative analyses of two minor mantle phases, liquid or fluid inclusions, and sulfides(?), together with the paucity of LIL elements observed in pure silicates, demonstrate the possible overwhelming importance of minor phases in determining mantle trace element characteristics.

## 5.9 Comparison of different generations of silicates

Each of three lherzolites studied has a texture indicative of partial recrystallization under upper mantle conditions. This recrystallization is evidenced by dual habits for each of the major silicate phases. Recrystallized grains, or neoblasts, are smaller than the porphyroblasts and are relatively free of inclusions. Modal analyses of the nodules, which appear in Table 5-1, were determined gravimetrically by complete separation of phases via magnetic properties, and subsequent sieving to permit an estimate of neoblast/porphyroblast ratios. The results in Table 1 indicate that PA 65 displays the most pervasive recrystallization, followed by SC 23, with PA 15 having the largest percentage of relict phases.

To determine the extent of equilibrium attained between different generations of the same phase, inclusion-free porphyroblasts and neoblasts of clinopyroxene, orthopyroxene and olivine, from SC 23, were separated and analyzed independently. Preliminary results indicate that K and Rb concentrations are marginally higher in neoblastic clinopyroxene and orthopyroxene than their porphyroblastic counterparts. However, higher concentrations of Sr, Nd and Sm were measured in the porphyroblasts, with the largest differences occurring for Sm. This results in significantly higher Sm/Nd ratios in the porphyroblasts than in the coexisting neoblasts.

Within the precision of the analyses, porphyroblasts ($^{87}Sr/^{86}Sr$ = 0.70318 ±2; $^{143}Nd/^{144}Nd$ = 0.512743 ±15) and neoblasts ($^{87}Sr/^{86}Sr$ = 0.70316 ±3; $^{143}Nd/^{144}Nd$ = 0.512715 ±15) of clinopyroxene have identical $^{87}Sr/^{86}Sr$ and $^{143}Nd/^{144}Nd$ ratios, but because differences in Rb/Sr and Sm/Nd are small, no significant time constraints on the age of recrystallization are derived. In contrast, the Sm/Nd ratio in the porphyroblastic orthopyroxene is ∿30% higher than in the neoblasts, but, unfortunately Nd in these samples was too low (total Nd ∿0.7 ng) to permit precise measurement of $^{143}Nd/^{144}Nd$.

## 5.10 Trace element partitioning

As a secondary results of our investigation, high-quality, mineral-mineral partition coefficients have been determined for major silicate phases (see Tables 5-10 and 5-11). Orthopyroxene and olivine values are reported relative to coexisting clinopyroxene. To facilitate use and comparison of our data, OPX/CPX and OL/CPX $K_D$'s are converted to OPX/1 and OL/1 $K_D$'s by using CPX/1 values from Hart and Brooks (1974) and Arth (1976). Our OPX/1 and OL/1 $K_D$'s for K, Sr, Nd, and Sm are significantly lower than values reported in the literature ( e.g., see: Hart and Brooks, 1974; Arth, 1976; or Frey, et. al., 1978).

The four sets of OPX $K_D$'s reported in Table 5-10 display remarkable consistency, given the concentration levels measured in the clean mineral separates. This is interpreted as a strong indication of the reliability of the $K_D$'s. K is the one exception and possibly indicates orthopyroxene samples from PA 15 and PA 65 were not as pure, with respect to inclusions, as those from SC 23. The olivine $K_D$'s in Table 5-11 vary over considerably larger ranges than the orthopyroxene $K_D$'s. It is believed that this results from the overall lower abundance of trace elements in olivine, and therefore, the greater difficulty in obtaining uncontaiminated mineral separates. Olivine samples SC 23 were the purest samples prepared in this investigation, and are considered to yield the most reliable OL/1 $K_D$'s.

The major effect of using the $K_D$'s reported in Tables 5-10 and 5-11 in melting models, will be to minimize the importance of olivine and orthopyroxene in melting residues. Although this is an important result, its effect is minimal when compared with the results for the minor phases discussed previously. Realistic melting models cannot be constructed without considering the melting behavior of sulfides (?) and silicates which contain liquid or fluid inclusions.

TABLE 5-10

Orthopyroxene/Clinopyroxene partition coefficients

| Sample | K | Rb | Cs | Ba | Sr | Nd | Sm |
|---|---|---|---|---|---|---|---|
| SC23(NEO) | <0.022 | <0.38 | -- | <0.37 | 0.00244 | 0.00613 | 0.0131 |
| SC23 (POR) | 0.023 | <0.78 | 0.14 | 0.34 | 0.00311 | 0.00828 | 0.0236 |
| PA 15 | 0.109 | 0.36 | 0.15 | 0.30 | 0.00256 | 0.00616 | 0.0119 |
| PA 65 | 0.21 | 0.79 | -- | -- | 0.00287 | 0.00887 | 0.0174 |

Orthopyroxene/liquid partition coefficients[*]

| Sample | K | Rb | Cs | Ba | Sr | Nd | Sm |
|---|---|---|---|---|---|---|---|
| SC23 (NEO) | <0.000029 | <0.00067 | -- | 0.00060 | 0.000175 | 0.000736 | 0.00236 |
| SC23 (POR) | 0.000031 | <0.0014 | 0.00051 | 0.00055 | 0.000224 | 0.000994 | 0.00425 |
| PA 15 | 0.00015 | 0.00063 | 0.00055 | 0.00049 | 0.000184 | 0.000739 | 0.00214 |
| PA 65 | 0.00028 | 0.0014 | -- | -- | 0.000206 | 0.00106 | 0.00313 |

[*]Calculated using CPX/liquid partition coefficients from Hart and Brooks (1974)

and Arth (1976): $D_K = 0.00134$; $D_{Rb} = 0.00175$; $D_{Cs} = 0.00367$; $D_{Ba} = 0.00162$;

$D_{Sr} = 0.0719$; $D_{Nd} = 0.12$; $D_{Sm} = 0.18$.

TABLE   5-11

Olivine/Clinopyroxene partition coefficients

| Sample | K | Rb | Cs | Ba | Sr | Nd | Sm |
|---|---|---|---|---|---|---|---|
| SC 23 (NEO) | <0.0029 | <0.27 | -- | 0.24 | 0.00137 | <0.00011 | <0.00025 |
| SC 23 (POR) | <0.0055 | <1.29 | <0.16 | 0.18 | 0.000416 | <0.00013 | <0.00014 |
| PA 10 | 0.030 | 0.76 | -- | -- | 0.000225 | <0.00022 | <0.0016 |
| PA 65 | 0.027 | 0.76 | -- | <0.62 | 0.000054 | 0.000286 | -- |

Olivine/liquid partition coefficients[*]

| Sample | K | Rb | Cs | Ba | Sr | Nd | Sm |
|---|---|---|---|---|---|---|---|
| SC 23 (NEO) | 0.0000039 | <0.00047 | -- | 0.00039 | 0.000099 | <0.000013 | <0.000045 |
| SC 23 (POR) | 0.0000074 | <0.0023 | <0.00059 | 0.00029 | 0.0000299 | <0.000016 | <0.000025 |
| PA 10 | 0.000040 | 0.00133 | -- | -- | 0.0000162 | <0.000026 | <0.00029 |
| PA 65 | 0.000036 | 0.00133 | -- | 0.00100 | 0.0000039 | 0.0000343 | -- |

*Calculated using CPX/liquid partition from Hart and Brooks (1974) and Arth (1976):

$D_K$ = 0.00134; $D_{Rb}$ = 0.00175; $D_{Cs}$ = 0.00367; $D_{Ba}$ = 0.00162; $D_{Sr}$ = 0.0719; $D_{Nd}$ = 0.12; $D_{Sm}$ = 0.18.

Further investigations along these lines can be expected to elucidate character-
istics of this behavior, but a definitive understanding will emerge only
through careful experimentation.

## 5.11  LREE enrichments in "depleted" peridotites

A significant problem, not solved by our data, is that of a potential
source for LREE enrichment in peridotite nodules with residual mineralogy,
such as PA 65.  The agreement of Nd and Sm concentrations in the whole rock
with the calculated clean bulk for PA 65, together with the observed con-
sistency of OPX/CPX $K_D$'s, demonstrates that these elements are in equilibrium
between orthopyroxene and clinopyroxene.  This argues against the possibility,
suggested by Frey and Green (1974), that crystallization of a metasomatic
liquid, exclusively as clinopyroxene, results in the observed LREE enrich-
ments.

The $^{143}Nd/^{144}Nd$ ratio measured in clinopyroxene from PA 65 (0.513084 ± 13)
is higher than the present-day bulk earth ratio (0.51262), suggesting that the
LREE enrichment in these nodules is a recent event.  Comparison of the clino-
pyroxene $^{143}Nd/^{144}Nd$ ratio with bulk-earth and "MORB-type" mantle evolution
for $^{143}Nd/^{144}Nd$ yields a "maximum enrichment age" of about 180 m.y. (see
Figure 3-6)  As this is based on evolution of a mantle segment with the
highest present-day $^{143}Nd/^{144}Nd$ ratio measured to date (0.51329 from O'Nions
et. al., 1977), a younger age is considered to be more likely.  The recent
nature of this "enrichment event" suggests that the enrichment may have
occured since the onset of volcanism in the Rio Grande rift.

The only documentation of long-term LREE enrichment in peridotite nodules,
is for several nodules from Cretaceous kimberlites in South Africa ( Menzies
and Murthy, 1980b).  It is noteable that, in this tectonic setting, kimberlite
"magmatism" has been occurring since the Proterozoic, and it is possible that the
observed LREE enrichments in the nodules result from interaction in the mantle

with ancient kimberlitic fluids. Hence, with regard to the nature and origin of metasomatic phases in the mantle, it is important to distinguish between metasomatic enrichment as a precursor to alkaline magmatism (Menzies and Murthy, 1980a) and metasomatic enrichment as a result of alkaline magmatism.

## 5.12    Summary and conclusions of chapter 5

Trace element characteristics of mantle–derived peridotites are inconsistent with predictions based on major element chemistry and modal mineralogy.  In addition, many isotopic investigations of constituent minerals from nodules have yielded nebulous results.  Because peridotite nodules represent a unique source of primary information about the upper mantle, it is important to reconcile first-order observations of them with models of the mantle based on information from mantle-derived volcanic rocks.  The results presented in this chapter represent a small but significant step toward attainment of this goal, but more importantly, they demonstrate the inadequacy of previous approaches to the study of nodule chemistry and related mantle processes.

Information from clean mineral separates was shown to be essential to the development of a realistic picture for trace element distributions in mantle peridotites.  Mass balance calculations, regardless of sample mineralogy, demonstrate that Ba and the alkali elements reside almost exclusively in minor phases such as liquid inclusions and sulfides, while Sr, Nd, and Sm in the whole rocks are consistent with measured concentrations of these elements in clean silicates.  These results indicate that major lherzolite phases are too depleted in LIL elements to yield basaltic magma by partial melting.

Equilibrium has been demonstrated between coexisting silicate phases on the basis of: (1) identical $^{87}Sr^{86}Sr$ in coexisting clinopyroxine and orthopyroxene and; (2) consistency of measured mineral-mineral partition coefficients from several nodules.  In light of these data, the observed LREE enrichment in peridotites with residual minerology cannot result from metasomatic introduction of clinopyroxene, but must represent an equilibrium distribution of REE's between major sili-

cate phases.

Semi-quantitative analyses of minor peridotite phases have qualitatively demonstrated the potential for interaction of these phases, with partial melts of fertile lherzolite, in the genesis of basaltic or alkaline magmas.

References

Ahorner, L, Present-day stress field and seismotectonic block movements
along major fault zones in Central Europe, in   N. Pavoni and
R. Green (Editors), Recent Crustal Movements, Tectonophys., 29,
233-249 (1975).

Allsopp, H.L., M.J. Viljoen, R.P. Viljoen, Strontium isotopic studies of
the mafic and felsic rocks of the Onverwacht Group of the Swaziland
Sequence, Geol. Rundsch. 62, 902 (1973).

Arndt, N.T., Thick, layered peridotite-gabbro lava flows in Munro Township,
Ontario, Can. J. Earth Sci. 14, 2620 (1977).

Arndt, N.T., A.J. Naldrett and D.R. Pyke, Komatiite and iron-rich tho-
leiitic lavas of Munro Township, northeast Ontario, J. Petrol. 18,
319 (1977).

Arth, J.C., Behavior of trace elements during magmatic processes -- A
summary of theoretical models and their applications, J. Res. U.S.G.S.,
4, 41 (1976).

Arth, J.G., N.T. Arndt and A.J. Naldrett, Genesis of Archean komatiites -
trace element evidence from Munro Township, Ontario, Geology 5, 590
(1977).

Basu, A.R., and V.R. Murthy, Ancient lithospheric lherzolite xenolith
in alkali basalt from Baja California, Earth Planet. Sci. Lett. 35,
239 (1977).

Basu, A.R., and M. Tatsumoto, Sm-Nd systematics in kimberlites and in the
minerals of garnet lherzolite inclusions, Science (1979).

Beall, G.H., Differentiation controls in subsiliceous gabbros, Ph.D. Thesis, M.I.T., unpublished (1962).

Beall, G.H., P.M. Hurley, H.W. Fairbairn and W.H. Pinson Jr., Comparison of K-Ar and whole-rock Rb-Sr dating in New Quebec and Labrador, Am. J. Sci. 261, 571 (1963).

Best, M.G., Mantle-derived amphibole within inclusions alkalic-basaltic lavas, J. Geophys. Res. 79, 2107 (1974).

Beswick, A.E., Authors reply to Comment on "Is phologopite the key?", Geochim. Cosmochim. Acta 42, 149 (1978).

Beswick, A.E., I.S.E. Carmichael, Nd isotope variations in basic magmas: a disequilibrium melting model, Geol. Soc. Am., Abstr. Progr. 9, 896 (1977).

Bibus, E., and A. Semmel, Uber die Auswirkung quartärer Tektonik auf die altpleistozänen Mittelrhein-Terrassen, Catena, 4, 385-408 (1977).

Bickle, M.J., A. Martin and E.G. Nesbet, Basaltic and peridotitic komatiites and stromatolites above a basal unconformity in the Belingwe greenstone belt, Rhodesia, Earth Planet. Sci. Lett. 27, 155 (1975).

Boyd, F.R., P.H. Nixon, Origins of the ultramafic nodules from some kimberlites of northern Lesotho and the monastery mine, South Africa, Phys. Chem. Earth, 9, 431 (1975).

Brooks, C., S.R. Hart, A. Hofmann, D.E. James, Rb-Sr mantle isochrons from oceanic regions. Earth Planet. Sci. Lett. 32, 51 (1976).

Brooks, C., S.R. Hart and I. Wendt, Realistic use of two-error regression treatments as applied to Rb-Sr data, Rev. Geophys. Space Phys. 10, 551 (1972).

Brooks, C., R. Wardle and T. Rivers, Helikian magmatism in Western Labrador, in prep.

Burwell, A.D.M., Pb-Sr isotope geochemistry of lherzolites and their constituent minerals from Victoria, Australia, Earth Planet. Sci. Lett., 28, 69 (1975).

Cantarel, P. and H.J. Lippolt, Alter und Abfolge des Vulkanismus der Hocheifel, Neues Jahrb. Geol. Palaontol. Monatsh., 600-612 (1977).

Carlson, R.W., J.D. Macdougall and G.W. Lugmair, Differential Sm/Nd evolution in oceanic basalts, Geophys. Res. Lett. 5, 229 (1978).

Carter, S.R., N.M. Evensen, P.J. Hamilton and R.K. O'Nions, Continental volcanics derived from enriched and depleted source regions: Nd- and Sr-isotope evidence, Earth Planet. Sci. Lett. 37, 401 (1978).

Chen, J.C., Petrology and chemistry of garnet lherzolite nodules in kimberlite from South Africa, A. Min., 56, 2098 (1971).

Dasch, E.J., and D.H. Green, Sr isotope geochemistry of lherzolite inclusions and host basaltic rocks, Victoria Australia, Am. J. Sci., 275, 461 (1975).

Davis, B.T.C., and J.F. Schairer, Melting relations in the join diopside-forsterite-pyrope at 40 kb. and at 1 atm., Carnegie Inst. Wash. Yearb. 64, 123 (1965).

DePaolo, D.J., Implications of correlated Nd and Sr isotopic variations for the chemical evolution of the crust and mantle, Earth and Planet. Sci. Lett., 43, 201 (1979).

DePaolo, D.J., G.J. Wasserburg, Inferences about magma sources and mantle structure from variations in $^{143}Nd/^{144}Nd$, Geoph. Res. Lett., 3, 743 (1976a)

DePaolo, D.J., G.J. Wasserburg, Nd isotopic variations and petrogenetic models, Geophys. Res. Lett., 3, 249 (1976b).

DePaolo, D.J., G.J. Wasserburg, The sources of island arcs as indicated by Nd and Sr isotopic studies, Geophys. Res. Lett. 4, 465 (1977).

DePaolo, D.J. and G.J. Wasserburg, Neodymium isotopes in flood basalts from the Siberian Platform and inferences about their mantle sources, Proc. Nat'l. Acad. Sci. USA 76, 3056 (1979).

DePaolo, D.J. and G.J. Wasserburg, Sm—Nd age of the Stillwater complex and the mantle evolution curve for neody mium, Geochim. Cosmochim. Acta, 43, 999 (1979).

Dimroth, E., W.R.A. Baragar, V. Bergeron and G.D. Jackson, The filling of the Circum—Ungava geosyncline, in Symposium on Basins and Geosynclines of the Canadian Shield (Ed. A.J. Baer), Geol. Surv. Can., Paper 70-40, 45 (1970).

Dimroth, E., P. Bowin, N. Goulet, M. LaRouche, Tectonic and volcanological studies in the Rouyn—Noranda area. Open—file Manuscript, Quebec Dept. Nat. Res. 1 (1973).

Duda, A. and H.-U. Schmincke, Quaternary basanites, melilite nephelinites and tephrites from the Laacher See area (Germany), neues Jahrb. Mineral. abh., 132, 1-33 (1978).

Evensen, N.M., P.J. Hamilton and R.K. O'Nions, Rare-earth abundances in chondritic meteorites, Geochim. Cosmochim. Acta 42, 1199 (1978).

Fahrig, W.F., Shabogamo Lake map area, Newfoundland-Labrador and Quebec (23GE 1/2), Geol. Surv. Can., Memoir 354 (1967).

Flower, M.F.J., H.U. Schmicke and R.N. Thompson, Phlogopite stability and the $^{87}Sr/^{86}Sr$ step in basalts along the Reykjanes Ridge, Nature 254, 404 (1975).

Francis, D.M., The origin of amphibole in lherzolite xenoliths from Nunivak Island, Alaska, J. Petrol. 17, 357 (1976).

Francis, D.M. and A.J. Hynes, Komatiite-derived tholeiites in the Proterozoic of New Quebec, Earth Planet. Sci. Lett. 44, 473 (1979).

Frechen, J. and H.J. Lippolt, K-Ar-Daten zum Alter des Laacher Vulkanismus, der Rheinterrassen und der Eiszeiten, Eiszeitalter Ggw., 16, 5-30 (1965).

Frey, F.A., The origin of pyroxenites and garnet pyroxenites from Salt Lake Crater, Oahu, Hawaii: trace element evidence, Am. J. Sci. in press (1979).

Frey, F.A., Trace element geochemistry: Applications to the igneous petrogenesis of terrestrial rocks, Rev. Geophys. Space Phys., 17, 803-823 (1979).

Frey, F.A., W.B. Bryan, G. Thompson, Atlantic Ocean floor: geochemistry and petrology of basalts from Legs 2 and 3 of the Deep-Sea Drilling Project, J. Geophys. Res. 79, 5507 (1974).

Frey, F.A., and Green, D.H., The mineralogy, geochemistry and origin of lherzolite inclusions in Victorian basanites, Geochim. Cosmochim. Acta 38, 1023 (1974).

Frey, F.A., D.H. Green, S.D. Roy, Integrated models of basalt petrogenesis: A study of quartz tholeiites to olivine melilitites from southeastern Australia utilizing geochemical and experimental petrological data, J. Petrol., 19, 463 (1978).

Frey, F.A., M.A. Haskin, J. Poetz, L.A. Haskin, Rare earth abundances in some basic rocks, J. Geophys. Res. 70, 6085 (1968).

Frey, F.A., and M. Prinz, Ultramafic inclusions from San Carlos, Arizona: petrologic and geochemical data bearing on their petrogenesis, Earth Planet. Sci. Lett. 38, 129 (1976).

Freyer, B.J., Age determinations in the Circum-Ungava geosyncline and the evolution of Precambrian banded iron-formations, Can. J. Earth Sci. 9, 652 (1972).

Gast, P.W., Trace element fractionation and the origin of tholeiitic and alkaline magma types, Geochim. Cosmochim. Acta, 32, 1057 (1968).

Gelinas, L., C. Brooks, Archean quench-texture tholeiites, Can. J. Earth Sci. 11, 324 (1974).

Goodwin, A.M., R.H. Ridler, The Abitibi orogenic belt, in Baer, A.J. ed., Symposium on basins and geosynclines of the Canadian Shield, Canada Geol. Survey Paper 70-40, 1 (1970).

Gray, C.M., D.A. Papanastassiou, G.J. Wasserburg, The identification of early condensates from the solar nebula, Icarus 20, 213 (1973).

Green, D.H., Composition of basaltic magmas as indicators of conditions of origin: application to oceanic volcanism, Philos. Trans. R. Soc. London, Ser. A 268, 707 (1971).

Griffin, W.L., Murthy, V.R., Distribution of K, Rb, Sr and Ba in some minerals relevant to basalt genesis, Geochim. Cosmochim. Acta, 33, 1389 (1969).

Hamilton, P.J., Sr isotope and trace element studies of the Great Dyke and Bushveld Mafic Phase and their relation to early Proterozoic magma genesis in Southern Africa, J. Petrol. 18, 24 (1977).

Hamilton, P.J., R.K. O'Nions, N.M. Evensen, Sm-Nd dating of Archaean basic and ultrabasic volcanics, Earth Planet. Sci. Lett. 36, 263 (1977).

Hamilton, P.J., R.K. O'Nions and N.M. Evensen, Sm-Nd dating of Archean basic and ultrabasic volcanics, Earth Planet. Sci. Lett. 36, 263 (1977).

Hamilton, P.J., R.K. O'Nions, N.M. Evensen, D. Bridgwater, J.H. Allaart, Sm-Nd isotopic investigations of the Isua supracrustals, West Greenland: implications for mantle evolution, Nature 272, 41 (1978a).

Hamilton, P.J., N.M. Evensen and R.K. O'Nions, Sm-Nd dating of Onverwacht Group volcanics, southern Africa, Nature 279, 298 (1979).

Harrison, N.M., The geology of the country around Que Que, Bull. Geol. Surv. Rhodesia 67, 125 (1970).

Hart, S.R., LlL-element geochemistry, leg 34 basalts, Initial Reports of the Deep Sea Drilling Project, Vol. XXXIV, eds. R.S. Yeats, S.R. Hart et al., 283 (1976).

Hart, S.R. and C. Brooks, Clinopyroxene-matrix partitioning of K, Rb, Cs, Sr and Ba Geochim. Cosmochim. Acta 38, 1799 (1974).

Hart, S.R. and C. Brooks, The geochemistry and evolution of the Early Precambrian mantle, Contrib. Mineral. Petrol. 61, 109 (1977).

Hart, S.R., J.G. Schilling and J.L. Powell, Basalts from Iceland and along the Reykjanes Ridge: Sr-isotope geochemistry, Nature Phys. Sci. 246, 104 (1973).

Hawkesworth, C.J. and M.J. Bickle, Rhodesian Rb/Sr geochronology from 3.6-2.0 b.a.: a brief review, Annu. Res. Rep., Dept. Earth Sci., Univ. Leeds, preprint (1977).

Hawkesworth, C.J., S. Moorbath, R.K. O'Nions and J.F. Wilson, Age relationships between greenstone belts and "granites" in the Rhodesian Archaean craton, Earth Planet. Sci. Lett. 25, 251 (1975).

Hawkesworth, C.J., R.K. O'Nions, R.J. Pankhurst, P.J. Hamilton and N.M. Evensen, A geochemical study of island-arc and back-arc tholeiites from the Scotia Sea, Earth Planet. Sci. Lett. 36, 253 (1977).

Hawkesworth, C.J., M.J. Norry, J.C. Roddick and R. Volmer, $^{143}Nd/^{144}Nd$ and $^{87}Sr/^{86}Sr$ ratios from the Azores·and their significance in LIL-element enriched mantle, Nature 280, 28 (1979).

Hofmann, A.W., S.R. Hart, An assessment of local and regional isotopic equilibrium in the mantle, Earth Planet. Sci. Lett. 38, 44 (1978).

Hutchinson, R., and J.R. Dawson, Rb Sr, and $^{87}Sr/^{86}Sr$ in ultrabasic xenoliths and host-rocks, Lashaine volcano, Tanzania, Earth Planet Sci. Lett. 9, 87 (1970).

Hynes, A.J. and D.M. Francis, Komatiitic basalts of the Cape Smith fold belt, New Quebec, Canada, in Komatiites and Related Rocks (eds. E. Nisbet and N.T. Arndt) (Cambridge Univ. Press) in press (1980).

Illies, J.H., Two stages Rhinegraben rifting, in I.B. Ramberg and E.-R. Neumann (Editors), Tectonics and Geophys. of Continental Rifts. Reidel, Dordrecht, 63-71 (1978).

Illies, J.H. and G. Greiner, Holocene movements and state of stress in the Rhinegraben rift system, in C.A. Whitten, R. Green and B.K. Meade (Editors), Recent Crustal Movements, Tectonophys., 52, 349-359 (1979).

Illies, J.H., C. Prodehl, H.-U. Schminke and A. Semmel, The quaternary uplift of the Rhenish shield in Germany, in T.R. McGetchin and R.B. Merrill (Editors), Plateau Uplift: Mode and Mechanism, Tectonophys., 61, 197-225 (1979).

Jackson, E.D., T.L. Wright, The magmas and xenoliths of the Honolulu volcanic series, Abstr. UMC Sympos. on Phase Transformations, Canberra (1969).

Jacobsen, S.B. and G.J. Wasserburg, Nd and Sr isotopic study of The Bay of Islands ophiolite complex and the evolution of the source of mid-ocean ridge basalts, submitted J. Geophys. Res. (1980).

Jacobsen, S.B. and G.J. Wasserburg, The mean age of mantle and crustal reservoirs, submitted J. Geophys. Res (1980).

Jagoutz, E., H. Palme, H. Baddenhausen, K. Blum, M. Cendales, G. Dreibus, B. Spettel, V. Lorenz, H. Wänke, The abundance of major, minor and trace elements in the earth's mantle as derived from primitive ultra-mafic nodules, Proc. Lunar Sci. Conf. (1979).

Jagoutz, E., R.W. Carlson, G.W. Lugmair, Equilibrated Nd Nd unequilibrated Sr Isotopes in mantle xenoliths, Nature (in press) (1980).

Jahn, B.J., C.Y. Shih, On the age of the Onverwacht Group, Swaziland Sequence, South Africa, Geochim. Cosmochim. Acta 38, 873 (1974).

Jakobsson, S.P., J. Jonsson, F. Shido, Petrology of the western Reykjanes Peninsula, Iceland, J. Petrol. 19, 669 (1978).

Klein, F.W., P. Einarsson, M. Wyss, Microearthquakes on the Mid-Atlantic plate boundary on the Reykjanes Peninsula in Iceland, J. Geophys. Res. 78, 5084 (1973).

Klein, F.W., P. Einarsson, M. Wyss, The Reykjanes Peninsula, Iceland; earthquake swarm of September 1972 and its tectonic significance, J. Geophys. Res. 82, 865 (1977).

Kramers, J.D., Lead and Strontium isotopes in cretaceous kimberlites and mantle-derived xenoliths from southern Africa, Earth Planet Sci. Lett. 34, 419 (1977).

Krogh, T.E., G.L. Davis, Zircon U-Pb ages of Archean metavolcanic rocks in the Canadian Shield, Carnegie Inst. Yearbook 70, 241 (1971).

Kuno, H., K.I. Aoki, Chemistry of ultramafic nodules and their bearing on the origin of basaltic magmas, Phys. Earth Planet. Inter. 3, 273 (1970).

Kurat, G.H. Palme, B. Spettel, H. Baddenhausen, H. Hofmeister, C. Palme, and H. Wänke, Geochemistry of ultramafic xenoliths from Kapfenstein, Austria: evidence for a variety of upper mantle processes. Geochim. Cosmochim. Acta 44 (1980).

Langmuir, C.H., J.F. Bender, A.E. Bence, G.N. Hanson, S.R. Taylor, Petrogenesis of basalts from the FAMOUS area: Mid-Atlantic Ridge. Earth Planet. Sci. Lett. 36, 133 (1977).

Langmuir, C.H., R.D. Vocke Jr., G.N. Hanson, S.R. Hart, A general mixing equation with applications to Icelandic basalts, Earth Planet. Sci. Lett. 37, 380 (1978).

Laughlin, A.W., D.G. Brookins, A.M. Kudo, and J.D. Causey, Chemical and strontium isotopic investigations of ultramafic inclusions and basalt, Bandera, Crater, New Mexico, Geochim. Cosmochim. Acta 35, 107 (1971).

Lorenz, V. and G. Büchel, Phreatomagmatische Vulkane in der südlichen Westeifel, ihr Alter und ihre Beziehung zum Talnetz, Nachr. Dtsch. Geol. Ges., 19, 30 (1978).

Lugmair, G.W., K. Marti, Sm-Nd-Pu timepieces in the Angra dos Reis meteorite, Earth Planet. Sci. Lett. 35, 273 (1977).

Lugmair, G.W. and K. Marti, Evolution of the lunar interior: Sm-Nd systematics of A15 green glass and the question of lunar initial $^{143}$Nd/$^{144}$Nd, Lunar Sci. Conf. Abstr., 597 (1977).

Lugmair, G.W. and N.B. Scheinin, Sm-Nd systematics of Angra dos Reis, Meteorit. Soc. 39th Ann. Meet., 108 (1976).

Lugmair, G.W., N.B. Scheinin, K. Marti, Search for extinct $^{146}$Sm, 1. The isotopic abundance of $^{142}$Nd in the Juvinas meteorite, Earth Planet. Sci. Lett. 27, 79 (1975).

Lugmair, G.W., Scheinin, N.B., Marti, K., Sm-Nd age and history of Apollo 17 basalt 75075: evidence for early differentiation of the lunar exterior., Proc. Lunar. Sci. Conf., 6, 1419 (1975b).

MacRae, N.D., Ultramafic intrusions of the Abitibi area, Ontario, Can. J. Earth Sci. 6, 281 (1969).

McCulloch, M.T. and G.J. Wasserburg, Sm-Nd and Rb-Sr chronology of continental crust formation, Science 200, 1003 (1978).

McCulloch, M.T., G.J. Wasserburg, Sm-Nd and Rb-Sr chronology of continental crust formation. Science 200, 1003 (1978).

Menzies, M., V.R. Murthy, Nd and Sr isotope geochemistry of metasomatized mantle nodules and their host alkali basalts: Implications for local mantle heterogeneities, Earth Planet. Sci. Lett., in press (1980a)

Menzies, M., V.R. Murthy, Enriched sub-continental mantle: Nd and Sr isotopes in diopsides from kimberlite nodules, Nature, in press (1980b).

Mertes, H. and H.-H. Schminke, K-Ar ages of Pliocene and Quaternary volcanoes in the West Eifel volcanic field, Neues Jahrb. Geol. Paleontol., Monatsh. (1979).

Minster, J.-F., L.-P. Ricard and C.J. Allegre, $^{87}Rb$-$^{87}Sr$ chronology of enstatite meteorites, Earth Planet. Sci. Lett. 44, 420 (1979).

Minster, J.F., C.J. Allegre, Systematic use of trace elements in igneous processes, Part III: inverse problem of batch partial melting in volcanic suites, Contrib. Mineral. Petrol., 68, 37 (1978).

Moorbath, S., J.H. Allaart, D. Bridgwater, V.R. McGregor, Rb-Sr ages of early Archaean supercrustal rocks and Amitsoq gneisses at Isua, Nature 270, 43 (1977).

Moorbath, S., R.K. O'Nions, R.J. Pankhurst, The evolution of early Precambrian crustal rocks at Isua, west Greenland - Geochemical and isotopic evidence. Earth Planet. Sci. Lett. 27, 229 (1975).

Muehlenbachs, K., A.T. Anderson, Jr., G.E. Sigvaldson, Low-$^{18}O$ basalts from Iceland, Geochim. Cosmochim. Acta 38, 577 (1974).

Mysen, B.O. and I. Kushiro, Compositional variations of coexisting phases with degree of melting of peridotite in upper mantle, Am. Min., 62, 843 (1977).

Nagasawa, H. and C.C. Schnetzler, Partitioning of rare earth, alkali and alkaline earth elements between phenocrysts and acidic igneous magma, Geochim. Cosmochim. Acta 35, 953 (1971).

Nakamura, N., Determination of REE, Ba, Fe, Mg, Na and K in carbonaceous and ordinary chondrites, Geochim. Cosmochim. Acta 38, 757 (1974).

Nakamura, N., Determination of REE, Ba, Fe, Mg, Na and K in carbonaceous and ordinary chondrites, Geochim. Cosmochim. Acta 38, 757 (1974).

Nakamura, N., M. Tatsumoto, P.D. Nunes, D.M. Unruh, A.P. Schwab, T.R. Wildeman, 4.4-b.y.-old clast in Boulder 7, Apollo 17: a comprehensive chronological study by U-Pb, Rb-Sr and Sm-Nd methods, Proc. 7th Lunar Sci. Conf., 2309 (1976).

Nakamura, N., D.M. Unruh, R. Gensho, M. Tatsumoto, Evolution history of lunar mare basalts: Apollo 15 samples revisited, Lunar Science Institute, Houston, Texas, Lunar Science VIII, 712 (1977).

Nixon, P.H., and F.R. Boyd, The discrete nodule association in kimberlites from northern Lesotho, in Lesotho Kimberlites (ed. P.H. Nixon) pp. 67-75, Lesotho National Development Corp. Museum, Lesotho (1973).

O'Hara, M.J., Geochemical evolution during fractional crystallization of a periodically refilled magma chamber, Nature 266, 503 (1977).

O'Nions, R.K., S.R. Carter, R.S. Cohen, N.M. Evensen, P.J. Hamilton, Pb, Nd and Sr isotopes in oceanic ferromagnanese deposits and ocean floor basalts, Nature 273, 435 (1978).

O'Nions, R.K., S.R. Carter, N.M. Erensen and P.J. Hamilton, Geochemical and cosmochemical applications of Nd isotope analysis, Ann. Rev. Earth Planet. Sci., 7, 11 (1979).

O'Nions, R.K. and K. Gronvold, Petrogenetic relationships of acid and basic rocks in Iceland. Sr-isotope and rare-earth elements in late and postglacial volcanics, Earth Planet. Sci. Lett. 19, 307 (1973).

O'Nions, R.K., P.J. Hamilton, N.M. Evensen, Variations in $^{143}Nd/^{144}Nd$ and $^{87}Sr/^{86}Sr$ ratios in oceanic basalts, Earth Planet. Sci. Lett. 34, 13 (1977).

O'Nions, R.K., and R.J. Pankhurst, Petrogenetic significance of isotope and trace element variations in volcanic rocks from the Mid-Atlantic, J. Petrol. 15, 603 (1974).

O'Nions, R.K., R.J. Pankhurst, K. Gronvold, Nature and development of basalt magma sources beneath Iceland and the Reykjanes Ridge, J. Petrol. 17, 315 (1976).

Ottonello, G. Rare earth abundances and distribution in some spinel peridotite xenoliths from Assab (Ethiopia), in press (1978).

Papanastassiou, D.A., The determination of small time differences in the formation of planetary objects. Ph.D. thesis, Calif. Inst. of Tech., Pasadena, Calif. (1970).

Paul, D.K., Sr isotope studies of ultramafic inclusions from Dreiser Weiher, Eifel, Germany, Contrib. Mineral. Petrol. 34, 22 (1971).

Philpotts, J.A. and C.C. Schnetzler, Phenocryst-matrix partition coefficients for K, Rb, Sr and Ba, with applications to anorthosite and basalt genesis, Geochim. Cosmochim. Acta 34, 307 (1970).

Philpotts, J.A., C.C. Schnetzler, and H.H. Thomas, Petrogenetic implications of some new geochemical data on eclogitic and ultrabasic inclusions, Geochim. Cosmochim. Acta 36, 1131 (1972).

Reid, J.B., and G.A. Woods, Oceanic mantle beneath the southern Rio Grande Rift, Earth Planet. Sci. Lett. 41, 303 (1979).

Rhodes, J.M., J.B. Dawson, Major and trace element chemistry of peridotite inclusions from the Lashaine Volcano, Tanzania, Phys. Chem. Earth, 9, 545 (1975).

Richard, P., N. Shimizu, C.J. Allègre, $^{143}Nd/^{144}Nd$, a natural tracer: an application to oceanic basalts, Earth Planet. Sci. Lett. 31, 269 (1976).

Ridley, W.F., and Dawson, J.B., Lithophile trace element data bearing on the origin of perdotite xenoliths, ankaramite and carbonatite from Lashaine volcano, N. Tanzania, Phys. Chem. Earth 9, 559 (1975).

Rivers, T., Geological mapping of the Wabush - Labrador City area, south-western Labrador, in Report of Activities for 1977 (Ed. R.V. Gibbons), Newfoundland Department of Mines and Energy, Mineral Development Division, Report 78-1, 44 (1978a).

Rivers, T. and N. Massey, Wabush-Sawbill Lake map area, western Labrador, in Report of Activities for 1978 (Ed. R.V. Gibbons), Newfoundland Department of Mines and Energy, Mineral Development Division, Report 79-1, 142 (1979).

Roedder, E., Liquid $CO_2$ inclusions in olivine-bearing nodules and phenocrysts from basalts, Am. Min., 50, 1746 (1965).

Rosasco, G.J., E. Roedder, Application of a new Raman microprobe spectrometer to nondestructive analysis of sulfate and other ions in individual phases in fluid includsions in minerals, Geochim. Cosmochim. Acta, 43, 1907 (1979).

Rosasco, G.J., E.S. Etz, The Raman microprobe: a new analytical tool, Res. Dev. 28, 20 (1977).

Schilling, J.G., Iceland mantle plume, geochemical evidence along the Reykjanes Ridge, Nature 242, 565 (1973).

Schilling, J.G., H. Sigurdsson, R.H. Kingsley, Skagi and western neovolcanic zones in Iceland, II. Geochemical variations, J. Geophys. Res 83, 3983 (1978).

Schmincke, H.-U., R. Risse, P. Bogaard and G. Wörner, Magma-und Warme-inhalt der Magmakammer des Laacher See Vulkans (Osteifel), Status Seminar "Geotechnik und Lagerstätten", Berlin, 65-77 (1978).

Schnetzler, C.C. and J.A. Philpotts, Partition coefficients of rare-earth elements between igneous matrix material and rock-forming mineral phenocrysts-II, Geochim. Cosmochim. Acta 34, 331 (1970).

Shaw, D.M., Trace element fractionation during anatexis, Geochim. Cosmo-chim. Acta 34, 237 (1970).

Shaw, D.M., G.A. Reilly, J.R. Muysson, G.E. Pattenden, and F.E. Campbell, An estimate of the chemical composition of the Canadian Precambrian Shield, Can. J. Earth Sci. 4, 829 (1967).

Shibata, T., G. Thompson and F.A. Frey, Tholeiitic and alkali basalts from the Mid-Atlantic Ridge at 43°N, Contrib. Mineral. Petrol. 70, 127 (1979).

Shimizu, N., An experimental study of the partitioning of K, Rb, Cs, Sr, and Ba between clinopyroxene and liquid at high pressures, Geochim. Cosmochim. Acta, 38, 1789 (1974).

Shimizu, N., Geochemistry of Ultramafic inclusions from Salt Lake Coates, Hawaii and from Southern African Kimberlites., Phys. Chem. Earth, 9, 655 (1975).

Shimizu, N. and I. Kushiro, The partitioning of rare earth elements between garnet and liquid at high pressures: preliminary experiments, Geophys. Res. Lett. 2, 413 (1975).

Sigvaldason, G.E., Basalts from the centre of the assumed Icelandic mantle plume, J. Petrol. 15, 397 (1974).

Sigvaldason, G.E., S. Steinthorsson, N. Oskarsson, P. Imsland, Composition-
al variation in recent Icelandic tholeiites and the Kverkfjoll hot spot,
Nature 251, 579 (1974).

Smewing, J.D., P.J. Potts, Rare-earth abundances in basalts and metabasalts
from the Troodos Massif, Cyprus, Contrib. Mineral. Petrol. 57, 245
(1976).

Smith, H.S. and A.J. Erlank, Aspects of the geochemistry of Archean
volcanic rocks: Lower Ultranif unit, Swaziland sequence, South Africa,
in Proceedings of the 1978 Archean geochemistry Conference (eds.
I.E.M. Smith and J.G. Williams) (Univ. of Toronto Press).

Staudigel, H. and A. Zindler, Nd and Sr isotope compositions of potassic
volcanics from the East Eifel, Germany: implications for mantle source
region, Geol. Soc. Am. Abstr. Vol. (1978).

Stockwell, C.H., Revised Precambrian time scale for the Canadian Shield,
Geol. Surv. Can., Paper 72-52 (1972).

Stosch, H.G., Carlson, R.W., G.W. Lugmair, Episodic mantle differentiation:
Nd and Sr isotopic evidence., Earth Planet. Sci. Lett. (in press)
(1980).

Stowe, C.W., Summary of the tectonics of the Rhodesian Archaean craton,
Spec. Publ. Geol. Soc. Aust. 3, 377 (1971).

Strong, D.F., J. Dostal, Dynamic melting of the Proterozoic upper mantle:
Evidence from rare earth elements in oceanic crust of eastern Newfound-
land, submitted to Contrib. Mineral. Petrol., in press (1980).

Strong, D.F., S.J. O'Brien, S.P. Taylor, P.G. Strong, D.H. Wilton, Aborted Proterozoic rifting in eastern Newfoundland, Can. J. Earth Sci., 15, 117 (1978).

Stueber, A.M., and M. Ikramuddin, Rubidium, strontium and isotopic composition of strontium in ultramafic nodule minerals and host basalts, Geochim, Cosmochim. Acta, 38, 207 (1974).

Sun, S.S., G.N. Hanson, Origin of Ross Island basanitoids and limitations upon the heterogeneity of mantle sources for alkali basalts and nephelinites. Contrib. Mineral. Petrol. 52, 77 (1975).

Sun, S.S., G.N. Hanson, Rare earth element evidence for differentiation of McMurdo volcanics, Ross Island Antarctica, Contrib. Mineral. Petrol., 54, 139 (1976).

Sun, S.S. and R.W. Nesbitt, Petrogenesis of Archean ultrabasic and basic volcanics: evidence from rare earth elements, Contrib. Mineral. Petrol. 65, 301 (1978).

Sun, S.S., M. Tatsumoto and J.G. Schilling, Mantle plume mixing along the Reykjanes Ridge axis: lead isotope evidence, Science 190, 143 (1975).

Tatsumoto, M., Isotopic composition of lead in oceanic basalt and its implication to mantle evolution, Earth Planet, Sci. Lett., 38, 63 (1978).

Taylor, F.C., Reconnaissance geology of a part of the Pre-cambrian Shield, northern Quebec and Northwest Territories, Geol. Surv. Can. Paper 74-21, (1974).

Tryggvason, E., Seismicity, earthquake swarms, and plate boundaries in the Iceland regions, Bull. Seismol. Soc. Am. 63, 1327 (1973).

Unruh, D.M., N. Nakamura, M. Tatsumoto, History of the Pasamonte achondrite: relative susceptibility of the Sm-Nd, Rb-Sr and U-Pb systems to metamorphic events. Earth Planet. Sci. Lett. 37, 1 (1977).

Viljoen, M.J. and R.P. Viljoen, The geology and geochemistry of the lower ultramafic unit of the Onverwacht Group, and a proposed new class of igneous rock, Geol. Soc. S. Afr. Spec. Publ. 2, 221 (1969).

Wanless, R.K., R.D. Stevens, G.R. Lachance and R.N.D. Delabio, Age determinations and geological studies, Geol. Surv. Can., Paper 74-2, 50 (1974).

Wanless, R.K., R.D. Stevens, G.R. Lachance and J.Y.H. Rimsaite, Age determinations and geological studies, Geol. Surv. Can., Paper 65-17, 98 (1966).

Wardle, R.J., Geology of the eastern margin of the Labrador Trough, Newfoundland Department of Mines and Energy, Mineral Development Division, Report 78-9 (1979).

Ware, M.J., Geology of the Sims Lake - Evening Lake area, western Labrador, in Report of Activities for 1978 (Ed. R.V. Gibbons), Newfoundland Department of Mines and Energy, Mineral Development Division, Report 79-1, 135 (1979).

Ware, M.J. and R.J. Wardle, Geology of the Sims Lake - Evening Lake Area, western Labrador, with emphasis on the Helikian Sims Group, Newfoundland Department of Mines and Energy, Mineral Development Division, Report 79-5 (1979).

Wasserburg, G.J., F. Tera, D.A. Papanastassiou, J.C. Huneke, Isotopic and chemical investigation on Angra dos Reis, Earth Planet. Sci. Lett. 35, 294 (1977).

White, W.M., J.G. Schilling and S.R. Hart, Evidence for the Azores Mantle Plume from Sr isotope geochemistry of the Central North Atlantic, Nature 263, 659 (1976).

Whittaker, E.J.W., and R. Muntus, Ionic radii for use in geochemistry, Geochim. Cosmochim. Acta, 34, 945 (1970).

Wilshire, H.G., N.J. Trask, Structural and textural relationships of amphibole and phlogopite in peridotite inclusions, Dish Hill, California, 56, 240 (1971).

Wilson, J.F., The Rhodesian Archaean craton – an essay in cratonic evolution, Philos. Trans. R. Soc. Lond., Ser. A, 273, 389 (1973).

Windheuser, H., Die Stellung des Laacher Vulkanismus (Osteifel) im Quartar. Sonderveröff. Geol. Inst. Univ. Köln, 31, 223 (1977).

York, D., Least squares fitting of a straight line, Can. J. Phys. 44, 1079 (1966).

Zodrow, E.L., Relationships of olivine gabbro and amphibolite schist at Carol west, Labrador Geosyncline, Geologische Rundschau 60, 1264 (1971).

Appendix I — <u>Chemical Procedure for Nd-Sm Separation</u>

A two column procedure is used; on the first, the REE are separated in bulk from other metals; on the second, the REE are separated from one another.

<u>Sample Preparation</u>

Fifty to 100 mg of sample powder is dissolved in $\sim$3-8 ml of $\sim$1:4 $HClO_4$:HF in a 10 ml TFE beaker. This solution is evaporated at $\sim$150°C until majority of HF is gone; temp. then increased incrementally to 280°C to drive off $HClO_4$. Sample is then brought up to 0.2 ml of 2.5 N HCl, centrifuged, and loaded onto first column.

<u>First Column</u>

The first column, which has been described by Hart and Brooks (1977), consists of a 0.5 cm (diam.) x 19 cm. (ht.) volume (in 2.5 N HCl) of cleaned (in 6.2 N HCl) Dowex AG50WX-8 (200-400 mesh) cation exchange resin obtained from Bio-Rad Laboratories. The sample is loaded in 0.2 ml of 2.5 N HCl, and washed with 3 aliquots of 2.5 N HCl totaling 1 ml. Elution with 20 ml of 2.5 N HCl follows. During this stage of the elution, alkalies and Sr are passed off the column and can be caught if desired (see Appendix II). The elutant is then changed to 6.2 N HCl and approx. 6-8 ml are required to remove the REE, before Ba comes off. When just Nd and Sm are desired, 2-3 ml are discarded and the next 5-6 ml contain the LREE fraction. When preparing these columns, care should be taken <u>not</u> to randomly size the resin while loading into the columns. If all columns have the same size distribution of resin, a given element will be removed from the column with an exactly predictable volume of elutant. Column is then cleaned with 30 ml 6.2 N HCl and backwashed with 2.5 N HCl.

Second Column

The column consists of 50 cm of 0.5 cm I. D. supersil quartz tubing

(obtainable from Amersil, Inc., 650 Jernees Mill Road, Sayreville, N. J.)

attached to a 100 ml round bottom flask (also of quartz from Amersil, Inc.)

which serves as a reservoir for elutant, and provides a constant pressure

head. The bottom end of the column is fitted with a polyethylene fiber

"frit" (from Bel-Art Products, Inc., Pequannock, New Jersey., 07440; or-

der #F-13650, 22 mm chromatographic disks; cut to 0.5 cm with cork cutter).

A 2 mm hole is blown into column 12.5 cm from bottom to allow for sample

loading. Teflon tape, cleaned in 1:1 $HNO_3$ can be wrapped around hole to

prevent leakage. Ten cm of column material is loaded into the column in

$H_2O$ and compressed uniformly to desired compaction ($\sim$10 ml/hr. flow rate)

by a combination of aspiration from the bottom and "tamping" from the

top with a glass rod. This column material is then capped with 0.5 cm

of Dowex AG1-X8 (200-400 mesh) anion resin to prevent teflon flotation.

Preparation of Column Material

Teflon powder (Marque Voltalef Déposée, License Kel-F 3M, 300

Ld Pl micro; Agent de Vente; Plastimer, 98, bd. Victor Hugo, 92-Clichy,

France/ more information on obtaining this powder is available from P.

Richard, Laboratoire de Géochimie et Cosmochimie, Département des

Sciences de la Terre, Université de Paris, 4, place Jussieu, 75230 Paris

CEDEX 05, France) is combined with HDEHP (Bis (2-ethylhexyl) hydrogen

phosphate, $[CH_3(CH_2)_3CH(C_2H_5) CH_2O]_2POOH$, F. W. 322.43) obtained from

Fischer Chemicals, stock #0-1453) in a wt. ratio of 10:1 (powder:

HDEHP) in an acetone slurry. Slurry is dried at room temperature;

can be stirred with teflon magnetic stirrer until it becomes too thick.

Dried powder is then slurried in $H_2O$ and loaded onto column as described

above.

REE are loaded onto column in 0.1 ml of 0.25 N HCL and washed with several 0.2 ml aliquots of 0.25 N HCl through hole 12.5 cm from bottom. Hole is then wrapped with clean teflon tape and elution started. Approximately 10 ml of $0.1^{-0}.15$ N HCl can be passed through column to effect separation of Ba and Ce from Nd. Reservoir is then emptied by inserting pipette tip through teflon tape covering hole in column. Elution is then begun with 0.25 N HCl and Nd is caught with 0.6 N HCl. Sm is caught between 2 and 4 ml. When loading column and reservoir with elutant, it is recommended that the reservoir is filled sufficiently to allow only very small changes in pressure head during elution. This allows the calibration of columns by time rather than volume, which is convenient.

Column Calibration

Column calibration must be carried out for second column because of sensitivity to acid normality, flow rate, and packing profile. Calibration is most easily carried out using the indicator Eriochrome Black-T (EBT). A solution of EBT is prepared by mixing a small amount of EBT ($\sim$10 mg) in 20 ml of 1:1 methanol + $NH_4OH$. At the proper strength, the color change from blue to red can be observed in 0.5 ml of solution with 200 ng of REE. (A white teflon beaker is ideal for this purpose). Typically, 5 min. fractions are collected after loading $\sim$20μg of Nd and/or Sm. Fractions are first buffered at pH 9-10 by adding several drops of $NH_4OH$. The number of drops to this point will be $\sim$proportional to the amount of metal in solution. A similar procedure may be used to calibrate first columns for Nd or REE. The major difference is the need for a much larger volume of $NH_4OH$. EBT is then added dropwise until solution turns blue or purple. The number of drops to this point will be $\sim$proportional to the amount of metal in solution. A similar procedure may be used to calibrate first columns for Nd or REE. The major difference

is the need for a much larger volume of $NH_4OH$ ($\sim$15 drops) to buffer at pH 9-10.

---

The procedure described for Nd-Sm separation has been modified after the technique of P. Richard (Richard et al., 1976).

Appendix II     Notes on chemistry and mass spectrometry

This appendix consists of a collection of observations and empirical intuitions about the chemical techniques (see Appendix I) and mass spectrometric techniques currently employed at M.I.T.  At the request of Cap'n. Stan, many small points are discussed in what may seem to the casual reader to be fairly excruciating detail.  It is hopeful that this way the potential Nd analyst (perhaps SRH?) will avoid some of the possible pitfalls and hours of frustration experienced by the author.  Appendix I should be considered required reading for this section.

## Sample dissolution

When one dissolves a silicate in HF, insoluble fluorides almost invariably form.  No problem results if: (1) the fluorides contain no trace elements, or (2) they can be subsequently broken down in hot HCI. With small samples (<100mg in 10 ml beaker), no problems are observed and one or both of the above conditions must hold.  However, should one decide, for whatever reason, to dissolve significantly more than 100 mg, a larger beaker should be used (naturally, more HF and $HCIO_4$) should be used as well).  The author's experience is that with ~400 mg, the REE yield is <100% and with 1.0 g, REE yield is approximately zero, even though Sr and alkali yields are not significantly affected.  At the other end of the sample-size spectrum, no such problems exist.  10 mg of clinopyroxene may be dissolved in pure HF (i.e., with no $HCIO_4$) with zero loss of REE.  In this case, the sample should be brought up in HCI

shortly after the HF has evaporated, avoiding excessive "cooking" of the fluorides. It has been suggested, on the basis of an old German wives' tale, that youthful fluorides are more easily dissolved (Emil Jagoutz, pers. comm.). As a third alternative for sample dissolution, one might consider HF and $H\ NO_3$ ($\sim$4.1). An old English wives' tale (Jo Hamilton, pers. comm.) has it that fluoride formation is inhibited by $HNO_3$.

For small samples, where blank-level contamination is a problem, it is advantageous to accomplish dissolution of the sample without using $HClO_4$ (This also has advantages with regard to long-term mass spectrometer stability, especially if mass spectrometer resides directly above chemistry lab, in close proximity to hood exhaust system). However, if $HClO_4$ is used, its quality can be considerably improved through distillation in a teflon, two-bottle still, but this procedure should be considered potentially dangerous, and only undertaken with the utmost care. To distill Ultrex $HClO_4$, temperatures in the range of $210°\ C$ are necessary and can be attained by using a heating "sock" on a 1 liter Teflon bottle. Heat lamps must then be focused on the upper part of the bottle to prevent condensation. Because $HClO_4$ does react with teflon to a finite extent, $HClO_4$ produced in this manner must be discarded until the still has been sufficiently cleaned.

## First column chemistry

The cation exchange column used for separation of transition metals from alkali metals, Sr, and REE's has presented minor problems from time to time. It was found that filling the column from an HCl slurry

(2.5N HCI) in a wash bottle was not a good technique, because of the lack of reproducibility with respect to sizing of the resin. The technique employed, which proved to be reproducible, was to transfer small aliquots of resin directly from the supplier's container, with a clean spatula, to a small polyethelyne beaker (~25 ml); slurrly with a few ml's 2.5 N HCI; pour directly into column; then rinse beaker with 2.5 N HCI and pour rinse into column. These steps are repeated until column is filled to 19 cm level. The result of this procedure is to obtain the same size distribution of resin beads in each column, which eliminates the need to calibrate individual columns (although this is not a bad idea).

Several methods of storing columns between periods of use were investigated. If the columns are to be used within a week, the best, and easiest, method is to loosely cover the top with a small poly vial, to keep flies out, and leave the column in the 6.2 N HCI form, and forget it. For longer periods of non-use, it may be advisable to cover both ends tightly with para film, although this is not clearly necessary. If the resin has started to crack and dry out when you return, backwash with 2.5 N HCI and keep going.

Mysterious positive volume changes are observed to occasionally occur, in the cation columns, which may seem to be caused by: (1) inadvertantly pouring $HCIO_4$ on column; (2) allowing extensive drying of resin; (3) temperature changes in clean lab; (4) change in normality of primary acid solutions; (5) pouring undissolved rock on column; (6) full moon during the Fall of an even numbered year; or (7) none of the above. Should one observe such a volume change, try cleaning

column well with a large volume of 6.2 N HCI, then backwashing with 2.5 N HCI, then cleaning, then backwashing, etc. If this doesn't help, and the volume change is less than 5%, try to ignore it, it may go away yet. In this case, the volume calibrations on the side of the column will have changed so that elution volumes will remain the same.

The column technique discussed in Appendix I is the straight, no frills approach, suitable for 30-50 mg of basalt or 20-30 mg of clinopyroxene. For larger samples, the column is overloaded to some degree, resulting in lower purity of element concentrates as well as an increase and a shift in the optimum collection volume for a given element (see Table A-1). Sr samples processed with the overload technique should be cleaned up by repeating the first column step with normal collection volumes. There is generally no problem with alkalis Nd, Sm, or Ba collected during the overload procedure. Extremely large samples (∿1.0 g), such as olivine or opx, may be processed by splitting the liquid from the dissolution into a number of aliquots so that ∿200 mg are loaded onto each of a number of columns, and eluted with the overload procedure. Sr's from all columns may then be combined and run through a single column; the alkali or Ba fraction from any one aliquot is usually enough to run. REE fractions should be combined and run through the second column.

## Drydown after first column step

Sr and Ba: Dry well-spaced samples on hotplate at ∿125°C until HCI is gone. Add ∿3 drops $HCIO_4$ and dry at 175 C for ∿15 min.; then

Table A-1        Optimum collection volumes* for first column chemistry

| | 2.5N HCl | | | | 6.2N HCl | | |
| | Wash | K-Rb-Cs | Wash | Sr | Wash | LREE | Ba |
|---|---|---|---|---|---|---|---|
| Normal sample (30-50 mg basalt or 20-30 mg cpx) | 6.5 | 5.0 | 3.5 | 4.0 | 3.0 | 5.0 | 4.0 |
| Overload (80-200 mg basalt or 50-150 mg cpx) | 5.0 | 5.0 | 2.0 | 7.0 | 2.0 | 6.0 | 4.0 |

*All volumes in ml's.

225 C for 15 min. Add 2 more drops $HClO_4$ and dry at $200°$ C for 15 min.; then increase temperature incrementally to $\sim 280°$ C over period of $\sim 45$ min. Cook for $\sim 1$ hr., turning beaker $180°$ at some point, to evaporate additional $HClO_4$. Let cool and add 2 drops of concentrated $HNO_3$ and dry at $\sim 150$ ; repeat twice. After this procedure, beaker may still have some $HClO_4$ near top. If this procedure is carried out immediately before loading on filament there will be no problem. If saved for a long period of time, it may have to be re-cooked before loading.

Alkalis: Dry at $125°$ C until HCl has evaporated. Add 1-5 drops 20% $H_2SO_4$ (depending on sample volume) and cook at 175 C for $\sim 30$ min. Increase temperature incrementally to 280 C over period of $\sim 45$ min. Cook for 1-2 hrs., turning beaker 180 at some point. Cool, add a few drops of $H_2O$, and dry at 125 C.

REE's: Dry at 125 C until HCl is gone. If so desired resin can be destroyed with $HClO_4$ as for Sr and Ba, reconditioning with 6.2 N HCl instead of $HNO_3$. This step is not essential.

## Second column step for Nd and Sm separation

LREE fraction from first column is brought up in 0.1-0.2 ml of 0.25N HCl, allowing $\sim 5$ -10 min. to completely dissolve. Scraping with clean pipette tip is recommended. Sample can then be loaded onto anion resin through small hole in column. Hole is then closed by wrapping tightly with clean teflon tape. At this stage, it is particularly tempting to break column into 2-7 pieces by applying seemingly harmless pressure to column with thumbs(typically more than 2...). If this should happen to you, have a beer, take a walk, or go bitch at somebody you care about, but do not touch another column for at least two hours (the

result can be disasterous). To prevent damaging columns, remove lower

end from plexiglass stand, reducing possible leverage. Breaking column is

still possible, but more challenging.

When changing normality of elutant, "punch" cleaned pipette tip

through teflon tape, and allow acid to drain on clothing (if so desired,

beaker can be placed behind pipette tip at this stage). If acid refuses

to drain, teflon tape has clogged the pipette tip. Simply remove pipette

and acid will drain, in one of numerous possible directions. To avoid

this predicament, slice end of pipette tip at an angle with razor blade

before cleaning.

Nd and Sm samples are heated at 125° C until liquid has evaporated.

Sample can be loaded onto filament at this stage, however it is difficult

to claim entire sample out of beaker with a small drop of liquid. To

facilitate this add 1 or 2 drops of $HClO_4$ and dry as described for Sr

and Ba above. This will consolidate sample in beaker and make it easier

to load.

## Filament Preparation

Filament beads are cleaned by immersing top half in 1:1 HF and

$HNO_3$ for 2-3 sec., rinsing in $H_2O$, then acetone. If rinsed thoroughly

in acetone, no drying at elevated temperatures is necessary. Single

filaments, for analyzing Sr, Ba, or alkalis, are prepared by welding

Ta strip (0.001"x0.0020") onto filament posts. Single filaments are

degased at 2.8 amps (3.2 amps for marz grade Ta) for ∿20 min. with a

vacuum better than $4.10^{-6}$ torr, then allowed to cool for ∿15 min., then

"flashed" for ∿10 sec. at 2.8 amps, and then degased at 0.95 amps

(∿1.0 amps for marz grade Ta) for 10 min. to remove alkalis which might

have condensed on filament. Double filament beads are cleaned as

described above. A Ta filament is welded on the side and degased as

described above. Zone-refined Re (0.0012"x0.030") is welded on center

posts which are bent away from sides at ∿15 angle, and degased at

∿5.5 amps for 20 min. at a pressure better than $4 \times 10^{-6}$ torr, then

allowed to cool for 15 min. and flashed at 5.5 amps for 10 sec. When

degasing, side filament should never be cold when center filament is hot.

If degasing separately, center is done first, then side.

### Sample loading

All samples are loaded using teflon pipettes skillfully manufactured

by drawing out shrinkable teflon tubing over flame and sealing the

rear end.

Alkalis: Alkalis should be brought up in water for loading. If

sample appears small and black, as from OPX, olivine or blank, a small

amount of water is sufficient. This is accomplished by putting a large

drop from dropper bottle in beaker and removing most of it with pipette.

This also serves as an extra rinse for the pipette. For large, cruddy

alkali samples, as from CPX or basalt, put 1 or 2 drops of water in

beaker. Small black alkali samples can be entirely loaded in center

of filament, drying at ∿0.6 amp (for regular Ta). Cruddy alkalis should

be loaded, avoiding all solid matter in beaker, and spread evenly over

1/2 to 3/4 of filament width. With these samples, especially from

CPX, it is difficult to load enough to get a strong Cs signal. Care

should be taken to avoid getting any $H_2SO_4$ on filament. The effect of

this is not certain, but it is clearly not good.

Sr: Sr should be brought up in a tiny drop of ∿0.1 N $HNO_3$ (∿3μl).

Sample should be scraped with pipette and allowed to sit in laminar

flow box for $\sim$5 min. to allow complete dissolution. In the interim, a thin, even, opaque coat of $Ta_2O_5$ should be loaded on center of filament in a water slurry. Theoretically, the smaller the white spot, the better, but for very small spots, sample must be loaded in a very small volume of $HNO_3$ to prevent it from spreading past the limit of $Ta_2O_5$. Sample can be loaded in several small aliquots. Sample and $Ta_2O_5$ can be dried at $\sim$1 amp and then heated briefly to dull read when sample is completely loaded. 20 ng of Sr will run to fair precision if you're careful and lucky and have a very pure sample (i.e., no Ca). 100 ng is more likely to be satisfying and 400-800 ng is optimum. Samples known to contain significantly more than 800 ng should only be partially loaded.

Ba: Ba is brought up in small amount of $HNO_3$ and loaded directly on center of Ta filament, dried at $\sim$1 amp and briefly heated to dull red.

Nd and Sm: Nd and Sm are brought up in a tiny drop of 1:1 0.3 N HCl and 0.2 N $H_3PO_4$. With small samples being run for Nd isotopic composition, care should be taken to claim entire sample from beaker. Experience has shown that leaving sample in the beaker makes long stable runs exceedinly difficult, if not impossible. Sample should be carefully loaded in tiny aliquots ($\sim$0,3$\mu$l) onto very center of side filament, drying aliquots at $\sim$1 amp. When sample is loaded, briefly heat to dull red. Using two pairs of tweezers, center filament is bent until it is again vertical relative to surface of glass bead. Center and side filaments should be as close together as possible without touching. Isotopic composition of Nd can be measured to good precision on 15-25 ng samples but this is very difficult. 50-100 ng is quite feasible and

200-500 ng is a piece of cake. Samples known to contain significantly
more than 500 ng should only be partially loaded. (For the large
samples, it is also conceivable for mass spectroscopist to be partially
loaded.)

## Measuring isotopic compositions on mass spectrometer

Measurements of a given element should routinely be taken with
similar ion currents, that is, on the same range of the Cary 401 VRE.
The Cary is not linear from range to range and can produce erroneous
results for high-precision isotopic composition measurements of Nd
and Sr (this is not so critical for ID measurements). Different ranges
can be used but should first be calibrated by measuring standards
(E&A $SrCO_3$, for Sr, =0.70800; BCR-1, for Nd, =0.512640) several times.
A note about focusing: the differential range on the Z lens is not as
large as might be desired, but can be enhanced, if necessary, by placing
a bar magnet normal to flight path at exit slit -- experimentation will
show best position. Filament current stability has been a significant
problem in the past. The digital voltmeters allow you to monitor this
very closely; fluctuations of more than ±0.01% indicates a problem --
normally supplies are stable to ±0.004%. During isotopic composition
funs for Nd or Sm (1C's), problems must be dealt with as they will
significantly affect the precision of the result. For ID's, this
is much less critical and you may get away with small current fluctuations.
Current fluctuations of all magnitudes typically result from bad connections
of one of the following types: (1) filament bead to connectors inside
source; (2) filament wire to posts; (3) power supply to source block;
(4) power supply to power cables; (5) you to the powers that be on a given

day.  Careful experimentation will usually produce ambiguous results.
In this case, you must consider the possibility that the power supply
is not functioning properly.  This can be ascertained by attaching a
dummy load ( $\sim 0.4\Omega$ ) across the power supply output.  However, do not
attempt this without prior clearance from SRH or KB.  Typically, this
test will also produce ambiguous results.  In dealing with these
supplies, one must remember, as is the case for all electronics and
machinery, never to underestimate the capacity for the simultaneous
failure of 2-6 completely independent components (algorithm of
Murphy's Law).

Alkalis:  Emission temperature for the alkali metals increases from K
to Rb to Cs.  Theoretically, it makes sense to measure them in this
order, except for two things:  (1) If you don't look for Cs immediately,
especially in clino pyroxene, it may not be there when you do look;
(2) breathing or expectorating in the direction of a loaded alkali
sample, or dropping cigarette ashes on filament, may cause significant
changes in K isotopic composition.  In all but the worst cases, this
will only be evident with a relatively small K ion beam ($<3 \times 10^{-11}$ amps).
Hence, it makes good sense to go to Rb or Cs before K.  The author tends
to prefer Cs – Rb – K, because of his fear of losing Cs.  Cs should be
measured on a 3-peak program, allowing for correction of in-run
fractionation (133, 135, 137).  Data can be taken on 100mv scale if
possible ($10^{11}\,\Omega$ input resistor), but usually 10-30mv is the upper limit.
Two good blocks of data (12 sets of ratios) is sufficient, but often
you will settle for much less.  Rb is measured on a 2-peak program
(85-87).  One should strive to run Rb's in a reproducible way, so as
to take data in a similar fractionation range from sample to sample;

(this is a good reason, incidentally, to measure Rb, rather than Cs,
first). Data for Rb is ideally taken on 1V to 10V range. There is
not much point to measuring $^{85}Rb/$ $^{87}Rb$ to much better than ± 0.2% as
you can never predict the fractionation better than this (unless,
of course, you happen to be S. Richardson or C. Allègre). K is
measured on a 3-peak program (39-40-41) and data can usually be ob-
tained on a 30V scale. After running alkalis for several hours, peak
shape will start to deteriorate and peaks will begin to resemble
rocket ships. You must be aware of this, as focusing and centering
will become more difficult. Peak shape can usually be improved by
defocusing with either the first thick lens or the Z lens. After
unusually long periods of measuring alkalis, machine blanks may occur
for K, so beware.

Ba: Ba, though typically measured on a 2-peak program, should be
measured on a 3-peak program (136, 137, 138), allowing fractionation
corrections to be made. Ionization efficiency for Ba is very high, and
it requires almost no thought or effort to run. Two good blocks of
data is sufficient.

Sr: For Sr's, ID's and IC's are measured together on the same, spiked
sample. Because of the purity of the $^{84}Sr$ spike, the correction
on the IC should be trivial. (Samples should be spiked for an
$^{84}Sr/^{88}Sr$ ratio in the range of 0.03 - 0.3 ) Sr samples may be "con-
ditioned" before running, by heating to just below emmission temperature
for one to two hours. ( ∿1.4 amps for std. purity Ta ribbon). This
may or may not enhance stability, but it certainly won't hurt. The

procedure may be carried out in the degasser, as opposed to the mass
spectrometer, so that valuable running time is not wasted. Alterna-
tively, Sr samples may be loaded and brought to running temperature
slowly ( $\sim$1.5 - 1.7 amps for std. purity Ta) over the period of $\sim$1
hour. Again the effect of this is not certain. The third choice,
which is the most esthetically appealing, is to immediately "flash"
sample to $\sim$2.2 amps, reduce current to running temperature, and start
taking data. Experimentation with the three approaches is suggested.
Sr's, particularly when loaded over a large portion of the filament,
tend to change focus (primarily Z direction) quite often and need to
be closely monitored. Often after "flashing" the focus will change
drastically. Flashing the sample to 1.9 - 2.7 amps is sometimes
advisable when encountering stability problems. This may not be wise
with very small samples, although a minor flash ( $\sim$2.0 amps) rarely
does major damage. Again one should experiment with flashing techniques.
Several good blocks of ID data (84, 86, 88) are usually taken for Sr
in the beginning of the run, after the signal has become stable.

Nd: Currently Nd I.D.'s and I.C.'s are measured on separate aliquots
of sample, which are split at the third HCl stage during dissolution.
Splitting liquids, as opposed to using separate powder aliquots is
probably more reliable for Sm/Nd ratios and probably a little less
reliable for absolute concentrations. As a result, liquids should
always be split for geochronological applications, whereas powder
aliquots are sufficient for young basalts. There is no inherent

reason not to measure Nd ID's and IC's on the same aliquot. This merely requires much more care in spiking. Because the $^{148}$Nd spike is not nearly as enriched as the $^{84}$Sr spike, smaller spike to normal ratios must be used to minimize the correction in $^{143}$Nd/$^{144}$Nd ($^{148}$Nd/$^{146}$Nd $\sim$ 0.01). It is then advisable to measure Nd on a 4-peak program (143, 144, 146, 148) which is currently not available. ID splits are run on a 3-peak program (144, 146,148) and several good blocks (< ±0.10%) should be taken.

With a reasonable amount of sample on the filament ( > 100mg), measurement of Nd is inherently easier than Sr. Because the hot spot on the center filament determines the point of emission, this changes little during the course of a run and the focus does not require as much attention as Sr. As for Sr, conditioning prior to running may help stability ( 1 - 6 hours with side filament at $\sim$1.2 amps and center at 2.5 amps). As a rule, regardless of conditioning, Nd seems to run better if brought to running temperature (1.5 - 1.8 side and 5.0 - 6.0 center) over the period of an hour or so. This also allows the chance to observe the level of fractionation early and predict the degree of care necessary for a good run. With a signal strength of $\sim$ 7 X 10$^{-13}$ amps, it is a good idea to take a block of data and check the fractionation: if$^{144}$ Nd/$^{146}$Nd > 1.390, crank it up to 2.8 X 10$^{-12}$amps and start taking data - it will probably run all day (or all night); if $^{144}$Nd/ $^{146}$Nd > 1.386, start collecting data, but use some care; if $^{144}$Nd/ $^{146}$Nd > 1.384, it's going to be a tough go, but still possible - don't take it as high as fast; if $^{144}$Nd/ $^{146}$Nd < 1.382; hang it up - go have a beer.

To judge the center filament current, check the ratio of $^{144}Nd/^{160}NdO$. It will always be higher in the beginning of the run, but by the time you start to collect data, it should be >20 and preferably >100. This ratio can be increased by increasing the center filament current to an upper limit of ~6 amps. More normally,you should run between 5.0 - 5.5 amps. If the oxide is still large at 6.0 amps, the center and side filaments are not close enough together. Clearly, for small samples, you don't want to be running a big oxide peak, purely from an efficiency standpoint.

The major interference to be concerned with for Nd, is Sm. The column separation is generally very good and this is not a problem. However, at some stage in the life of an Nd column, the separation begins to deteriorate (~1-2 years). You should calibrate columns often enough to observe changes on this time scale. At any rate, $^{147}$Sm should be checked routinely on the 30mv scale ($10^{11}\Omega$). Pr, La, Ce, and Ba will almost always be present in Nd samples. The only potential problem is $^{146}$BaO, but $^{130}$Ba is very small and luckily Ba runs with a very large metal to oxide ratio. These elements are not observed to affect the stability of Nd emission.

A good Nd run reaches a precision of < ± 0.004% in 100-150 ratios. Normal runs attain this precision in 150-300 ratios. If by 300 ratios, the precision is not < ±0.004%, it may never get there, because of a bumpy signal, and you may settle for a less precise answer.

Data should only be taken with a fairly flat signal. Rapid growing or dying may result in an erroneous answer. Aside and singular phenomena, such as "blips" and current ups and downs, all data are used for

calculation. On a medium-bad run, it becomes a matter of discretion as to whether or not a bad linearity or mean deviation for a given block results from singular phenomena or "gaussian" changes in the sample emission. In this case, one theory of how to treat the data is as good as another. The best thing is simply to avoid bad runs. Duplicate analyses have shown that the quoted precision for a bad run may be unrealistically low.

Appendix III    Fractionation Models

A model for isotopic fractionation in a thermal ion source has been
developed.  The model is based on a formulation for the rate of evaporation
of a thin film solid as a function of temperature,

$$G = n \sqrt{(kT/2\pi m)} \ e^{-U_0/kT}, \tag{1}$$

where G is the number of atoms which escape per unit time, and n is the total
number of atoms.  This formulation is derived from Maxwell's velocity distri-
bution law, and has been described by J. Frenkel in <u>Kinetic Theory of Liquids</u>
(1955, Dover Publications).  If we consider the ratio, X, of two isotopes of
the same element, the expression reduces to

$$X_i = X_f \sqrt{(m_{x2}/m_{x1})}, \tag{2}$$

where $X_i$ indicates the isotopic ratio in the first fraction of solid to
evaporate from a filament; $X_f$ indicates the ratio on the filament prior
to evaporation; and $x_1$ and $x_2$ are the numerator and denominator of the
ratio X, respectively.  We can then write

$$\frac{X_i - X_f}{X_f} = \sqrt{(m_{x2}/m_{x1})} - 1 . \tag{3}$$

This expression can be thought of as a differential equation because it
is defined only where $X_f$ is an unfractionated solid and $X_i$ is the first
differential increment to evaporate.  Thus,

$$dx/x = \sqrt{(m_{x2}/m_{x1})} - 1 = K_x - 1 \tag{4}$$

where $K_x$ is defined for convenience.  Similarly, for a second isotope ratio

of the same element, we can write

$$dy/y = K_y - 1 \qquad\qquad (5)$$

This yields

$$dx/x = dy/y \ (K_x - 1)/(K_y - 1) \qquad\qquad (6)$$

which can be integrated for measured and true values of the isotope

ratios X and Y to obtain

$$Y_t = Y_m \ (X_t/X_m)^K \qquad\qquad (7)$$

where

$$K = (K_x - 1)/(K_y - 1) \ .$$

Equation (7) describes the relative fractionation between two pairs of

isotopes in a thermal ion source. The expression has a general form and

can be used for any pairs of isotopes of any element. Constants for

geologically interesting elements are listed in Table A-2.

To date, the implications of this model have not been fully ex-

plored. A major result, is the ability to estimate the absolute istopic

composition of an element in nature. Equation (2) dictates that the

isotopic ratio in the first fraction of solid to leave the filament will

be equal to a constant times the isotopic ratio of the solid on the

filament, which initially has an unfractionated composition. Hence, to

estimate the natural isotopic composition of an element, one should utilize

a ratio measured immediately after the ion beam is turned on. Interesting-

ly, there is no reason to expect that the average of a large number of

measurements of a isotope ratio should yield the true value for that ratio.

Table A-2   Constants* for fractionation equasion:   $Y_t = Y_m \left(\dfrac{X_t}{X_m}\right)^K$

| ELEMENT | X | Y | Kx | Ky | $K = \left(\dfrac{Ky-1}{Kx-1}\right)$ |
|---------|-----|-----|-----|-----|-----|
| Nd | 144/146 | 148/146 | 1.006935 | 0.993204 | -0.979972 |
| Nd | 144/146 | 143/144 | 1.006935 | 1.003494 | 0.403730 |
| Sr | 86/88 | 84/88 | 1.011552 | 1.023511 | 2.035232 |
| Sr | 86/88 | 87/86 | 1.011552 | 0.994233 | -0.499256 |
| Sm | 154/152 | 149/152 | 0.993474 | 1.010031 | -1.537027 |
| K | 39/41 | 40/41 | 1.02532 | 1.01241 | 0.490126 |
| Cs | 137/135 | 135/133 | 0.992665 | 0.992558 | 1.014593 |

*  All values calculated using atomic masses corrected for nuclear binding energy.

The model described by equation (7) is termed Model A and is compared to two commonly used models in Figures A - 1 to A - 4. The other models are described by the following expressions

$$(X_t - X_m)/ X_t = C (Y_t - Y_m)/ Y_t \qquad \text{Model B}$$

$$(X_t - X_m)/ X_m = C (Y_t - Y_m)/ Y_m \qquad \text{Model C .}$$

Figure A - 1    Comparison of Nd fractionation models.

S indicates $^{148}$Nd - enriched spike currently used at M.I.T.

N indicates normal Nd.   Fractionation lines for the three

models are drawn through S, N, and two intermediate com-

positions on the spike - normal mixing line.   Model A -

dashed - dotted line; Model B - unbroken line; Model C -

dashed line.   Note that only Model A describes a family of
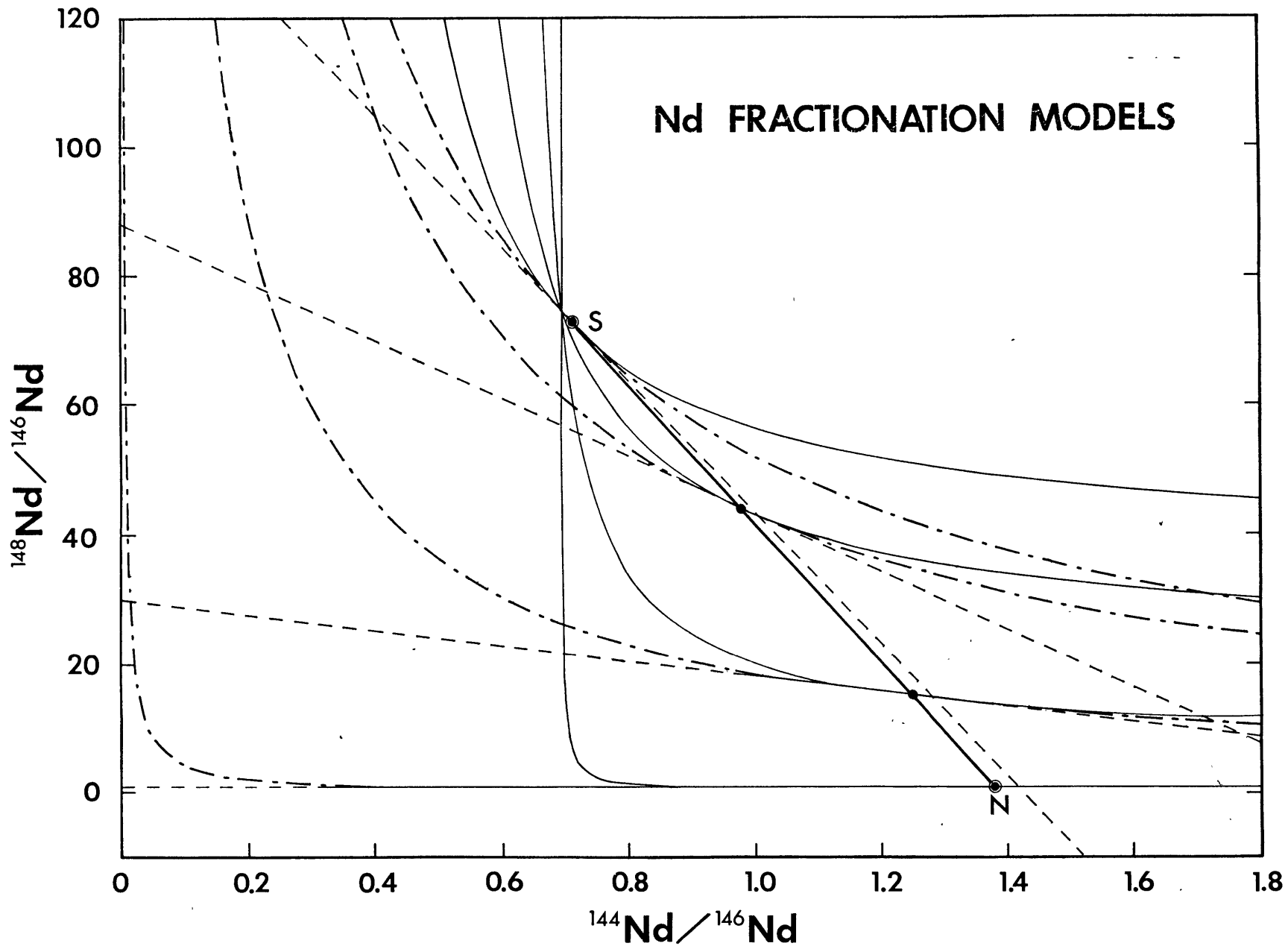
curves in the differential sense.

Nd FRACTIONATION MODELS

Figure A - 2    Comparison of Sm fractination models.

S indicates the $^{149}$Sm - enriched spike currently in use

at M.I.T.   N is normal Sm.   Fractionation lines drawn

for S, N, and two intermediate compositions.   Legend as
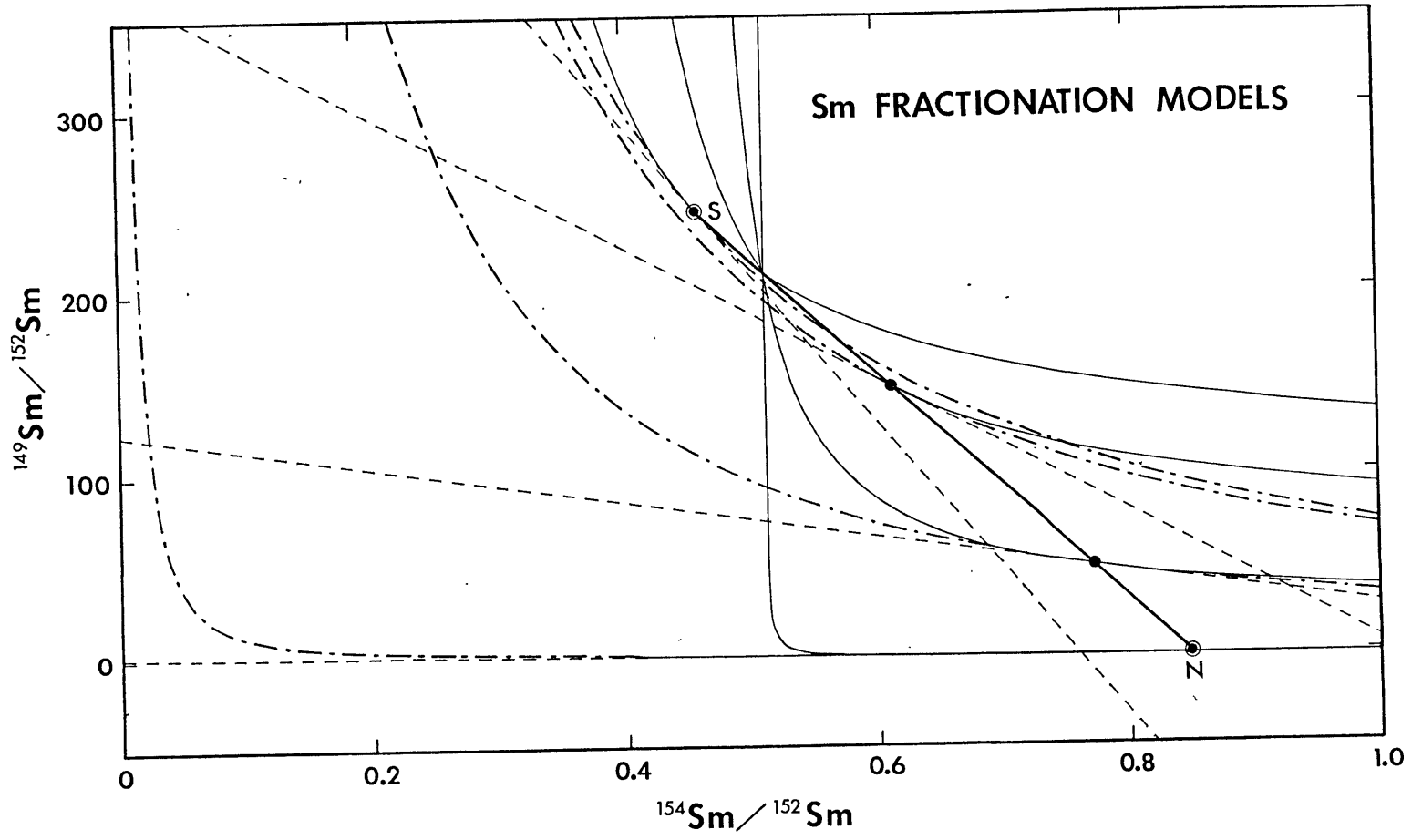
in Figure A - 1.

Sm FRACTIONATION MODELS

$^{149}Sm/^{152}Sm$

$^{154}Sm/^{152}Sm$

FIGURE A-2

Figure A - 3    Comparison of Sr fractionation models.

S indicates $^{84}$Sr - enriched spike currently in use at M.I.T.

N is normal Sr.   Fractionation lines drawn through S, N,

and three intermediate compositions.   Legend as in Figure

A - 1.  Note that there is one Model A curve which is tan-

gent to the spike - normal mixing line at $^{84}$Sr/$^{88}$Sr equals

about 200.   All other Model A curves cross the mixing line

twice.

Sr FRACTIONATION MODELS
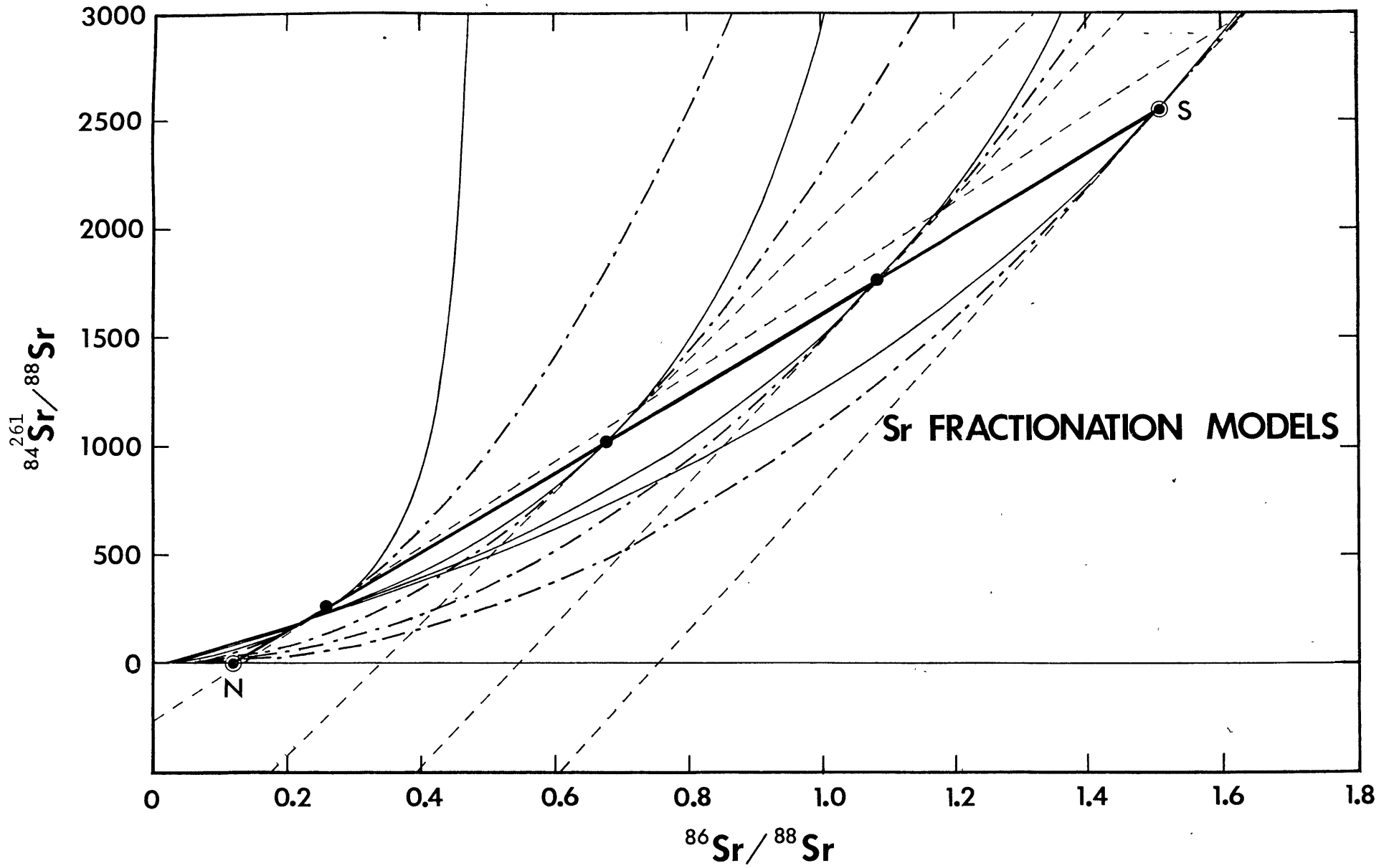
FIGURE   A-3

Figure A - 3     Comparison of Sr fractionation models.

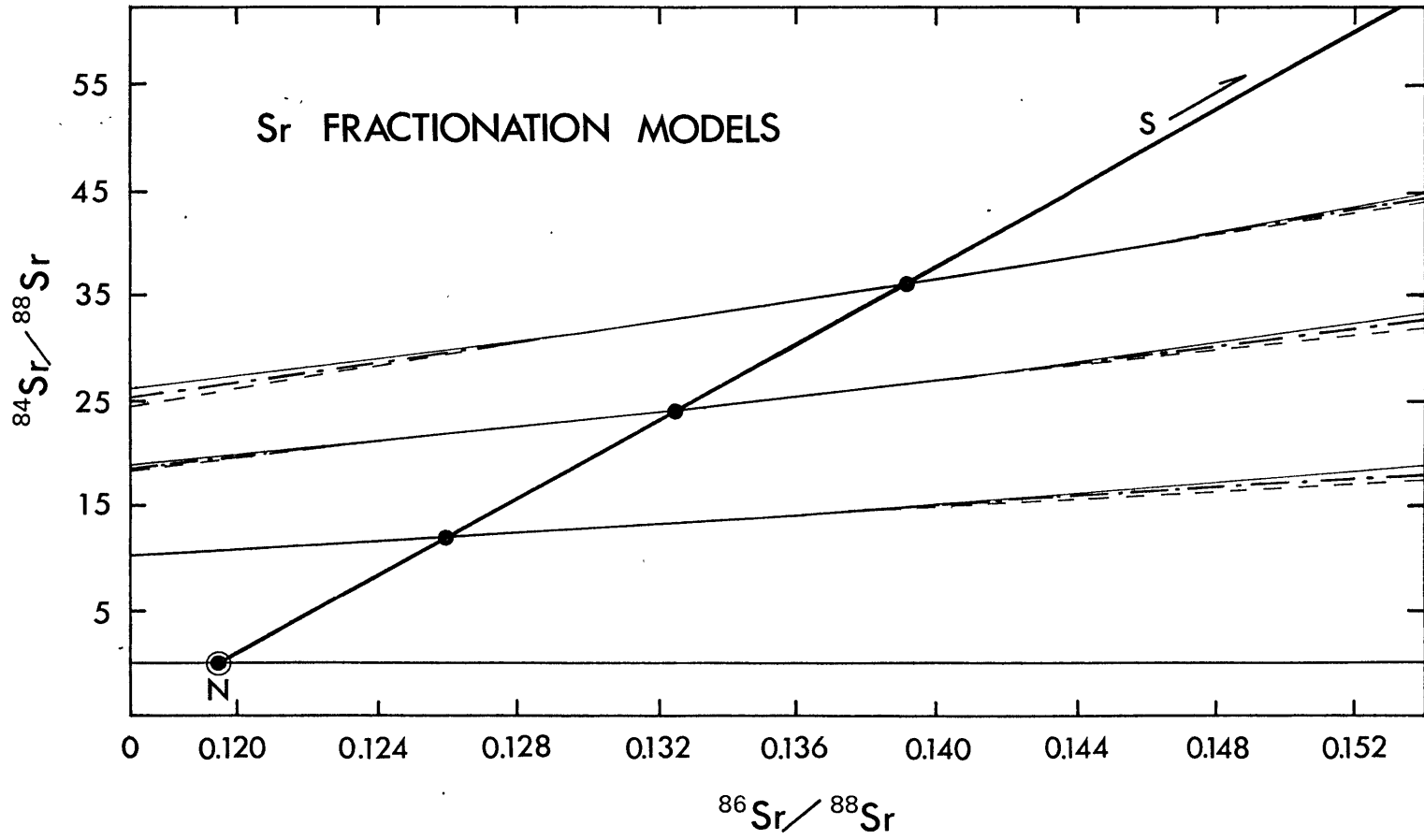Expanded view of the low $^{84}Sr/^{88}Sr$ range.   Legend as in

Figure A - 3.

Sr FRACTIONATION MODELS

FIGURE A-4